FLYWCH1, a Novel Transcription Regulator with Potential Tumour Suppressor Activity

Sheema Almozyan, BSc., MSc.

Thesis submitted to the University of Nottingham in fulfilment for the degree of Doctor of Philosophy

August 2021

Declaration

I hereby declare that this thesis is entirely my own work, except where otherwise acknowledged in the text, and was prepared by me in Cancer Genetics & Stem Cell Group, under the supervision of Dr Abdolrahman Shams-Nateri at the School of Medicine, Faculty of Medicine and Health Sciences, University of Nottingham.

Sheema Almozyan

ID: 4251035

Abstract

Colorectal cancer (CRC) remains the world's third most deadly cancer. The molecular mechanisms underlying cancer development are multifactorial; however, hyperactivation of the Wnt pathway is the most common and primary molecular driver of this disease. Therefore, a better characterisation of the molecular mechanisms underlying the differences of Wnt/β-catenin signalling pathway action in normal versus cancer cells is warranted. Identifying specific protein(s) regulating Wnt/β-catenin differentially in healthy versus cancer cells are particularly of clinical interest.

Previous work in Dr Nateri's lab used a modified yeast two-hybrid Ras-Recruitment System (RRS) and identified several new proteins that bind β-catenin protein. One of the β-catenin interacting proteins was FLYWCH1, a previously uncharacterised protein product of the human *FLYWCH*1 gene. Hitherto, only a few published studies investigated the interplay of physiological and molecular mechanisms of FLYWCH1. For example, FLYWCH1-mediated transcriptional regulation was particularly crucial for the cardiovascular system. Another study reported that in humans, FLYWCH1 mutation variants might be deleterious and associated with familial mitral valve prolapse (MVP) in humans.

Furthermore, the roles of FLYWCH transcription factors (known as FLH-1 and FLH-2) regulating microRNAs (miRNAs) were previously reported in *C. elegans*. Therefore, the FLYWCH1 protein likely plays an essential role in regulating gene expression. Our lab has also shown that overexpression of FLYWCH1 antagonises

β-catenin/TCF4 signalling during cell polarity/migration in cultured CRC cells and influences the AML cells proliferation.

However, we are beginning to provide insights into the molecular mechanisms through which the FLYWCH proteins function. More recent unpublished in-situ hybridisation (ISH) data from our lab reported the high *Flywch1* expressing population of normal and adjacent tumour-free crypt-based cells (2-6 cells), to be the stem cells and transiently amplifying cells. In contrast, *Flywch1* expression was not detected in differentiated epithelial cells in the villi and highly down-regulated at the crypt-based cells of a tumour in Apc^Min mouse.

Considering the FLYWCH1 expression data, we hypothesised that FLYWCH1 might play a critical role in regulating Wnt/β-catenin mediated colon/intestinal development and tumour formation activities. Therefore, this project was aimed to explore the biological significance, cellular and molecular mechanism(s) of FLYWCH1 via several *in vitro* approaches through gain and loss of function analysis of FLYWCH1 in cultured human skin fibroblast cells (TIG119), CRC cell lines, 3D-organoids models, and eventually clinically orientated CRC TMA analyses.

As a result, herein, Chapter 3 demonstrated that *Flywch*1 crypt-expression is crucial for maintaining the growth and proliferation of the intestinal crypt using murine intestinal organoids. Loss of *Flywch*1 accelerates the proliferation (Ki-67+ cells) of normal intestinal organoids via increasing the transcription of *Lgr5/Olmf4* intestinal stem cell markers. In CRC patient-derived tumour organoids (PDOs), over-expressing human FLYWCH1 protein significantly reduces PDOs sizes and growth by regulating a subset of Wnt target genes involved in cancer invasion, stemness and EMT. Furthermore, we showed that loss of *FLYWCH*1 in SW620 cell

lines conferred more stemness activity *in vitro* by increasing the colonosphere forming efficiency. Our data provided proof of concept regarding the role of FLYWCH1 in regulating Wnt-mediated biological responses in CRC. Additionally, the data suggested that an over-activation of Wnt signalling decreases FLYWCH1 expression, affecting its stability and cellular localisation. More importantly, our immunohistochemistry-based analysis revealed a significant reduction in FLYWCH1 protein expression in patient's tumour tissues compared to normal samples. Further analyses indicated a significant correlation between low FLYWCH1 expression, cytoplasmic localisation, CRC staging and overall survival. The data indicate that a low expression of FLYWCH1 could predict a poor prognosis in CRCs. In Chapter 4, the data demonstrated for the first time that FLYWCH1 could play as a novel participant in DNA-damage/ repair pathways, co-localising with γH2AX and overexpressing FLYWCH1 induces the expression of γH2AX protein (Almozyan S., et al. 2021).

Altogether, these findings suggest that deregulation of FLYWCH1-WNT signalling and/or FLYWCH1-γH2AX axis via DNA repair pathway could be a significant modulator of tumorigenesis in CRC. However, future studies integrating omics data with *in vivo* models will allow us to understand the flow of our current developed data that underlies intestinal tissue homeostasis and cancer.

Acknowledgment

Publication list

- **<u>Almozyan, S,</u>** Coulton, J, Babaei-Jadidi, R, and Nateri, A.S. FLYWCH1, a Multi-Functional Zinc Finger Protein Contributes to the DNA Repair Pathway. Cells 2021

- Almars A, Panagiota S, Emenike K, **<u>Almozyan S</u>**, Seedhouse, C, Babaei-Jadidi R and S. Nateri A. Increased FLYWCH1 Expression is Negatively Correlated with Wnt/β-catenin Target Gene Expression in Acute Myeloid Leukemia Cells. Int. J. Mol. Sci. 2019

- Muhammad B*, **<u>Almozyan S *,</u>** Babaei-Jadidi R*, Onyido E, Saadeddin A, Kashfi1 S, Spencer-Dene B, Ilyas M, Behrens A and Naeri AS. FLYWCH1, a Novel Suppressor of Nuclear β-catenin, Regulates Migration and Morphology in Colorectal Cancer. Molecular Cancer Research, 2018. <u>*Co-first authors</u>

- Kashfi S<u>, **Almozyan S,**</u> Jinks N, Koo BK, and Nateri AS. Morphological alterations of cultured human colorectal matched tumour and healthy organoids. Oncotarget. 2018 Jan 19;9(12):10572-10584.

Table of content

Abbreviations

APC	Adenomatous Polyposis Coli
BIO	6-bromoindirubin-30-oxime
BMP	Bone Morphogenic Protein
BRCA1	Breast cancer type 1 susceptibility protein
Brg-1	Brahma/Brahma-related gene 1
BSA	Bovine Serum Albumin
β-TRCP	Beta-Transducin Repeat-Containing Protein
C2H2	Cystein2-Histidine2
CAMKII	Calcium/calmodulin-mediated kinase II
CBC	Crypt Base Columnar
CBP/p300	CREB-binding protein
cDNA	Complementary DNA
CHX	Cycloheximide
CK 1	Casein Kinase 1
CIN	Chromosomal instability pathway
CIMP	CpG island methylator phenotype
CMS	Consensus molecular subtypes
CRC	Colorectal Cancer
CRISPR	Clustered regularly interspaced short palindromic repeats
Crm-1	Chromosomal region maintenance 1 protein
CSCs	Cancer Stem Cells
DAPI	4′,6-diamidino-2-phenylindole
DDR	DNA Damage Repair
Dkk	Dickkopf Family
DMEM	Dulbecco's Modified Eagle Medium
DMSO	Dimethyl Sulfoxide
DNA	Deoxyribonucleic acid
dH2O	Distilled Water
dsRNA	Double stranded RNA
DSB	Double-strand breaks
Drosha	Double-stranded RNA-specific ribonuclease (RNase) III
Dvl	Dishevelled
ECIS	Cell-substrate impedance sensing
ECM	Extracellular matrix
EDTA	Ethylenediaminetetraacetic acid
eGFP	Enhanced Green Fluorescent Protein
EMT	Epithelial Mesenchymal Transition
FAP	Familial Adenomatous Polyposis
FBXW7	F-box and WD repeat domain-containing protein 7
FLYWCH1	FLYWCH-type zinc finger 1
Fz	Frizzled
GFP	Green Fluorescent Protein
gRNA	Guide RNA
GSK-3β	Glycogen Synthase Kinase 3 beta
GST	Glutathione SH-Transferase
H2AX	Histone H2A variant
HDAC	Histone Deacetylases

HPA	Human Protein Atlas
HP1a	Heterochromatin protein 1 isoform a
HP1BP3	Heterochromatin protein 1 binding protein 3
HR	Homologous recombination
ICAT	Inhibitor of β-catenin and TCF4
IF	Immunofluorescence
IHC	Immunohistochemistry
ISC	Intestinal Stem Cell
ISH	In situ hybridization
JNK	Jun N-terminal Kinase
Kb	Kilo base
KDa	Kilo Dalton
KLF6	Kruppel-like factor 6
KO	Knockout
LB	Luria Broth
LEF	Lymphoid Enhancer Factors
Lgr5	Leucine-rich Repeat-containing G-protein Coupled Receptor
LRC	Label-retaining Cells
LRIG1	Leucine-rich repeats and immunoglobulin-like domains protein 1
LRP	Lipoprotein Receptor-related Protein
MAPK	Mitogen- activated protein kinases
MET	Mesenchymal Epithelial Transition
MMR	Mismatch repair
MSI	Microsatellite Instability
MSS	Microsatellite Stability
NER	Nucleotide excision repair
NES	Nuclear export
NHEJ	Non-homologous end-joining
NLS	Nuclear localisation signals
PAM	Protospacer adjacent motif
PBS	Phosphate Buffered Saline
PCR	Polymerase Chain Reaction
PDO	Patients derived organoids
PEI	Polyethyenimine
PFA	Paraformaldehyde
PI3K	Phosphoinositide-3-kinase
PTM	Post-translational modifications
PVDF	Polyvinylidene difluoride
PYG	Pygopus
qPCR	Quantitative PCR
RHOA	Ras homolog gene family, member A
RNA	Ribonucleic Acid
ROS	Reactive Oxygen Species
Ror1/2	Tyrosine protein kinase transmembrane receptor 1 or 2
Rpm	Round per minutes
RPMI	Roswell Park Memorial Institute
RSPO3	R-spondin 3
RT	Room Temperature
Ryk	Receptor tyrosine kinase
SCF	SKP1–Cullin–F-box

SD	Standard Deviation
SDS-PAGE	Sodium Dodecyl Sulphate-Polyacrylamide Gel Electrophoresis
SFRPs	Secreted frizzled-related proteins
SMAD4	Mothers against decapentaplegic homolog 4
SNP	Single Nucleotide Polymorphism
Sox9	SRY-box containing gene 9
SR	Serine/arginine-rich
TAs	Transit-amplifying cells
TAE	Tris-acetate-EDTA
TBL1-TBLR1	Transducin β-like proteins
TBS-T	Tris buffer saline-Tween-20
TCF	T-cell Factor
TCGA	The Cancer Genome Atlas
TGFβR2	Transforming Growth Factor Beta Receptor 2
TF	Transcription factor
TIC	Tumour-initiating cells
TME	Tumour microenvironment
TNM	Tumour-node-metastasis
UV	Ultraviolet
WT	Wild Type
ZEB1	Zinc finger E-box-Binding Homeobox 1
ZFPs	Zinc Finger Protein

List of figures

List of tables

CHAPTER 1

General Introduction

1.1 A Brief Introduction to Colorectal Cancer

Colorectal cancer (CRC) is the fourth most diagnosed cancer and the third most deadly cancer in the world (1, 2). It is anticipated for over 1.93 million new cases and almost 935,173 deaths in 2021, according to the World Health Organization GLOBOCAN database (1, 3). According to Cancer Research UK (2017), around 42,317 people are diagnosed with bowel cancer in the UK each year, accounting for 10% of all cancer deaths. Both hereditary and environmental risk factors are important drivers in CRC development. Around 70% of all cases develop sporadic CRC, with no family history or genetic predisposition, mainly caused by different somatic mutations (4). In comparison, the hereditary colorectal cancer syndromes represent 25% of cases and can be sub-divided as non-polyposis (i.e. mainly Lynch syndrome) and familial polyposis adenomatous (FAP) (5-7). Other forms of hereditary CRC entail rare genetic syndromes named Hamartomatous Polyposis Syndromes (HPS) (<1%), and result from less penetrant inherited mutations (8). Similar to other forms of cancer, the risk of developing CRC depends on many other factors, among which, the intrinsic factors include age, genetics, diabetes mellitus, stomach ulcer or inflammatory bowel disease, whereas, the extrinsic factors include some potentially avoidable lifestyle factors such as smoking, alcohol intake, high-fat diets and lack of physical exercise (9). Fortunately, in recent years, overall survival has increased due to significant improvements in surgery, treatment strategies, early diagnosis, and more importantly, advancement in our current understanding of the molecular basis of CRC.

1.2 The Multi-Step progression of CRC

CRC is a heterogeneous disease, and the underlying causes of CRC are complex. To date, CRC is considered the prime example of multi-step carcinogenesis (6), where several genetic and epigenetic changes accumulate sequentially over time to drive CRC through a multi-step process known as the adenoma-carcinoma sequence (10). This process can be described as a series of histopathologic events associated with distinct molecular alterations that accumulate over the years, to form tumour (Figure 1-1) (11).

In general, multi-step cancer development starts with the gradual formation of benign adenomas or so-called adenomatous polyps which accumulate within the lining of the intestinal mucosa, causing an initial genetic change (9). Later, the balance at the innermost lining of the mucosa in the small intestine is progressively interrupted. This interruption promotes the acquisition of more mutations in multiple genes including tumour suppressor genes/oncogenes, DNA stability genes, as well as several critical genes associated with cell proliferation and apoptosis (12). This ultimately results in the inactivation of these genes and gradual tumour formation. In CRC, this process takes place over a long period of about 10–15 years (9).

In 1990, Fearon and Vogelstein (13) presented the concept for a multi-step genetic model for CRC development. This model is based on understanding the key genetic alterations in CRC (13, 14). Later, researchers further explored the importance of the timing of these mutations in tumour progression. It was found that, for example, *KRAS* and p53 mutations can co-exist within a tumour (15). Also, it is generally believed that the severity of intestinal cancer highly depends on the

initiation mutations (16). Therefore, increasing our understanding of the initiating mutation drivers and early events of CRC development is essential for resolving the complexity of colorectal tumorigenesis.

Amongst several genetic and epigenetic defects, disruption of the adenomatosis polyposis coli (APC) gene was proposed as the key driver for adenoma initiation, at the early stage of CRC initiation (17, 18). It triggers the stabilisation of β-catenin and leads to constitutive active transcription by the β-catenin/TCF complex (19). Consequently, this drives the expansion and transformation of the stem cell compartment and later the development of adenomatous polyps (20). Several studies have confirmed the crucial role of APC in CRC (21-23), revealing the significance of Wnt (wingless-related integration site)/β-catenin signaling in the initiation and progression of CRC.

During tumorigenesis, additional mutations can be acquired in other oncogenes and tumour suppressors (24). The most frequently mutated genes after *APC* (70%) are: tumour suppressor protein (p53, 50%), Kirsten rat sarcoma viral oncogene homolog (*KRAS*, 40%) and mothers against decapentaplegic homolog 4 (*SMAD4*, 25%). Additional but less frequently mutated genes include: TGF-β receptor 2 (*TGFBR2*), F-box and WD repeat domain-containing protein 7 (*FBXW7*) and phosphatidylinositol-4,5-biphosphate 3-kinase catalytic subunit alpha (*PIK3CA*) (6, 25, 26). Overall, the early events in the transition from normal colonic epithelium to adenoma are mainly driven by mutations of *APC*, *KRAS* and *BRAF*. In contrast, the late-stage is mostly driven by mutations of *PIK3CA*, *SMAD4* and p53, which eventually generate a malignant tumour that has potential for invasion (17).

Chapter 1: General Introduction

The progression from adenoma to carcinoma can arise from one or a combination of three different mechanisms/major pathways, namely: the chromosomal instability pathway (CIN), the MSI pathway (MSI) and the CpG island methylator phenotype (CIMP) pathway (10, 27). Each of them features different genetic, epigenetic and molecular events. Occasionally, these pathways can be correlated, and one pathway can occur as a result of another (28).

Among these pathways, the CIN pathway represents most sporadic CRCs (80–85%) (6, 28). It is mainly driven by inactivating mutations in tumour-suppression genes, such as the adenomatous polyposis coli (*APC*) gene, together with activating mutations in proto-oncogenes, such as the Kirsten rat sarcoma viral oncogene homolog *(KRAS)* gene (Figure 1-1). Also, it has been considered the model pathway for an adenoma-carcinoma sequence (29). On the other hand, the CIMP pathway refers to the widespread hypermethylation of CpG at several loci and is mainly characterized by promoter hypermethylation of various tumour-suppressor genes, most importantly the DNA repair genes O^6-methylguanine-DNA methyltransferase (*MGMT*) and mutator L homologue 1 (*MLH1*) (30). This hypermethylation is often associated with *BRAF* mutation and MSI. Finally, the MSI pathway is a hallmark condition in familial Lynch syndrome (LS) (which appears in ~15% of sporadic CRC cases), and is mainly caused by inactivation of the DNA mismatch repair genes such as h*MLH1*, h*MSH2*, h*MSH6* and h*PMS2* (4). Indeed, CIN, MSI and CIMP often overlap in molecular tumour subtypes, which have considerable prognostic implications (28).
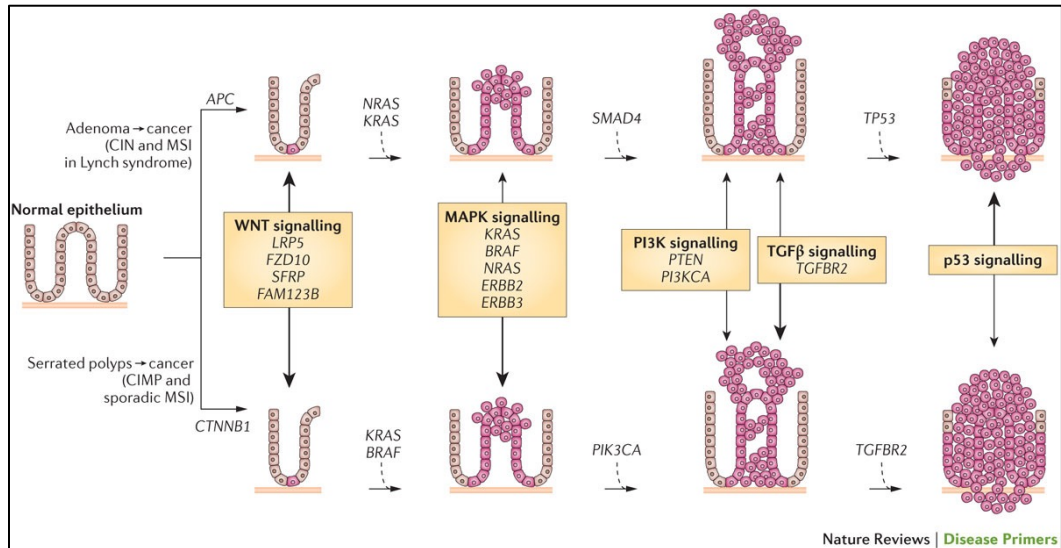
Figure 1-1 The multi-stage development and progression of CRC. The top panel shows the traditional or classic model of adenoma-carcinoma sequence and chromosomal instability (CIN) in CRC. The bottom panel demonstrates an alternate pathway involves serrated polyps and their progression to serrated colorectal cancer. Reprinted from (9).

1.3 Classification of CRC

CRC diagnosis and prognostic stratification are based on histopathologic assessments of cell or nuclear pleomorphism, aberrant mitotic figures, altered glandular architecture and other phenomics abnormalities (31). Classically, tumour-node-metastasis (TNM) classification is the well-established cancer staging system and is an important determinant in judging the prognosis and guiding treatment of CRC. It is a widely used worldwide system that assigns to each cancer a stage of disease by evaluating the size and extension of the primary tumour (T), regional lymph node involvement (N) and the presence of metastasis (M) (32, 33). However, CRC is very heterogeneous at the molecular level, and each subtype or group of patients displays distinct pathological and genetic signatures. This heterogeneity represents a major challenge to the precise interpretation of

prognostic and predictive markers. It also confers primary or secondary resistance to targeted treatments. Therefore, molecular classification of CRC or gene expression-based subtyping is being increasingly accepted as a relevant source of disease stratification (5). Several molecular classifications have been established to provide better understanding and better therapies. These classifications are mainly based on tumour fate, genetic features, cellular specifications, tumour microenvironment (TME), and more recently, immunological characteristics. However, despite the several classification methods available for CRC, there is no gold-standard method that can resolve inconsistencies in data processing and algorithms applied to diverse patient cohorts, studies' inclusion and exclusion criteria, and sample preparation methods. Recently, CRC consensus molecular subtypes (CMS) classification system has gained great attention since being published by Guinney et al. in 2015 (34).

1.3.1 CMS classification

The CRC Subtyping Consortium (CRCSC) has recently unified six independent molecular classification systems, based on gene expression data, into a single consensus system, known as the CMS (35). Using gene expression data from six different cohorts, CMS is mainly divided into four subtypes of CRC, from CMS1 to CMS4. Each subtype has a characteristic molecular biological background. Briefly, CMS1 is defined by upregulation of immune genes and is highly associated with microsatellite instability (MSI-h) (MSI immune, 14%). CMS2 reflects the canonical pathway of carcinogenesis as defined by the adenoma-carcinoma sequence (canonical, 37%). CMS3 is defined by metabolic dysregulation, with higher activity

in glutaminolysis and lipidogenesis (metabolic, 13%). Finally, CMS4 (mesenchymal, 23%) is defined by an activated transforming growth factor (TGF) beta pathway and by epithelial-mesenchymal transition (EMT), making it, in general, more invasive and chemoresistant (36-38). Overall, CMS classification offers more profound insights into the biology of CRC and may better inform clinicians of prognosis, therapeutic response, and potential novel therapeutic strategies (36, 39).

Even though CMS represents the current best description of heterogeneity at the gene expression level, to date it has had no impact on clinical decision-making process (35). Dedicated efforts are currently ongoing to improve the CMS and make it more clinically applicable.

1.4 The CRC cell of origin

The development and identification of intestinal stem cell (ISC) expression markers have enabled the researcher to test the hypothesis of the cell of origin for intestinal cancer, or the so-called the monoclonal origin of cancer (i.e., CRC originates from the clonal expansion of one hyperproliferating cell). However, there is still an ongoing debate over the cell of origin of CRC. First, in 2001, Shin et al. (40) suggested the top-down model of adenoma morphogenesis, which refers to tumour initiation that begins at the top of the crypt and then spreads laterally and downward, displacing the normal crypt epithelium (41). This model was evidenced by the several spontaneous adenomas found at the top of colonic crypts without any contact with the stem cell compartment (42). It was also

thought to be representative of patients with FAP. Later, Preston et al. (43), suggested the bottom-up model, when it was shown that *Lgr5+* or *Bmi1+* stem cells could act like the cells of origin of intestinal cancer in mice (43-45). This model was defined by the division of the crypt at the base, also named crypt fission. Several lines of evidence indicated that crypt fission is the primary mode of adenoma progression in FAP (46), as well as in sporadic adenomas (47).

Moreover, several studies have pointed out that ISCs are the primary cells of origin of CRC, wherein mutation in ISCs causes tumour initiation in genetically modified mice. For example: it was reported that the specific deletion of *APC* in ISCs expressing markers such as Lgr5, LRIG1 or CD133 could induce rapid adenoma generation (44, 48). Likewise, cancer initiating mutations in key signaling pathways, such as the Wnt, Notch and Hedgehog pathways, can enable the wild-type ISCs to escape from the control of regulatory signals and lead to precursor lesions development (49, 50). Few other reports have demonstrated non-stem cell-based CRC origin model, suggesting the role of differentiated cells in serving as the cell of origin for cancer (51). These studies also indicated the significance of environmental factors combined with genetic events in advancing the development of CRC. For example, the loss of *APC* in tuft cells accompanied by microenvironmental disturbances was found to induce colonic tumours (52). It is noteworthy, however, that many direct evidence for the preferential cell of origin in CRC development were obtained via mouse models. This enabled the induction and tracking of transformation events specifically in either stem cells or in more differentiated cells. Nevertheless, further aspects must be considered when describing the origin of CRC in humans. First, most of the adenoma formation

modelled by mouse genetic models occurs in the small intestine, while human malignancies appear mainly in the colon. Second, the progression from adenoma to full carcinomas is sporadic in CRC genetic mouse models (53, 54). Finally, the significant contribution of environmental factors such as chronic inflammatory conditions is not usually present in genetically modified mice (55, 56). Overall, CRC is a prolonged disease that takes over a decade to develop and progress, yet the presence of underlying conditions and environmental factors (such as carcinogen exposure and intestinal inflammation) confers a functional advantage for tumour development and progression.

To date, intestinal and colorectal cancer is increasingly being recognised as a disease maintained by mutations and disruption of the major signaling pathways responsible for tissue homeostasis. Thus, understanding the mechanisms that regulate normal ISCs and homeostasis is fundamental to gain insights into the biology of their malignant counterparts.

1.5 The Dynamics of ISCs

The human intestinal epithelium is one of the most rapidly regenerating tissues in our body; approximately all intestinal epithelium cells are replaced every week in the human colon (57). This incredible epithelial turnover rate is mainly mediated by a dynamic pool of stem cells in the intestine (58). The single epithelial layer of the small intestine is made up of stem cells, transit-amplifying cells (TAs) and terminally differentiated cells that vary in their location, function, and regulation (59, 60). Together, they all form a multi-layered structure which brings out a uniquely dynamic environment to maintain intestinal homeostasis (61, 62). As

demonstrated in Figure 1-2, the histological architecture of the small intestinal epithelium is divided into two main parts: crypts and villi (63). The crypt area is the main proliferative compartment that disseminates the multipotent stem cells (58). In contrast, the villus is a polyclonal compartment made up of several differentiated cells such as goblet cells, enteroendocrine cells and enterocytes (59). In a healthy intestine, the undifferentiated epithelial or transit cells at the bottom of crypts sequentially duplicate to give rise to progeny cells which migrate throughout the crypt–villus axis to produce specific cell lineage precursors. The latter can be either absorptive precursors (which give rise to enterocytes) or secretory precursors. Each can further subdivide into distinct mature differentiated cells while moving toward the tip of the villus (64). This upwards movement of intestinal progenitor and differentiated cells is mainly powered by ISCs [11].
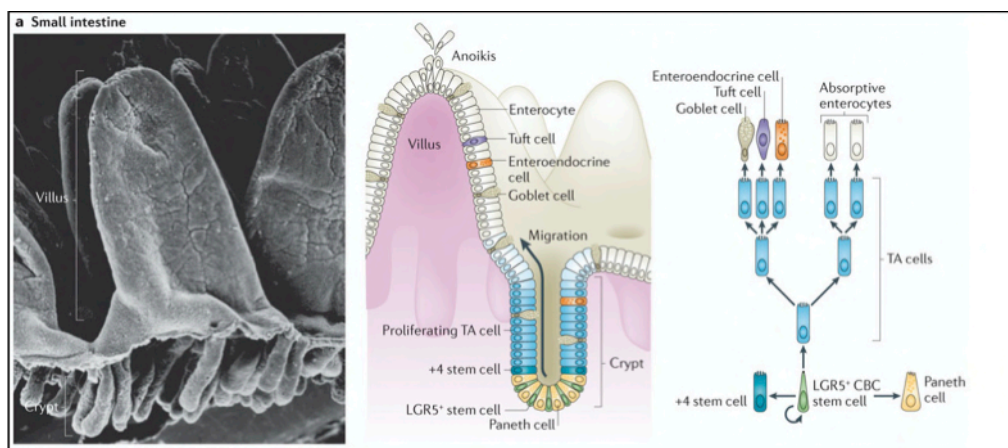
Figure 1-2 The structural organization of small intestine, showing the dynamics of ISCs and the mechanism of epithelial self-renewal. Adapted from (63).

Due to the high renewal ability, the ISC compartment is susceptible to cytotoxic injury. Once the damage occurs, ISCs undergo apoptosis, and under the influence of niche signals, the progenitor cells gain ISC activity to replace the lost ISCs.

Recent studies suggested that two types of regenerative cells can fill the loss of Lgr5+ cells in the damaged epithelium. This can be either driven by the downward de-differentiation of Lgr5+-derived reserve stem cells (65), or by the de-differentiation of +4 cell position-derived cells that migrate down from the TA zone to regenerate the stem cell niche (66, 67). More recently, however, Murata and colleagues indicated that +4 positioned cells do not migrate to the site of injury to rescue their damaged counterparts (68). It was, therefore, suggested that the damaged epithelium is replaced mainly by Ascl2-dependent de-differentiation of recent Lgr5+ progeny, with less contribution from the ''reserve'' stem cells (or older crypt cells) (68). Yet, this was challenged by Tan et al. 2021, indicating that a constant pool of Lgr5+ ISCs, regardless of their origin, is crucial for maintaining intestinal homeostasis (69). While studies indicate that Lgr5+ cells can act as regenerative stem cells, it remains controversial whether Lgr5+ cells in the newly generated crypts are directly derived from Lgr5+ cells of adjacent crypts (due to preservation of a small population of cells) (70), or de-differentiation of their primed progeny cells (71, 72). The molecular basis of cellular plasticity in intestinal homeostasis and disease is still ambiguous.

Moreover, many evidence from both genetic lineage tracing and single-cell transcriptional analysis showed that Paneth cells and enterocyte precursor cells can act as stem cell reservoirs under the depletion of Lgr5+ stem cells or the so-called Crypt Base Columnar cells (CBCs) (61, 73). Hence, various types of crypt

cells, including differentiated cells, can be considered as potential stem cell sources, particularly following injury, or tissue damage. This remarkable plasticity of the intestinal epithelium has changed the view and definition of the ISC population. It was thought that ISCs are restricted to the actively proliferating ISC CBCs (ISC, Lgr5+), and the quiescent cells, also known as label-retaining cells (LRCs) (45, 74). Now, it is widely accepted that ISCs can be distinct populations and/or sub-populations of stem-like cells that are located at different parts of the intestine (75).

Accordingly, the ISC population cannot be a static entity and is not limited to those cells at the bottom of crypt (75, 76). The ISC pool can be defined as a niche of several populations working in synchrony. Each population sustains a unique functional role in this niche yet having the ability to replace one another. Importantly, the complexity of the intestinal niche and the fast turnover of its lining epithelium increases the potential of mutation acquisition and expansion, leading to higher susceptibility to developing oncogenic mutations, as discussed below.

1.5.1 ISC Mutations, Clonal Expansion and Vulnerability to Disease

Although somatic mutation is a normal event that can affect any cell based on exposure to environmental agents, the difference is in the outcome of this mutation and the expansion of the mutated cells. In healthy crypts, stem cells continuously replace each other in a random fashion (77). Once the stem cells acquire a mutation, stochastic differentiation usually eliminates many mutant clones and expands the normal ones to restore the normal balance (78). Accordingly, there is an equal competition for clonal expansion between neutral

mutated stem cells and unmutated stem cells. However, evidences from clonal analysis and lineage tracing studies show that some cancer- or disease-driving mutations have the potential to expand over the normal ones to initiate illness (Figure 1-3) (79). For example, cells with mutations such as in *APC* have more ability to expand over the wild-type (WT) cells (80). Also, they have substantial ability to colonize the whole crypt, resulting in a higher probability of developing cancer, particularly with the acquisition of additional mutations over time (79).
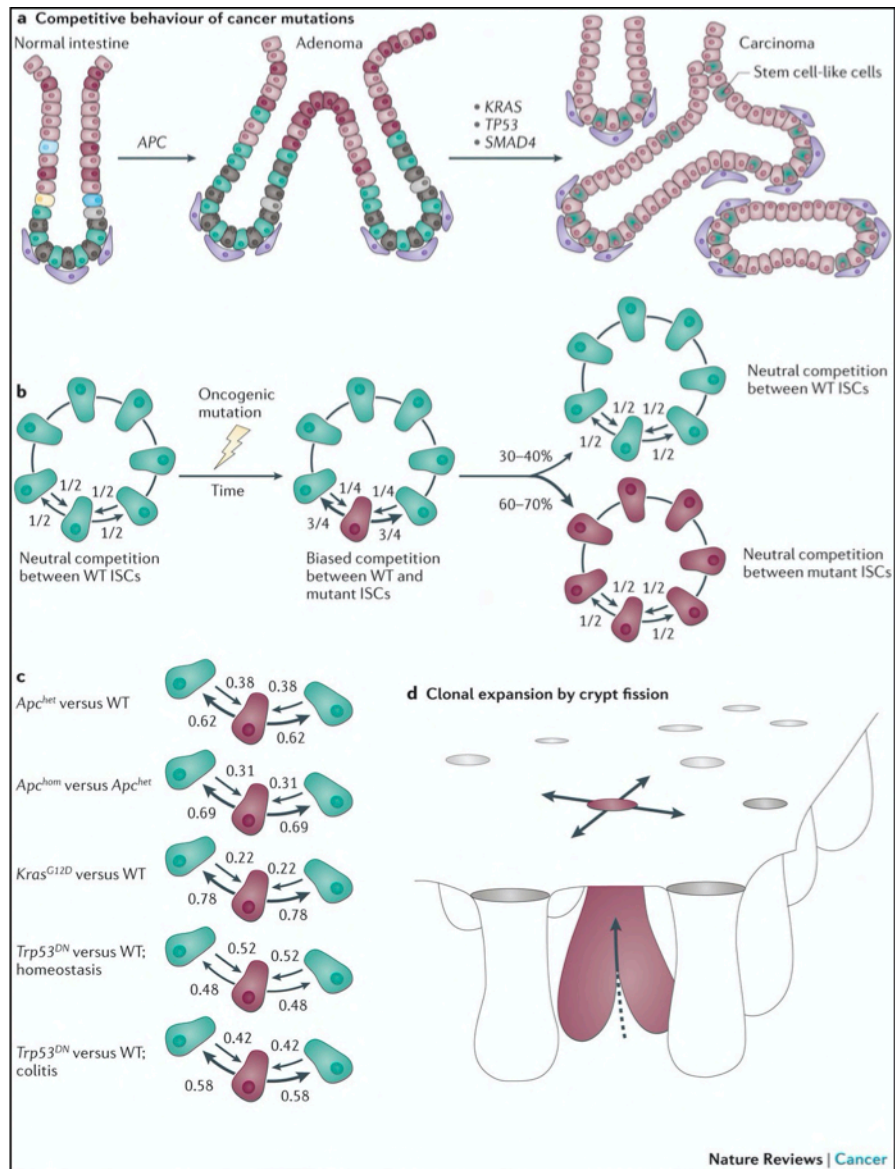
Figure 1-3 Schematic representation of the competitive fitness of intestinal stem cells, and clonal expansion under oncogenic mutations. A) Schematic representation of the adenoma–carcinoma sequence**. B)** The competitive fitness of intestinal stem cells (ISCs) with respect to their wild-type (WT) neighbours. The diagram indicates a higher chance that a mutant ISC will displace a WT-neighbouring ISC (clonal expansion). However, there is still a chance that ISCs with an advantageous mutation will be displaced from the niche and become extinct. Between ISCs containing the same mutation, replacement events are neutral again**. C)** Diagram highlights the context-dependent nature, and the relative competitive advantage for different cancer mutations, such as in the case of Trp53 mutations in homeostasis versus colitis. **D)** Crypt fission is the likely mechanism by which mutant cells expand through the crypt's epithelium. Reprinted from (75).

Of note, the competition between normal and mutated stem cells in the crypt is strongly influenced by genetic and environmental factors, as well as niche factors (80). For example: under inflammation, *P53* mutated clones tend to prevail over WT stem cells in an inflamed intestine, but not in healthy conditions (Figure 1-3 C). Furthermore, reports have shown that the degree of stem cell clonal advantage is highly affected by the ISC microenvironment. Dysregulation in the ISC niche plays a key role in triggering these mutations and driving CRC (51).

Nowadays, the ISC niche has become an attractive target for cancer researchers, and many studies have focused on the regulatory pathways and how they direct the behaviour of stem cells in health condition versus disease. The next subsection will briefly introduce some critical mediators of the ISC microenvironment (or the ISC niche) and their role in maintaining the stem cell pool and intestinal homeostasis.

1.5.2 The ISC Niche: Key Signaling Pathways

In the niche, the maintenance of stem cells is mainly governed by four main signaling pathways: Wnt, Notch, Hedgehog and BMP signaling pathways. These pathways are the most studied pathways for their roles in early intestinal development and homeostasis (81-84). The Wnt pathway is involved in cellular commitment or the fate determination of intestinal lineages (secretory versus absorptive) (85, 86), in addition to its role in the positioning and maturation of Paneth cells (87). Likewise, the Notch pathway is crucial for developmental patterning and stem cell differentiation (88). The BMP cascade is mainly known for inducing cellular differentiation (86, 89), and the Hedgehog pathway is

responsible for mesenchymal–epithelial interactions (90). Intriguingly, under stress signals, the niche tunes the ratio between these pathways to restore and maintain the balance. For example, in the case of ISC over-proliferation, several cellular and acellular interactions within the niche reduce the level of Wnt signaling and keep it below the threshold (91, 92). Similarly, the activity and cross-talks of the BMP and Hedgehog signaling cascades contribute significantly to fine-tuning the output of the Wnt pathway to prevent ISC over-proliferation (93, 94). Therefore, any dysregulation or mutations of these key molecular pathways have the potential to drive disease, including cancer.

In cancer, a specific compartment of tumour cells similar to normal stem cells known as CSCs was identified more than 10 years ago and represent a subset of the tumour population that has the extraordinary ability of self-renewal and can induce hierarchical differentiation (95). The following section will discuss CSCs and the importance of the TME in promoting cancer initiation and progression, contributing to therapy resistance, recurrence, and metastasis.

1.5.3 CSCs and the TME

Cancer stem-like cells CSCs, also called tumour-initiating cells (TICs), have been studied intensively due to their rapid proliferation, migration, and role in the recurrence of cancer (95-97). According to the CSC hypothesis, only CSCs have the capacity to generate primary tumour, recurrence, and metastasis (98, 99). However, interestingly, CSCs themselves do not exist as a static population. Several reports have suggested the interconversion between CSCs and non-CSCs

through self-differentiation and dedifferentiation (100). For example, the overexpression of a few stemness-related transcriptional factors was reported as a mediator for transforming non-CSCs into CSCs in both glioblastoma and colon cancer (101, 102). Moreover, increasing evidences demonstrate the critical role of the TME in regulating CSCs and their contribution in tumour progression (103). CSCs not only reside in their niches, but also actively crosstalk with different elements therein. Therefore, CSCs are strongly regulated by their microenvironment, giving rise to a heterogeneous population with discrepant dependencies and a wide variety of resistance mechanisms (104). Correspondingly, the TME is a key driver of the heterogeneity, plasticity and evolution within the CSC population. The TME is composed of diverse cellular (such as mesenchymal stem cells, endothelial cells, fibroblasts or immune cells) (105) and non-cellular components, defined as an extracellular matrix (ECM). This is constituted of macromolecules such as collagens, glycoproteins, proteoglycans, and integrins (96, 106). Studies have shown that ECM molecules can regulate CSC activities by modulating both cell-cell signaling and immune surveillance (104).

The bidirectional cross-talk between TME and CSCs is a fundamental and crucial component of tumour growth and evolution, maintenance of stemness, and therapeutic resistance (97, 107). Several pathways are implicated in maintaining a stem-supportive microenvironment in cancer development, such as the Wnt, Notch, TGF-β and Hedgehog signaling pathways (108). Amongst these pathways, Wnt signaling plays an indispensable role in promoting the maintenance of CSCs (109, 110). Given the significance of the Wnt signaling pathway in intestinal health

and disease, the next sections will be focused on the Wnt signaling pathway and its role in ISCs regulation and CRC initiation and progression.

1.6 The Wnt Signaling Pathway

Wnt was named after the discovery of the *Drosophila* wingless (*Wg*) gene and the mouse *Int1* (mouse mammary tumour virus integration site 1) gene. In 1982, the first *WNT* gene, known as *Int1*, was discovered as a gene overexpressed in breast cancer (111). Later, it turned out that *Int1* is highly conserved across multiple species and is particularly similar to *Wg*, a gene involved in wing development and segmentation of the body axis during flight development (112). Hence, the name WNT comes from a fusion of Wg and iNT (113). Decades later, the Wnt pathway is recognised as an evolutionarily conserved signal transduction pathway and has been broadly implicated in a wide range of cellular functions during embryonic development and adulthood, including adult tissue homeostasis and regeneration (112).

1.6.1 Canonical and Non-Canonical Wnt Signaling Pathways

Once extracellular ligand-receptor bindings initiate the pathway, the intracellular transduction of Wnt signals can be divided into either β-catenin-dependent (canonical) or β-catenin-independent (non-canonical) signalling routes (114, 115). The canonical Wnt pathway is the most characterized and relies on β-catenin as its main effector protein. In the absence of Wnt stimulus, the cytoplasmic β-catenin is tightly associated with a multimeric destruction complex composed of the tumour suppressors AXIN1, APC, the kinases casein kinase 1 (CK1) and

glycogen synthase kinase 3β (GSK3β). This protein complex captures and regulates the N-terminus domain of β-catenin by several phosphorylation events mediated mainly by GSK-3β and CKIb. The phosphorylated domain is then recognised by β-TrCP, a component of SKP1-Cullin-F-box (SCF) ubiquitin ligase, which in turn marks β-catenin for degradation by 26S proteasome machinery (Figure 1-4). However, when a specific secreted glycoprotein or Wnt ligand is bound to its corresponding Frizzled receptor (ON-state, right panel), they form a heterodimeric complex by further binding to co-receptors such as LGR5/6. Subsequently, this complex interacts with and activates a family of transmembrane receptors called Dishevelled transmembrane receptor by phosphorylation events. The activation of this protein triggers the displacement of the destruction complex from β-catenin and accumulates it in the cytoplasm. The stabilised β-catenin is then translocated into the nucleus via trafficking factors such as Rac1, where it binds to a family of transcription factors (TFs) known as TCF/lymphoid enhancer (LEF) TFs (116). Finally, after the displacement of transcriptional inhibitors such as Groucho from the DNA, the nuclear localisation of β-catenin and its association with the TCF/LEF complex activates the transcription of Wnt target genes such as c-Myc, Axin2, Cyclin D1 and Lgr5 (114, 117, 118).
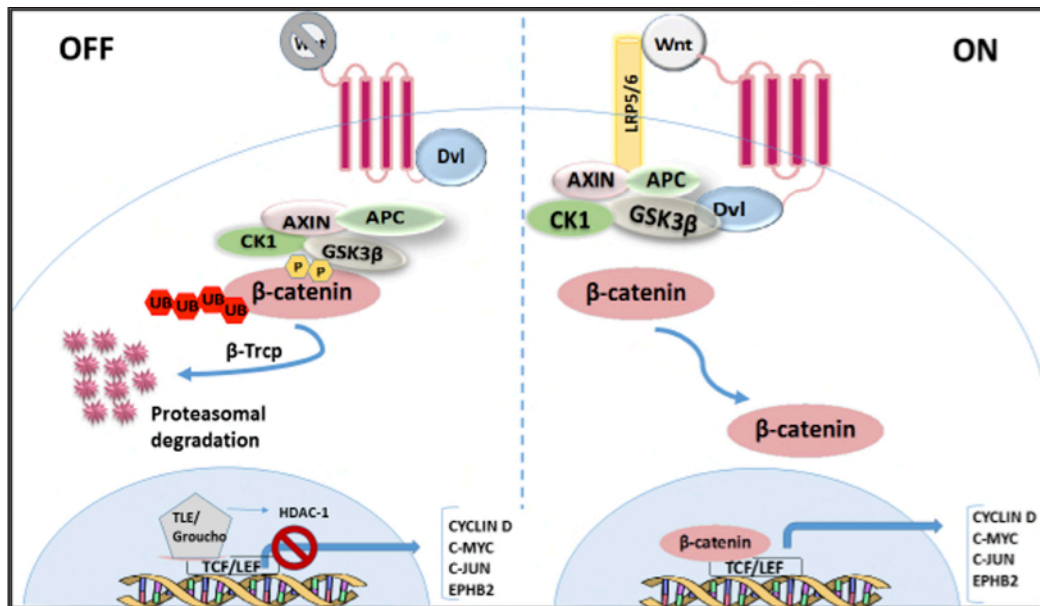
Figure 1-4 Wnt/β-catenin signaling pathway. The left panel shows the OFF-state of Wnt pathway. In the absence of Wnt stimulus, the destruction complex composed of (APC-AXIN1-GSK-3β-CK1) tightly regulates the cytoplasmic β-catenin by phosphorylation events, rendering it for proteasome-mediated degradation. The absence of nuclear β-catenin enables transcriptional repressors such as a transducing-like enhancer protein (TLE/Groucho) to bind and interact with TCF/LEF complex and recruits HDACs to repress the transcription of target genes. The right panel shows the activated state of Wnt pathway (ON-state). Upon binding of Wnt to its corresponding Fzd receptor and Lpr5/6 co-receptor, a transmembrane receptor called Disheveled (Dvl) protein is recruited to form a complex with Frz-Lpr5/6, leading to Axin downregulation, GSK-3β inactivation and β-catenin stabilisation. Consequently, β-catenin will be stabilised in the cytoplasm and then shuffled into the nucleus, where it forms a complex with TCF/LEF family and recruits co-activators to regulate gene transcription.

However, several negative feedback regulators act to prevent excessive signaling and tune the WNT-induced responses. For example, AXIN2, an Axin paralog exhibiting similar domain architecture (a.k.a., Conductin) downregulates β-catenin-mediated transcription by facilitating the formation of new destruction complexes (119, 120). Likewise, Ring Finger Protein 43 (RNF43) and Zinc and Ring Finger Protein 3 (ZNRF3) help to attenuate WNT-signaling, by inducing the ubiquitylation and subsequent lysosomal degradation of FZD receptor proteins

(121, 122). Furthermore, it was recently reported that RNF43 enables the restoration of destruction complex activity, to prevent β-catenin-mediated transcription, via a mechanism that involves CK1α- phosphorylation of the cytosolic tail of truncated RNF43 (123). Nonetheless, the secreted proteins of the R-spondin (RSPO) family, can act to counterbalance the activity of the Wnt negative regulators and thereby potentiating WNT signalling (124, 125). Predominantly, in stem cells, R-spondins form a complex with Leucine-rich repeat-containing G-protein-coupled receptor 4/5 (Lgr4/5) to promote the membrane clearance of RNF43/ZNRF3, facilitate Wnt receptor stabilization, and thereby increase Wnt responsiveness of stem cell populations (126-128).

On the other hand, the hallmark of the non-canonical signaling pathway is its β-catenin-independent actions. Principally, this signaling is initiated by binding several Wnt or Frizzled proteins with other co-receptors which contain a cysteine (Cys)-rich binding domain. An example is a receptor tyrosine kinase (Ryk) or tyrosine protein kinase transmembrane receptor 1 or 2 (Ror1/2), which drives a specific downstream effect by the given Wnt ligand (129-131). Mostly, noncanonical Wnt signaling encompasses: Wnt–PCP (planar cell polarity) signaling (132, 133), Wnt–cGMP–Ca^{2+} signaling (134), Wnt–ROR2 signaling (135), Wnt–PKA signaling, Wnt–GSK3–microtubule (MT) signaling (130), Wnt–aPKC signaling (136), Wnt–RYK signaling and Wnt–mTOR signaling (137). In many cases, these categories are poorly defined or less characterized. Also, it is likely these pathways highly overlap with one another. Beyond that, increasing evidence suggests an

overlap between non-canonical Wnt signaling with other signaling pathways, including Hippo-YAP/TAZ signaling (138, 139).

The best-characterized β-catenin-independent pathway (non-canonical) is the planar cell polarity (PCP) pathway (140). As shown in Figure 1-5, a cascade of downstream effectors containing the small GTPases RAC1, and Ras homolog gene family member A (RHOA), and c-Jun N-terminal kinase (JNK), is activated via Fzr receptors to control rearrangements in the cytoskeleton and gene expression (130, 141). The PCP pathway controls cell polarity in morphogenetic processes in vertebrates, such as gastrulation and neural tube closure (140). Furthermore, another important but less understood subdivision of the noncanonical Wnt pathway is the Wnt/Ca^{2+} signaling pathway (Figure 1-5, right panel). It is stimulated via G proteins, causing the induction and activation of phospholipase C (PLC), as well as the movement of intracellular Ca^{2+}. Subsequently, this leads to the activation of several Ca^{2+}-dependent effectors, including calcium/calmodulin-mediated kinase II (CAMKII), protein kinase C (PKC) and calcineurin (142). The PLC pathway is mainly involved in cancer, inflammation, and neurodegeneration, via regulating the transcription of genes associated with cell fate and cell migration (142, 143).
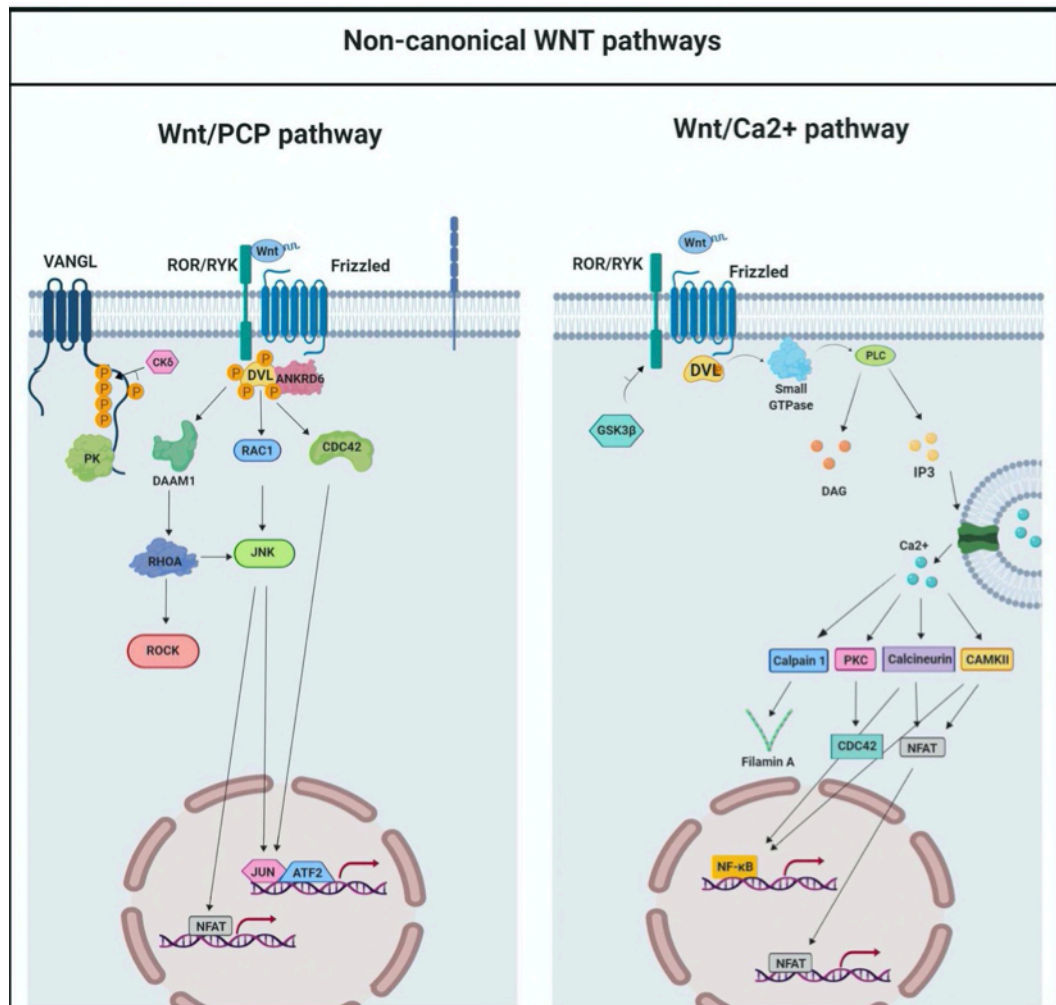
Figure 1-5 Overview of non-canonical Wnt signaling. Diagram showing the signal transduction pathway of Wnt-PCP (Left panel) and Wnt-Ca2+ signaling (Right panel). Adapted from (144).

However, the best-studied and most critical Wnt pathway is the canonical Wnt/β-catenin pathway, which functions by regulating the amount of the transcriptional co-activator β-catenin to control essential developmental gene expression programs. The following sections will be focused on the significance of the canonical Wnt/β-catenin pathway in intestinal health and CRC development.

1.7 The Significant Role of Wnt/β-catenin Signaling in Intestinal Health and Disease

Among the numerous signaling pathways in the ISC niche, Wnt/β-catenin signaling is the most crucial pathway in the intestinal homeostasis, morphogenesis and regulation of stem cells (145). It plays critical roles in several aspects of ISC health, including maintaining stemness activity and inhibition of differentiation via cell cycle (86, 92). It also controls the migration of cells through the crypt-villus axis and is essential for directing the terminal differentiation of Paneth cells and early secretory lineage (87, 146).

Typically, the crypt base cells of the small intestine exhibit the most potent Wnt signaling, represented by the highest nuclear levels of β-catenin, which is gradually decreased to reach the minimum at the luminal side of the crypt-villus axis (86). Nonetheless, the level of Wnt signaling in both compartments needs to be kept within the physiological range to maintain homeostasis and prevent disease development (147). Any aberrant activity of Wnt/β-catenin signaling can lead to lethal outcomes. Reports have shown that external activation of the Wnt pathway, e.g. by injecting Wnt agonists, can significantly induce stemness activity by increasing the number of Lgr5+ cells in the intestine (148). Likewise, several studies have emphasized the critical role of the canonical Wnt pathway in intestinal self-renewal and development (92, 149). For example, studies showed that neonatal mice lacking murine intestinal *Tcf7l2* (transcription factor 7-like 2, a.k.a., *Tcf4*) proliferative crypts do not develop (150-152). *Tcf7l2* plays significance roles in intestinal tissue homeostasis (153, 154). However, the role of *TCF7L2* in human colorectal carcinogenesis remains uncertain. Evidence has indicated that

TCF7L2 is indispensable for tumour initiation (153). More recently, a study has shown that loss of the TCF7L2 gene increases the invasion and migration of CRC cell lines (155).

Furthermore, a study in a transgenic mouse model expressing *Dkk1* (a Wnt inhibitor) revealed complete loss of the crypts and reduction in the size of the villus (156, 157). Similar phenomena were seen after specific deletion of β-catenin (*CTNNB1*) from the intestinal epithelium (158). Therefore, dysregulation of the Wnt pathway is highly implicated in cancer development, particularly, CRCs (138).

1.7.1 Wnt/β-Catenin Signaling and CRC Development

The connection between Wnt signaling and CRC was first indicated after the discovery of *APC* mutations in FAP (159, 160). As highlighted above, the loss of *APC* is the most frequent driver mutation that accounts for more than 80% of CRC cases (12, 22). Individuals with a germline APC mutation can develop multiple adenomas by acquisition of additional somatic APC mutations or loss of heterozygosity (LOH) at this locus (161, 162). Moreover, patients with CRC normally exhibit biallelic protein-truncating mutations in *APC* (163). However, distinct *APC* genotypes in CRC can be associated with different outcomes, including tumour type, location, and level of Wnt/β-catenin signaling (164, 165). In addition, it was reported that Wnt target genes are expressed differently in each *APC* genotype. For example, mutational analysis studies have indicated the association between the expression levels of Wnt target genes and the overall survival rate (34, 166). Likewise, *in vivo* studies using the *Apc*^Min mouse model suggested that adenoma can be reverted to normal tissue upon restoration of *Apc* function in the mouse (165).

Apart from the well-known *APC* mutations, several mutations in *AXIN1* and *CTNNB1* have been identified in several cases of CRC. Furthermore, some driver mutations in the Wnt-dependent tumours are found to be mutually exclusive to *APC*. For example, mutations in *RNF43* were demonstrated in 19% of CRC cases, whereas R-spondin 3 (*RSPO3*) mutations and *RSPO* gene fusions were identified in 10% of CRCs. Interestingly, the major consequence of all mutations in the Wnt pathway is the abnormally high level of nuclear β-catenin, which is often linked to CIN and is known as an indicator of poor prognosis of CRC (11).

Nonetheless, along with the rapid progress in genome screening and sequencing tools, several novel components in the Wnt pathway, ranging from co-receptors to nuclear co-factors, have been discovered. This discovery has refined our current understanding of the molecular levels involved in the canonical Wnt pathway and has significantly contributed to improvements in the prevention and treatment of CRC. In this context, the current understanding of nuclear events will be detailed in the next section.

1.7.2 Current Understanding of the Nuclear Events Involved in the Wnt/β-catenin Pathway

The primary indicator of Wnt pathway activation is the transcriptional activity of β-catenin, which is mediated by a complex network of nuclear TFs and β-catenin/binding proteins. In the nucleus, the transactivation domain of β-catenin often recruits specific DNA-binding TFs to activate the target genes (167). These TFs act by binding defined response elements located in the promoter region of their target gene to drive their expression. The most documented and well-known

example of nuclear TFs is the TCF/LEF family, which binds directly to β-catenin and promotes the transcription of its target genes (168, 169). Yet, this process is tightly regulated by several co-factors (co-activators and co-repressors) in order to maintain normal homeostasis.

These co-factors act as a safeguard to regulate transcriptional activity and fine-tune the outcome of the Wnt pathway via various mechanisms. Some interact directly with β-catenin, others might function as nuclear trafficking molecules (170). Additionally, the majority of co-factors are themselves controlled by the Wnt pathway, and many of them are found to be mutated or disrupted in cancer (168).

1.7.2.1 Co-activators and Co-repressors

It is well known that β-catenin initiates transcription by recruiting various transcriptional co-activators to its C-terminus. These co-activators can be defined as mediator proteins that induce the transcription of Wnt target genes by direct or indirect interaction with β-catenin and/or TCF4. Hitherto, several co-activators have been identified, including chromatin modifiers and remodeler. Of these, BCL9 is a well-studied co-activator, also known as an Wnt enhanceosome (171). B-cell lymphoma 9 (BCL9) and its homologue B-cell lymphoma 9-like (BCL9L) binds directly to nuclear β-catenin and enhances its transcriptional activity (171, 172), regardless the mutational status of the Wnt signaling component (173). Additionally, it regulates the recruitment of Pygopus, (a histone methylation reader and context-dependent LEF/TCF anti-repressor) to the nuclear β-catenin-TCF complex (167, 174). Of interest, a recent report has shown that BCL9/9L are required for an oncogenic β-catenin-mediated transcriptional programme which

permits the acute transformation of the murine intestine following APC loss (175).

Currently, there is a growing interest in targeting the β-catenin–BCL9 association in the Wnt enhanceosome. And several small molecules have shown promise in APC-deficient cells both *in vitro* and *in vivo* (176, 177). Other examples of less studied co-activators include: Brahma/Brahma-related gene 1 (Brg-1) (178), CREB-binding protein (CBP/p300) (179), parafibromin/Hyrax (180), Sox4 (181), PITX2 (182) and many others.

On the other hand, numerous co-repressor proteins, the so-called Wnt antagonists, have been identified and described as essential gatekeepers for maintaining Wnt signaling. These factors function through diverse mechanisms, including, a direct interaction with TCF4 and/or β-catenin to disrupt the formation of the complex. Examples include Groucho/TLE family protein, which is a well-studied repressor that recruits the HDAC enzyme to inactivate chromatin status and transcription via direct binding to TCF/LEF TFs (183, 184). Chibby is another example of a co-repressor that binds directly to β-catenin (185), while ICAT is an example of a protein that interacts with β-catenin and/or TCF/LEF to disrupt the formation of the β-catenin/TCF complex (186). Other suppression mechanisms could be by reducing or weakening the binding affinity within the TCF/β-catenin complex, such as in the case of RUNX3 (187, 188), or by repressing the TCF binding ability to DNA, such as SMRT/NCoR (189). Other proteins can function by inhibiting the recruitment of co-activators, such as Krüppel-like factor 4 (KLF4), which binds to the C-terminal domain of β-catenin and inhibits the recruitment of p300/CBP (190). Nonetheless, a combinatory mechanism is also possible, as in the case of Sox9 protein, which competes with TCF/LEF for β-catenin binding sites. At the

same time, Sox9 induces the ubiquitin-mediated phosphorylation and degradation of β-catenin (191, 192). Additionally, some co-repressors can act in TCF4-independent mechanisms, whereby their interaction with β-catenin is sufficient to modulate transcription activity. For example, Prop1 was found to interact directly with β-catenin and regulate cell lineage determination during pituitary gland development, independently of TCF4 activity (193).

In summary, these auxiliary proteins (both co-activators and co-repressors, Figure 1-6) are the safeguards of the Wnt pathway, maintaining the balance between activation/repression and maintaining the appropriate threshold of β-catenin/TCF4 interaction. Understanding the mechanisms of their action would enhance the therapeutic window of Wnt-dependent CRC.
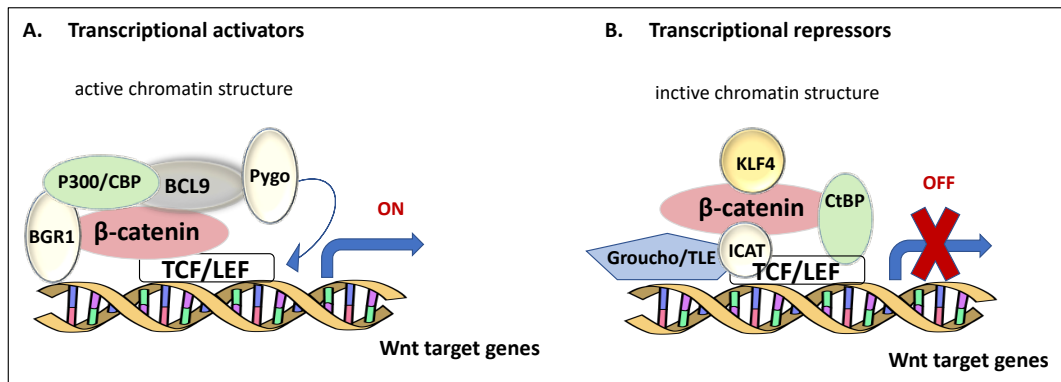
Figure 1-6 Schematic presentation of the nuclear regulation of β-catenin and TCF4 activity by: A) Transcriptional co-activators **B)** Transcriptional co-repressor.

Of note, apart from TCF4, the majority of identified TFs (including KLF4, GLIS2, GLIS3 and OSX) belong to a family of proteins called the Zinc Finger Protein (ZNF) family, which is characterized by multiple Cys2-His2 (C2H2)-type zinc finger DNA-binding domains (194, 195). This unique feature makes them outstanding players

in the recruitment of nuclear β-catenin, to the promoter of specific target genes independently of TCFs. At the same time, they can interact with β-catenin and/or TCFs and disrupt the formation of the β-catenin/TCF complex (196). The recent findings of TCF-independent mechanisms have challenged the current view of β-catenin/TCF4 interactions. Yet, it is still the least understood aspect of the Wnt/β-catenin pathway.

Due to the impact of these nuclear co-factors on regulating the biological outcomes of the Wnt signaling pathway, great efforts have been made to uncover and identify novel nuclear β-catenin partners and regulators that could play crucial roles in Wnt-driven tumorigenesis. To this end, several catenin-interacting proteins (CIP) that bind β-catenin in a GSK-3β phosphorylation-dependent and/or -independent manner were initially identified in our lab by employing a modified yeast two-hybrid Ras recruitment system (RRS) on a mouse embryonic cDNA library (197) (Figure 1-7). Among others, FLYWCH1 (198), a previously uncharacterized protein product of the human *FLYWCH1* gene, has gained the most attention owing to its unique features as a ZFP with C2H2-type zinc finger DNA-binding domains.
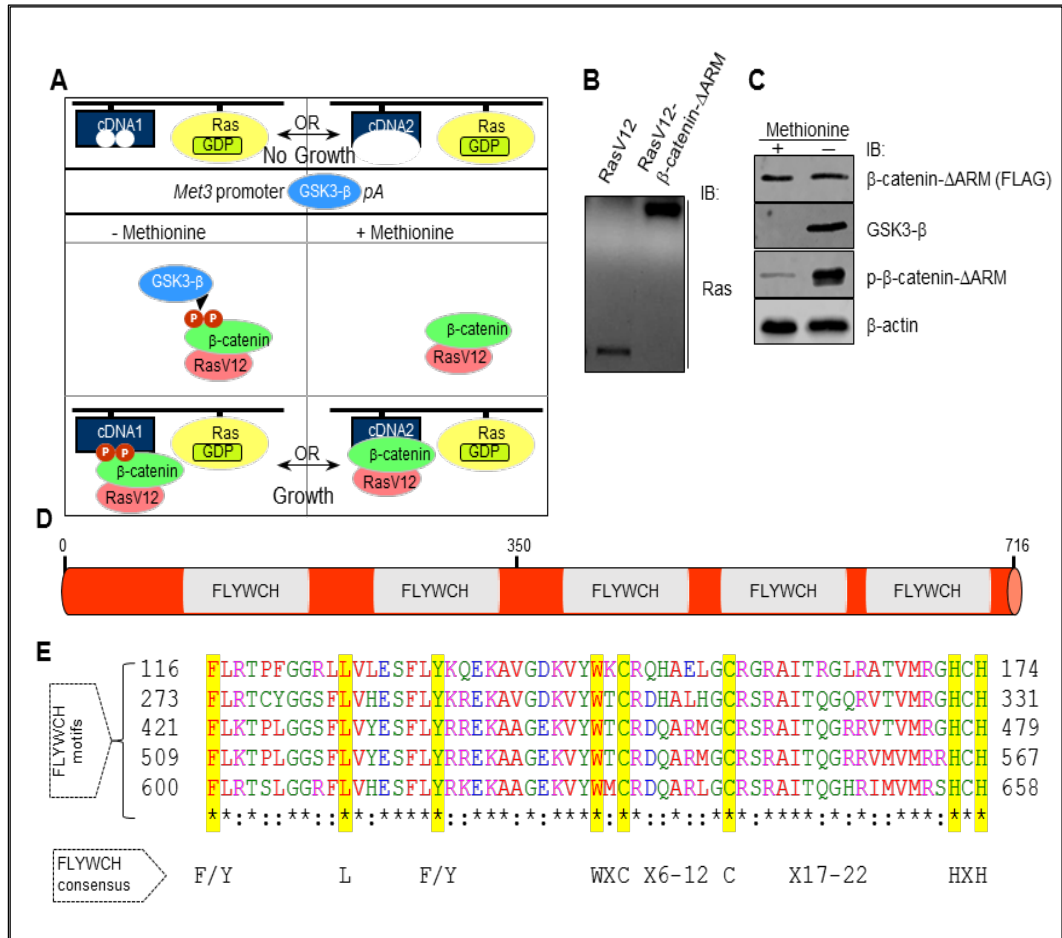
Figure 1-7 Identification of FLYWCH1 as an unphosphorylated-β-catenin interacting protein in yeast cells. A) Schematic representation of the modified yeast two-hybrid Ras Recruitment System (RRS). GDP, guanosine diphosphate; pA, polyA signal; P, phosphorylated amino acid. **B)** Ras, GSK-3β, FLAG and phospho-β-catenin protein expression in yeast. **C)** Phospho-β-catenin is induced by withdrawal of methionine. **D)** Tandem repeats of five FLYWCH encoding domains across human FLYWCH1 protein. **E)** Alignment of FLYWCH domain sequences of human FLYWCH1 shows the core aa residues (F, L, Y, W, C and H) of FLYWCH consensus sequence highlighted in yellow. The starting and ending residue numbers given for each domain indicate the aa numbering within the FLYWCH1 protein sequence. Identical residues are indicated by asterisks (*) at the bottom line and the non-identical residues by colons (:) Adapted from (198).

Before elaborating on the characterization and significance of FLYWCH1, the

unique features of C2H2-type ZNFs are highlighted below.

1.8 C2H2 Zinc Finger Family of Proteins

The Zinc Finger Protein family forms one of the largest TF families. ZNFs are known for their finger-like structure and their ability to bind zinc (199), and are mainly categorized into nine subfamilies based on the order of the cysteine (Cys) and histidine (His) residues in their secondary structures, such as the C2H2, C3H, C3HC4, C2HC5, C4HC3, C2HC, C4, C6 and C8 subfamilies (200). Among these, C2H2-type ZNFs represent the largest, but still poorly understood, class family of human TFs (201).

In classical C2H2-ZNFs, the zinc finger domains have two β-sheets and one α-helix as revealed by crystallography (202). The two conserved Cys-residues at one end of the β-sheet are coordinated by a zinc ion with two conserved His-residues at the α-helix C-terminus (202). The distinctive features of C2H2-ZNFs include strong and specific binding to long and unique DNA sequences reaching several tens of base pairs. In addition, the C2H2 proteins can bind to DNA effectively as monomers, unlike most other TFs that bind to short palindromic sequences as homo- or heterodimers (200). Also, it is believed that some C2H2 domains can enable a variety of interactions with protein complexes, individual TFs and RNAs. These distinctive features make them promising candidates for regulatory roles such as promoters, enhancers, insulators, and silencers (194, 201).

Moreover, ZNFs are involved in several cellular processes, and have key roles in the development and differentiation of several tissues. Additionally, ZNFs are implicated in tumorigenesis and cancer progression (195, 199). Examples of the most studied members of C2H2 ZNFs include: KLF4, KLF5, EGR3, ZFP637, SLUG, ZNF750, ZNF281, ZBP89, GLIS1 and GLIS3 (199, 201). Of interest, many C2H2 ZNFs

are implicated in the regulation of the intestinal epithelium under normal physiological and pathological conditions. For example, KLF5 (C2H2-type TF) is crucial for regulating the proliferation of intestinal epithelium (203). Additionally, studies have reported the role of ZNFs in cancer progression and metastasis via their TF function and as recruiters of chromatin modifiers or as structural proteins that regulate cancer cell migration and invasion (195). ZEB1 (C2H2-type TF) is one of the most important ZNFs involved in tumour invasion and metastasis and is known as a master regulator of EMT (204). Other examples include *ZNF281* (C2H2-type), reported as an oncogene in CRC by regulating metastasis (205), as well as *ZBP89* (C2H2-type TF), also known as *ZNF148*, which is a well-characterized zinc finger factor involved in cancer growth and apoptosis, and reported as a tumour-suppressor gene in CRC (206).

1.9 FLYWCH1 Characterization and Identification

Human FLYWCH1 is a conserved nuclear protein with multiple FLYWCH-type zinc finger domains. The FLYWCH motif is annotated based on the presence of five amino acid residues (F (phenylalanine), L (leucine), Y (tyrosine) and W (tryptophan)). It was first characterized and identified in our lab as a novel TF that binds directly to nuclear β-catenin and represses its transcriptional activity (Figure 1-7). Nonetheless, the FLYWCH zinc finger motif was previously characterized and identified in *Drosophila* and *Caenorhabditis elegans*. In *Drosophila*, the FLYWCH motif was initially identified from modifier of mdg4 [*mod* (*mdg4*)] encoded proteins (207). In *C. elegans*, it was identified in two other proteins derived from FLYWCH TFs, namely, FLH-1, FLH-2 and FLH-3 (208), and PEB-1 (209). Also, FLYWCH

motifs were found to be highly conserved in mammals (Gene ID: 84256). An overall view of the genetic and bioinformatic analysis of this novel protein will be highlighted below.

1.9.1 Bioinformatics of Human FLYWCH1

Based on NCBI data, the human *FLYWCH* gene located on chromosome 16, is composed of 15 exons and 2151 nucleotides encoding a protein of 716 amino acid residues (https://www.ncbi.nlm.nih.gov/gene/84256). At least 14 transcripts (splice variants), five of which are protein-coding isoforms, and a paralogue gene named *FLYWCH2*, have been described. *FLYWCH2* is a small gene comprised of four exons, which encodes a protein of 140 amino acids and is mainly associated with RNA binding (210) (Gene ID: 114984).

Human FLYWCH1 protein has a putative nuclear localisation signal (NLS) motif (KRAK) that closely resembles the classical NLS motif consensus sequences (K-R/K-X-K/R) (211). According to expression data obtained from the Human Protein Atlas (HPA), FLYWCH1 is mainly localised to the nuclear bodies and can localise to the nucleoplasm and cytosol (212). Of interest, the HPA Tissue Atlas expression profiles of human FLYWCH1 protein showed the highest expression of FLYWCH1 protein in the brain, particularly in neuronal cells, whereas the lowest expression in soft tissues, and it was not detected in blood cells. In intestinal and colon tissues, FLYWCH1 is highly expressed in the glandular cells, and less expressed in endothelial cells and other cell types (212).

Likewise, RNA expression profiling of FLYWCH1 suggested the highest expression in the brain and endocrine tissues and the lowest detectable expression levels in

blood cells and soft tissues (all expressional data available from HPA, https://www.proteinatlas.org/ENSG00000059122-FLYWCH1).

Moreover, based on the tissue microarray (TMA) data obtained from 216 cancer patients (corresponding to 20 different types of The Cancer Genome Atlas (TCGA) cancer tissue) and stained with anti-FLYWCH1, the expression of FLYWCH1 was generally low and showed strong cytoplasmic positivity in endometrial cancers. However, malignant lymphomas, testicular, urothelial, renal, and liver cancers along with several malignant gliomas were negative for FLYWCH1 (available from HPA: https://www.proteinatlas.org/ENSG00000059122-FLYWCH1). In CRC, the HPA database suggested a moderate level of expression, which was mainly cytoplasmic. However, these are qualitative antibody-based protein profiles, therefore, they only provide an overall idea or pattern of the spatial distribution of FLYWCH1 protein, rather than their exact expression in these tissues. Nonetheless, according to TCGA PanCancer Atlas studies, the highest percentage of mutations in *FLYWCH1* is found in undifferentiated stomach adenocarcinoma and breast invasive carcinoma (Figure 1-8, based on data generated via TCGA Research Network: https://www.cancer.gov/tcga).
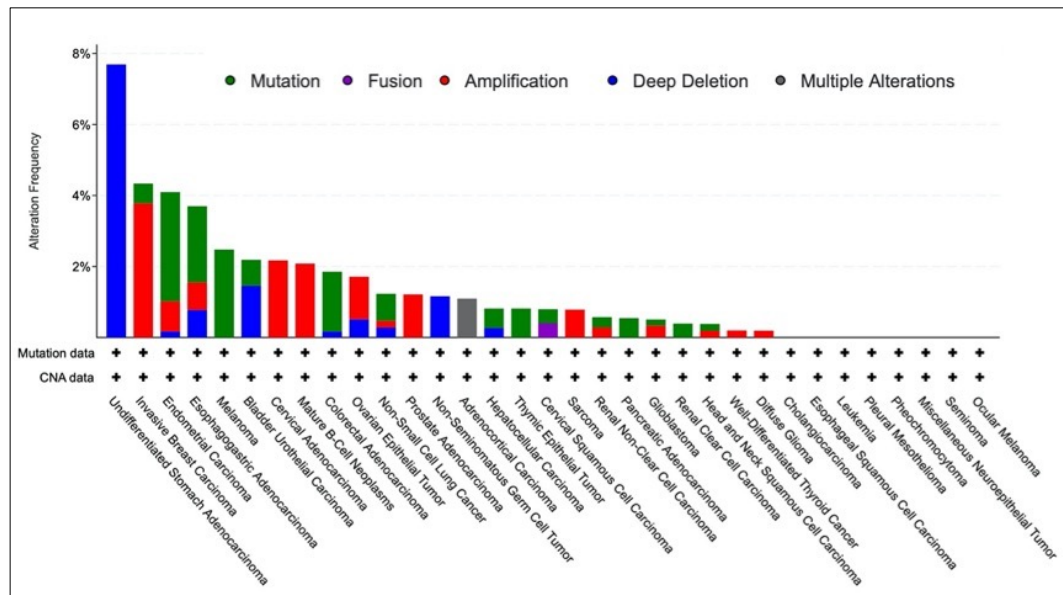
Figure 1-8 Alteration frequency and mutational analysis of *FLYWCH1* in various human cancers. Obtained from TCGA, National Cancer Institute**.**

Furthermore, the analysis of the Colon Adenocarcinoma dataset (obtained from TCGA PanCancer data) using the cBio Portal for Cancer Genomics (cBioPortal) (213) showed that only 11 of 594 cases (2%) had *FLYWCH1* mutation. Nine of the 11 cases showed missense mutations, one case had a truncating mutation (spotted in the C-terminal domain of *FLYWCH1*), and one case showed an in-frame mutation detected in the N-terminal (E345del) (Figure 1-9). Of interest, patients without alteration in *FLYWCH1* showed better survival curves, yet the p-value was not significant (213, 214) (https://bit.ly/2SALiSb). However, there is no evidence that FLYWCH1 can be a driver mutation in cancers. Also, till date, all these analyses were generated from small sample sizes/small projects and therefore may not accurately represent the significance of FLYWCH1 expression and/or mutations in cancers.
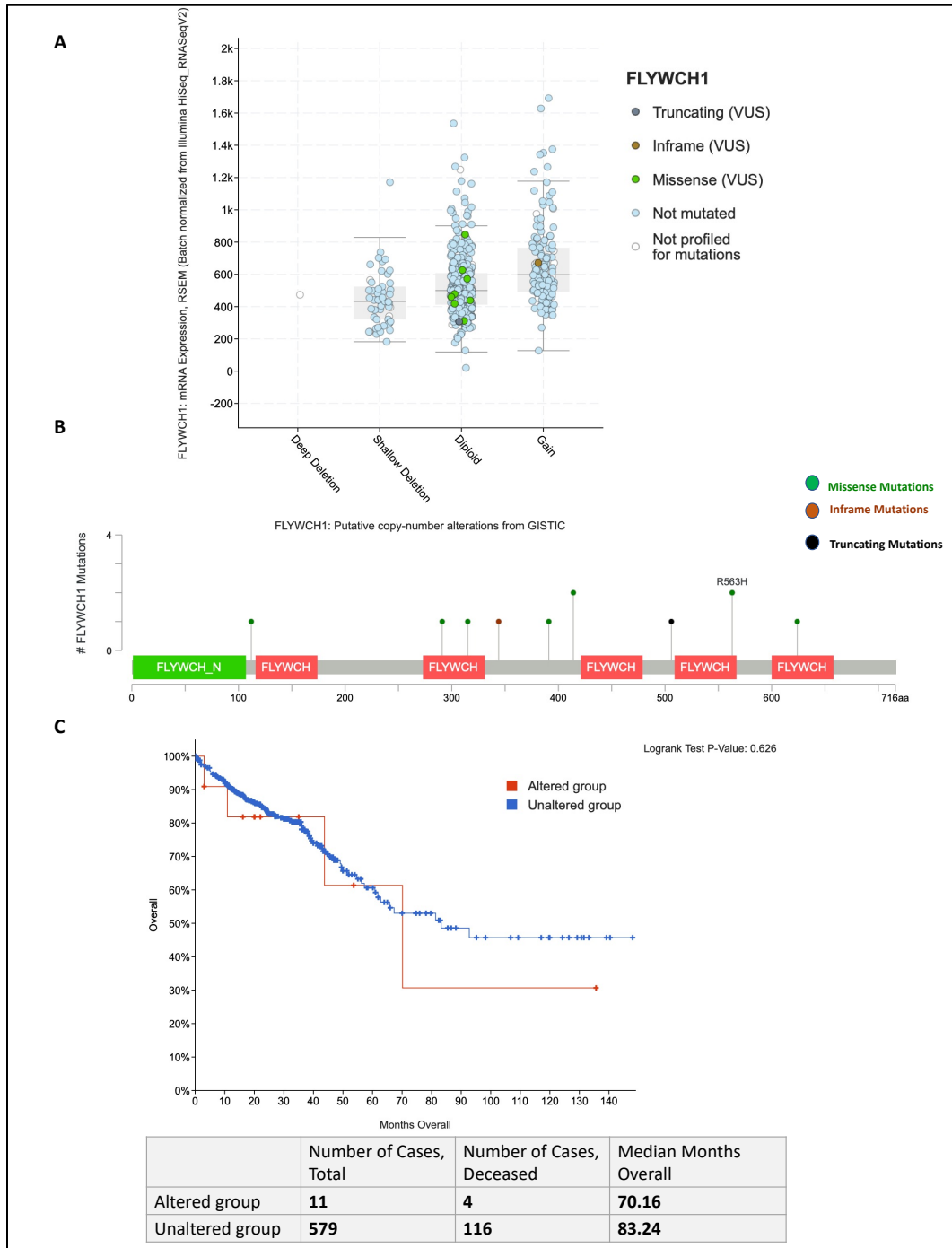
Figure 1-9 Mutational analysis of *FLYWCH1* in colorectal adenocarcinoma.
Diagrams showing the A) types and **B)** location of mutations detected in the
FLYWCH1 gene (sample size: 594 patients/samples). **C)** The association of altered
FLYWCH1 with overall patient survival status in colorectal adenocarcinoma. Data
were generated by cBioPortal (213, 214).

1.9.2 Biological Significance of FLYWCH1

Although the actual role of the FLYWCH domain is still poorly understood, two separate studies based on *Drosophila* and *C. elegans* studies, suggested that FLYWCH motifs may function in protein–protein interactions and serve as DNA- and RNA-binding domains (207, 208). Accordingly, FLYWCH motifs in human FLYWCH1 protein may have similar activities; however, the role of human FLYWCH1 was not fully established when I began my PhD study.

To date, during this PhD project we reported the role of FLYWCH1 in CRC and more recently in acute myeloid leukaemia (AML) (198, 215). We showed that overexpression of FLYWCH1 reduces the motility and increases cell attachment in colorectal cancer (CRC) cells via modulating Wnt/β-catenin signaling (198). In AML cells, FLYWCH1-overexpression increased the number of cells in G0/G1 arrest, while decreasing the number of cells at S and G2/M transitions by repressing nuclear β-catenin activity (215).

Prior to our laboratory work, there were only two published studies reporting the significance of the *FLYWCH1* gene in cardiovascular development. One study indicated *FLYWCH1* as a candidate master regulator of atherogenesis, where it was shown that *FLYWCH1*-mediated transcriptional regulation might be particularly crucial for the cardiovascular system (216). Likewise, the other study suggested that mutation variants in *FLYWCH1* (*FLYWCH1 p.R540Q at 16p13.3) may be deleterious and associated with familial mitral valve prolapse (MVP) in humans, implying the role of the *FLYWCH1* gene in the cardiovascular system (217).

Very recently, during the submission of this thesis, a new potential role of FLYWCH1 in chromatin-related processes has been suggested by Santos-Barriopedro et al. (218). Experiments have shown that a knock-in GFP-FLYWCH1 localises to centromeric regions through binding with a subset of H3K9me3-marked (peri)centromeres in human cells (218). These findings indicate a putative function for FLYWCH1 in centromere regulation and cellular homeostasis without direct interaction with H3K9Me3, confirming our finding of no complete localisation of FLYWCH1 with HP1a (219) (Chapter 4, Figure 4-3).

According to our recent evidence, we anticipated the potential roles of FLYWCH1 in various aspects of CRC progression, including cell morphology, metastasis, and invasion. Briefly, we reported a direct interaction of FLYWCH1 with the unphosphorylated (nuclear) β-catenin. FLYWCH1 efficiently suppresses the transcriptional activity of Wnt/β-catenin signaling, and this is not rescued by TCF4 (198). Our findings also highlighted a selective regulation of β-catenin/TCF4 transcriptional activity by FLYWCH1. We showed that altered FLYWCH1 expression modulates specific downstream genes associated with CRC cell migration and morphology, including ZEB1, EPHA4, and E-cadherin (198). Furthermore, a small pilot TMA screening of patients' samples derived at different stages of CRC revealed a heterogeneous expression of FLYWCH1 in early and advanced CRCs, using ISH assay (Figure 1-10 A) (198). The expression of FLYWCH1 was negatively correlated with the expression level of ZEB1 and EPHA4 in normal versus primary and advanced CRC tissues in patients (Figure 1-10 B). This study mainly established a molecular mechanism by which FLYWCH1 represses β-catenin-induced ZEB1 and

increases cadherin-mediated cell attachment, suppressing cultured colorectal

cancer cells migration (Figure 1-11).

Tumour type	Total	N/A	Stained	ISH			Staining
				High	Medium	Not detectable	
				Strong	Moderate	Weak	Intensity
Early tumour	73	3	70 (100%)	23 (32.8%)	29 (41.4%)	18 (25.7%)	
Advanced tumour/ Metastatic	74	2	72 (100%)	8 (11.1%)	15 (20.8%)	51 (70.8%)	
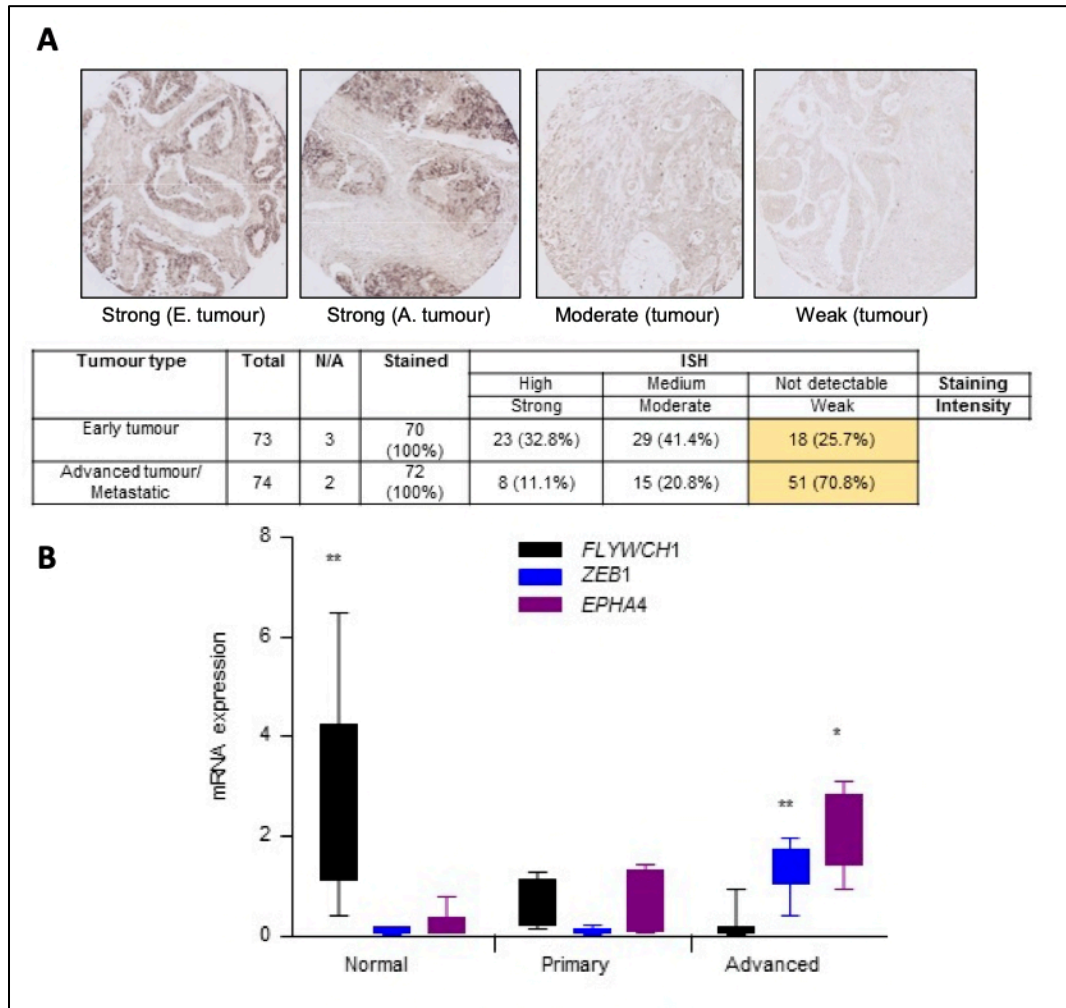
Figure 1-10 Low FLYWCH1-mRNA expression significantly associated with advanced tumours A) Upper panel shows photomicrographs of CRC-TMA specimens analysed by ISH using a specific FLYWCH1 probe with strong (left panel), moderate (middle panel) and weak (right panel) expression. The lower panel shows a correlation between FLYWCH1 expression and tumour staging. Weak expression of FLYWCH1 is associated with more advanced stage of a tumour. N/A: samples were not available on slides after staining and perhaps wiped off through the ISH process. Scale bars; 50mm. **B)** qPCR analysis of FLYWCH1, EPHA4 and ZEB1 mRNA expression in a cohort of thirty-three; normal, primary, and metastatic tumour tissues from patients in Nottingham, UK, normalized to HPRT. Data are mean ± SEM (n = 3; 36 *p ≤.05; **, p ≤.01). Experiments were performed in triplicate for each sample and repeated on two independent occasions (198).
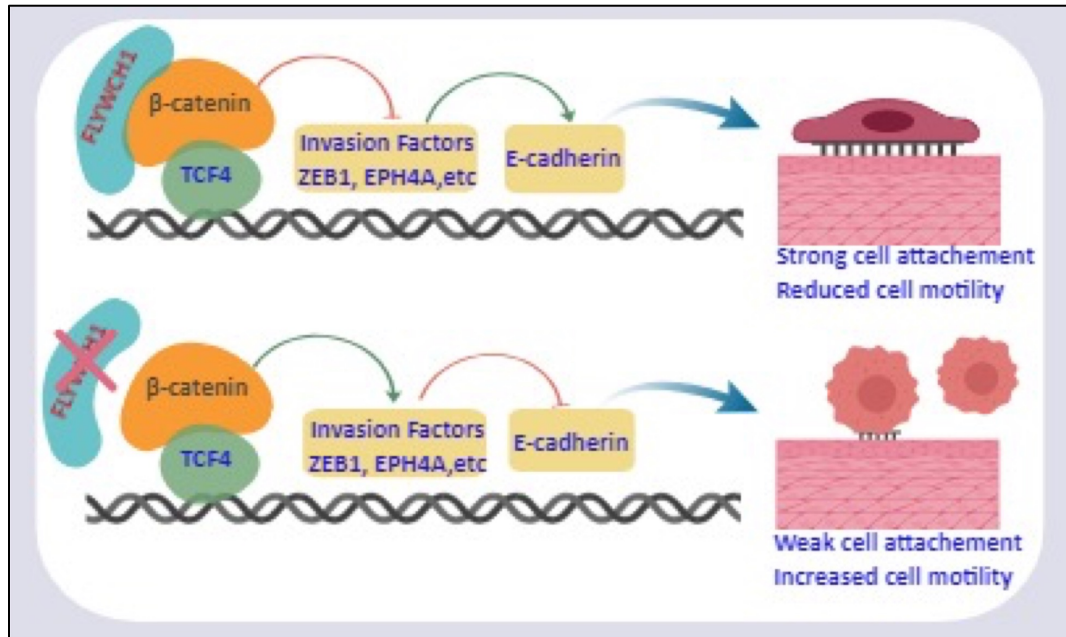
Figure 1-11 Schematic representation shows the adverse effect of FLYWCH1 on cancer cell migratory potentials through inhibition of β-catenin signalling pathway. Re-printed from (198).

Moreover, unpublished data from our lab using the *in situ* hybridization (ISH) analysis of mouse tissues demonstrated that *Flywch1* is mainly expressed in the crypt base columnar cells (CBCs), which also function as stem cells, and is undetectable in the differentiated epithelial cells of intestinal villi of $Apc^{Min/+}$ mice (Figure 1-12). This was also confirmed in Apc^{WT} mice, which showed similar expression pattern (Data not provided). On the other hand, the data showed that *FLYWCH1* expression was strongly downregulated in CRC cell lines and was restricted to subpopulations of transformed cells in both humans and $Apc^{Min/+}$ mice. Therefore, it can be postulated that the expression of FLYWCH1 might undergo gradual reduction (or loss) during cell differentiation and/or tumour progression.
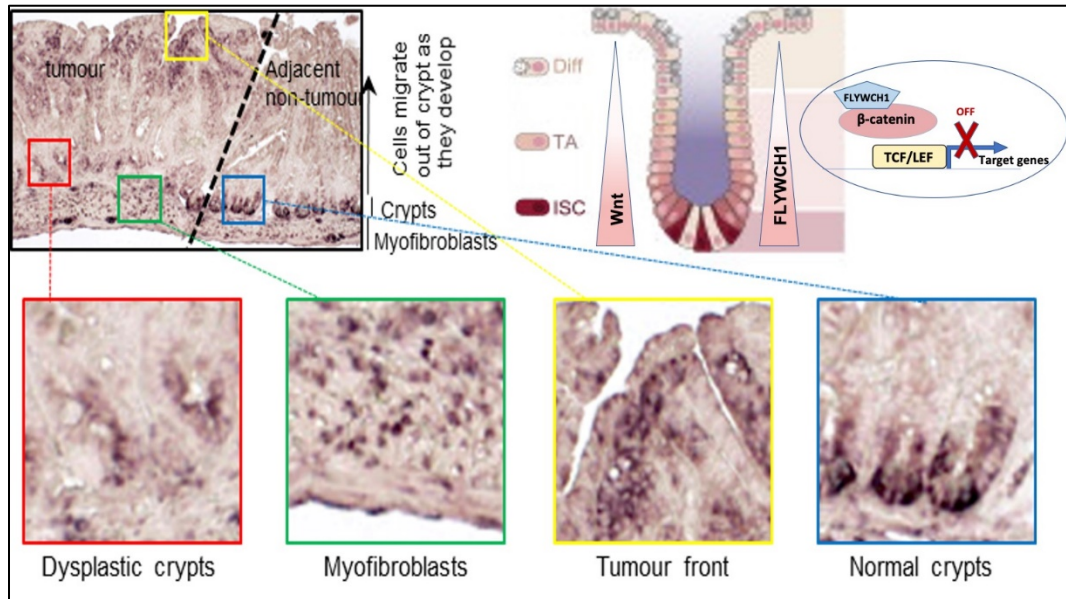
Figure 1-12 *FLYWCH1* mRNA expression in mouse and colorectal tumour tissues. ISH for *flywch1* on representative intestinal sections from 16-weeks old *Apc*^{Min} mouse. Boxes indicate magnified tumour crypts (red), the front of the intestinal tumour (yellow), the sub-epithelial intestinal myofibroblast (green) and the tumour adjacent normal-appearing crypts (blue). (Unpublished data from Dr Nateri's lab, Personal communication)

On the strength of these findings, it can be speculated that FLYWCH1 and its interaction with β-catenin would play critical roles in normal intestinal development, and colorectal cancer development and progression.
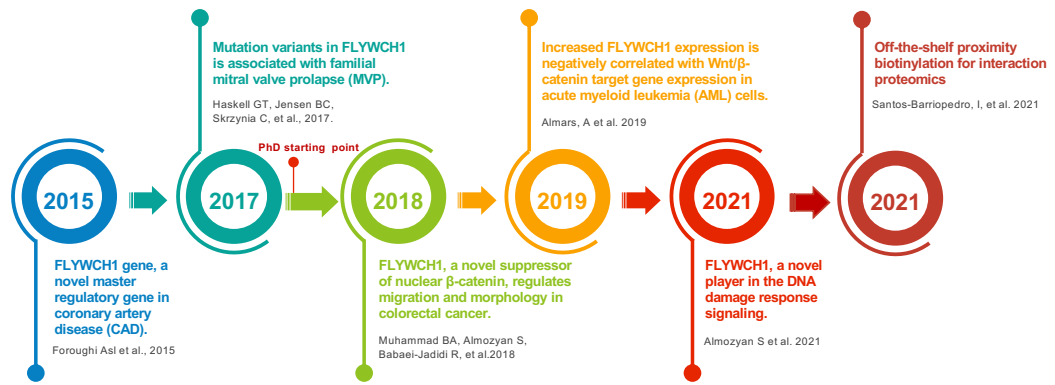
Figure 1-13 Timeline depicts key milestones in the FLYWCH1 research.

1.10 Rationale, Aims and Objectives

Sustained activation of the WNT/β-catenin pathway provides cancer cells with enduring self-renewing and growth properties, which is associated with therapy resistance in CRC. In a healthy intestinal crypt, core transcription suppressors and negative feedback regulators tightly controlled the WNT pathway activity. In CRC, the picture is far more complex, in which these regulators are often mutated, dysregulated, or inactivated during CRC development. These changes strongly affect the biological characteristic that gives information about the clinical outcomes in CRC patients.

Several studies have shown the therapeutic potential of targeting Wnt/β-catenin signaling in suppressing tumorigenesis in CRC patient-driven xenograft and animal models (220, 221). More recently, cancer-specific Wnt signaling regulators have been identified as potential future candidates for treating Wnt signaling-associated cancers (220, 222).

Therefore, identifying novel Wnt/β-catenin regulators would be valuable to develop innovative therapeutic approaches for CRC.

Chapter 1: General Introduction

Our recent findings on FLYWCH1 as a novel suppressor of nuclear β-catenin transcriptional activity revealed the potential roles of FLYWCH1 in regulating Wnt-mediated growth and migration in CRC cells. However, our current understanding of FLYWCH1 biological functions is very limited. Therefore, this study initially aimed to gain fundamental knowledge on the biological and clinical significance of FLYWCH1 expression in CRC and intestinal organoids models. The primary long-term aim of this project is to evaluate the impact of FLYWCH1 as a Wnt-suppressor and understand its roles in regulating Wnt-mediated biological responses during CRC development. This may enable the discovery of an alternative strategy to target the oncogenic Wnt signaling in CRC.

Hence, we explored the multi-faces, functions, and regulation of FLYWCH1, with a focus on the bidirectional crosstalk between FLYWCH1 and WNT-driven activities in normal physiological conditions versus cancers.

To this end, the main objectives of this project were to:

1. Evaluate the significance of FLYWCH1-crypt expression in maintaining the normal crypt activity by employing a 3D intestinal mouse organoid model and examining the impact of FLYWCH1 loss on the proliferation and stem cell transcriptional activity.

2. Examine the potential tumour suppressive functions of FLYWCH1 in patient-derived CRC organoids (PDOs), focusing on the impact of FLYWCH1 overexpression on tuning the transcriptional activity of Wnt-mediated tumour growth and proliferation.

3. Investigate the association of FLYWCH1 with cancer stem-like properties in SW620 cells via applying an *in vitro* 3D-colonosphere culture.

44

4. Understand the regulation of FLYWCH1 by the Wnt/β-catenin signaling pathway in normal versus cancer cell lines.

5. Explore the mechanism(s) and effects of Wnt modulation on FLYWCH1 protein stability and cellular distribution.

6. Address the prognostic value and clinical significance of FLYWCH1 (expression and cellular distribution) for CRC patients via TMA analysis of a patient cohort containing 1000 CRC tissues.

7. Uncover new roles of FLYWCH1 in the DNA-damage response pathways and explore the potential mechanism(s) of action.

CHAPTER 2

Materials and Methods

Chapter 2: Materials and Methods

2.1 Materials

2.1.1 Reagents and buffers

All common materials, reagents, and chemicals for biochemical, molecular, and cellular experiment purposes were purchased from Sigma-Aldrich (UK) unless otherwise stated.

2.1.2 Cell lines

Four different immortalized human colorectal cancer cell lines were used in this study; HCT116, SW480, SW620, and DLD-1 (Table 2-1), together with human embryonic kidney HEK293T cells. All cell lines were initially purchased from the American Type Culture Collection (ATCC). HEK293T-HA-Rspo1-Fc cells stably expressing murine R-spondin1 were kindly gifted from Prof Hans Clevers laboratory. Human skin fibroblast cells (TIG119 cells) was a gift from Dr Peter Gordon laboratory (CRUK London Research Institute, London). All cell lines were routinely tested to exclude mycoplasma contamination.

Table 2-1: CRC cell lines used in this study (36, 223, 224).

Name	Cell line origins	TP53	KRAS	BRAF	PIK3CA	PTEN	MSI	CIMP	CMS
HCT116	Tissue: Colon Disease: Colorectal carcinoma, primary tumour, Dukes' D	WT	p.G13D	WT	p.H1047R	WT	MSI	CIMP+	CMS1
DLD-1	Tissue: Colon Disease: Dukes' C, Colorectal adenocarcinoma.	p.S241F	p.G13D	WT	p.E545K p.D549N	WT	MSI	CIMP+	CMS1
SW480	Tissue: Colon Disease:Dukes' B, Colorectal adenocarcinoma.	p.R273H; p.P309S	p.G12V	WT	WT	WT	MSS	CIMP-	CMS2 (TGF-B)
SW620	Tissue: colon; derived from metastatic site: lymph node Disese: Dukes' type C, colorectal adenocarcinoma	p.R273H; p.P309S	p.G12V	WT	WT	WT	MSS	CIMP-	CMS2 (ErpB-Hippo-Wnt)

2.1.3 Human biopsy tissue

Human normal/tumour biopsy tissues were collected with informed written consent from CRC patient who underwent colectomy at Nottingham Health Sciences Biobank (NHSB), Queens Medical Center (QMC), University of Nottingham.

2.1.4 Antibodies

Different types of primary and secondary antibodies were used throughout this study for both Western blotting and immunofluorescence analysis. Details about the source of these antibodies and the dilution factors are given in (Table 2-2, 2-3).

Table 2-2: The list of primary antibodies used for Western blotting and Immunofluorescence analysis. "NA" means not applied.

Primary antibodies	Source	Supplier & catalogue number	Dilution used	
			WB	IF
MYC (9E10)	Mouse	Sigma, M4439	1:2000	1:200
GFP	Rabbit	Invitrogen, A-11122	1:2000	NA
FLYWCH1	Rabbit	Sigma, HPA040753	NA	1:200 IHC 1:300
FLYWCH1	Rabbit	Prestige Antibodies Powered by Atlas Antibodies, HPA041001	1:400	1:200
FLYWCH1 (V8)	Goat	Santa Cruz, sc- 242855	NA	1:100
FLYWCH2	Rabbit	Prestige Antigens Powered by Atlas Antibodies, HPA041354	1:500	1:100
β-Catenin	Mouse	BD Biosciences, 610181	1:1000	1:100
β-actin	Mouse	Abcam, ab6276	1:5000	NA
α/β-Tubulin	Rabbit	Cell Signalling, 2148	1:1,000	NA
Phospho-β-Catenin (Ser45)	Rabbit	Cell signalling, 9564	1:1000	NA
β-catenin (Clone 8E7)	Rabbit	Santa Cruz, sc- 220	1:2,000	1:100
Phospho GSK-3β (S9)	Rabbit	Cell Signalling, 9322	1:2,000	1:50
GSK-3β (D5C5Z) XP	Rabbit	Cell signalling 12456	1:1000	1:100
c-Jun	Rabbit	Cell Signaling, 9165	1:1000	1:100
c-MYC (9E10)	Mouse	Santa-Cruz, sc-40	1:1000	NA
JNK1/3 Antibody (F-5)	Mouse	Santa-Cruz , sc-514539	1:1000	NA
p-JNK Antibody (14.Thr 183/Tyr 185)	Mouse	Santa-Cruz, sc-293136	1:1000	NA
SC-35	Mouse	Abcam, ab11826	1:1,000	1:100
Twist-1	Mouse	Abcam, 2F8E7	1:100	NA

Table 2-3: List of secondary antibodies used for Western blotting and Immunostaining.

Secondary Antibody	Source	Supplier and catalogue number	Dilution used	
			WB	IF
IRDye® 800CW anti-Mouse IgG	Donkey	Licor, P/N:926 32212	1:10.000	NA
IRDye® 800CW anti-Rabbit IgG	Goat	Licor, P/N: 926-32211	1:10.000	NA
Alexa Fluor® 488 anti-rabbit	Donkey	Life Technologies, A-21206	NA	1:500
Alexa Fluor® 594 anti-mouse	Goat	Life Technologies, A-21155	NA	1:500
Alexa Fluor® 594 anti-rat	Goat	Life Technologies, P1379	NA	1:500
Alexa Fluor® 488 anti-rabbit	Donkey	Life Technologies, A-21206	NA	1:500
Alexa Fluor® 594 anti-mouse	Goat	Life Technologies, A-21155	NA	1:500

2.1.5 DNA plasmid constructs

All plasmids used in this study are listed in (Table 2-4). These plasmids were previously fully validated and used in Dr Nateri's laboratory.

Table 2-4: List of DNA plasmids used throughout the thesis.

Plasmid	Supplier	Cat.No.	Backbone vector
pEGFP-C2	Clontech	6083-1	NA
pLVX-EGFP	Dr Nateri's lab	NA	pLVX-Puro
pLVX-Puro- FLYWCH1-GFP	Dr Mohammed Belal Dr Nateri's lab	NA	pLVX-Puro
pCMV delta R8.74 ,pMDG2	Dr Nateri's lab	NA	
GFP-FLYWCH1	Dr Mohammed Belal Dr Nateri's lab	NA	EGFP2 vector
MYC-tagged FLYWCH1 clones (WT, ΔC350 and ΔN350)	Dr Mohammed Belal Dr Nateri's lab	NA	pIRES2-EGFP
gRNA, pLV-U6g-EPCG CRISPR-Cas9	SIGMA	Custom CRISPR	pLV-U6g-EPCG
pLv5-Cas9-Neo	SIGMA	CAS9NEO-1EA	pLv5-Cas9-Neo
pLV-U6g/FLH1-Puro-2A-tBFP	SIGMA	CRISPR 03291733MN	pLV-U6g-PPB
pSpCas9(BB)-2A-Puro	Addgene	48139	(PX459) V2.0 vector
ATM-gRNA-CRISPR	Dr Makhliyo Normatova Dr Nateri's lab	NA	pX459

2.1.6 Oligonucleotides

All oligonucleotides used in this study (Table 2-5) were designed using NCBI-primer designing tool (https://www.ncbi.nlm.nih.gov/tools/primer-blast), for standard PCR and quantitative real-time polymerase chain reaction (qRT-PCR). For qRT-PCR, the primers were designed to target two consecutive exons within the gene of interest, and to amplify a region of 100-200 bp of size. The specificity of the primers was checked by blasting the primer sequences against the NCBI human transcript database (http://www.ncbi.nlm.nih.gov/tools/primer-blast/). Upon receipt, the primers were spun down, re-suspended in an appropriate volume of distilled water to give a final concentration of 100 µM, and stored at -20°C until used.

Table 2-5: List of primers and their sequences used in this study.

	Primer sequences 5'- 3'
FLYWCH1	Forward: CTGGATGCAGCCCCTCAGT Reverse: TTGGCGGCACTTCCAGTAC
FLYWCH2	Forward: T CAGGAGCCTGAGCAGAAAC Reverse: CACAGAGCAGGGGGCAAAG
HPRT	Forward: AGATGTGATGAAGGAGATG Reverse: GTGTCAATTATATCTTCCA
B-actin	Forward: GCGCGGCTACAGCTTCA Reverse: CTTAATGTCACGCACGATTTCC
CD44	Forward: AGAAGGTGTGGGCAGAAGAA Reverse: AAATGCACCATTTCCTGAGA
LGR5	Forward: GACAACAGCAGTATGGACG Reverse: GCATTACAAGTAAGTGCCAG
CDX2	Forward: AGCCAAGTGAAAACCAGGAC Reverse: CCAGATTTTAACCTGCCTCTCA
KRT20	Forward: TGAAGAGCTGCGAAGTCAGAT Reverse: TCCTCTCTCAGTCTCATACTTCAGTC
CCND1	Forward: GCTGGAGGTCTGCGAGGA Reverse: CATCTTAGAGGCCACGAACA
BMI-1	Forward: CCAGGGCTTTTCAAAAATGA Reverse: CCGATCCAATCTGTTCTGGT
N-cadherin	Forward: GACAATGCCCCTCAAGTGTT Reverse: CCATTAAGCCGAGTGATGGT
FRZ8	Forward: GGAGTGGGGTTACCTGTTGG Reverse: GTAGCCGATGCCCTTACACA
FRZ7	Forward: TGTCGTTCTCTGTGCGAGC Reverse: GAGCCGTCCGACGTGTTCT
FRZ1	Forward: GAAAGTGCAGTGTTCCGCTG Reverse: CGAACTTGTTCATGAGCGCC
WNT11	Forward: TATCCGGCCTGTGAAGGACT Reverse: GTCTTGTTGCACTGCCTGTC
BCL9	Forward: TGTCTTGATACCAGGAGGCCA Reverse: TGGGCCCACATTCAGTCCTTTTT
P21	Forward: AGCTGAGGTGTGAGCAGC Reverse: TTCTGACATGGCGCCTCC
p53 (TP53)	Forward: AAGTCTAGAGCCACCGTCCA Reverse: GCAGTCTGGCCAATCCAGG

Table 2-6: FLYWCH1 isoform-specific or exon specific oligos used in this study.

Target genes	Primer sequences 5'- 3'
FLYWCH-type zinc finger 1 (FLYWCH1) Full length	Forward: TGGATGCAGCAGCCCCT Reverse: GTTGGCGGCACTTCCAGTA
FLYWCH1- (Exon1)	Forward: AAGGTGTACTGGAAGTGCCG Reverse: CTGGGCAGTTTCTCCCTCTG
FLYWCH1- Exon 2	Forward: GGGCTAGATTGCGGAGTGTT Reverse: CCACATAGGGTGCTGACAGG

2.2 Methods

All procedures were performed under aseptic conditions under the guidance of strict safety regulations. Standard protocols of the techniques used throughout the project were followed from previously established templates and optimized where necessary or otherwise, developed in our laboratory.

2.2.1 General tissue culture techniques

2.2.1.1 Cell culture and maintenance

Cell lines (low passage) were recovered from liquid nitrogen and thawed in a water-bath at 37°C. Cells were then propagated in a 75 cm^2 flask (Cellstar, 658975) using a complete medium composed of RPMI1640 medium (Sigma Aldrich, R0883), supplemented with 10% fetal bovine serum (FBS, Sigma Aldrich, F7524), and 2 mM L-glutamine (Thermo Fisher Scientific, 25030-024), in a humidified, 37°C, 5% CO_2 incubator. Cells were maintained at 70-80% confluence and were sub-cultured every 2-3 days. After discarding the medium, adherent cells were washed with 2 ml of a sterile phosphate buffer solution (PBS, Sigma, D8537) followed by 5-10 min incubation at 37°C with 1 ml 1x Trypsin /ethylenediaminetetraacetic acid (EDTA) (Sigma, T3924) solution to detach the cells. Next, the trypsin/EDTA solution was neutralised by adding 6 ml of the complete medium and then was diluted according to the experimental protocol and future needs.

2.2.1.2 Cell freezing

For cell freezing, cells were first trypsinized and centrifuged, as mentioned above. The supernatant was then discarded, and the pellet was resuspended in 1 ml freezing medium comprising of 10% DMSO and 90% FBS in Cryogenic vials, on ice. All vials were kept overnight at -80°C for short storage, before transferring to the -150°C freezer, or liquid nitrogen for long term storage.

2.2.1.3 Cell cycle synchronization

To synchronize the cells in G0 phase of the cell cycle, the complete cell culture medium was replaced with a serum-free RPMI-1640 medium (Sigma Aldrich, R0883), supplemented with 2 mM L- L-glutamine (Thermo Fisher Scientific, 25030-024), and kept in a humidified, 37°C, 5% CO_2 incubator for 18h. Prior to the wound healing assay and/or any drug treatment experiments, various cell lines were cultured at similar passage numbers and subjected to serum starvation to avoid any proliferation advantage or differences in the growth conditions between cell lines.

2.2.1.4 Cell counting

Neubauer haemocytometer (MARIENFELD, Germany) was used to estimate the number of cells in a suspension. Trypsinized cells were diluted in a complete medium as necessary (by a factor of 2 or 4), depending on their confluence. In Eppendorf tubes, 10 µl of the diluted cell suspension was mixed with 10 µl of Trypan Blue (Sigma, T8154). Trypan Blue is used to stain and exclude the non-viable cells from the counting. Thence, 10 µl of the well-mixed Trypan Blue-cell suspension was loaded onto a haemocytometer slide, and the number of living

transparent cells in each of the four large corner squares was counted under the microscope using the 10X objective lens. The average number of cells was calculated. Lastly, the final number of cells per ml of suspension was determined by multiplying the average cell count by the applied dilution factors.

2.2.1.5 Transient transfection

Several transient transfections of mammalian cell lines were carried out in this study for different purposes. At first, an appropriate number of cells were seeded and allowed to reach 70% confluency to achieve optimum transfection efficiency. On the day of transfection, an ideal concentration of the DNA plasmids (calculated based on the number of cells) was diluted in the optimum medium. In a separate sterile tube, 4 µl of PIE transfection reagent (for each µg of plasmid DNA) was diluted in an optimum medium. Then, the plasmid DNA and transfection reagent mixture were mixed in one tube, incubated for 30 min at room temperature (RT). At this stage, the growth medium was discarded, and cells were washed with an optimum medium. Next, a suitable volume of the transfection mixture was added into each plate/well and incubated in a humidified, 37°C, 5% CO_2 incubator for 6-8 h, before adding a complete cell culture medium. The transfected cells were incubated for 30-48 h before assessment, and the transfection efficiency was analysed by microscopic examination of GFP expression. Finally, transfected cells were validated by WB and IF staining for different experiments.

2.2.1.6 Lentivirus production (transduction)

To produce lentivirus particles, HEK293T cells were cultured in 75T flasks (at least 3 flasks) and maintained in 15 ml of virus production medium composed of (DMEM

high glucose (Sigma, D5796), 1 mM sodium pyruvate (Sigma, S8636), 1% v/v L-glutamine (Invitrogen, 25030- 081), 1% v/v penicillin/streptomycin (100 Units/ml) (Invitrogen, 15140-122) and 10% v/v fetal bovine serum (FBS) (Sigma, F7524). On the day of transduction, 80-90% confluent cells were co-transfected with 2 packaging plasmids (6 µg of pCMV delta R8.74 and 3 µg of pMDG2), as well as a 9 µg of the plasmid of interest (e.g. pLV-U6g-EPCG CRISPR-Cas9 construct contains FLYWCH1-gRNA). All plasmids were diluted in an Optimum medium and incubated for 5 min, before mixing with a 4 µl/µg of PIE transfection reagent. The mixture was kept for 30 min at RT. Later, cells were washed from the residual growth medium by adding 9 ml Optimum medium. Then, 4 ml of transfection mixture was added gently and left overnight in a humidified, 37°C, 5% CO_2 incubator. Afterwards, the medium containing the transfection mixture was discarded and replaced with a fresh complete culture medium. On the second day after transfection, the supernatant or the viral soap (culture medium enriched with virus particles) was collected into a clean labelled 50 ml tube and cells were fed with a fresh complete growth medium. The virus harvesting was repeated for three consecutive days and tubes were stored at 4°C until purification. The collected tubes (viral soap) were then centrifuged at 4000 rpm at 4°C for 10 min, and filtered by 0.45 µm pore filter (to clear any contaminants in the soap). Next, the purified soap was layered equally into specific centrifuge tubes filled with 1ml of 20 % Sucrose solution. Virus particles were precipitated by centrifugation at 4000 rpm for 2h at 4°C (using ultracentrifuge). After centrifugation, the supernatant was discarded, and the pellet enriched with virus particles were re-

suspended in 40 µl of PBS, and kept overnight at 4°C. Finally, particles were aliquoted and stored at -80°C for later use.

2.2.1.7 Mammalian cell transduction

To generate stable cell lines by viral transduction, cells were seeded into a 24-well plate in triplicates or duplicates. The infection mixture was prepared by diluting 20, 30 or 50 µl of the concentrated viral particles in a complete DMEM medium mixed with Hexadimethrine bromide (Sigma, H9268) at a final concentration of 8 µg/ml. Later, 70-80 % of confluent cells were infected by adding the infection mixture gently into each well. Cells were then incubated for 24-48 h in a humidified, 37°C, 5% CO_2 incubator. Later, infected cells were examined for GFP expression, selected by Puromycin treatment, and amplified as previously mentioned.

2.2.1.8 Generation of Stable cell lines transfected with CRISPR-Cas9 and gRNA expressing vectors

Several stable long-term knockout cell lines were generated (for the candidate genes: *FLYWCH*1 and *ATM*) using CRISPR-Cas9 technology. Guide RNA designing and cloning into the backbone vector are explained in Section 2.4.1 below. To generate the stable cell lines, we utilised (pLV-U6g-CRISPR-Cas9) vectors. All lenti-vectors used in this study contained a puromycin resistant gene which enables the selection of transfected cells. Briefly, cells were seeded equally in a 6 well-plate and were then transfected with 5 µg of lenti-vector constructs, using PEI (4 µl/1 µg) transfection reagent as outlined above (See section 2.2.1.5). 48 h later, transfected cells were selected based on their resistant to Puromycin treatment. Un-transfected control cells usually failed to integrate the resistant gene and died

upon treatment with puromycin. Only transfected cells can survive and develop resistance to the drug. This was accomplished by introducing 3-6 μg /ml of Puromycin (Sigma-Aldrich, P8833) into the culture medium every 48h for 7-14 days or until all transfected cells had developed resistance to the drug. The concentration of Puromycin was adjusted for depending on the cell line. TIG119 cells were treated with 3 μg of puromycin whereas CRCs were treated with 5 μg of puromycin, as previously reported (225). Following the selection, the few Puromycin-resistant colonies (Puro[R]) were transferred into T75 flask, amplified in RPMI medium, and maintained in culture before proceeding with single-cell cloning. Confluent cells were then frozen and stored in -150°C freezer or under liquid nitrogen storage.

Moreover, single cell cloning via serial dilution was performed to obtain a single knockout clone of the protein of interest. Firstly, confluent cells were trypsinized and counted as previously described. The cells were then diluted with the required volume of RPMI media to make a 1:10 dilution. Diluted cell mixtures were thoroughly pipetted up and down to sort 1 cell into each well and then carefully distributed across a 96 well-plate with 200 μl/well. The wells were observed under the microscope over the following week to look for colonies derived from single-cell clones. Thenceforth, the colonies were amplified and expanded under normal tissue culture conditions for further validation by immunoblotting and qPCR analyses.

2.2.2 Gene cloning techniques

In the current research, methods such as Polymerase Chain Reaction (PCR), enzymatic digestion and were employed for genetic engineering and CRISPR/Cas9 technology.

2.2.2.1 gRNA designing tool

Two pairs of gRNA (Table 2-7) were designed for each target protein using (http://tools.genome-engineering.org)(226). For the highest efficiency and efficient Cas9-cleavage, all designed gRNAs were 20 nucleotides in size, with a protospacer adjacent motif (PAM) sequence downstream of the target sequence. Importantly, the nearest to 5' the better the chance of having frameshift mutation and non-functional product (227). Furthermore, to facilitate the efficient U6 transcription of sgRNA, the presence of a G is preferable at 5' position, corresponding to the first base of the 20-bp target site (226). Accordingly, at least 2 pairs of gRNAs were employed based on the highest quality score with the lowest number of off-target sites. In addition, two Sanger FLYWCH1-gRNA constructs were kindly provided by Sanger (Table 2-8).

Table 2-7: Two pairs of guide sequence oligos used to generate FLYWCH1-CRISPR plasmid construct. Restriction enzyme sites for BbsI within primers are underlined.

Primer Use	Primer sequence 5'-3'	Restriction Site
FLYWCH1-CRISPR (1ˢᵗ set, on-target locus: chr16:-2979861)	**F:** CACCGCAGGACGCAGTGCACTTCCT	BbsI
	R: AAACAGGAAGTGCACTGCGTCCTGC	BbsI
FLYWCH1-CRISPR (2ⁿᵈ set, on-target locus: chr16:-2979965)	**F:** CACCGTGTTCAGGCATCTCTAGGGC	BbsI
	R: AAACGCCCTAGAGATGCCTGAACAC	BbsI

Table 2-8: Details and sequences of the Sanger FLYWCH1-gRNA constructs used for organoids transduction. Both gRNA target the same exon, one gRNA targets the sense strand, and the other gRNA targets the antisense. PAM is underlined in red (Sigma, UK).

Primer Use	Primer sequence 5'-3'	Gene ID	Exon ID	Restriction Site
FLYWCH1-CRISPR (1st set, on-target locus: chr16:-2990071)	**CCT**GAAAGCCAGCAGATTTATGG	ENSG00000059122	ENSMUSE00001153016	BbsI
FLYWCH1-CRISPR (2nd set, on-target locus: chr16:-2990071)	CCTGAAAGCCAGCAGATTTA**TGG**	ENSG00000059122	ENSMUSE00001153016	BbsI

2.2.2.1.1 Preparation of the sgRNA inserts for cloning

Phosphorylation and annealing of sgRNA oligos (top and bottom strands) were performed according to the Nature protocol (226). In thermocycler, the following strategy was applied: 37°C for 30 min; 95°C for 5 min; and then ramping down the temperature to 25°C by decreasing the temperature 1°C/min. Afterwards, each annealed gRNA set was cloned into the digested backbone plasmids (pSpCas9(BB)-2A-Puro (PX459) V2.0 vector) by restriction-ligation cloning techniques (explained below).

2.2.2.2 Restriction enzyme digestion

DNA plasmids were digested with suitable restriction enzymes (such as EcoRI, NotI, HpaLI, etc.). The choice of the enzyme was determined in accordance with the restriction sites demonstrated in each DNA plasmid map. All enzymes were purchased from New England BioLabs (NEB). Following the manufacturer's instruction, plasmids were incubated under the optimal temperature condition with a suitable buffer mixture. For example, in our experiments, digestion reactions were incubated for 4-6 h at 37°C. A single reaction mixture was

composed of 1 µg/µl of DNA, 1-2 µl of each restriction enzyme and 10 % of suitable NEB buffer, topped up with ddH$_2$O to a final volume of 20 µl.

2.2.2.3 DNA Agarose gel electrophoresis

Following the complete DNA digestion, 1-2 % (w/v) Agarose gel was prepared in 1X Tris Acetate EDTA (TAE, Sigma Aldrich, T9650) buffer. This was achieved by heating the solution in the microwave to dissolve the agarose, before adding 10 µl of Ethidium Bromide (Sigma, E1385). This was then poured into a secured tray and allowed to solidify for 40 min at room temperature. Later, a mixture of 20 µl digested plasmids and 5 µl of 5X loading dye was loaded into each well and run by gel electrophoresis in 1X TAE buffer, at 80 volts for 1 h. To determine the size of DNA plasmids, 1 kb DNA ladder (Bio Labs, NO467G) was used as a loading control. Following gel electrophoresis, the Bio-Rad Gel-Doc EZ system was utilised to visualise the DNA and/or RNA bands. The percentage of agarose gel used was selected based on the product size. The lower % of agarose gives a better resolution for higher molecular weight PCR products and vice versa. For example, 2 - 2.5% agarose gel was prepared for 100–130 bp PCR products, and a 100 bp DNA ladder was used accordingly.

2.2.2.4 DNA ligation

The recombinant DNA constructs or inserts (freshly isolated) were ligated into linearized vectors by overnight incubation with T4-DNA ligase enzyme (NEB, M0202S). For this, the cohesive ends ligation strategy was employed. This was attained by adding one volume of pre-digested plasmid backbone vector into seven volumes of the DNA inserts, and then mixed with 1X T4 DNA ligase buffer

(NEB, # B0202S) and 2 μl T4 DNA ligase enzyme (NEB, # M0202S). Afterwards, an appropriate volume of Nuclease-free water was added to the reaction mixture to make a final volume of 20 μl. The samples were then incubated overnight at 4°C. Lastly, the ligated DNA was amplified by bacterial transformation and further validated by digestion and/or DNA sequencing.

2.2.2.5 DNA extraction from agarose gel

At first, UV-light was utilised to visualise the agarose gel. This enables an accurate removal of the DNA bands out of the agarose gel. Then, the excised piece (the band of interest) was placed into a labelled micro-centrifuge tube. Using the QIAGEN Gel extraction kit, the sample was purified from TAE agarose gel following the manufacturer's instruction. A similar protocol was applied for the purification of PCR products from PCR reactions, with only difference in the volume of capture buffer (500 μl) used. Moreover, to isolate the DNA samples from agarose gel, the gel was first dissolved by heating the tubes in the thermocycler (until complete dissolving). Then, 10 μl of Capture buffer was added to every 10 μg of agarose gel. The capture-buffer-sample mixture was next placed in a Micro-spin column inserted into a collection tube, and incubated for 1 min at RT. This was then centrifuged at 14000 rpm for 30 sec to obtain a pellet, washed with 500 μl of washing Buffer, and followed by another centrifugation at 14000 rpm for 30 sec to dry the pellet. Tubes were then incubated for 1 min at RT before cleansing the left-over proteins and lubricating the DNA sample with 30-50 μl of Elution Buffer. The elution buffer was added directly into the column and incubated for 1 min at RT. Later, the final concentration and purity of extracted DNA was measured by Nanodrop.

2.2.2.6 Standard Polymerase Chain Reaction (PCR)

PCR was performed in a 25 µl reaction mixture containing 1-2 µl of cDNA, 0.25 µl of dNTPs (0.25 mM) (Qiagen, 201913), 5 µl 5x PCR buffer (Promega, M7805), 2 µl of $MgCl_2$ (2 mM) (Promega, M7805), 0.125 µl Taq DNA polymerase (1.25 U) (Promega, M7805), 0.25 µl forward and reverse primers (1 pmol/µl). The mixture was diluted in nuclease-free water to reach a final volume of 25 µl. Next, PCR reactions were incubated in Veriti Thermal Cycler (Applied Biosystems). The PCR reactions were carried out by first heating to 94 °C for 3min, followed by 30-39 cycles of denaturation at 94 °C for 40sec, then annealing at 52-60°C for 40 sec and extension at 72°C for 30-60 sec. A final extension at 72°C was carried out for 10min. Later, PCR products were visualised and validated by agarose gel electrophoresis (Section 2.2.2.3).

2.2.3 Plasmid/vector DNA preparation and manipulation

2.2.3.1 DNA transformation

Plasmids DNAs were transformed into commercially available competent DH5a bacterial cells. For each transformation, 100 ng of DNA was added into 50 µl of competent cells, mixed and incubated on ice for 30 min, and then heat shocked for 1 min at 42°C. Next, the mixture was cooled on ice for 10 min before transferring into a new sterile tube containing 500 µl of Luria Broth (LB) medium. Tubes were then incubated for 1-2 h on a rotary shaker at 37°C. Later, the bacterial mixture was grown in a 5 ml tube contains LB medium supplemented with the suitable antibiotics and incubated for 6 h (or until the mixture becomes cloudy) at 37°C using the shaking incubator (300 rpm). Thereafter, the bacterial growth was

further amplified in 100 ml LB medium supplemented with an appropriate antibiotic [Kanamycin (30 µg/ml) or Ampicillin (50 µg/ml)] and incubated overnight or 16 h in the shaking incubator.

2.2.3.2 DNA Purification (Midi prep)

DNA was isolated and purified using the Midiprep Kit purchased from (Roche, 03143414001) or (QIAGEN Plasmid Midi Kit, 12143). Following the manufacturer's protocol illustrated in Figure 2-1, DNA was extracted and harvested from transformed bacterial cells. The purity and concentration of DNA yield were measured by Nanodrop. This is based on OD at 260 x dilution factor x 50 ng/ul for DNA concentration, and A260A260/A280 ratio for DNA purity.
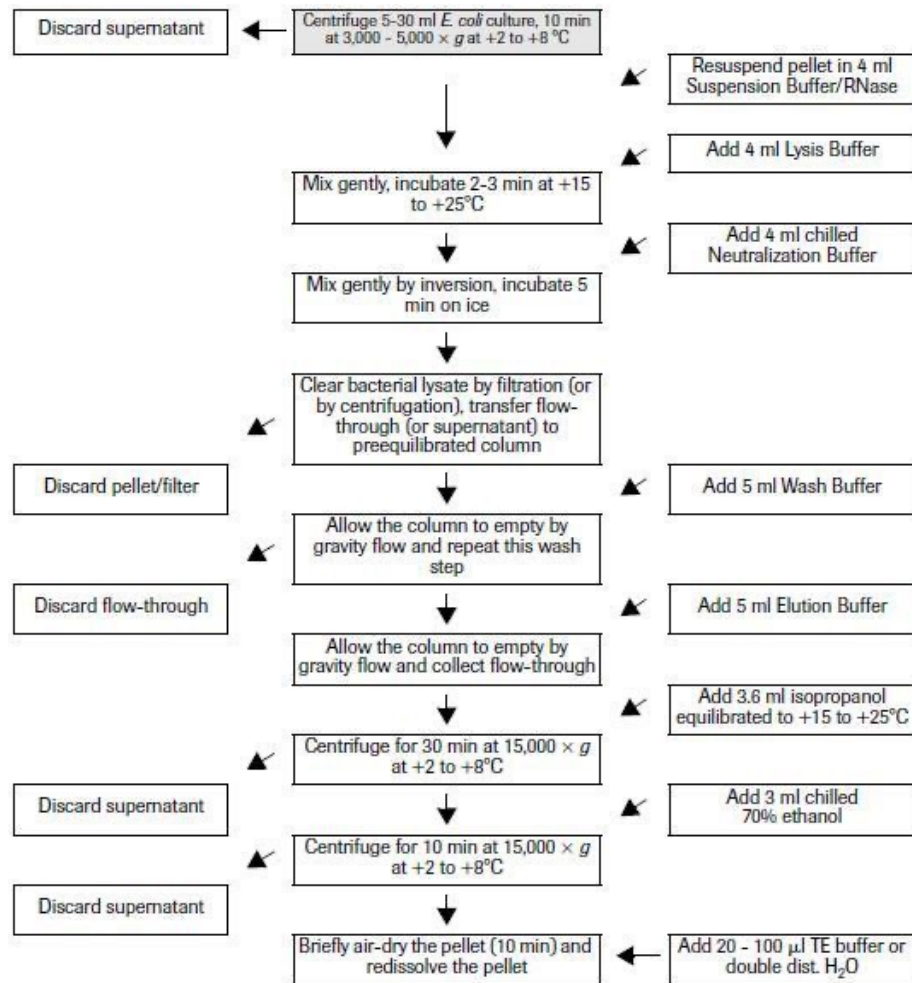
Figure 2-1 Plasmid DNA isolation and purification: the isolation procedure using Roche Genopure Plasmid Midi Kit.

2.2.4 Ribonucleic acid (RNA) isolation and reverse transcription

2.2.4.1 RNA extraction using TRIzol reagent

Total RNA was extracted from cultured cells (10 cm plates) by adding 1 ml of TRIzol reagent into the cells for 5 min at RT. Lysates were next transferred into sterile Eppendorf tubes, and 200 µl of chloroform was added into each tube and mixed vigorously. Tubes were centrifuged at 12000 g at 4°C for 15 min. Afterwards, the upper aqueous phase (containing the RNA) was transferred into a new sterile tube, mixed with 500 µl of isopropanol, and incubated for 10 min at RT. RNA was then

precipitated by centrifuging the tubes at 12000 g for 10 min at 4°C. Later, tubes were washed with 70% absolute ethanol by centrifugation at 7400 g for 8 min. The supernatant was then discarded, the pellet was air-dried, and then re-suspended in 20-50 μl of RNA free distilled water. Finally, the RNA concentration and purity were measured by Nanodrop and stored at -80°C for later use.

2.2.4.2 RNA extraction using RNeasy Mini kit

Total RNA was extracted from colonospheres or organoids by using the Qiagen RNeasy Mini Kit (Qiagen, 74104). According to the manufacturer's instructions, cells were first lysed directly with an appropriate amount of RLT buffer, then homogenized and centrifuged for 3 min at maximum speed (16000 rpm). The supernatant was transferred into a new labelled tube and 70% ethanol was added to the lysate to provide ideal binding conditions. The mixture was then loaded onto the RNeasy silica-membrane (RNeasy Mini spin column) and centrifuged briefly for 15 sec. All contaminants were efficiently washed away by centrifugation steps and RW1 and RPE washing buffers at this stage. After washing, the flow-through was discarded, and the column (contains RNA with up to 100 μg capacity) was transferred into a new collection tube. The pure and concentrated RNA was eluted in 30–100 μl RNase free water by final centrifugation. The RNA concentrations was measured by Nanodrop and samples then stored at -80°C for later use.

2.2.4.3 Reverse transcription (RT)

For cDNA synthesis, PrimeScript RT Reagent Kit (Perfect Real Time, Takara-Clontech Laboratories, RR037A) was utilised following the manufacturer's

instructions. Briefly, 0.5-2 µg of total RNA was added into a mixture of 1x Prime

Script buffer, 25 pmol of oligo dT primers, 50 pmol of random six-mers primers,

0.5 µl of reverse transcription (RT) enzyme. The volume was topped up with RNase

free distilled water to a final volume of 20 µl (Invitrogen, 10977035). The reaction

mixture was then incubated at 37°C for 15 min, followed by 5 sec at 85°C to

inactivate the reverse transcriptase and stop the reaction. All cDNA samples were

stored at -20°C for later use.

2.2.4.4. Quantitative real-time PCR (qPCR)

For different purposes, quantitative real-time PCR was implemented to measure

the gene expression changes at the mRNA level. First, Primers were designed using

Primer3 and Blast design tool available at

http://www.ncbi.nlm.nih.gov/tools/primer-blast/. Principally, primers were

designed to target two consecutive exons within the gene of interest (to prevent

amplification of contaminating genomic DNA), and to amplify a region of 100-200

bp of size. NCB1 blast tool was then employed to validate the specificity of the

designed primers.

To make the PCR reaction, a master mix was composed of 2 µl of cDNA (10x

diluted), 10 µl of LightCycler 480 SYBR Green I Master (Roche, 04707516001), 1 µL

of reverse and forward primers, and 6 µl of DNase/RNase free water for a final

volume of 20 µl. Reactions were performed in triplicates per sample using a 96

well plate provided by Roche (LightCycler® 480 Multi-well plate 96). According to

the manufacturer's instructions, the plate was run under appropriate

amplification parameters. The expression of housekeeping genes β-actin or

glyceraldehyde 3-phosphate dehydrogenase (GAPDH) housekeeping genes was

measured as an internal control for data normalization. All primers used in this study are listed in Table 2-5. The qRT-PCR data were analysed using the comparative Ct ($2\text{-}\Delta\Delta CT$) method, in which the Ct values obtained from two different experimental RNA samples (control and experimental) are directly normalized to a housekeeping gene and then compared (228). Threshold cycle (Ct) values were calculated and generated by light-cycler 480 II software (Roche), and further data analysis was performed using GraphPad Prism 8 software.

2.2.4.5. RT2-profiler PCR arrays-Pathway-focused PCR array for gene expression profiling

To analyse the gene-expression profile, the Human WNR Signaling RT2 Profiler™ PCR Array (QIAGEN, Cat. no. PAHS-043Z) and Stem Cell Signaling RT2 Profiler PCR Array (QIAGEN, Cat. no. PAHS-047Z) were utilised according to the manufacturer's instructions. Every array contains 84 genes from each signaling pathway. Five housekeeping genes [beta-2-microglobulin (B2M), hypoxanthine phosphoribosyltransferase 1 (HPRT1), ribosomal protein L13a (RPL13A), glyceraldehyde-3-phosphate dehydrogenase (GAPDH), actin beta (ACTB)] and controls were incorporated in the array for genomic DNA contamination detection, RNA quality, and general PCR performance. (A complete list of genes contained in the plate is available from the manufacturer website). Predominantly, the thermal cycling was performed using Real-Time PCR system (LightCycler® 480 software, Roche) under the following conditions: 10 minutes at 95°C, and 40 cycles of 15 seconds at 95°C, and one minute at 60°C. For quality control, fold changes in the gene expression and statistical analysis (two-tailed Student's *t*-test with the significance threshold set to P<0.05) was analysed using

RT2 Profiler PCR Array Data Analysis Workbook (Qiagen data analysis web portal at http://www.qiagen.com/geneglobe). A validation assay was then achieved by qPCR for a differential gene expression pattern of 10 selected genes.

2.2.5 Protein biochemistry techniques

2.2.5.1 Protein extraction

For total protein lysate, cultured cells were first washed once in a cold PBS to remove any residual medium, scraped and collected into sterile labelled Eppendorf tubes. Cells were pelleted by centrifugation at 1500 rpm for 5 min and the pellet was then lysed directly by adding 500-800 µl of RIPA buffer (Sigma, R0278), supplemented with 1X Protease inhibitor cocktail (Sigma, P8340). Tubes were placed on ice and mixed every 5-10 min for 30 min followed by centrifugation at 14000 rpm for 15 min at 4°C. Supernatants enriched with protein lysates were then collected into sterile tubes and stored in -20°C for later use.

2.2.5.2 Sub-cellular fractionation

Nuclear/cytosol protein separation was performed using the Bio-Vision Nuclear/cytosol fractionation kit (K266-25). This kit is composed of 3 main buffers: Cytosol Extraction Buffer A (CEB-A), Cytosol Extraction Buffer B (CEB-B), and Nuclear Extraction Buffer (NEB).

First, CEB-A and NEB-A buffer mixtures were prepared separately by adding protease inhibitor cocktail and DTT (For each ml of buffer, 2 µl of 1x protease inhibitor, and 1 µl of DTT (1M) were added and mixed gently). Following the manufacture's protocol, cells were washed from any residual medium and

collected by centrifugation. The pellet was first re-suspended in 0.2 ml of CEB-A buffer mix, vortexed for 20 sec and kept on ice for 10min. After incubation, 11 µl of ice-cold CEB-B buffer was added into the mixture, kept on ice and vortexed vigorously for 15 sec. To separate the cytosolic protein, the sample was centrifuged at the highest speed 16000xg at 4°C for 5 min, and the supernatant (contains the cytosolic fraction) was transferred into a sterile labelled Eppendorf tube. For nuclear fraction, on ice, the pellet was re-suspended in 100 µl of NEB-A buffer and mixed vigorously by vortexing the sample every 5-10 min for 40 min. Later, the tube was centrifuged for 15 min at 16000xg at 4°C, and the nuclear protein was collected into a sterile Eppendorf tube and stored at -20°C for short term storage or -80°C for long term storage.

2.2.5.3 Protein quantification BSA-assay

The extracted proteins (total protein or sub-cellular fraction proteins) were quantified utilising the Bio-Rad protein Assay reagent. First, BSA standards with concentrations ranging from 0.05-0.25 µg/µl were prepared by diluting Bovine Serum Albumin (BSA, Sigma 4503, stock concentration 1 mg/ml) in different volumes of distilled water. The lysates were then diluted (1:30 or 1:20 dilution), depending on the expected protein yield. Later, 20 µl of each standard or protein sample was loaded (in triplicate) in a 96-well microplate (Scientific Laboratory Supplies) and mixed with 200 µl of the diluted Bradford solution (1:5). Subsequently, the absorbance of each sample was measured at a wavelength of 595-620 nm, by Magellan software provided within the TECAN machine. Finally, a BSA standard curve was generated in an Excel sheet, and the average concentration of proteins was calculated accordingly.

2.2.5.4 Western blotting (WB) analysis

For WB analysis, protein samples were first prepared by mixing the cell lysates (50-100 µg) with the appropriate amount of 5X loading buffer. The samples were denaturized by heating at 95°C for 5 min, then cooled briefly on ice before loading into 4-20% or 10% Mini-PROTEAN TGX Precast Protein Gels (Bio-Rad, 4561096). A Pre-stained colour plus protein ladder (Bio-Rad, UK) was used as a molecular marker to determine the molecular mass of the protein bands. Electrophoresis of SDS PAGE gel was carried out at 80-100V for 1-1.5 h, in 1X TGS running buffer (Tris/Glycine/SDS). Subsequently, gels were transferred into a polyvinylidene difluoride PVDF membrane for 30 min at 15V, via the semi-dry Electrophoretic transfer cell (Bio-Rad, UK). The membrane was then blocked for 1h with 5% skimmed milk powder dissolved in Tris-Buffered Saline, 0.1% Tween-20 (Sigma, 1379) (TBS-T) buffer. After blocking, the membrane was washed in TBST and probed with the recommended concentration of primary antibodies (1:500-1:1000, diluted in 1% BSA in TBST) for overnight, at 4°C and under constant rotation. The following day, the membrane was washed in TBST and incubated with a compatible anti-mouse, rabbit, or goat secondary Ab for 1h at RT. As suitable, antibodies against β-actin, β-tubulin, or Histone H3 were used as a loading control.

2.2.5.5 Co-Immunoprecipitation (co-IP) assays

For the analysis of protein-protein interactions and *in-vitro* Ubiquitination/Phosphorylation assays, Pure Proteome Protein A and G Magnetic beads (Merck Millipore, LSKMAGG02) were used to pull down the protein of interest. First, 50-60 µl of homogenized bead suspension was added into a labelled

1.5 ml Eppendorf tube, placed on the Dynal MPC magnetic stand to capture the magnetic beads. At first, the storage buffer was discarded by aspiration. The beads were then washed 3 times with 1 ml PBS-tween (0.01-0.1% tween20 in PBS) by disengaging the beads from the stand and mixing with the washing buffer at least 3 times. After the last wash, the beads were re-suspended in 100 µl of PBS-T, and a volume equal to 6-8 µg of primary antibody was added and mixed well with beads. The mixture was kept at 4°C for 4 hours under continuous mixing to capture the immune complex. Later, the tubes were placed on the magnetic rack to capture the beads-Ab complex, the buffer was discarded, and the complex was then washed twice in PBS-T to remove unbound beads. Afterwards, 400-500 µg of the protein lysate was added and mixed well with the beads-Ab complex by pipetting. The tubes were incubated overnight at 4°C on a rotary shaker. After overnight incubation, the beads-immune complexes were re-engaged using the magnetic stand, while the non-crosslinked Ab/beads were washed out after three washes in PBST. Finally, the immune-precipitated complex was dissociated from the beads by adding RIBA buffer. Thence, the eluted samples were transferred into new tubes, denatured by mixing and heating with the loading buffer at 95°C, before proceeding with WB for IP validation and co-I result analysis.

2.2.6 Functional analysis

2.2.6.1 Colonosphere formation efficiency assay

The formation of colonospheres derived from SW620 control and FLYWCH1^{KO} cells was examined as described by (229). Briefly, cells were seeded equally into a 6-well plate (1000 cells/well), in triplicate, and cultured in (DMEM/F-12) medium

supplemented with 1 U/ml penicillin/streptomycin antibiotics, 10 ng/ml human recombinant basic fibroblast growth factor (bFGF), 10 ng/ml human recombinant epidermal growth factor (EGF) and 100 X N-2 supplements, and incubated in a 5% CO_2 incubator at 37°C. Stem cell medium was only partially replaced (about one-third) every 3- 4 days. On day 14, well defined colonospheres were subjected to microscopic analysis and further immunofluorescence studies. For IF staining, colonies were fixed with 4% paraformaldehyde for 10 minutes at room temperature and stained with CD44 antibody. The number of colonospheres ranging between 50–250 μm diameters was counted using a DMI3000 B fluorescence microscope (Leica Microsystems), and the percentage of colonospheres was calculated and analysed using Microsoft Office Excel 2007.

2.2.6.2 Luciferase reporter assay

Herein, R-spondin1 and Wnt-3a conditioned media were validated by the TOP/FOP flash dual-luciferase reporter assay system (Promega, E1910), following the previously described protocol (230). Using two plasmids: *A)* TOP-flash plasmid, a luciferase reporter plasmid containing two sets of three copies of the TCF/LEF binding site upstream of a Firefly luciferase reporter gene (Promega, E1910). *B)* FOP-flash plasmid, a negative control, contains three mutated copies of the TCF/LEF binding site. Additionally, as an internal control, a vector carrying constitutively active Renilla luciferase gene was employed. First, HEK293T cells were seeded into a 24-well plate (in triplicate) and kept overnight in a humidified, 37°C, 5% CO_2 incubator. On the next day, cells were transiently transfected with Renilla luciferase vector (0.05 μg DNA/well) together with either TOP-flash or FOP-flash (0.2 μg DNA/well) for 6-8 h. Later, the transfection mixture was discarded

and replaced with R-Spondin 1/Wnt3A conditioned medium. At this stage, cells were incubated for 48 h before analysing the luciferase activity.

Following the manufacturer's instructions, the cell monolayer was first washed with a cold PBS and then lysed with the passive lysate buffer included in the kit. Approximately 10 μl of each lysate was loaded (in triplicate) in a 96-well plate (Thermo Fisher Scientific, MPA-560-040A). Next, a 50 μl/well of Luciferase Assay Reagent II (LAR II) was added, and the bioluminescence produced was detected using the Luminoskan Ascent Microplate Luminometer (Thermo Fisher Scientific, UK). Additionally, the activity of the internal control or Renilla luciferase activity was examined, after adding 50 μl/well of Stop and Glo® Reagent into the corresponding wells. Later, data were exported into Microsoft Office Excel and analysed by first normalising the firefly luciferase reading to the Renilla luciferase readings and then to the activity of the control samples.

2.2.6.3 Wound healing assay

The wound-healing assay was performed as described previously (231). Briefly, SW620 cells (GFP control and FLYWCH[KO]) were seeded in a 6-well plate (in triplicate) and cultured in a complete medium. 80-90% of Confluent cells were then starved overnight in a serum-free medium to synchronise the cell cycle status (232). Later, using a sterile 200 μl pipette tip, three parallel straight wounds were created in each well. Any detached cells were washed gently with PBS twice, before adding a complete growth medium containing 10% FBS. For time 0, cells were examined under the microscope, immediately after the wound creation, using a phase-contrast and GFP filter with the 10X lens fluorescence microscope (DMI3000, Leica Microsystems). Cells were imaged again after 24 h and 48 h for

each time point. Finally, quantitative analysis was performed using Image J software. The distance between each side of the scratch was measured in each image using the Freehand Selections command of the Image J software at the different time intervals (e.g. 0, 24 and 48 hours). The rate of cell migration under the experimental condition was determined by comparing the averaged percentage of cell movement obtained from at least three readings/well.

2.2.6.4 WST-1 Cell Proliferation Assay

Following the manufactures' protocol, tumour organoids viability and proliferation in response to GSK-3B inhibitor (BIO) and/or FLYWCH[OE] was measured by WST-1 cell proliferation assay (Roche, UK). The assay is based on the cleavage of a tetrazolium salt, MTS, by mitochondrial dehydrogenase. Here, control tumour organoids and FLYWCH1-expressing Organoids were treated with 5 µM of BIO for 48 h. Later, WST-1 reagent (11 644 807 001, Roche) was added and incubated for 2 h, the medium was then aspirated and transferred into another 96 well-plate, and the absorbance was measured at a wavelength of 450 nm by Magellan software provided within TECAN (ELISA) reader. Tumour organoid medium was used as a blank control.

2.2.7 Immunofluorescence (IF) staining

IF assay was used to visualise the expression pattern, location, and the distribution of a specific protein within the cell. For IF staining, an appropriate number of cells were cultured on sterile coverslips, placed in a 6 or 12 well- plate. Depending on the nature of experiments, seeded cells were transfected or treated as required. After overnight incubation, growth medium was discarded, cultured cells were

washed twice in a cold PBS, and fixed in 4% Paraformaldehyde (PFA, diluted from a 16 % stock solution in PBS), (Avocado, 043368) for 30 min at RT. The fixed cells were then washed twice in PBS and permeabilized at RT for another 30 min using 0.1% TritonX-100 (diluted in PBS). The permeabilization buffer was then aspirated and cells were washed again with PBS for 5 min.

To avoid non-specific bindings, cells were blocked with 3% Bovine Serum Albumin (BSA prepared in PBS) for 1 h, at RT. Afterwards, cells were washed once with PBS and incubated overnight with an appropriate concentration of the primary antibody diluted in 2% BSA-PBS at 4°C. The day after, cells were washed (at least 4 washes, 5 min each) in a special washing buffer composed of 0.1% PBS-Tween20, and prepared in 1% BSA. Cells were then incubated with an appropriate volume of secondary antibody diluted in 2% BSA-PBS (1:400 µl), covered with aluminium foil and kept in the dark for 1 hour at RT. Next, the immunostained cells were washed 4-5 times (5 min each) in the same washing buffer. Finally, coverslips were gently removed with forceps and placed upside down on a clean-labelled slide contains a drop of DAPI Gold anti-fade mounting medium. Slides were sealed with nail varnish and allowed to dry (in a dark and cool atmosphere) before microscopic examination.

2.2.8 Phalloidin staining

Phalloidin is a commonly used dye for cytoskeletal and morphological analysis. This dye has a strong binding affinity to F-actin that enables the display of the cell shape (233). Cells were initially grown on sterile coverslips, fixed, and permeabilized with 0.1% Triton X-100, using the same approach explained above.

Following permeabilization, the cells were incubated (in the dark) with a diluted (50 µg/ml in PBS) fluorochrome-conjugated Phalloidin conjugate solution (Sigma-Aldrich, 1951) for 40 min at room temperature. Subsequently, cells were washed twice or thrice with PBS (5 min per wash), before mounting the coverslips upside down on a slide with a drop of DAPI.

2.2.9. Organoids culture

2.2.9.1 Noggin conditioned medium by transient transfections in HEK293T cells

HEK293 cells were cultured and maintained for (at least) 2 passages in 75T flasks, then sub-cultured into 10X 10 cm^2 dishes and maintained overnight in RPMI+10% FBS. Around 80-90% confluent cells were transiently transfected with 15 µg pcDNA3-neo-mouse Noggin-Fc (234), using PIE reagent as outlined above (See section 2.2.1.5). Later, the medium was replaced with an advanced DMEM/F-12 (Gibco, 12634010), supplemented with 10% FBS, 2 mM L-glutamine and 100 U/ml Penicillin/Streptomycin, and left for one week in a humidified, 37°C, 5% CO$_2$ incubator. The Noggin conditioned medium was then collected in falcon tubes, centrifuged at 400rpm for 5 min and the supernatant was filtered via 0.22 µm filters, aliquoted and stored at -80°C. Afterwards, the produced Noggin protein was validated with WB analysis by loading 25 µl of the conditioned medium mixed with 5X loading buffer directly into a 10% precast gel. DMEM medium mixed with loading buffer was loaded in a single well and used as a negative control.

2.2.9.2 Preparation of R-Spondin 1 conditioned medium

R-spondin1 stable cells (293T-HA-Rspo1-Fc) were thawed and initially cultured in a 75 cm^2 flask in DMEM growth medium without Zeocin. Later, confluent cells were sub-cultured into 5 x 75T flasks and maintained in DMEM supplemented with 300 µg/ml Zeocin for selection. After 3 days, the medium was replaced with serum-free conditioned medium (Advanced DMEM F12, supplemented with 100 U/ml penicillin/streptomycin (Invitrogen, 15140-122), 2mM L-glutamine (Invitrogen, 25030-024), and 5 mL HEPES from 1M stock (Invitrogen, 15630-122)). Cells were kept in culture for another week prior to the harvesting of R-spondin1 conditioned medium. At the day of harvesting, the medium was collected, centrifuged to precipitate any debris and dead cells, the supernatant was then filtered using 0.22 µm filter, aliquoted, and stored in -80 or -20°C for short storage.

2.2.9.3 Wnt-3a conditioned medium

For Wnt-3a production, 293T-HA-L-cells stably expressing Wnt-3a were recovered from the liquid nitrogen, cultured in DMEM medium supplemented with 20% FBS, pen/strep and Zeocin (1.25 µl/ml). On the first passage, confluent cells were sub-cultured into 5 x T75 cm^2 flasks and maintained in DMEM (without Zeocin) for 3-4 days. Later, confluent cells were trypsinized, pooled in 600 ml of medium without Zeocin, and then distributed equally into 30x150 cm^2 dishes (20 ml/dish). One week later, the conditioned medium was harvested, centrifuged, and filtered. Wnt-3a conditioned medium was then aliquoted into 25 ml tubes and stored at -20°C.

2.2.9.4 Small intestinal crypts isolation and organoid culture

In this study, organoids were grown from small intestinal crypts isolated from a normal or tumour human colon mucosa provided from tissue banking. All procedures were conducted following the Declaration of Helsinki and local ethics committee approval. Organoids were cultured as previously established and characterized in our lab (235, 236). The tissue was cut into pieces of around 5-10 mm, sterilized in 0.04% sodium hypochlorite for 15 minutes at room temperature, and then washed once in PBS. The tissue fragments were then collected into a 15 ml centrifuge tube, washed with a cold PBS 3-4 times (or until the PBS become clear) by mixing and inverting the tube several times. After the last wash, the crypts and villi were separated by chelation (the chelation reagent composed of 3 mM EDTA + 0.05 mM DTT in PBS). This was achieved by adding and mixing a 25 ml of the EDTA/DTT solution with the sample for 45-90 minutes at 4°C under continuous agitation. Later, EDTA/DTT solution was removed and replaced with a 15 ml sterile PBS. The tube was tightly sealed and mixed vigorously for 30 seconds, then the PBS was replaced with a fresh PBS (10 ml). This process was repeated at least 3 times. Next, the tube was centrifuged briefly at 400rcf for 2 min, and the supernatant was partially and carefully aspirated (leaving about 400 µl). Samples were kept on ice, and 20-25 µl of the pelleted or concentrated crypts were gently distributed into Eppendorf tubes containing 150 µl of Matrigel (Corning® Matrigel® Growth Factor Reduced (GFR) Basement Membrane Matrix, *LDEV-Free) (Corning®, 356230), and mixed slowly. Afterwards, 20 µl of the mixture (crypts-containing Matrigel) was loaded directly into a pre-warm 48-well plate (at the canter of each well), and the plate was then kept in a 37°C, 5% CO_2 incubator

for 5 min to solidify the Matrigel. Finally, a freshly prepared organoid culture medium was added (250-300 µl/well), (Table 2-9, 2-10). Crypts were maintained in a humidified, 37°C, 5% CO_2 incubator, checked visually by inverted microscope and the organoid medium was replaced with a fresh one every 48 h.

Table 2-9: Mice intestinal organoid medium components.

Component	Final concentration/ for 10 ml total volume	Supplier
advanced DMEM/F12	8 ml DMEM/F12 supplemented with 2mM L-glutamine, 100U/ml Penicillin/Streptomycin and 10mM HEPES	Invitrogen, 12634-028
N2 supplement	250 µl, 1x Supplement	Invitrogen, 17502-048
B27 supplement (1x)	200 µl, x50 stock	Invitrogen, 12587-010
N-acetylcysteine	1 mM, stock 500mM	Sigma Aldrich, A9165
murine recombinant epidermal growth factor (mEGF)	50 ng/ml	Invitrogen, PMG8043
R-spondin	1 µg/ml	In-house CM
Noggin	100 ng/ml	In-house CM

Table 2-10: Medium preparation for culturing patient-derived tumour organoids.

Component	Final concentration/ for total volume (10ml)	Supplier
Advanced DMEM/F12	Supplemented with 2mM L-glutamine, 100U/ml Penicillin/Streptomycin and 10mM HEPES	Invitrogen, 12634-028 Invitrogen, 15630-122
R-spondin-CM	20%	In-house CM
Noggin	20%	In-house CM
B27	2% (200 µl, x50 stock)	Invitrogen, 12587-010
n-Acetyl Cysteine	5 µl of 1.25 mM	Sigma, A9165
Nicotinamide	50 µl of 10 mM	Sigma, 98-92-0
EGF	5 µl of (100 µg/ml)	Sigma, E4127
A83-01 (TGF-β inhibitor)	1 µl of 0.5 µM	Tocris, 2939
SB202190 (p38 inhibitor)	1 µl of 3 µM	Sigma, S7067
Primocin	20 µl (100 µg/ml)	InvivoGen, ant-pm-1

2.2.9.5 Transduction and generation of stable organoid lines

For lentivirus particles production, HEK293-T cells were used as explained above (Section 2.2.1.6). Both primary patient-derived and mouse intestinal organoids were infected by lentiviral transduction according to the published protocol (237). Briefly, organoids were seeded into enough wells prior to the LV-transduction

(typically 10 confluent organoids per well, and at least 4 wells were used per transduction). On the day of transduction, organoids were collected and washed thrice in a chilled PBS to clear the Matrigel, by gentle mixing and centrifugation (3 min for 300xg). After the last wash, the pellet was dissociated from any basement matrix residue and resuspended in a fresh PBS to break down the organoids into small fragments using a 200 µl pipette. After a gentle centrifugation, the final pellet was resuspended in LV-particles mixed with polybrene. (For this experiment, virus particles were diluted in an appropriate organoid medium upon precipitation). To maximize the transduction efficacy, the mixture was incubated for 6 h in the 37°C, 5% CO2 incubator under continuous agitation (by gentle pipetting, every 45 min). Afterwards, transduced organoids were centrifuged for 3 min at 300xg, and the supernatant was discarded carefully. The pellet was then mixed in the basement matrix and seeded in a 48 well-plate (25 µl / well). After 5 min of incubation, a fresh complete organoid medium was added and the plate was incubated in a humidified, 37°C, 5% CO_2 incubator. Two-days post-transduction, the infected organoids were selected using puromycin (1 µg/µl) for 5 days (only PDOs were selected with puromycin). Non-transduced organoids were served as negative control samples. Later, survived, (or stably transduced) organoids were expanded in a free-antibiotic organoid medium, and the medium was carefully changed every 2 days. Subsequently, organoids growth and morphology were monitored by Leica DMI3000 B Manual Inverted Microscope throughout their culture.

2.2.10 Histological analysis of the organoids

2.2.10.1 Organoids preparation for histological analysis

Prior to histological analysis, the transduced mice intestinal organoids were first washed gently with enough volume of PBS, and then fixed in 4% paraformaldehyde (PFA) overnight at 4°C. On the following day, the fixative was aspirated carefully, and the organoids were collected in 15ml tubes and washed twice with PBS by centrifugation. The final pellet was carefully resuspended in a 2% Low-melting agarose (Sigma Aldrich, A9045), and stored in enough volume of 70% absolute ethanol. Subsequently, for the paraffin embedding, organoids were placed gently into several histology cassettes and samples were then dehydrated by Leica TP1020 semi-enclosed benchtop tissue processor, via automatic passages from ethanol (70%, 90% and 100%) to methanol, xylene and, lastly, paraffin. Afterwards, the blocks were sectioned into 4 µm-thick sections using a microtome and placed onto labelled polylysine glass slides (231).

2.2.10.2 Haematoxylin and eosin (H&E) stain

Haematoxylin and eosin (H&E) stain is a fundamental technique used to examine the structure of normal and pathological tissues. Haematoxylin stains different basophilic molecules within the cells (such as nucleic acids) in blue-purple colour. Whereas Eosin stains the basic compounds (such as cytoplasmic proteins) in pink-orange colour. Briefly, slides were processed for immunohistochemistry analysis or Hematoxylin and Eosin (H&E) staining as previously reported (238). First, the slides were dewaxed in two xylene chambers for 5 mins each, rehydrated with 100%, 90% and 70% ethanol containers, for 2 min each and then rinsed under

running tap water for 1 min. Next, sections were immersed in a pre-filtered Haemalum (Thermo Fisher Scientific, LAMB-170-E) chamber for 3 mins, washed under the running tap water for 1 min, and then stained with a pre-filtered Eosin (Thermo Fisher Scientific, LAMB-100-D) for 3 mins. This followed by dehydrating the sections in three gradual 70-100% ethanol chambers (1 min each), and two xylene containers (3 mins each). Lastly, the slides were mounted with DPX (Sigma Aldrich, 317616) neutral mounting medium and examined under the microscope.

2.2.10.3 Immunohistochemistry (IHC) staining and quantification of the organoids

Immunohistochemistry (IHC) combines histological, immunological, and biochemical techniques to evaluate a particular molecule/protein expression within the tissues. This is mainly achieved via the formation and detection of antigen (target protein)-antibody complexes (239). As outlined for H&E staining, slides were dewaxed, rehydrated, and briefly rinsed in a distilled water (dH$_2$O). Antigen retrieval was then achieved by placing the sections into a pre-heated citrate buffer pH 6 (Sigma Aldrich, 25114) for 15 mins in the microwave. The sections were then cooled to room temperature (RT). Next, the endogenous peroxidase activity in tissue samples was blocked with 1.6 % H$_2$O$_2$ (Scientific Laboratory Supplies, CHE2194), prepared in PBS for 10 mins. To terminate the reaction, samples were washed with distilled water for 5 mins. Importantly, using the Dako pen (Vector Laboratories, H-4000), the samples were carefully confined within an invisible hydrophobic barrier. For blocking, slides were incubated for 30 min at RT in a 10% serum (derived from the host animal of the secondary

antibody), prepared in 1% bovine serum albumin/PBS (BSA, Sigma Aldrich, 4503) to minimise background staining. Afterwards, the slides were incubated overnight at 4°C, with an appropriate concentration of the primary antibody (Ki67 1:200, FLYWCH1 1:300 and GSK-3β 1:250) diluted in 1% BSA/PBS. On the next day, slides were washed thrice in PBS (5 mins each), and the suitable biotinylated secondary antibody was applied for 45 mins at RT. During incubation with secondary antibody, avidin-biotin-peroxidase complex (ABC, Vector Laboratories, PK-6100) was prepared according to the manufacturer's instructions and then added to the slides for 30 mins at RT. At least three washes with PBS followed this. For protein visualisation, the chromogenic reaction was catalysed using DAB substrate solution (Vector Laboratories SK-4100). Sections were monitored under the microscope to develop the brown staining, and the DAB reaction was immediately terminated by distilled water. Lastly, sections were counterstained with Mayer's Haematoxylin (Thermo Fisher Scientific, LAMB-170-E), dehydrated, cleared in xylene, and mounted as described above for H&E stain.

2.2.11 TMA Immunohistochemical Analysis and H-scoring

TMA Immunohistochemical staining for FLYWCH1 and GSK-3β carried out in a collaboration with the Histopathology unit, City hospital, University of Nottingham, as outlined in 2.2.10.3. The stained slides were then scanned at 20x magnification using VENTANA DP 200 slide scanner (ROCHE, UK) and the images were analysed using QuPath software. The staining intensity was scored by H-scoring system and calculated as previously described by (240). The H-score is ranged from 0 to 300, using the formula: (1 × % weakly stained nuclei) + (2 × %

moderately stained nuclei) + (3 × % strongly stained nuclei). All cases were scored blindly without prior knowledge of the patients' pathological or outcome data. Furthermore, cores with less than 15% of invasive tumour tissue or intact (epithelial) were excluded (i.e. not scored). Double Scoring and interclass correlation coefficient (ICC) test were independently verified by our collaborator Abrar Aljohani, The city hospital, University of Nottingham.

2.2.12 Statistical analysis

Statistical analyses were obtained by Student's *t*-test, or analysis of variance (ANOVA), using GraphPad Prism 8 software or Microsoft Office Excel. For image analysis, Fiji (Image-J) software was used. The statistically tested experiments were repeated in three independent times, and the results are shown as mean ± standard deviation (STDEV). The P-value of ≤ 0.05 was considered statistically significant unless otherwise stated.

CHAPTER 3

Roles of FLYWCH1 in Intestinal Crypt Growth and CRC

3.1 SUMMARY

The intestinal epithelium is one of the most dynamically renewing tissues, within 5-7 days, the entire epithelial layer can be renewed (241). In the mammalian intestine, stem cells are located in the intestinal crypts (63). They can replenish the whole crypt-villus axis, generating all differentiated cell types that are required for various physiological functions of the intestine (242). Predominantly, four main signaling pathways govern the maintenance of stem cells; these are the Wnt, Notch, Hedgehog, and BMP signaling pathway. However, Wnt signaling is the main driving force for crypt proliferation (243). Moreover, secretion of Wnt3 from Paneth cells and ISC-expression of R-spondin1 create the WNT/β-catenin gradient along the crypt-villus axis (243-245). Several regulators tightly maintain this gradient to restrict Wnt-signals, such as Axin2 (246), RNF43 (247), and APCDD1 (248). Some of these examples are stem cell-expressed-Wnt target genes that simultaneously act as negative feedback regulators to tune the Wnt/β-catenin and maintain ISC homeostasis. Additionally, these regulators are considered as tumour suppressors in various cancers (249).

Human FLYWCH1 was first identified in Dr Nateri's lab as a nuclear β-catenin interacting protein that negatively modulates the transcriptional activity of β-catenin (198). Notably, murine *Flywch1* mRNA was detected in the crypt-based cells using in-situ hybridization (ISH) assay in normal intestinal tissues (Data not shown, personal communication to Dr Nateri) and normal adjacent adenoma tissues in the *Apc*Min mouse intestinal tumour model (Chapter 1, Figure 1-12). However, this was undetectable in the differentiated epithelial cells of intestinal

villi, and *Flywch*1 expression was highly decreased in cancer cells (Chapter 1, Figure 1-12). Moreover, a negative correlation between *FLYWCH*1 expression and tumour staging was detected in 149 CRCs samples using ISH assay on a tissue microarray (TMA) (198). Therefore, this led to a hypothesis that tumour cells have developed a mechanism(s) to suppress FLYWCH1 expression in both cancer and differentiated cells in the intestine. However, the role of FLYWCH1 and how FLYWCH1 expression is regulated in normal versus cancer cells were unknown. Having a robust model that can recapitulate the *in-vivo* intestinal tissue structure is indispensable to enhance our understanding of FLYWCH1 function and mechanism of action. Recently, long-term 3-dimensional (3D) organoid culture systems became available from both normal and tumour tissues, maintaining the basic crypt and intestinal epithelial cells (236, 250-252). Hence, in this chapter, we utilised murine intestinal and CRC patient-derived organoids (CRC PDOs) to understand the roles of FLYWCH1 in the context of Wnt-driven activities involved in intestinal homeostasis and tumorigenesis. Moreover, we applied multiple CRC cancer cell lines to explore the molecular details and mechanism(s) of FLYWCH1 functions and regulation. In parallel, we aimed to uncover the potential clinical relevance of FLYWCH1 expression including its cellular localisation in CRC patients using tissue microarray (TMA) and immunohistochemistry (IHC) analyses.

In brief, the data in this chapter suggest that;

- FLYWCH1 regulates crypt's cells growth and proliferation based on the analysis of proliferation specific marker (Ki-67) and the significant morphological defects in murine intestinal organoids.

- In CRC PDOs, FLYWCH1 over-expression revealed a significant potential in suppressing the organoids size and growth.

- In contrast, knockout of FLYWCH1 enhances the colonosphere forming efficiency and cancer stem cell markers in SW620 cells.

- Alteration of FLWYCH1 expression changes the transcriptional signatures of selected intestinal and CRC stem cells markers and Wnt target genes.

- Wnt activation by Wnt-3A or BIO (GSK-3β inhibitor) significantly decreased the endogenous FLYWCH1 expression in cultured cells.

- Further biochemical analysis suggested that the Wnt signaling regulates FLYWCH1 stability and cellular distribution.

- The CRC TMA-immunohistochemistry analyses suggest that FLYWCH1 expression may significantly affect CRC staging, and this can be correlated with its cellular localisation and the expression of GSK-3β.

3.2 RESULTS

3.2.1 *Flywch*1 expression is critical for the murine intestinal organoid growth

Our lab has previously established culture conditions to grow and maintain both mouse and human colonic organoids from normal and tumour intestinal/ colon tissues and genetically manipulate them (198, 253-255). Following the established protocol, essential organoid culture components were first prepared and validated to be used throughout the project. To investigate the functional role of FLYWCH1 in the murine intestinal organoids, we have initially knockout (KO) the

Flywch1 gene by transduction of lentivirus particles expressing Flywch1-single guide RNA (gRNA) into the Cas9-expressing intestinal organoids. The Cas9-expressing intestinal organoid line was generated using pLv5-Cas9-Neo lentiviral transduction by Dr Hossein Kashfi in our lab (255). The Flywch1-gRNA was targeting both mouse and human FLYWCH1 genes (gRNA details and sequence, Method section 2.2.2.2, Table 2-8).

3.2.1.1 Generation and validation of FLYWCH1KO normal intestinal organoids

LV-particles were produced from two different copies of FLYWCH1-gRNAs constructed in lentiviral vectors. Initially, we transfected HEK293T cells with pLV-U6g-PGK-Puro-2A-BFP plasmids expressing the FLYWCH1-gRNA, BFP and a puromycin-resistant gene as outlined at Methods section 2.2.1.6. In parallel, pLVX-EGFP expressing eGFP was used as a control (Figure 3-1 A). Transfection efficiency was estimated over 90-95% in HEK293T cells using the standard fluorescence microscopy examination based on GFP and BFP expression (Figure 3-1 B). Virus harvesting was carried out for 4 consecutive days, as explained in Methods section 2.2.1.6.
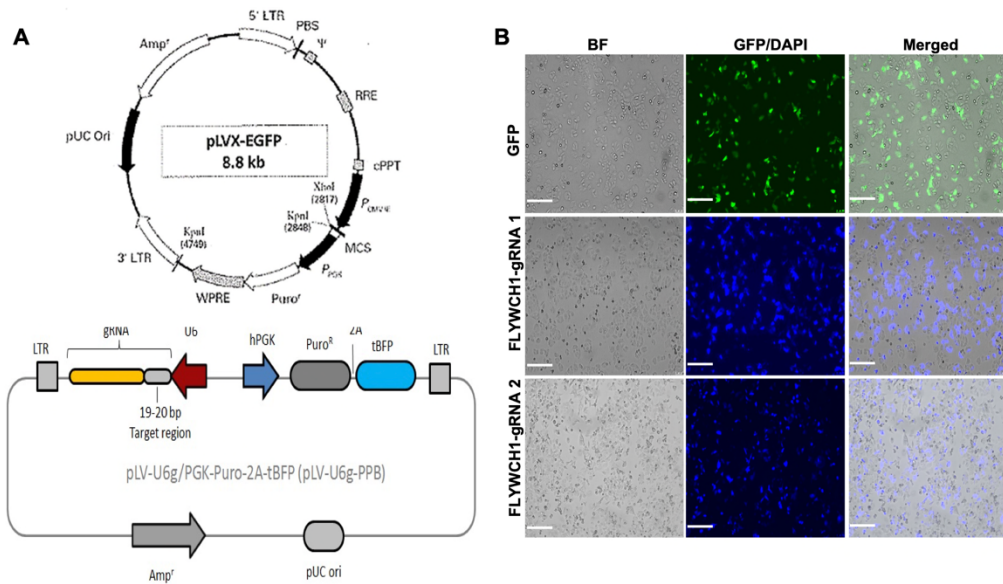
Figure 3-1 Schematic presentation of plasmids constructs used for LV-production. A) The map of control pLVX-EGFP plasmid expressing eGFP, and pLV-U6g-PGK-Puro-2A-BFP plasmid expressing the FLYWCH1-gRNA, BFP and a puromycin-resistant gene. **B)** The fluorescence microscopic images show the HEK293T transfected with above plasmids and the expression GFP and BFP fluorescent proteins. Magnification, 10x, scale bars 75μm.

Purified virus particles were then used to infect organoids using previously explained transduction method (256). Briefly, organoids were collected and incubated with LV-particles for at least 6 hrs. Infected organoids were then diluted in the Matrigel and incubated for 2-3 days before detecting Blue/GFP fluorescence. Transduced organoids were maintained healthy for 14 days in culture by replacing the medium with a fresh one every 2-3 days.

Typically, in cultured cell lines, transduced cells are first treated with puromycin and then sorted, or serially diluted into a single cell expressing BFP and GFP to minimize off-target activities. However, it is challenging to determine the best concentration of puromycin in cultured organoids due to cells heterogeneity, and a mixed epithelial cell population of un-transduced and transduced cells. Likewise,

for flow cytometry cell sorting, the organoids need to be dissociated into single cells, and this process will dramatically decrease the viability of stem cells and influence organoids growth efficiency. Hence, we examined intact cultured organoids transduced with LV particles to ensure that all organoid cells retained healthy.

48-72h post-transduction, transduced organoids were tested as a bulk population and the *FLYWCH1*-gRNA expressing organoids (*FLYWCH1*KO) were chased based on their BFP-expression and compared to GFP-transduced organoids. Furthermore, RNA was extracted from control and *FLYWCH1*KO organoids using TRIzol, and FLYWCH1 depletion was confirmed by qPCR analysis (Figure 3-2).
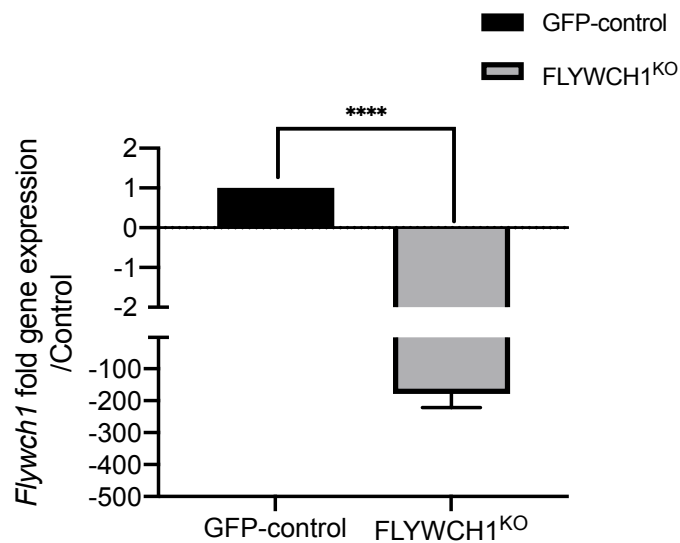
Figure 3-2 qPCR analysis validating the reduction of Flywch1 mRNA level. mRNA was obtained by (2^-(ΔΔCt) method, (****=P ≤ 0.0001).

3.2.1.2 Loss of FLYWCH1 expression induces the growth potential of normal intestinal organoids

With consideration of recent studies on loss- and gain-of-function analysis of genes expression and their influence on the developing organoids (252, 254, 257), we have analysed organoids morphological changes within 12 days of culture by the fluorescence microscopy, before the organoids were processed or sub-cultured for other purposes. For this, FLYWCH1^{KO} organoids were compared to the GFP-expressing organoids as a control for morphological differences, growth patterns, and transcriptional analysis, as outlined in Figure 3-3 A-C.
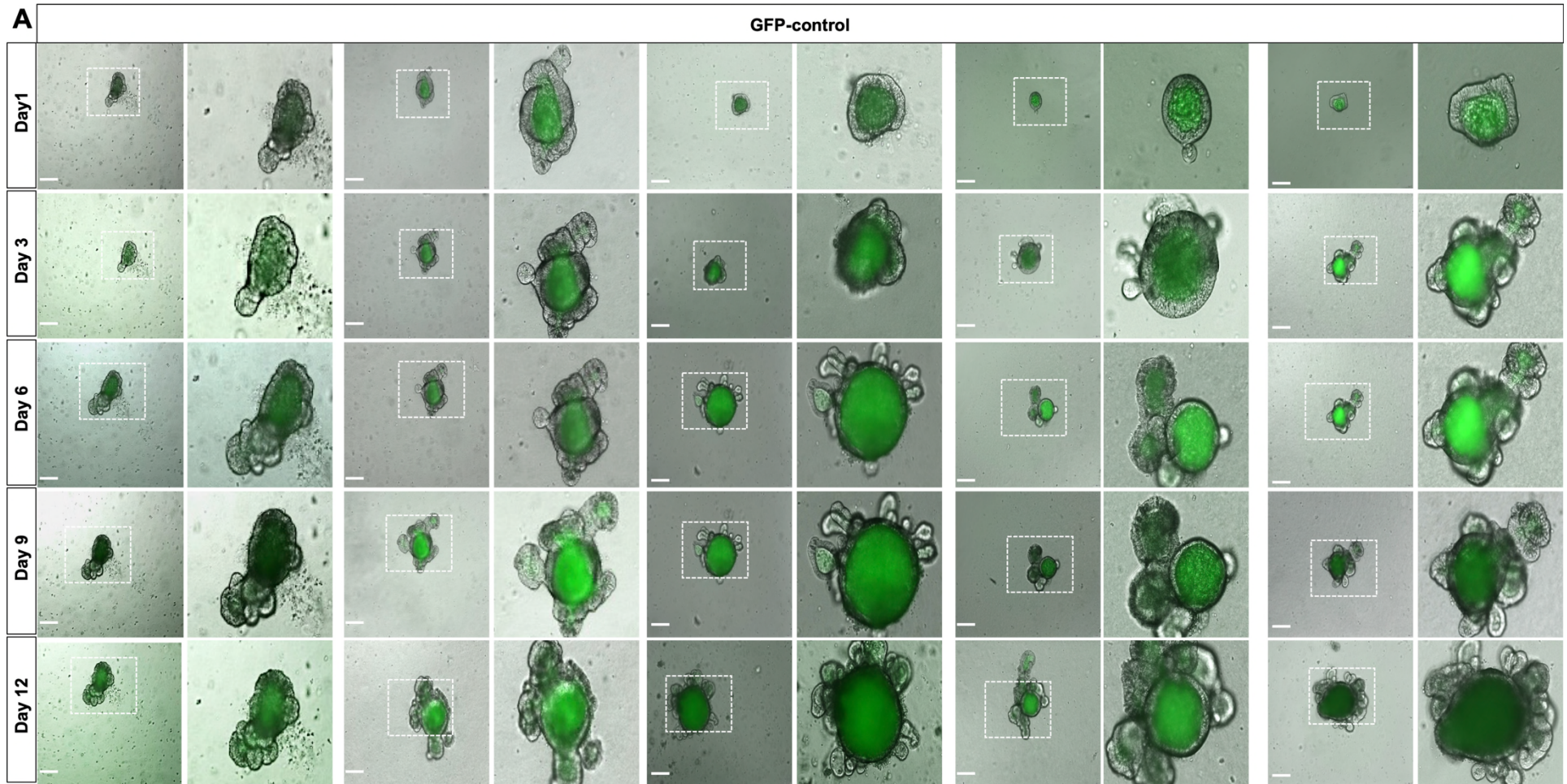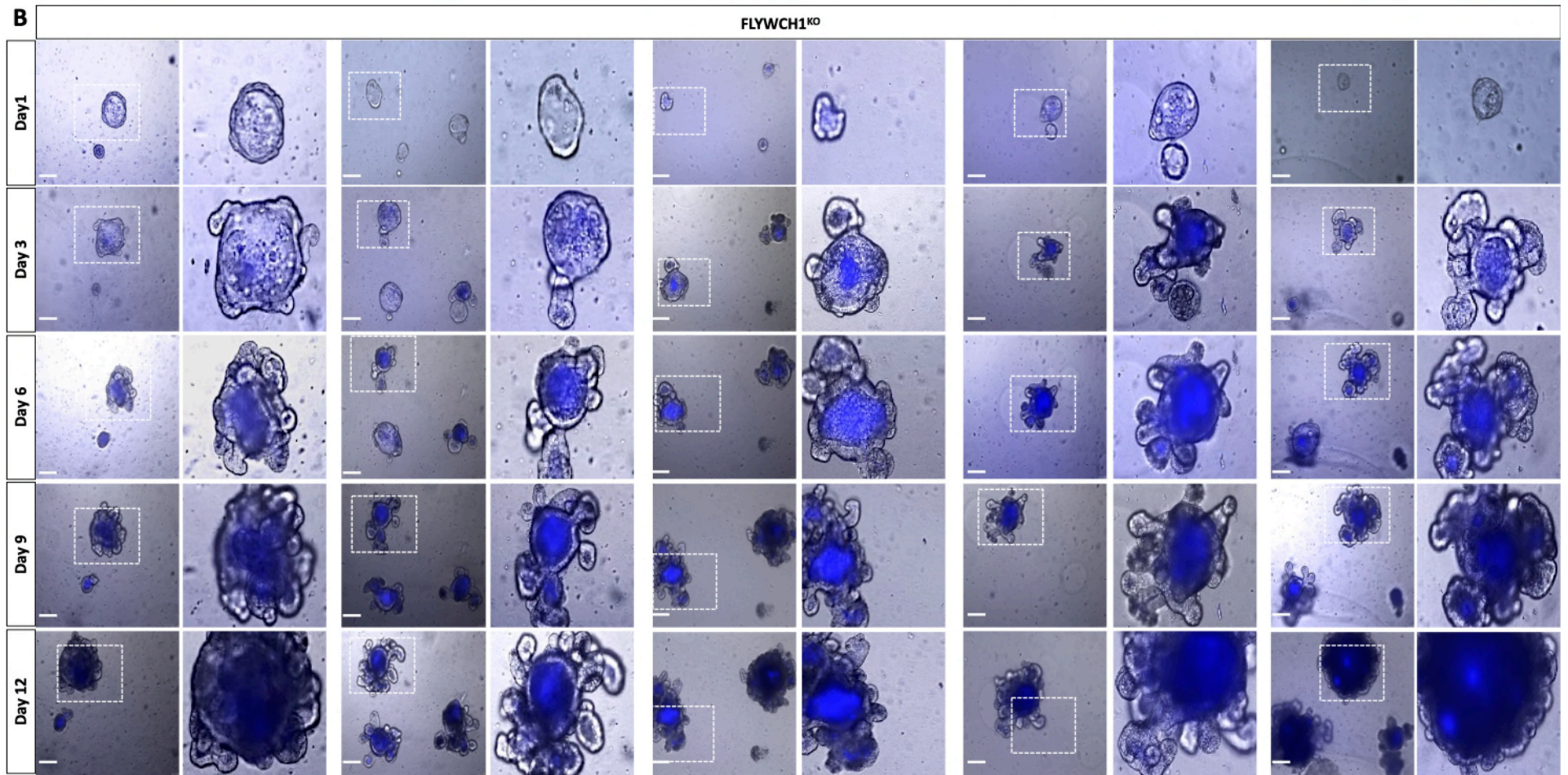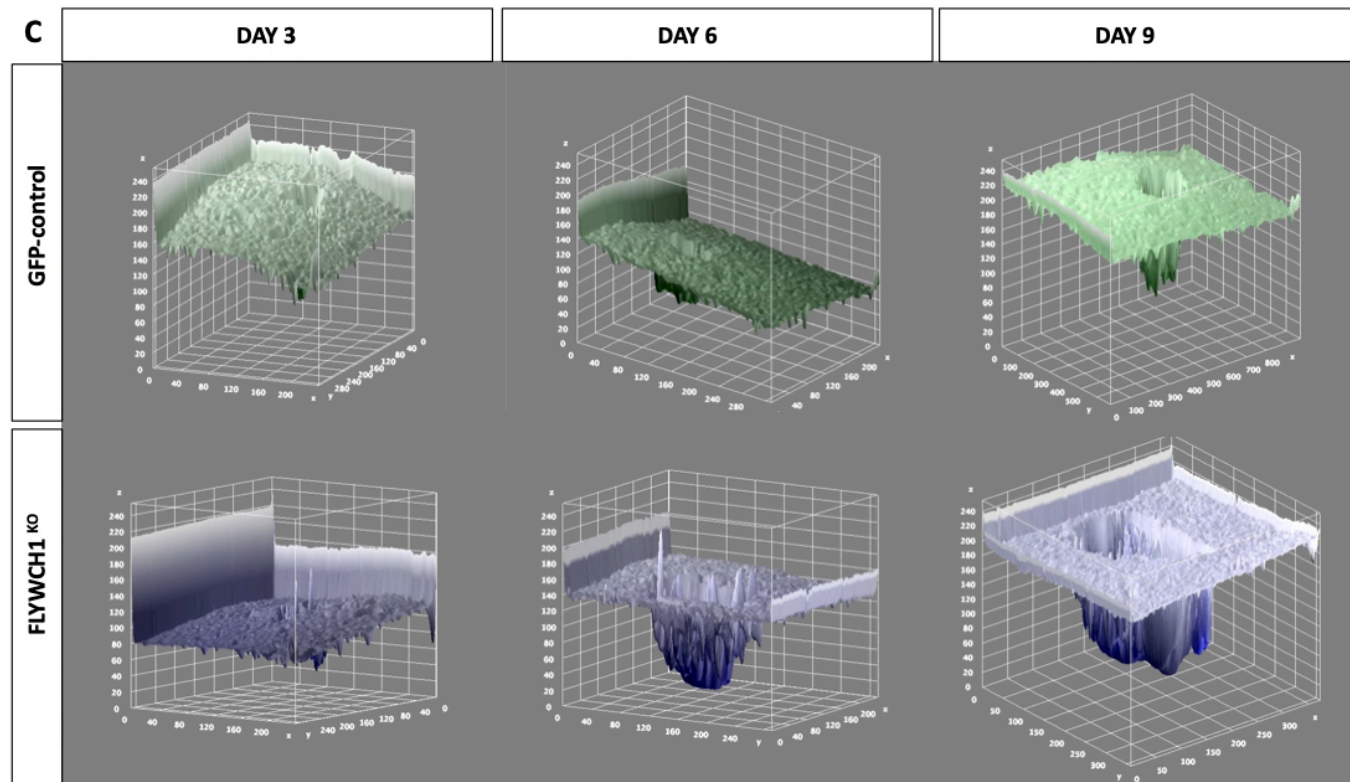
Figure 3-3 FLYWCH1 knockout influences the morphology and growth pattern of mouse intestinal normal organoids. A, B) Morphological analysis showing the changes in the growth pattern of FLYWCH1[KO] organoids compared to GFP-control. Images were taken using Leica microscope. Scale bar 7.5µm. **C)** A representative 3D interactive surface plots, illustrating the 3D-morphological differences between GFP-control versus FLYWCH1[KO] organoids at indicated days. Blots were generated using image J 3D Surface Plot Plugins.

Knocking out FLYWCH1 in the mouse 3D- organoids influenced their morphology and growth patterns. Wherein, FLYWCH1^{KO} organoids seemed bigger, formed a more complex budding phenotype, after three days in culture, compared to GFP-control organoids (Figure 3-3 A, B).

Considering the 3D structure, we next quantified organoids 3D volume and surface area (Figure 3-4). Organoids 3D volume was measured as previously reported (258), by taking 3-4 separate diameters from different directions for a single organoid, at different time points. Half of the average value of these diameters was then considered as the radius (r), and organoid volume was estimated using the following formula: V=4/3 πr^3, (Figure 3-4 A). Additionally, measuring the surface area (the circumference) of over 20 organoids (for each group) has further confirmed the differences in their size and growth at the indicated days (Figure 3-4 B). The surface area expansion rates were also calculated as previously established (259-261), using the formula (Present Day Area / First Day Area) * 100 (Figure 3-4 C).

In the FLYWCH^{KO} organoids, the volume was significantly greater, particularly after day 6. This was also supported by the significant increase in their expansion rates (Figure 3-4 C). Results together might reflect an increase in their proliferation and/or stem cells activities.
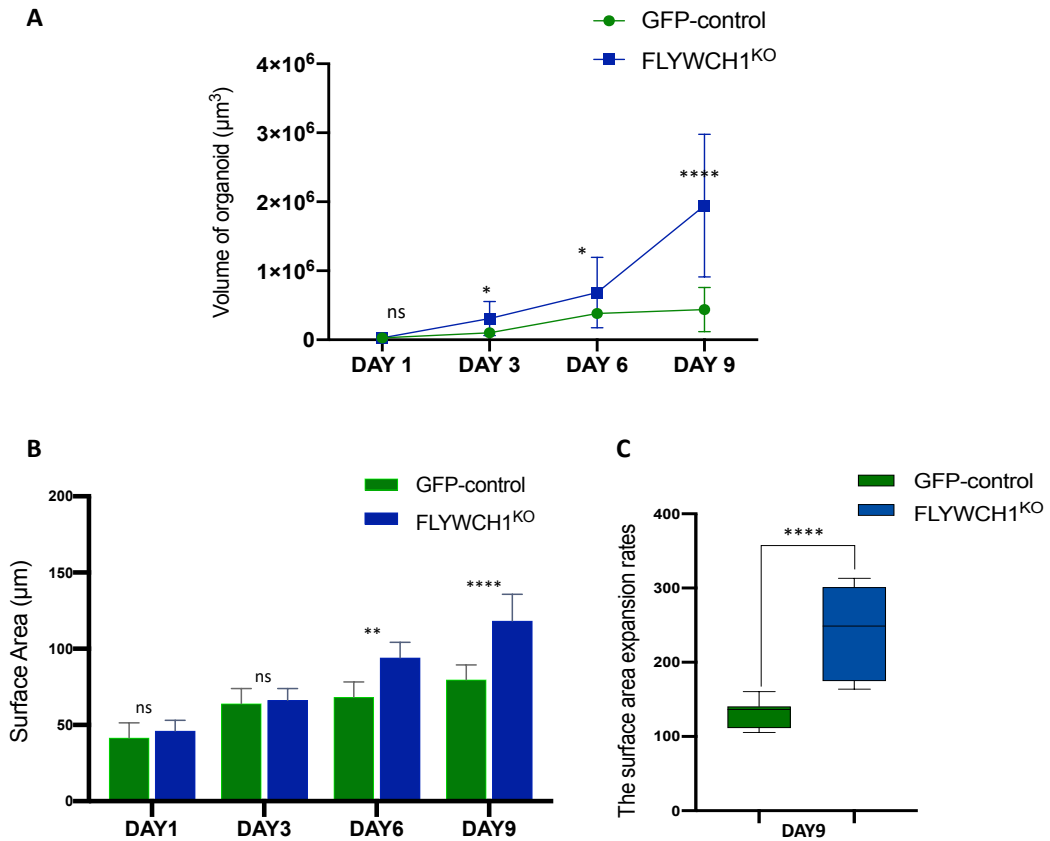
Figure 3-4 FLYWCH1 depletion induces the growth of normal intestinal mice organoids. A) Volumes of organoids were measured every 3 days over the culture time, using the formula: $V = 4/3\pi r3$. (20 Organoids were measured for each group). **B)** The surface area (circumference) of organoids was measured in 20 organoids for each category, every 3 days. **C)** The surface area expansion rate of organoids shows a significant induction in the growth of $FLYWCH^{KO}$ organoids compared to control organoids. The graph represents the average of the surface area (circumference) calculated from 20 organoids, using the formula (Day 9 Area /Day1 Area) * 100. The same organoids were followed up over all the different time points. Image-J software was applied to measure the circumference of organoids. Data are mean ± S.D., p-values were calculated based on a Student's *t*-test. (ns; not significant, *=P ≤ 0.05, **= P ≤ 0.01, ***= P ≤ 0.001, ****=P ≤ 0.0001).

To further understand the impact of FLYWCH1 loss on the growth and proliferation, organoids were then processed for paraffin embedding and immunohistochemistry analysis, as explained in Chapter 2 (Methods section 2.2.10). For this, I implemented several optimisation experiments to establish an optimal staining condition for the organoids using different antigen retrieval

approaches and different Ab concentrations. However, these were only stained

for Ki-67 (proliferation marker) (Figure 3-5) due to the time limitations of my PhD

course.
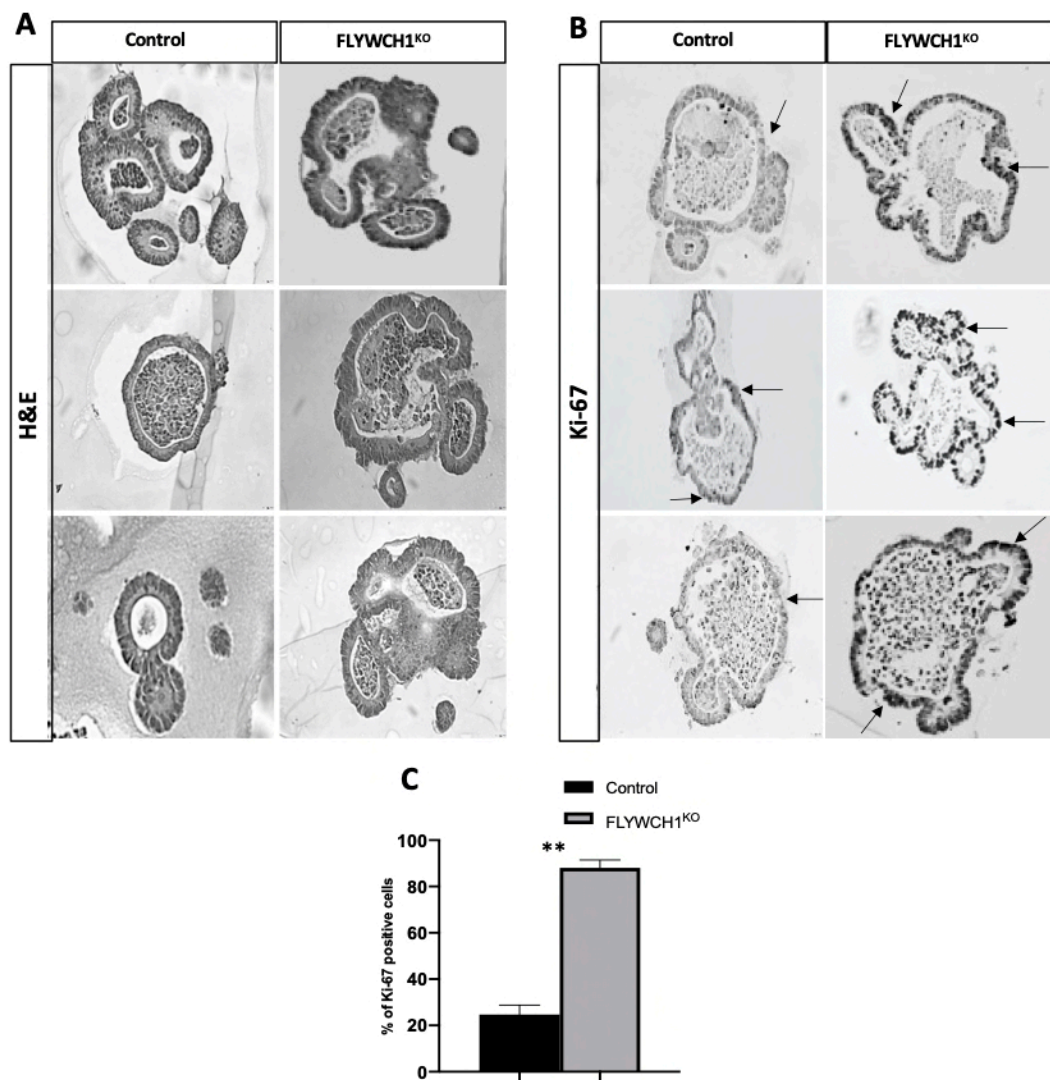
Figure 3-5 IHC staining and quantification of Ki-67 in mouse intestinal organoids. Representative images of A) H&E (Haematoxylin & Eosin) showing the structures or organoids, and **B)** IHC staining of Ki-67 showing the proliferation induction in FLYWCH^{KO}-organoids. Magnification: 100x. **C)** Quantificational analysis of Ki-67. The Ki-67 positive cells were quantified from 10 organoids per group and the data presented as the percentage Ki-67 positive cells (**= $P \leq 0.01$).

Beside the evident morphological changes perceived in FLYWCH1^{KO} organoids (Figure 3-4), our pilot histological evaluations revealed a clear induction of Ki-67+ proliferating crypts in FLYWCH1^{KO} organoids (Figure 3-5). Taken together, loss of FLYWCH1 expression induces the growth potential of normal intestinal organoids. However, further research is required to elucidate the mechanism of action and the potential effects of FLYWCH1 on differentiation and lineage-specific markers in the normal intestinal crypt.

3.2.1.3 FLYWCH1 knockout changes the transcription of intestinal stem cell markers.

To further investigate the mechanism underlying the observed morphological changes, qPCR analysis of key intestinal stem cell markers was conducted (Figure 3-6). In comparison to GFP-control, our results show a significant upregulation of the stem cells and Wnt target genes *Lgr5 and Olmf4;* in FLYWCH1^{KO} organoids (Figure 3-6 A, B). The Olmf4 and Lgr5 positively marking the cycling ISCs (57, 262). Notably, further qPCR data indicated a significant reduction in the transcriptional products of the quiescence ISC markers *Tert* and *Lrig1* in FLYWCH1^{KO} organoids compared to controls (Figure 3-6 C, D). These data may lead to the speculations that FLYWCH1 restricts the stemness of intestinal stem cells, although further investigations of their genes signature are required.
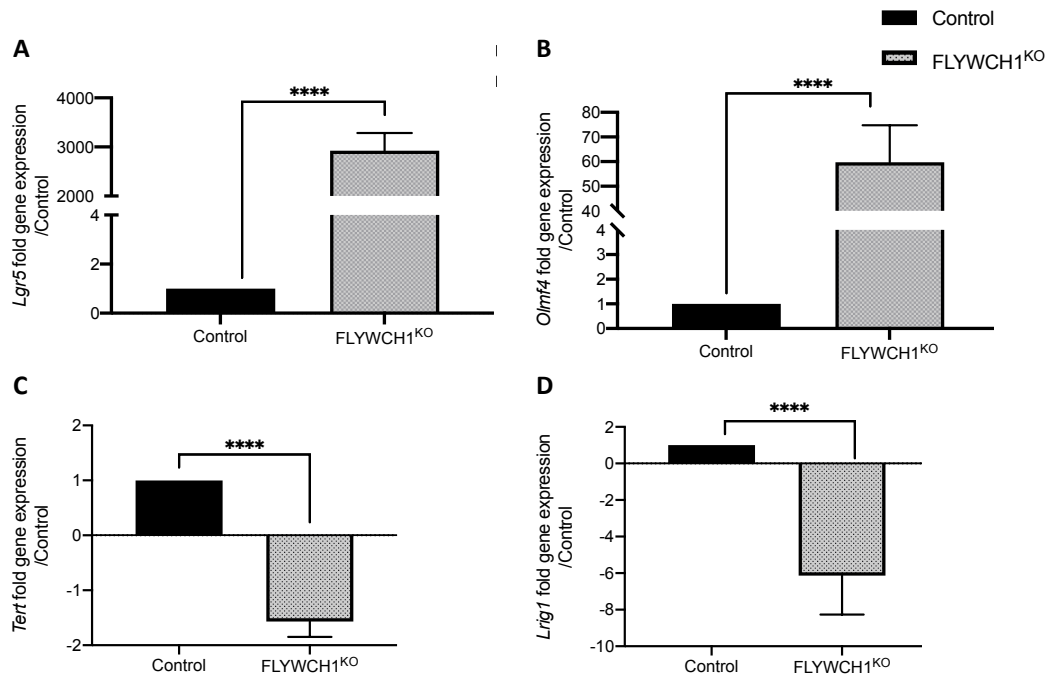
Figure 3-6 FLYWCH1 expression may control the expression of intestinal stem cell markers genes. qPCR analysis indicating that loss of FLYWCH1 upregulates the transcription of A) *Lgr5+*, **B)** *Olmf4* (cycling ISCs), while reduces **C)** *Tert+* and **D)** *Lrig1+* (quiescence ISCs). mRNA was obtained by ($2^{\wedge}$-($\Delta\Delta$Ct) method. Experiments were carried out in triplicates and repeated on three independent occasions, data are mean and SD. p-values were calculated based on a Student's *t*-test (****=$P \leq 0.0001$).

3.2.2 Evaluation of anti-FLYWCH1 antibody

Importantly, before proceeding with following experiments, we examined the specificity of the anti-FLYWCH1 antibody used for Immunofluorescence (IF) and Western Blotting (WB) assays in this study in normal and CRC cell lines at the endogenous level, cells over-expressing FLYWCH1 and/or depleted for FLYWCH1 (Figure 3-7).
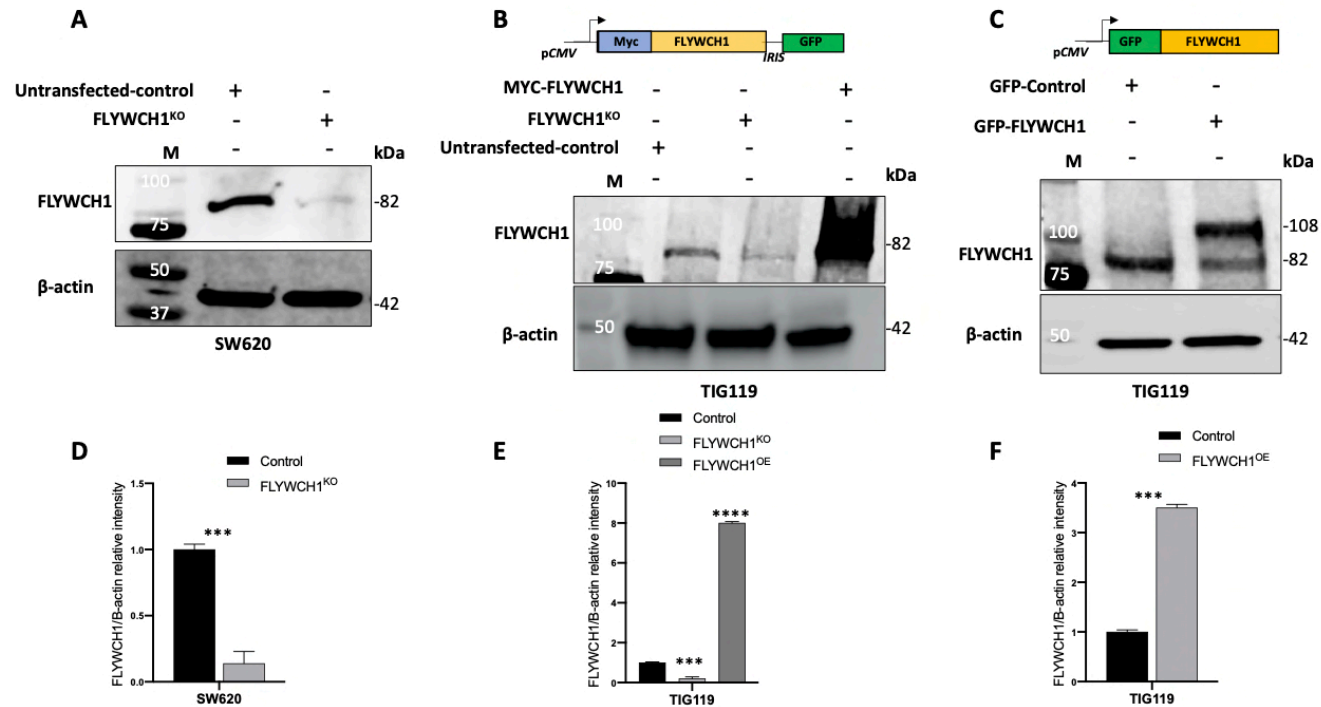
Figure 3-7 Validation of anti-FLYWCH1 antibody and cell lines used throughout the study by WB. A, D) WB and quantification analysis validates the knockout of FLYWCH1 in SW620 cells used in this study. **B, E)** WB and quantification confirms the depletion of endogenous FLYWCH1 in TIG119-FLYWCH1KO and shows the over-expression of FLYWCH1 using Myc-tagged construct used throughout the project. **C, F)** WB and quantification analysis confirms the over-expression of FLYWCH1 (GFP-FLYWCH1, band size 108kDa) in TIG119 cells using GFP-tagged FLYWCH1 construct. Histograms show the relative densitometric quantification of FLYWCH1 band intensities normalized to β-actin and presented as the mean fold changes obtained from three independent experiments. P-values were calculated by a Student's *t*-test (***= P ≤ 0.001, ****= P ≤ 0.0001).

Furthermore, to evaluate the FLYWCH1 antibody for immunofluorescence (IF) assays, we initially carried out a co-localisation analysis of anti-FLYWCH1 antibody with GFP-tagged FLYWCH1 (GFP-FLYWCH1), versus GFP-overexpressing TIG119 cells (Figure 3-8 A). Un-transfected cells were used as an internal control for the endogenous FLYWCH1 protein expression (Figure 3-8 A, top panel). No primary antibody controls were used as negative controls (i.e. cells stained with DAPI/secondary Ab only), (Figure 3-8 B). These data validate the specificity of anti-FLYWCH1 antibody used in the following experiments and throughout the project.
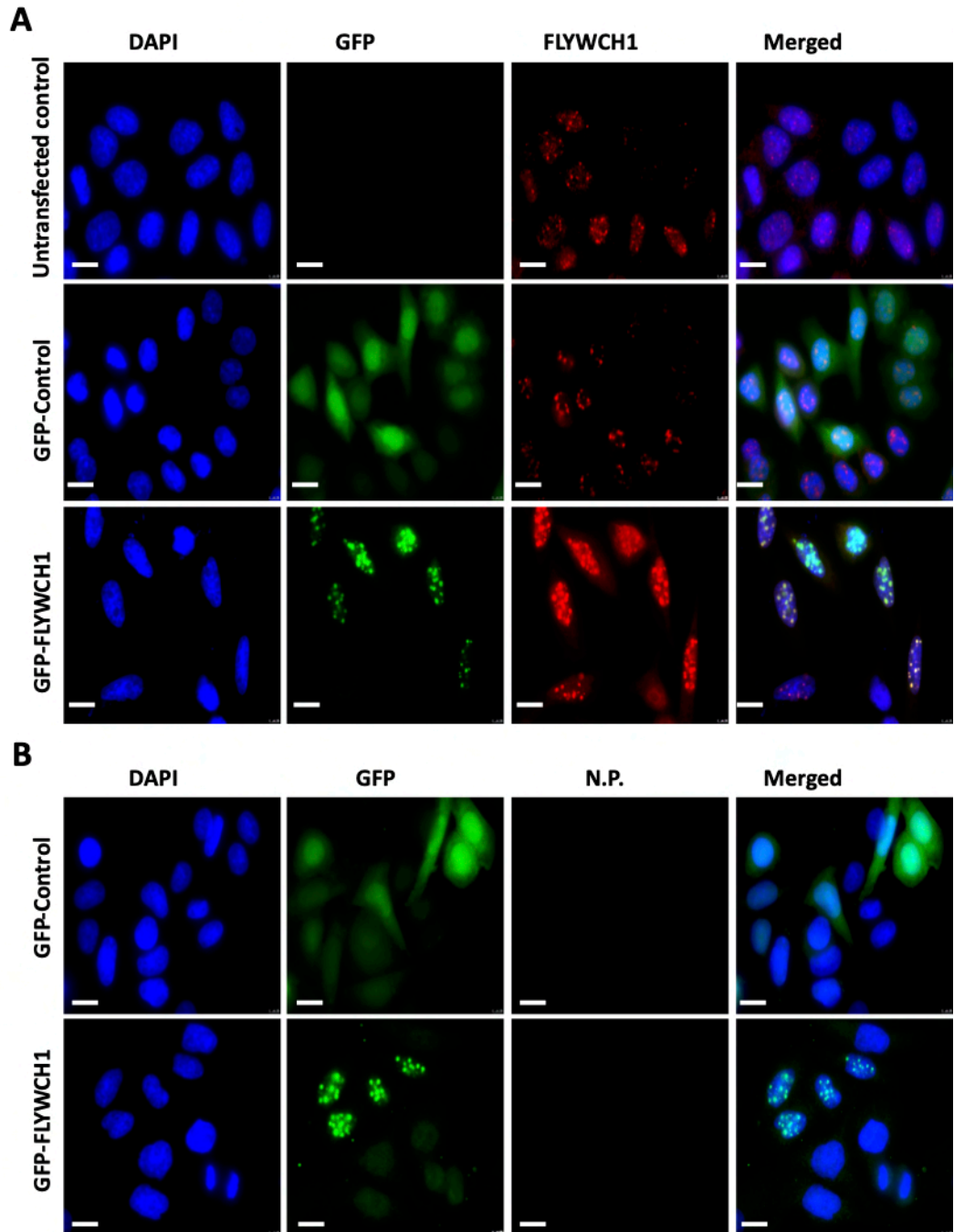
Figure 3-8 Immunofluorescence analysis of FLYWCH1 protein expression in TIG119 cell lines using anti-FLYWCH1 antibody. A) Top panel shows the endogenous expression of FLYWCH1 protein in parental cells, while middle and bottom panels show the co-localisation of GFP-control (empty vector) and GFP-tagged FLYWCH1 with Anti-FLYWCH1 Ab, confirming the specificity of the Ab. **B)** No primary antibody (N.P.), used as negative controls for both GFP-Control & GFP-FLYWCH1 cells. Magnification, 100x. Scale bars, 7.5µm.

3.2.3 Over-expression of FLYWCH1 reduces the size and growth of human CRC PDOs via modulating specific Wnt target genes

If aberrant Wnt signalling mediates a downregulation of FLYWCH1 in colorectal cancer cells, what role does FLYWCH1 play in Wnt responses? And does the expression of FLYWCH1 contribute to the maintenance of ''cancer stemness'?. Therefore, here we examined if FLYWCH1 over-expression plays a role in controlling Wnt-mediated intestinal tumorigenesis (263, 264), using patient-derived CRC organoids (PDOs) cultures. For this, FLYWCH1 was over-expressed in PDOs, as explained below.

3.2.3.1 Generation and validation of CRC PDOs over-expressing FLYWCH1

Dr Hossein Kashfi in our lab established a mini-bank of patient-derived organoid lines (PDOs) from 17 patients with CRCs from Nottingham's QMC hospitals (235). In this work (235), we reported two main phenotypical features of CRC PDOs. While about fourteen of patients PDOs grew as Cystic (spherical) organoids, four of the patients-PDOs were growing as Floral organoids (budding form), (Figures 3-9 & 3-10). Unfortunately, the healthy adjacent to tumour tissues did not survive after thawing them, and therefore we excluded them in our study. Importantly, the heterogeneity of CRC PDOs could be due to the variation of genetic background, mutations, treatment regimen and characteristics of each patient, as well as the location of the tumour (265, 266). Dr Nateri's lab would address the DNA sequences of our entire CRC PDOs lines, including the Cystic and Floral organoids I used in this study, (i.e. from two separate patients), using the whole genome sequencing (WES) whole-genome sequencing (WGS) analysis.

The frozen Cystic and Floral CRC PDOs were thawed and cultured as explained in Chapter 2 (section 2.2.9.4). To over-express FLYWCH1, pLVX-lentivirus particles expressing pLVX-Puro-eGFP-FLYWCH1 cDNA (or pLVX-lentivirus expressing empty vector) were produced and infected into the two different types of PDOs (Type 1: Floral and Type 2: Cystic). This was achieved using a similar Lentiviral-based transduction strategy, as explained above (See section 3.2.1).

Besides, HEK293T cells were transduced with pLVX-Puro-eGFP-FLYWCH1 virus particles, to validate the efficiency of LV-particles by fluorescence microscopy (Figure 3-9 A). The level of FLYWCH1 was also validated by WB analysis against GFP-FLYWCH1 using anti-GFP antibody (Figure 3-9 B, Top panel) and using anti-FLYWCH1 antibody (Figure 3-9 B, middle panel). However, validating FLYWCH1 over-expression in PDOs by WB analysis requires a massive number of organoids to extract enough protein lysate for WB analysis. This was not possible, particularly for FLYWCH1-overexpressing organoids, which were much smaller and were growing slower than control. Therefore, we validated the induction of FLYWCH1-mRNA by qPCR analysis in the transduced organoids (Figure 3-9 C).
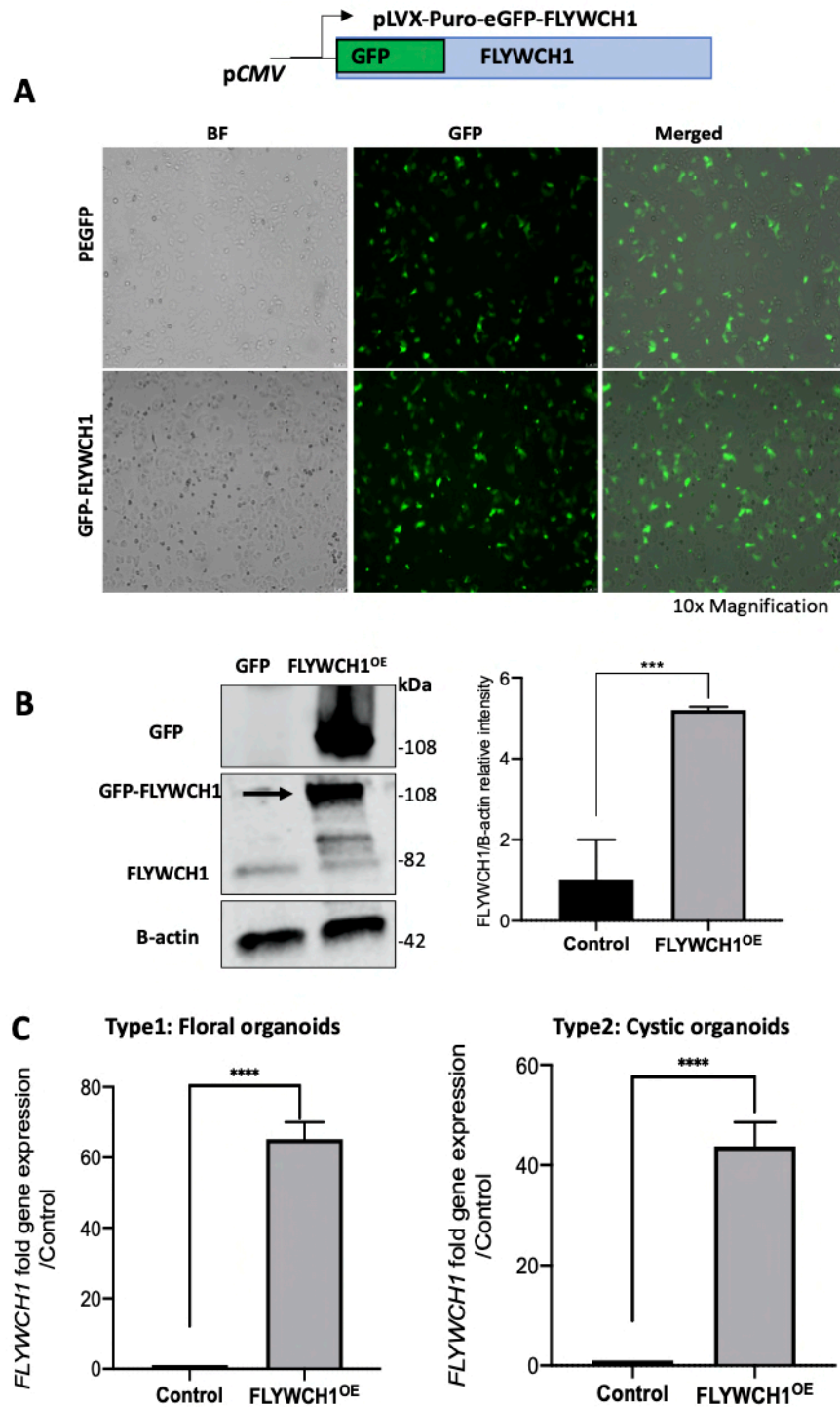
Figure 3-9 Validation of FLYWCH1 over-expression in HEK293T cells and PDOs. A) Schematic presentation of pLVX-Puro-eGFP-FLYWCH1 construct used to generate FLYWCH1-OE organoids and images showing the transfection efficiency of the LV in HEK293T cells. **B)** WB and quantification analysis validates FLYWCH1 over-expression in HEK293T cells using anti-GFP and anti-FLYWCH1 antibodies. The graph shows the relative densitometric quantification of FLYWCH1 band intensities normalized to β-actin and presented as the mean fold changes obtained from three independent experiments (***= $P \leq 0.001$). **C)**

Validation of FLYWCH1 mRNA expression in the PDOs via qPCR analysis. mRNA was obtained by $(2^{\wedge}-(\Delta\Delta Ct)$ method, $(****=P \leq 0.0001)$.

3.2.3.2 Over-expressing FLYWCH1 reduces the CRC PDOs growth

The morphology and growth analyses were then carried out every two/three days, and over 9 days in culture. Figure 3-10 below represents the morphological analysis of Type 1 (Floral organoids), showing the dissimilarities in size and growth of FLYWCH1-overexpressing organoids compared to control organoids. PDOs morphological differences were further quantified based on the size and 3D volume (Figure 3-10), as outlined above for murine intestinal organoids.
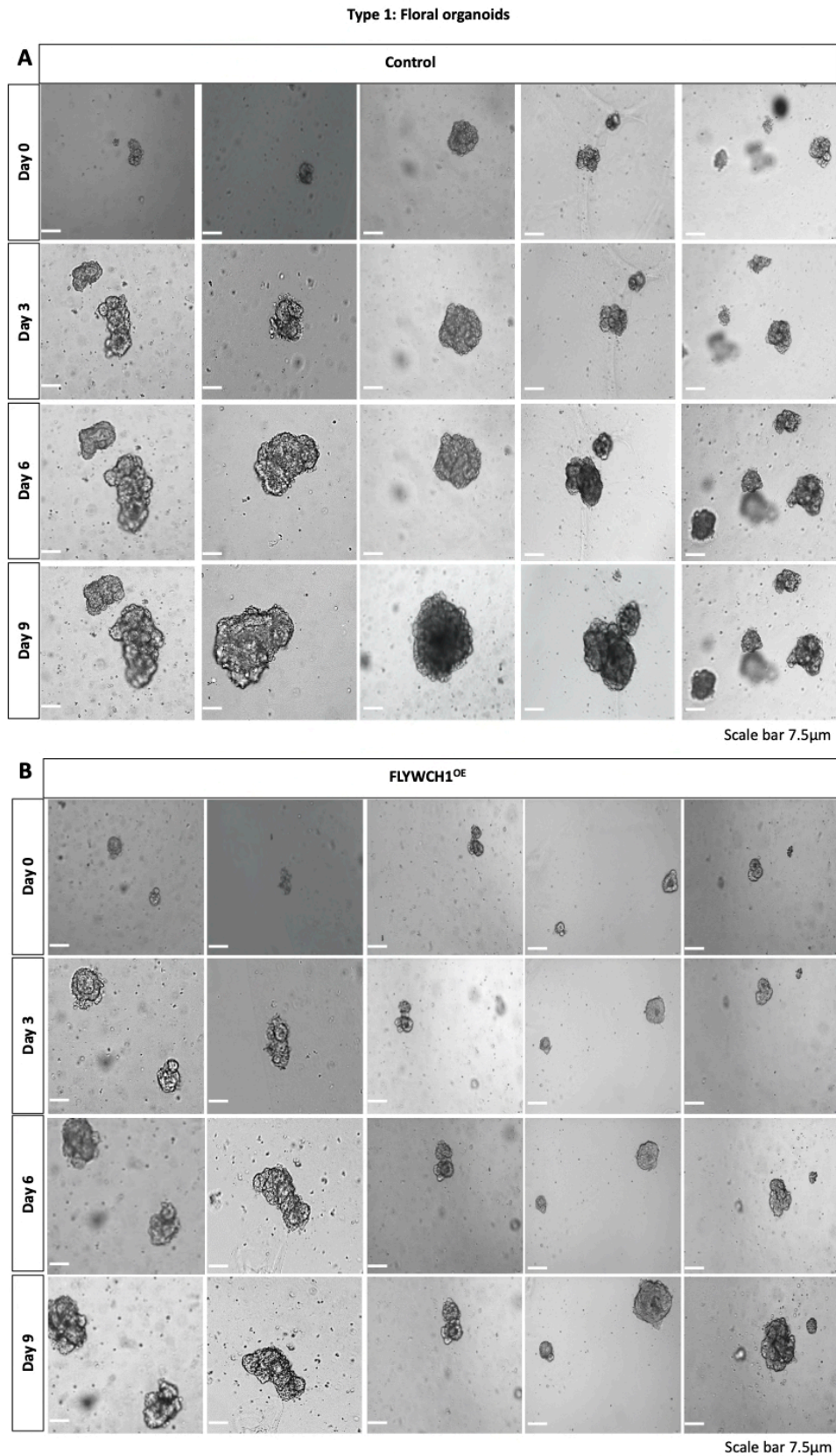
Figure 3-10 Morphological alterations and growth variations of Type 1 patient-derived tumour organoids. Representative images of A) Control versus

B) FLYWCH1-overexpressing organoids for 9 days in culture. Images were taken using a Leica microscope. Scale bar: 7.5 μm.

To assess the morphological changes, quantification analyses were carried out by measuring the surface area and 3D volume of organoids every 3 days over the culture time, using image J (Figure 3-11 A, B). This was calculated in 25 organoids obtained from two independent experiments and presented as the mean of the surface area (Figure 3-11 A), and the volume ($V=4/3\ \pi r)^3$ (Figure 3-11 B). Data suggested a significant size reduction of FLYWCH1-overexpressing organoids relative to controls.
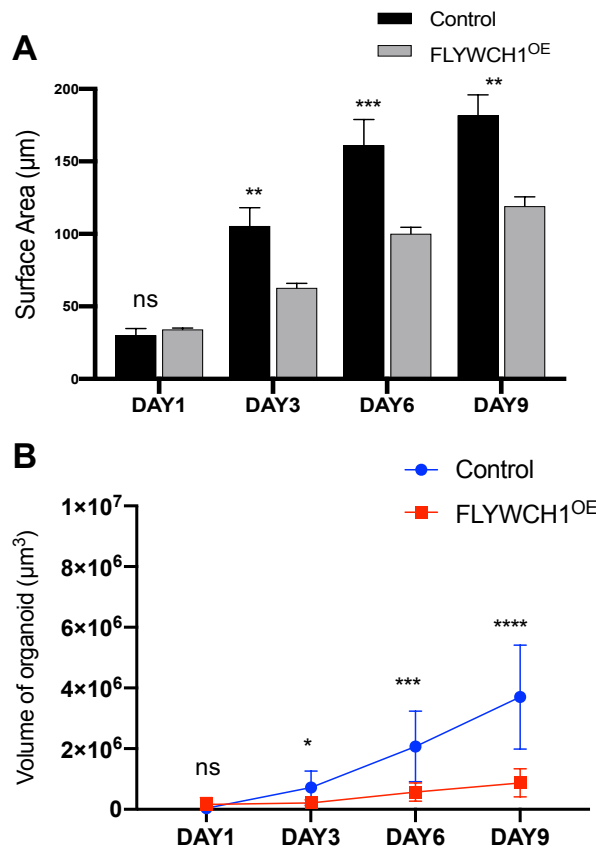
Figure 3-11 Overexpression of FLYWCH1 reduces the size and growth in Type 1-Floral tumour organoids. A) Graph represents the average of the surface area in FLYWCH1^{OE} organoids compared to control. The surface area (circumference) was measured every 3 days using image J. **B)** Volumes of organoids were measured every 3 days over the culture time. Organoid volume was

calculated using the formula: $V=4/3\pi r3$. The same organoids were followed up over all the different time points. (n= 25; control, n= 25, FLYWCH1^{OE}). Error bars represent mean $\pm$ S.D. (ns; not significant, *=P $\leq$ 0.05, **= P $\leq$ 0.01, ***= P $\leq$ 0.001, ****=P $\leq$ 0.0001). P-values were calculated using a Student's *t*-test.

Results suggest a morphology change and growth retardation caused by FLYWCH1

over-expression in Type 1 organoids. Hence, to examine if a different patient

similarly responds to over-expression of FLYWCH1, we further explored the effect

of FLYWCH1 over-expression in the second PDO line (i.e. Type 2 organoids or Cystic

tumour organoids), (Figure 3-12).
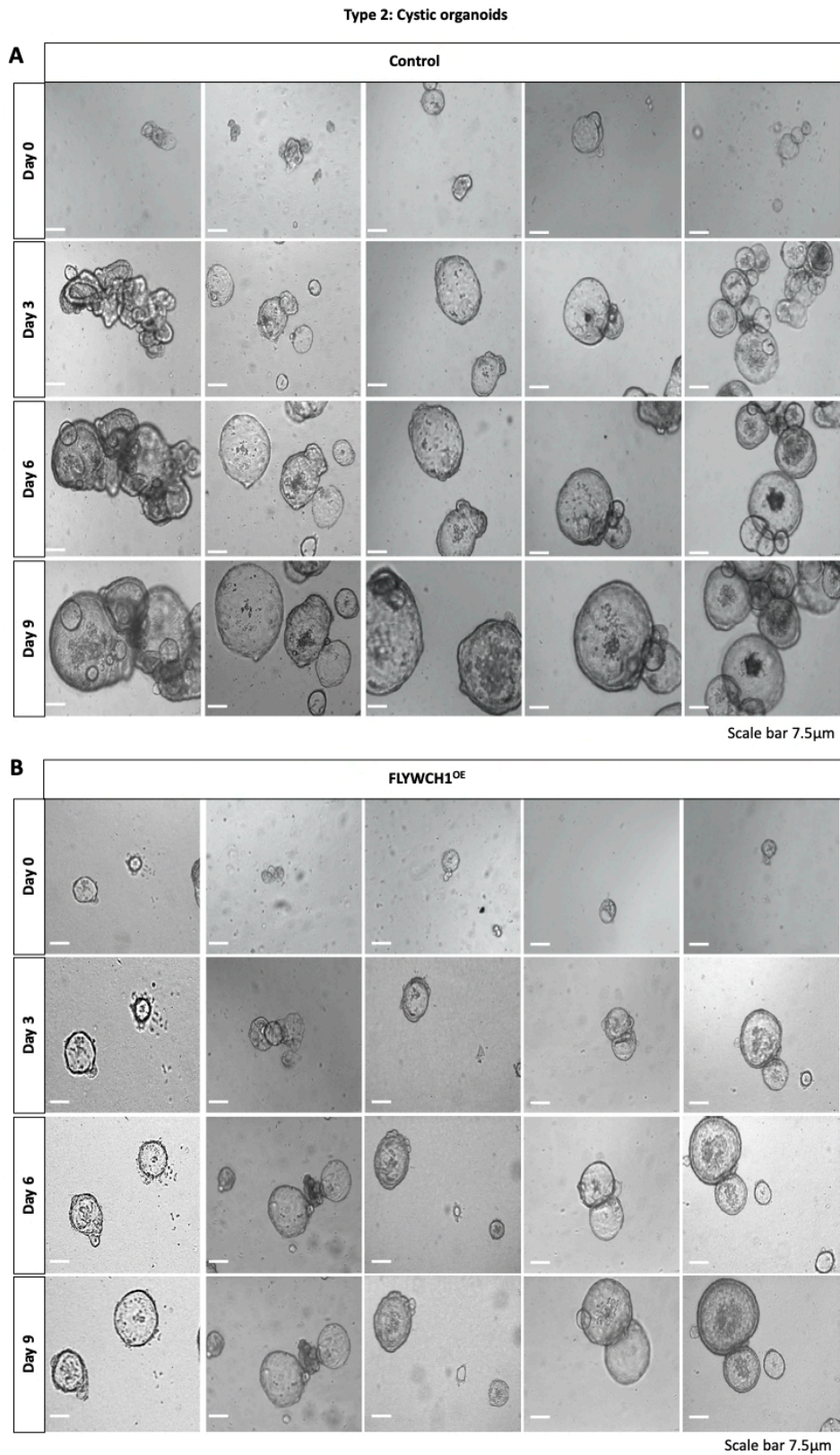
Figure 3-12 Morphological analysis showing variations in growth and size of FLYWCH1-overexpressing Type 2 tumour organoids. Representative images of **A)** Control, **B)** FLYWCH1^{OE} organoids throughout the culture time. Images were taken using a Leica microscope. Scale bar: 7.5 μm.

Of note, FLYWCH1- overexpressing organoids (Figure 3-12 B) appeared smaller in size and showed a slower growth rate over the culture time, in a comparison to control organoids (Figure 3-12 A). This was then analysed and quantified by measuring the surface area and volumes of these organoids, as explained above. Despite the high growth rate of the Cystic organoids, over-expressing FLYWCH1- significantly impaired their size and growth potential (Figure 3-13).
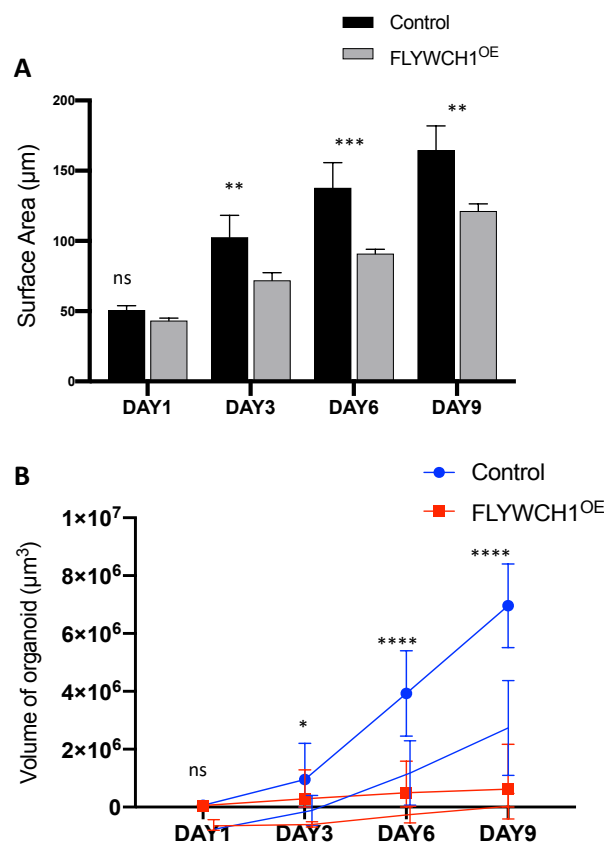
Figure 3-13 FLYWCH1^{OE} hindered the growth of Type 2-Cystic tumour organoid. A) Histogram shows the average of surface area in FLYWCH1^{OE} organoids compared to control. The surface area (circumference) was measured every 3 days using image J. **B)** Diagram demonstrates a significant reduction in organoids volumes by over-expressing FLYWCH1. The volume was calculated using the formula: $V = 4/3\pi r3$. The same organoids were followed up over all the different time points. (n= 25; control, n= 25, FLYWCH1^{OE}). Error bars represent mean $\pm$ S.D. (ns; not significant, *=P $\leq$ 0.05, **= P $\leq$ 0.01, ***= P $\leq$ 0.001, ****=P $\leq$ 0.0001).

Findings from both PDOs indicated that FLYWCH1 over-expression is efficient in suppressing tumour organoids growth, irrespective to the heterogeneity and variations of these PDOs. Yet, the underlying molecular changes driven by altered FLYWCH1 expression and signaling pathways involved could vary depends on the genetic background of each type.

3.2.3.3 FLYWCH1-overexpression in CRC PDOs changed the transcription profile of Wnt-associated genes

In keeping with the established role of FLYWCH1 in regulating Wnt/β-catenin transcriptional activity (198, 215), we studied the effect of FLYWCH1-overexpression on key Wnt-target genes by qPCR analysis in CRC PDOs (Figure 3-14). Remarkably, in both types of tumour organoids, FLYWCH1-overexpression reduced the stemness markers *CD44* and *LGR5*, but significantly augmented the transcription of *E-CADHERIN* in Type 2 cystic organoids only (Figure 3-14 B). The effect on *C-JUN* also varied between the PDOs. It is, therefore, possible that FLYWCH1 suppresses the growth of PDOs by driving specific transcriptional changes in each type, and possibly in a genetic background dependent manner. The genetic profiling of these organoids would help to further understand the underlying differential mechanisms of FLYWCH1 function in these PDOs as outlined above.

A

B
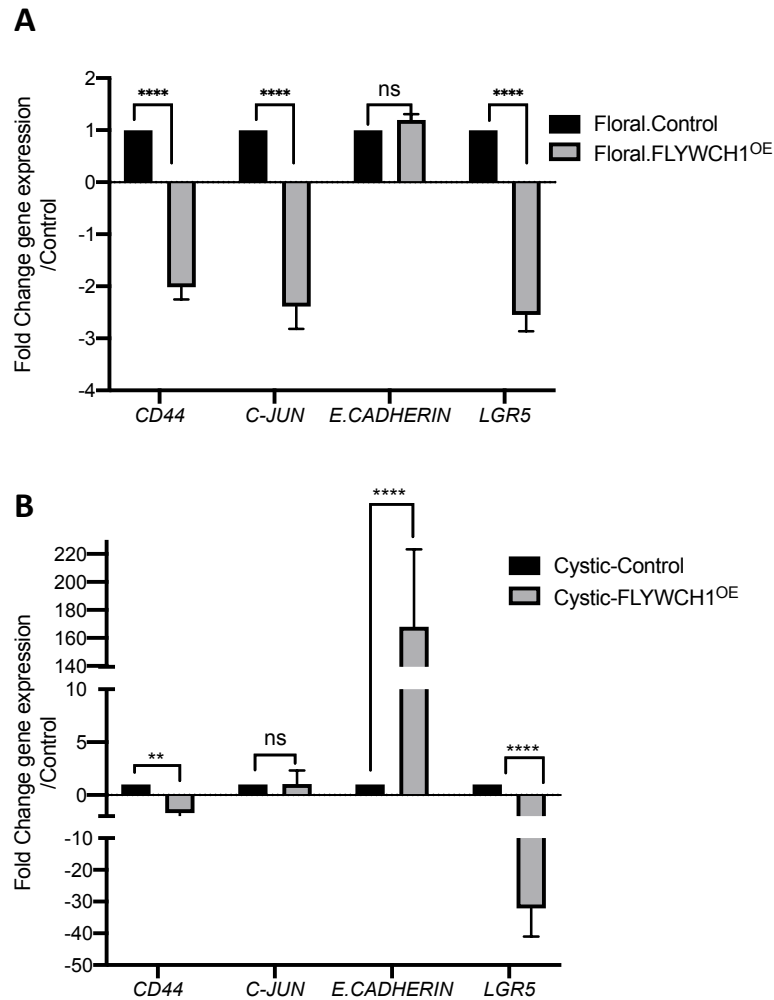
Figure 3-14 qPCR analysis showing the effect of FLYWCH1-overexpression on stemness and Wnt target genes in A) Type 1 (Floral), and **B)** Type 2 (Cystic 2) organoids. mRNA expression was obtained by using the $2^{\wedge}-(\Delta\Delta Ct)$ method. Each set of experiment was carried out in triplicate and repeated on three independent occasions. Data are mean $\pm$ SD (ns; not significant, *=$P \leq 0.05$, **= $P \leq 0.01$, ***= $P \leq 0.001$, ****=$P \leq 0.0001$). p-values were calculated using the two-way ANOVA test.

To obtain a more specific interpretation on the transcriptome changes associated with FLYWCH1-overexpression and its impact on Wnt-target genes, a small microarray using RT² Profiler™ PCR Array of Human WNT Signaling Pathway was performed on type 2 (Cystic organoids). The PCR array comprises a cDNA-library of 84 Wnt target gene. Primarily, we compared gene expression after over-

expression of FLYWCH1 with control organoids (transfected with an empty vector), and any altered gene expression was considered specific to FLYWCH1 modulation only if the up-or down-regulation was higher than 2-fold.

Overall, as demonstrated in Figure 3-15, the expression analysis of Wnt target genes showed a significant downregulation in certain genes associated with cell motility, and invasion in CRC (such as FOSL1 (267), WISP1 (268)), or transcriptional activators (such as FOXN1 (269)). Intriguingly, among other FZD receptors, FLYWCH1[OE] only reduced FZD8, which is known to promote cell proliferation through the canonical and non-canonical Wnt signaling pathway (270, 271). On the other hand, several Wnt-suppressive components were upregulated, including: WNT11, a non-canonical Wnt protein that represses the canonical Wnt signaling (272), and WNT9A, a non-canonical ligand that suppresses β-catenin protein, and is known to inhibit human colorectal cancer cell proliferation *in vitro* (273). A further qPCR analysis of selected target genes confirmed the results in agreement with the array data, for most of the genes (Figure 3-16).

A

Genes Over-Expressed in FLYWCH1-OE versus Control Group		
Position	Gene Symbol	Fold Regulation
E01	NFATC1	29.98
F09	WNT1	14.48
G11	WNT8A	4.91
G03	WNT3	4.4
G07	WNT5B	4.16
G01	WNT2	3.8
G12	WNT9A	2.28
F11	WNT11	2.26
E07	PRICKLE1	2.02

Genes Under-Expressed in FLYWCH1-OE versus Control Group		
Position	Gene Symbol	Fold Regulation
A02	APC	-1.57
A03	AXIN1	-1.71
A11	CTBP1	-3.24
B08	DVL1	-2.13
B12	FBXW4	-1.54
C02	FOSL1	-1.83
C03	FOXN1	-3.96
D01	FZD8	-2.27
D03	GSK3A	-1.52
E12	SFRP1	-2.7
F01	SFRP4	-1.62
F08	WISP1	-1.63
F12	WNT16	-2.05
G04	WNT3A	-2.08
G10	WNT7B	-2.68

B
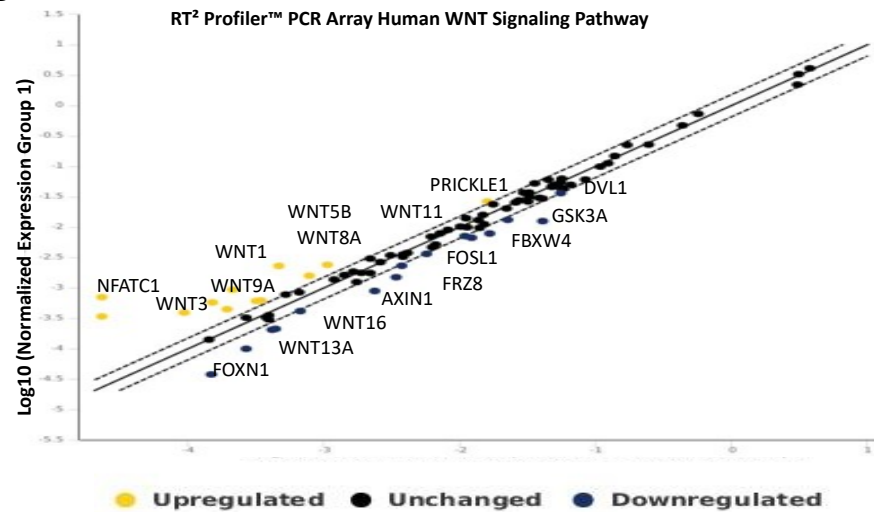
Figure 3-15 FLYWCH1 expression changes the transcriptional signature of PDOs to selectively regulate genes involved in Wnt-mediated biological responses. A) Table list of genes upregulated (Yellow) or downregulated (Blue) by FLYWCH1 expression obtained from RT² Profiler™ PCR array of human WNT signaling pathway. **B)** Scatter plot compares the normalized expression of every gene on the array between FLYWCH1^{OE} versus control by plotting them against one another. The central line indicates unchanged gene expression. The dotted lines indicate the selected fold regulation threshold. Fold threshold, and regulation cut off =2. The p-values are calculated based on a Student's *t*-test of the replicate 2^ (-Delta CT) values, p-value cut off=0.05.
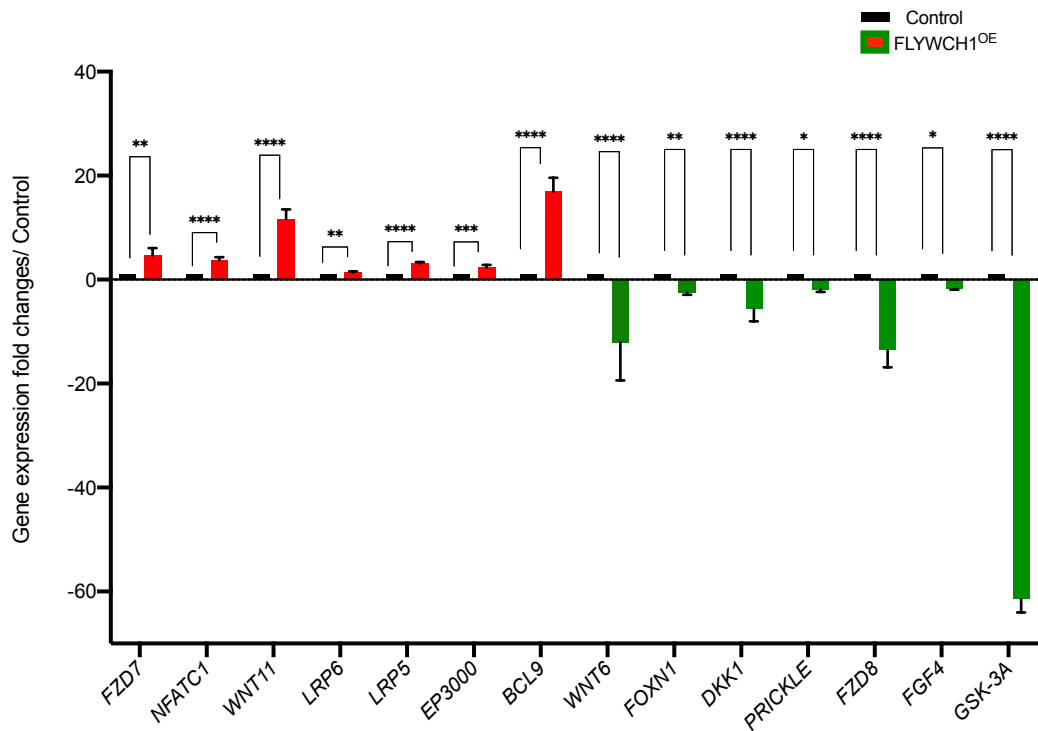
Figure 3-16 qRT-PCR validates the transcriptional changes associated with FLYWCH1^OE in PDOs. Expression of selected downregulated genes showed in green or upregulated genes in Red. mRNA expression was examined by the 2^-(ΔΔCt) method. Data are mean and SD, and P-values were estimated using the two-way ANOVA test. (ns; not significant *=P ≤ 0.05, **= P ≤ 0.01, ***= P ≤ 0.001, ****=P ≤ 0.0001).

Our above data together suggest that FLYWCH1 overexpression in tumour-organoids suppressed their size and growth, partly via modulating selected Wnt-dependent target genes for their stemness and malignancy potential. We have therefore speculated that FLYWCH1 might have a role in cancer cells stemness activity.

3.2.4 Loss of FLYWCH1 alters the *in vitro* cancer stem-like properties of CRC SW620 cells in culture

Cancer stem-like cells (CSCs), are a small sub-population of poorly differentiated cancer cells (i.e. also known as cancer-recurrent cells) (274-277), that play a critical role in the metastasis and relapse of colorectal cancer (276, 278). It was postulated that FLYWCH1^{KO} might alter the efficiency of colonospheres formation, a 3D spheroids culture derived from single cells in a conditional stem-cell medium (229, 279). Thus, we explored the functional consequence of FLYWCH1^{KO} on the colonosphere forming efficiency, and acquisition of stem-like properties in SW620 cells, by using a 3D-colonosphere formation assay.

3.2.4.1 Generation and validation of FLYWCH1^{KO} SW620 cell line

SW620 cells were used as a metastatic CRC cell line (280) (derived from a lymph node metastasis) and FLYWCH1^{KO} SW620 cell line. The FLYWCH1^{KO} SW620 cell line was accomplished by transfecting the cells with pX459 plasmid expressing simultaneously Cas9 nuclease, and FLYWCH1 sgRNA targeting *Exon*1 of *FLYWCH1* gene (for gRNA design and generation of CRISPR construct, see Methods section 2.2.2.1). FLYWCH1 level was then validated in both control and KO cells by qRT-PCR and WB analysis (Figure 3-17). Results showed a significant depletion in *FLYWCH1* mRNA, particularly Exon 1 (Figure 3-17 B). This was further confirmed by the WB analysis of the FLYWCH1 protein (Figure 3-17 C). Due to time and budget limitations, we could not complete the whole genomic sequencing analysis, but these already planned together with CRC PDOs as outlined above in our lab.
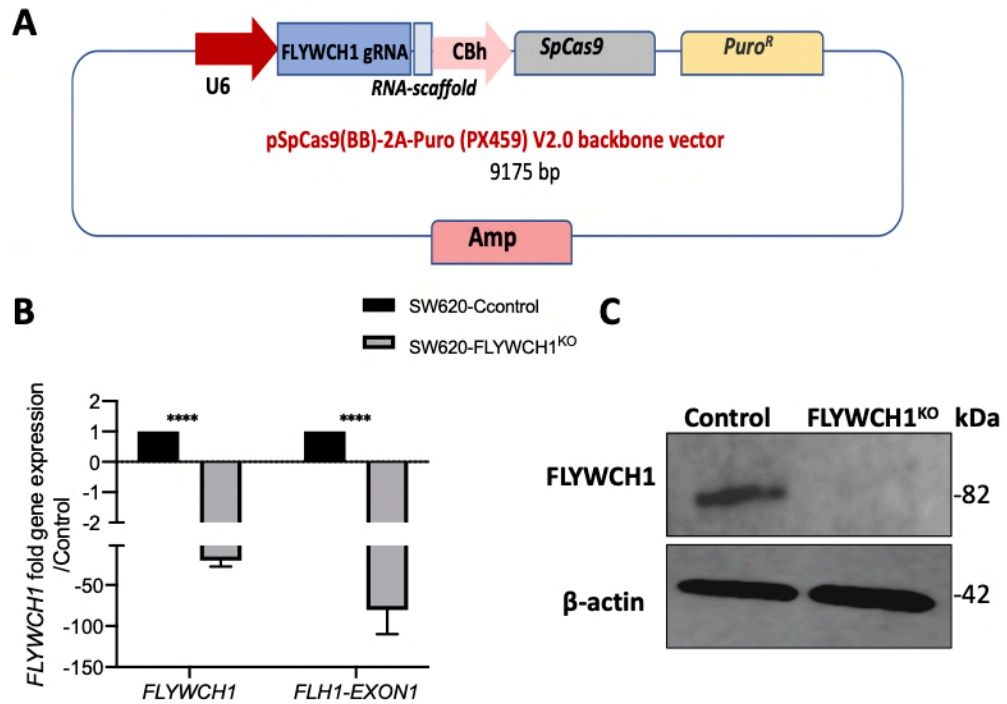
Figure 3-17 Generation and validation of SW620 FLYWCH1^{KO} cells. A) Schematic presentation of pX459-FLYWCH1gRNA-Cas9 expressing plasmid used to generate FLYWCH^{KO} (FLYWCH-gRNA was designed to target Exon1 of FLYWCH1 gene and cloned in backbone pX459-cas9 plasmid from Addgene). **B)** Validation of *FLYWCH1* depletion by qRT-PCR. mRNA expression was obtained by the 2^-(ΔΔCt) method. Experiment was carried out in triplicate and repeated on three independent occasions. Data are mean and SD (****= P ≤ 0.0001). **C)** WB validation of FLYWCH1 expression in SW620^{KO} cells. The level of FLYWCH1 protein was frequently checked to ensure the stable reduction of FLYWCH1 expression, before using the cell line in each experiment.

3.2.4.2 FLYWCH1^{KO} enhances the colonosphere forming efficiency in SW620 cell lines

FLYWCH1-depleted SW620 cells were then tested for their stemness activity, in 3D-colonosphere culture. Briefly, equal numbers of parental control and FLYWCH1^{KO} cells were seeded (1000 cells/ well) in triplicate, in a 6 well plate. Cells were then grown in a conditioned cancer stem-like cells medium (as detailed in Chapter 2, Methods section 2.2.6.1). On day 14, fully grown colonospheres (i.e.

Colonospheres that are bigger than 50 µm) were manually counted, and the forming efficiency of control versus FLYWCH1^{KO} cells was determined as reported in (281). The forming efficiency (%) = scored sphere number/total plating CRC cells (Figure 3-18 C). Thence, colonospheres were disassociated (trypsinized) into single cells, re-plated and allowed to grow again in a suspension stem cell medium, for a new round of sphere forming assay (P2). Later, spheres with diameters >50 µm were scored and the colonosphere forming efficiency (%) was calculated and presented as P2 (Figure 3-18 B). Furthermore, colonospheres size (diameter) was quantified from at least 50 colonospheres for each group (i.e. control versus FLYWCH^{KO}), averaged and presented as the mean averaged size of the colonospheres (Figure 3-18 C).
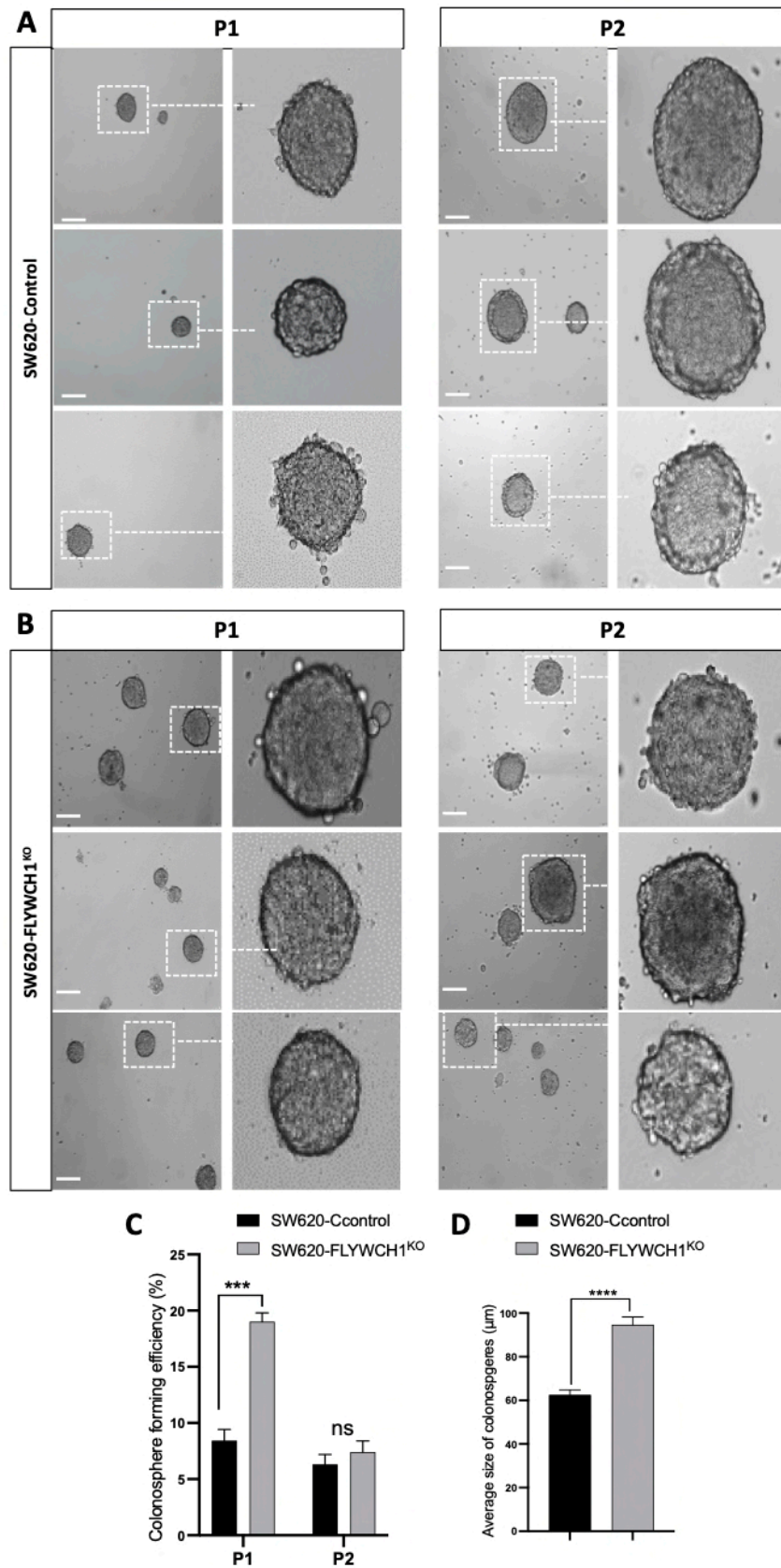
Figure 3-18 Loss of FLYWCH1 increases the colonosphere forming efficiency in SW620 cell lines. A, B) Representative images of the colonospheres formed by both parental control and FLYWCH1^{KO} cells in P1= passage 1 and P2= passage 2.

C) Histogram shows the induction in the colonospheres forming efficiency in FLYWCH1^{KO} compared to control cells in P1 & P2. Colonospheres that are bigger than 50 μm were counted for the analysis. (ns; not significant, ***, P < 0.001). **D)** Graph shows the size differences (diameter) of colonospheres formed by FLYWCH1^{KO} cells compared to control cells (n=50). (****= P ≤ 0.0001). Values represent means and standard deviations (SD) obtained from three independent experiments. The p-values are calculated based on a Student's *t*-test.

Overall, FLYWCH1^{KO} cells formed a greater number of colonospheres in comparison to controls in the first passage. The colonosphere forming efficiency assay showed a significant increase in the forming efficiency of FLYWCH1^{KO} cells compared to their parental SW620 cells (19% versus 8.4%). The increase was still detectable in the second passage (6% versus 7.4% for FLYWCH1^{KO}). Yet, this was not significant (only a 1.4% increase in P2, compared to a 10.5% increase in P1). Also, colonospheres formed by FLYWCH1^{KO} cells were significantly larger (i.e. ranged between 70-110μm) relative to control cells (ranged between 50-70μm). Results indicated that loss of FLYWCH1 promotes the sphere formation capacity of SW620 cells.

To evaluate related changes in stemness activity, we examined the expression of CD44 (a marker of poorly differentiated cells (282)) in colonospheres derived from both control and FLYWCH1^{KO} cells, by immunofluorescence assay (Figure 3-19 A-C). In addition, the transcriptional changes of cancer stem cell markers (LGR5, and CD44) was studied by qPCR assay (Figure 3-19 D).
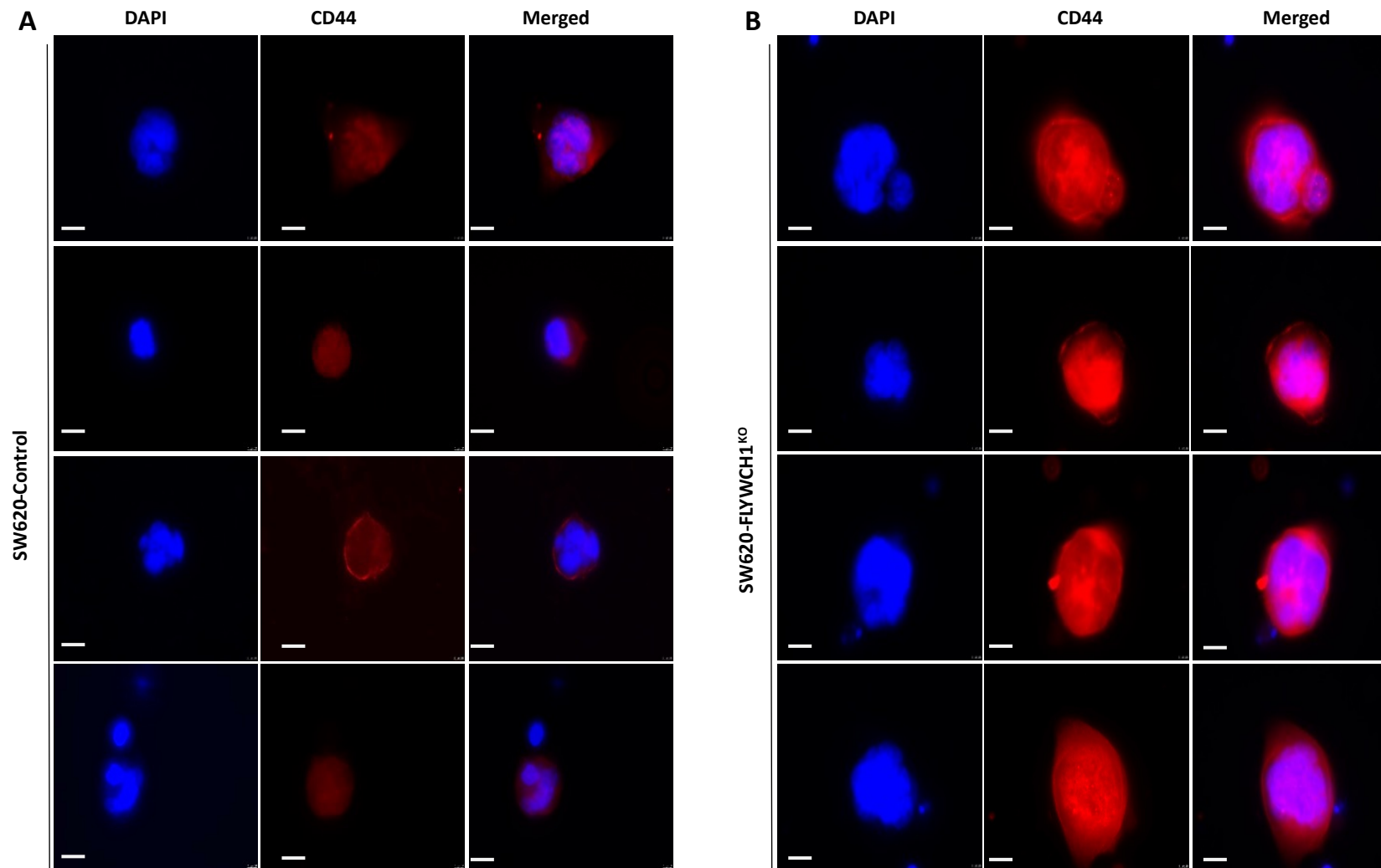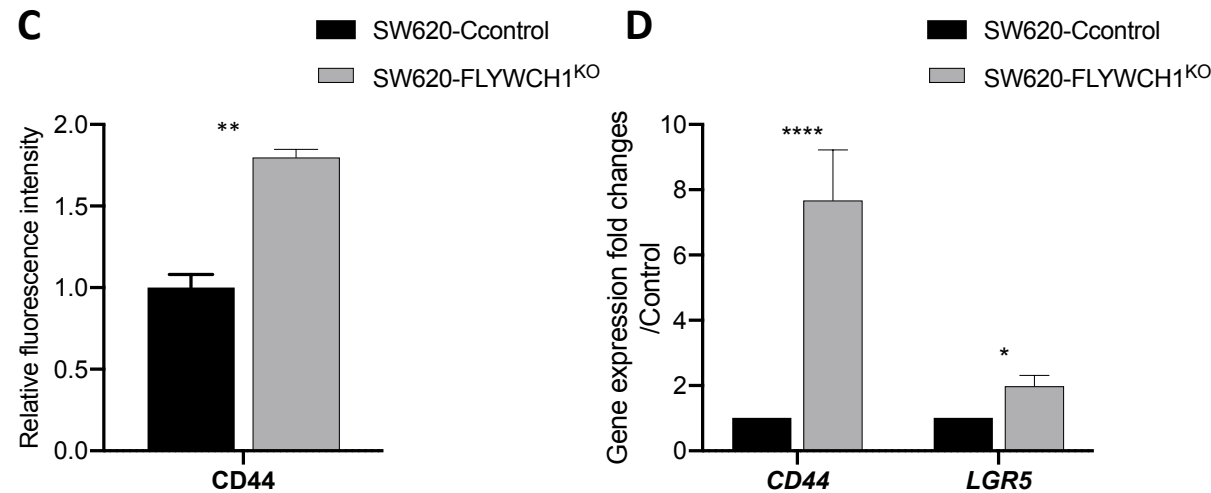
Figure 3-19 Loss of FLYWCH1 confers to more stemness activity in colonospheres derived from SW620 cells. A, B) Immunofluorescence staining shows the expression of CD44 in colonospheres derived from **A)** parental control and **B)** FLYWCH1^{KO} cells. Scale bar 7.5µm. **C)** Histogram confirms the induction of CD44 in spheres obtained from FLYWCH1^{KO}. CD44 relative fluorescence intensity (fold) was measured from at least 25 individual colonospheres obtained from two independent experiments, using ImageJ software. **D)** qPCR analysis indicates an upregulation of *CD44*, and *LGR5* in FLYWCH1^{KO} colonospheres. mRNA expression was obtained by the 2^-(ΔΔCt) method, data are mean and SD, P-values were calculated using a Student's *t*-test. (*=P ≤ 0.05, ****= P ≤ 0.0001).

Collectively, knocking out FLYWCH1 increases the cancer stem-like properties in SW620, by upregulating the stem cell markers *LGR5* and *CD44* and enhancing their colonospheres forming efficiency.

3.2.4.3 FLYWCH1-depletion changes the stem-like cell associated genes expression in SW620-derived colonospheres

To acquire a global view of FLYWCH1-mediated effects on cancer stem-like gene signature, another RT² Profiler™ PCR Array of Human Stem Cell Signaling was performed using isolated RNAs from colonospheres (Figure 3-20). Among others, the expression of genes associated with cell invasion, and migration was upregulated as a consequence of FLYWCH1-depletion, including: FGFR2 (283), Gli1,2 (284), ZEB2 (253), TGF-β binding proteins (LTBPs) (285), and FRZ1(286). Conversely, genes with Wnt-suppressive activities, such as EP300 (249), LRP5, 6 (287), and/or genes with anti-proliferation/metastatic functions, such as CDX2 (288), NOTCH1 (289), FZD7 (290) were substantially downregulated.

A

Genes Under-Expressed in FLYWCH1-KO versus Control Group		
Position	**Gene Symbol**	**Fold Regulation**
A02	ACVR1B	-2.51
A08	BCL9	-2.28
A09	BCL9L	-5.05
A12	BMPR2	-2.44
B01	CDX2	-10.17
B03	CTNNB1	-2.23
B06	EP300	-5.26
B07	FGFR1	-15.31
B10	FGFR4	-3
B12	FZD2	-5.3
C03	FZD5	-11.13
C06	FZD8	-2.76
C07	FZD9	-3.47
C12	LEF1	-5.96
D02	LRP5	-15.2
D03	LRP6	-2.46
D06	LTBP3	-33.97
D08	NCSTN	-6.95
D12	NFATC3	-3.4
E02	NOTCH1	-3.57
E06	PSEN1	-5.12
E07	PSEN2	-2.8
E08	PSENEN	-3.07
E11	PYGO2	-6.9
F01	RBL2	-2.08
F04	SMAD1	-3.7
F09	SMAD6	-8.32
G01	SP1	-2.71
G02	STAT3	-4.02
G04	TCF7	-3.62
G07	TGFBR1	-2.51
G08	TGFBR2	-3.33
H01	ACTB	-5.64

Genes Over-Expressed in FLYWCH1-KO versus Control Group		
Position	**Gene Symbol**	**Fold Regulation**
A06	ACVRL1	3.57
A07	AMHR2	8.78
A11	BMPR1B	2.3
B04	E2F5	2.08
B05	ENG	6
B08	FGFR2	7.97
C04	FZD6	2.08
C05	FZD7	2.16
C08	GLI1	6.52
C09	GLI2	6.79
C10	GLI3	5.91
D01	LIFR	5.29
D04	LTBP1	5.37
D05	LTBP2	7.75
D10	NFATC1	4.18
D11	NFATC2	5.37
E03	NOTCH2	6.47
E04	NOTCH3	7.08
E05	NOTCH4	3.82
E10	PTCHD2	8.08
F02	RBPJL	5.4
F03	RGMA	2.45
F11	SMAD9	6.52
F12	SMO	7.54
G05	TCF7L1	2.23
G11	VANGL2	5.04
G12	ZEB2	3.24
H04	HPRT1	3

B

RT² Profiler™ PCR Array Human Stem Cell Signaling

Layout	01	02	03	04	05	06	07	08	09	10	11	12
A	ACVR1 1.92	ACVR1B -2.51	ACVR1C 1.92	ACVR2A -1.20	ACVR2B 1.09	ACVRL1 3.57	AMHR2 8.78 A	BCL9 -2.28	BCL9L -5.05	BMPR1A -1.17	BMPR1B 2.30	BMPR2 -2.44
B	CDX2 -10.17	CREBBP -1.03	CTNNB1 -2.23	E2F5 2.08	ENG 6.00	EP300 -5.26	FGFR1 -15.31	FGFR2 7.97 A	FGFR3 -1.58	FGFR4 -3.00	FZD1 -1.84	FZD2 -5.30
C	FZD3 1.31	FZD4 1.19	FZD5 -11.13	FZD6 2.08	FZD7 2.16 A	FZD8 -2.76 A	FZD9 -3.47 A	GLI1 6.52	GLI2 6.79 A	GLI3 5.91	IL6ST -1.58	LEF1 -5.96
D	LIFR 5.29	LRP5 -15.20	LRP6 -2.46	LTBP1 5.37	LTBP2 7.75	LTBP3 -33.97	LTBP4 -1.23	NCSTN -6.95	NFAT5 -1.72	NFATC1 4.18 A	NFATC2 5.37 A	NFATC3 -3.40
E	NFATC4 1.65	NOTCH1 -3.57	NOTCH2 6.47	NOTCH3 7.08 A	NOTCH4 3.82	PSEN1 -5.12	PSEN2 -2.80	PSENEN -3.07	PTCH1 -1.39	PTCHD2 8.08 A	PYGO2 -6.90	RBL1 1.44
F	RBL2 -2.08	RBPJL 5.40	RGMA 2.45	SMAD1 -3.70	SMAD2 -1.95	SMAD3 -1.72	SMAD4 1.21	SMAD5 -1.00	SMAD6 -8.32	SMAD7 -1.64	SMAD9 6.52 A	SMO 7.54 A
G	SP1 -2.71	STAT3 -4.02	SUFU -1.53	TCF7 -3.62	TCF7L1 2.23	TCF7L2 -1.19	TGFBR1 -2.51	TGFBR2 -3.33	TGFBR3 1.57	TGFBRAP1 -1.43	VANGL2 5.04	ZEB2 3.24

Magnitude of log2(Fold Change)

-5.086   0   5.086

Figure 3-20 Loss of FLYWCH1 changing the transcriptome of essential stemness markers and Wnt target genes. A) Table shows the list of upregulated (yellow) or downregulated (blue) genes by FLYWCH1 expression obtained from

the PCR array. **B)** Heat map visualises the fold changes in expression between the selected groups for every gene in the array in the context of the array layout. Fold threshold and Regulation cut off =2. The p-values are calculated based on a Student's *t*-test of the replicate 2^ (- Delta CT) values for each gene in the control group, and FLYWCH1^{KO} groups, p-value cut off=0.05.

The array results were then post-validated by qRT-PCR analysis, which aligned with array readings for a sub-set of the genes (Figure 3-21).
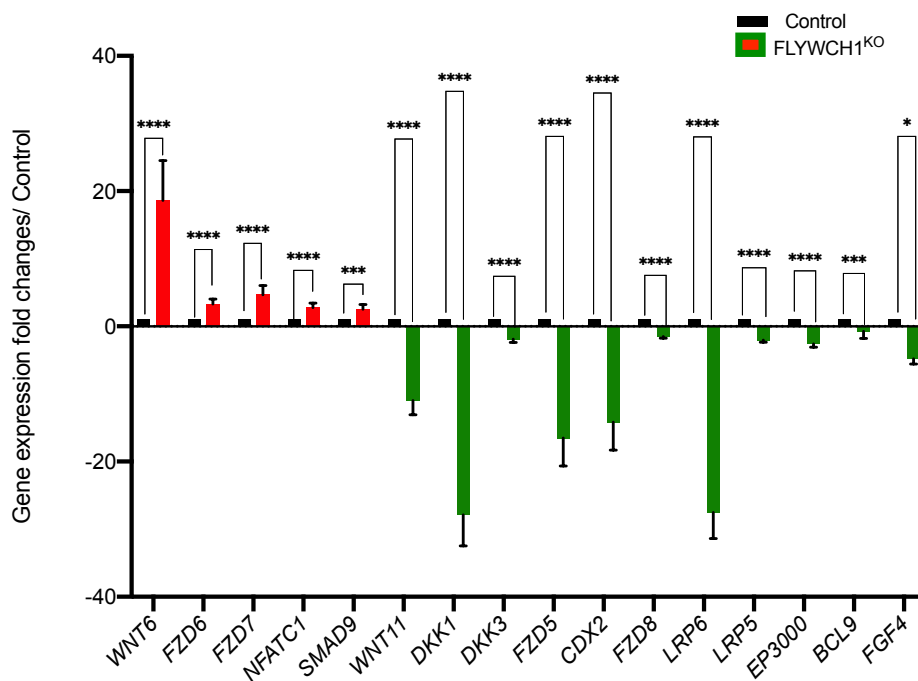
Figure 3-21 qRT-PCR validates the transcriptional changes associated with FLYWCH1^{KO} in SW620-derived colonospheres. Expression of selected downregulated genes showed in green or upregulated genes in Red. mRNA expression was examined by the 2^-($\Delta\Delta$Ct) method. Data are mean and SD. P-values were estimated using the two-way ANOVA test. (*=P $\leq$ 0.05, ***= P $\leq$ 0.001, ****= P $\leq$ 0.0001).

Together, loss of FLYWCH1 triggers the colonosphere forming ability, relatively, by modulating Wnt-mediated biological response to functionally promote a stem-like cell phenotype in a colonosphere culture.

3.2.5. The regulation of endogenous FLYWCH1 by Wnt/β-catenin signaling

To this point, we have proposed FLYWCH1 as an important repressor element for Wnt/β-catenin signaling, regulating stemness, cell-cell attachment, and invasion in CRC cells. This could be partially via its direct interaction and suppression of nuclear β-catenin activity in association with TCF/LEF transcription factors (198). However, the interplay between FLYWCH1 and the Wnt pathway appears more complex. In fact, many β-catenin regulators [such as SOX9 (291) and AXIN2 (292)] are themselves regulated by Wnt/β-catenin (293). Our findings here upraised the questions about the potential regulation of FLYWCH1 expression by Wnt/β-catenin signaling and whether FLYWCH1 constitutes one of its downstream targets. Thus, we here explored the potential regulation of FLYWCH1 by Wnt signaling in cultured normal versus cancer cell lines. This was primarily attained by activating Wnt signaling using Wnt3A-conditioned medium and GSK-3β inhibitor. However, prior to this, we carried out an IF analysis on a panel of CRC cell lines (HCT116, SW480, SW620 and DLD-1), alongside normal cell lines; TIG119 (Human skin fibroblast cells), CCD 841 CoN (normal colon epithelial cell line) and HEK293T (human embryonic kidney cells), to explore the pattern of FLYWCH1 expression in normal versus cancer cells (Figure 3-22).
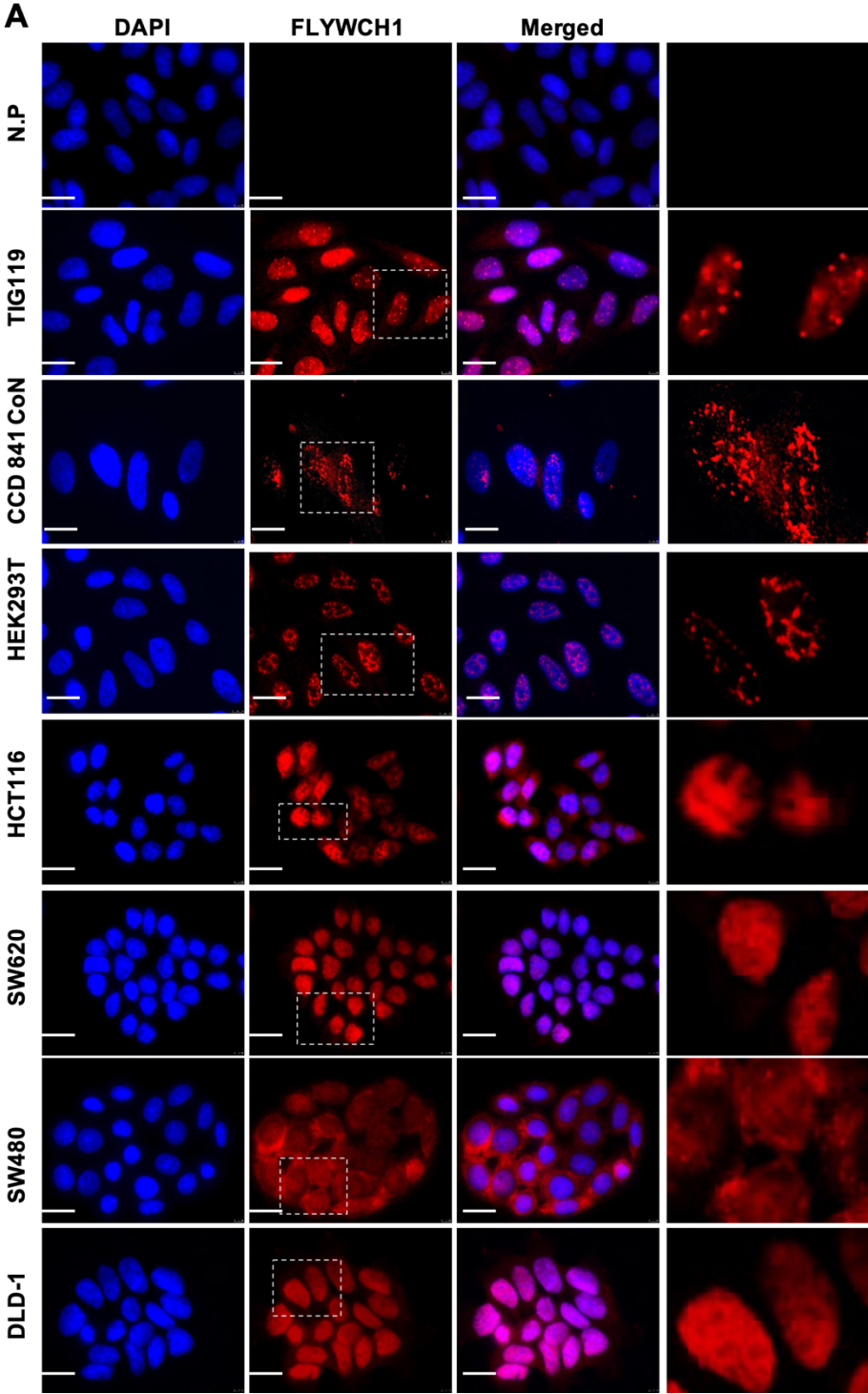
Figure 3-22 IF staining showing the pattern and distribution of FLYWCH1 protein in normal (TIG119, CCD841CoN, and HEK293T) versus CRC cell lines (HCT116, SW620, SW480 and DLD-1). N.P is a Negative control (no primary antibody using TIG119 cells). Dotted boxes indicate enlarged cell/s. Magnification, 100x. Scale bars, 7.5µm.

The IF data shows that the pattern of FLYWCH1 protein expression varied between normal and cancer cells. FLYWCH1 formed clear nuclear foci in normal cell lines. Whereas, in CRC cells, FLYWCH1 protein showed a diffused pattern of nuclear expression (Figure 3-22). Results provided an overall idea about the variation of FLYWCH1 expression pattern in the several cell lines used throughout the project.

3.2.5.1 Wnt activation downregulates the expression of FLYWCH1 in normal and CRC cells

Considering the functional roles of FLYWCH1 in colorectal cancer cells and organoid growth outlined above, we tested if FLYWCH1 expression was modulated by Wnt signalling. To test the Wnt dependence, we initially examined FLYWCH1 mRNA and protein expression under activated Wnt signaling. Wnt stimulation was achieved in cultured cells, using the Wnt3A conditioned medium (Wnt3A-CM) (Chapter 2, Methods section 2.9), which was validated by luciferase activity and used for culturing the organoids (Appendix 2). Furthermore, we validated the activation of Wnt signalling in Wnt3A treated cells via immunofluorescence staining for Wnt target genes (c-Jun and Cyclin-D1) (Figure 3-23 A), and western blotting assays for β-catenin, phosphorylated β-catenin (inactive form), c-Jun and Cyclin-D1 (Figure 3-23 B). Untreated HCT116 lysate was used as a negative control.
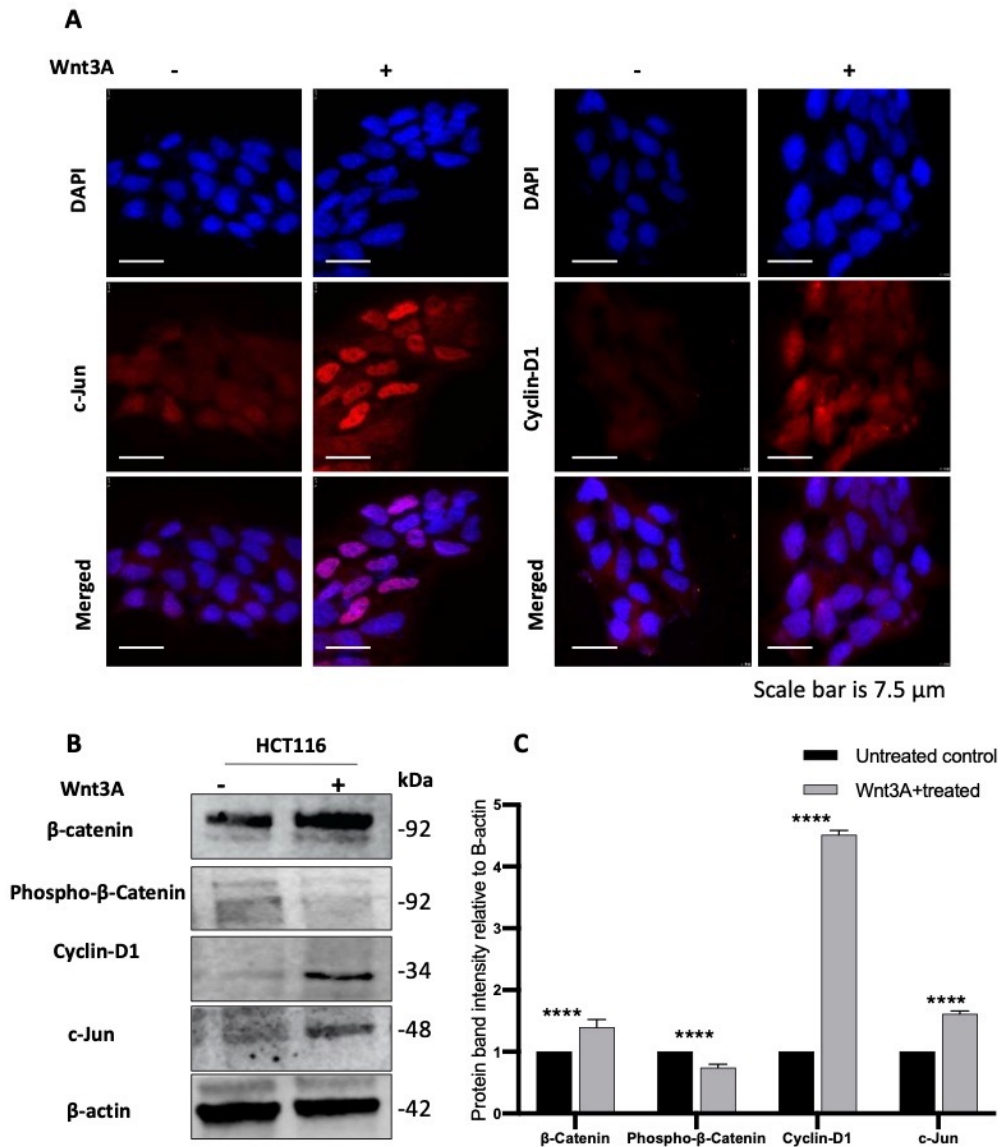
Figure 3-23 Validation of the activation of Wnt-pathway in HCT116 cell line treated with Wnt3A-CM. A) Immunofluorescence staining of c-Jun and Cyclin-D1, Magnification: 100x, Scale bars: 7.5µm. **B)** WB analysis of HCT116 cells treated with Wnt3A-CM for 24h, showing the induction in Wnt target genes. N=3 (Validation was repeated for each batch of Wn3A-CM). **C)** Histogram shows the relative densitometric quantification band intensities of β-catenin, phospho-β-catenin (Ser33/37/Thr41), c-Jun, Cyclin-D1 proteins normalized to β-actin and presented as the mean fold changes obtained from three independent experiments. P-values were calculated by a Student's *t*-test (****= P ≤ 0.0001).

Figure 3-23 demonstrated an induction of Wnt targets (c-Jun and Cyclin-D1) in Wnt3A treated cells, suggesting an increase in the transcriptional activity of Wnt/β-catenin pathway after 24h stimulation with Wnt3A-CM.

Subsequently, the potential effects on FLYWCH1 transcription and protein expression were examined following Wnt3A-CM treatment (Figure 3-24). The expression of FLYWCH1 mRNA was measured by standard RT-PCR and qRT-PCR analysis (Figure 3-24 A, B). In parallel, lysates were extracted and examined by WB for FLYWCH1 protein expression (Figure 3-24 C, D).
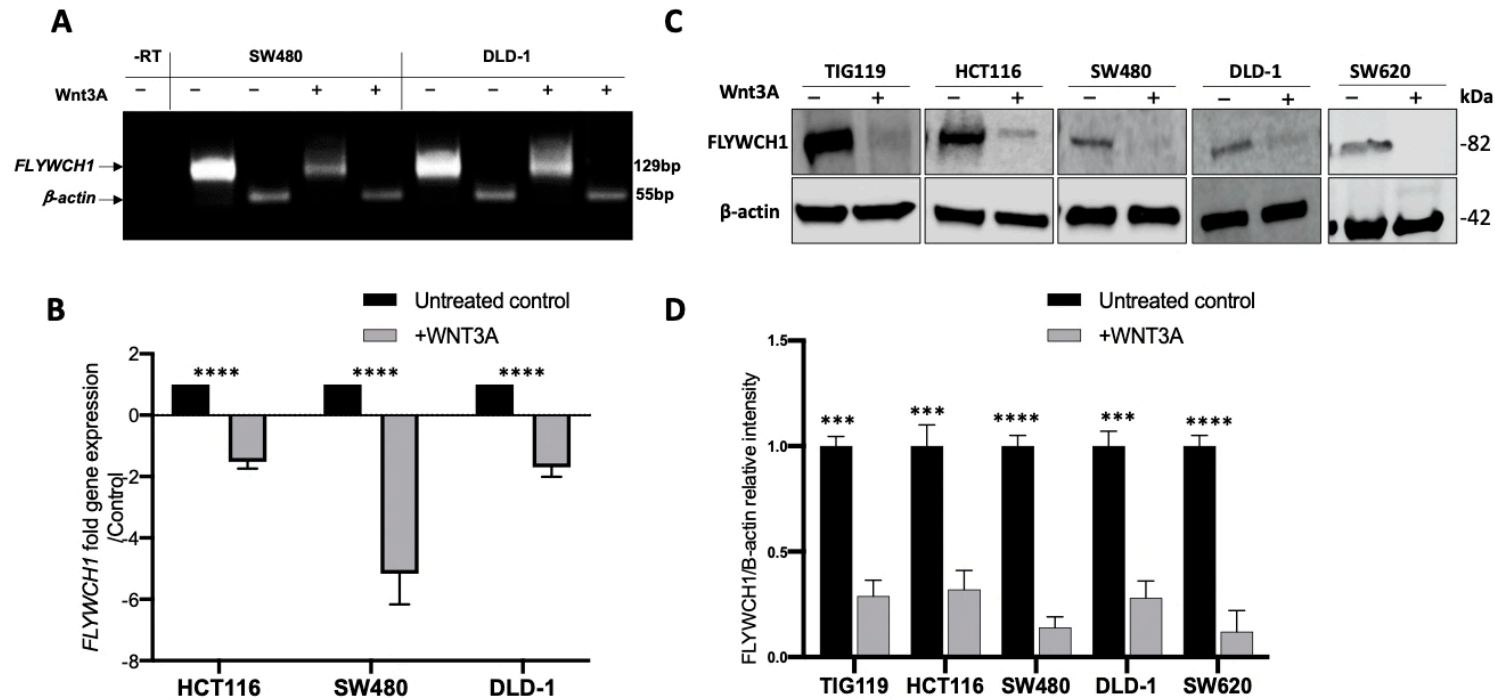
Figure 3-24 Wnt activation downregulates the transcription and protein expression of FLYWCH1 in various cell lines. CRC cell lines were treated with Wnt3A-CM or mock treated (medium only) for 24h. RNA was extracted and FLYWCH1 mRNA expression was assessed by **A)** Standard PCR (N=3, 100bp marker was used) and **B)** qRT-PCR (mRNA expression was obtained by using the 2^- (ΔΔCt) method. Each set of experiment was carried out in triplicate and repeated on three independent occasions. Data are mean ± SD. **C)** WB analysis showing the reduction in FLYWCH1 total protein expression in TIG119, and CRC cells treated with Wnt3A-CM. Experiments were repeated in three independent times. **D)** Graph shows the relative densitometric quantification of FLYWCH1 band intensities normalized to β-actin and presented as the mean fold changes obtained from three independent experiments. P-values were calculated by a Student's *t*-test (***= P ≤ 0.001, ****= P ≤ 0.0001).

Our findings indicate a significant downregulation of FLYWCH1 mRNA and protein level following 24h treatment with Wnt3A, in cultured cell lines (Figure 3-24).

We further examined if the cellular distribution and pattern of FLYWCH1 expression influenced by Wnt-3A treatment in various cell lines via immunofluorescence assay and WB analysis of nuclear/cytoplasmic protein expression (Figure 3-25).
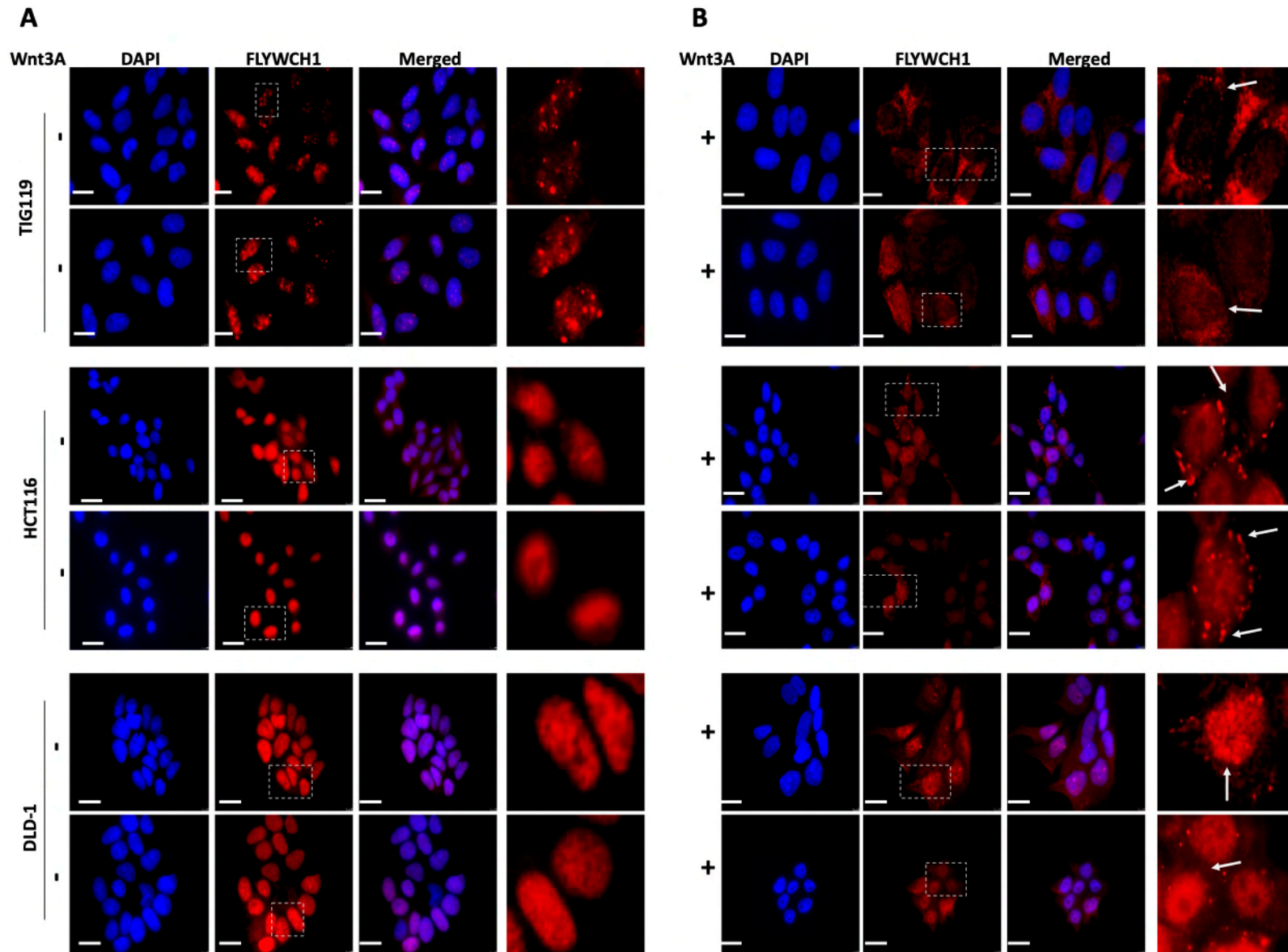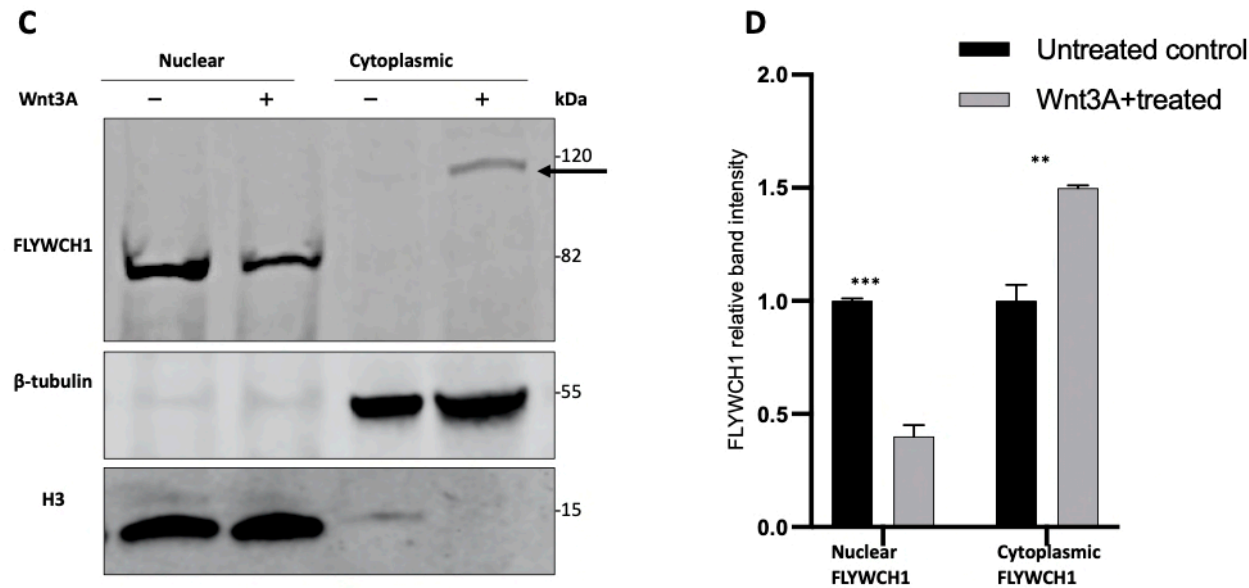
Figure 3-25 Wnt activation changes the cellular distribution of FLYWCH1 protein. A, B) Immunofluorescence staining showing the effect of Wnt3A on the cellular distribution and pattern of FLYWCH1expression in TIG119 and CRC (HCT116 and DLD-1) cell lines. Dotted lines indicate enlarged cell/s. Magnification: 100x, Scale bars: 7.5μm. **C)** Immunoblots show the nuclear and cytoplasmic distribution of FLYWCH1 in HCT116 cells following Wnt3A-CM treatment. **D)** Graph shows the relative densitometric quantification of western blot band intensities for the ratio of nuclear FLYWCH1 normalized to H3 and the ratio of cytoplasmic FLYWCH1 normalized to β-tubulin and presented as mean fold changes of three independent experiments. (**= $P \leq 0.01$, ***= $P \leq 0.001$). P-values were estimated by a Student's *t*-test**.**

Of note, Wnt3A treatment triggered changes in the cellular distribution of FLYWCH1, particularly in normal cells (TIG119), where FLYWCH1 was clearly shifted into the cytoplasm, and no nuclear foci were detected in the treated cells (Figure 3-25 B, Top panel). In CRC cells, the changes were less evident, and FLYWCH1 nuclear level was slightly affected. This could be due to the overactivated nature of Wnt signaling in CRC cells, as well as the low level of FLYWCH1 in cancer cells relative to normal cells. Nonetheless, cytoplasmic foci were formed in Wnt-3A treated cancer cells which were not detected in the untreated cells (Figure 3-25 B, middle and bottom panel). Cytoplasmic foci could be related to several cellular processes, such as post-transcriptional modifications (294) and posttranslational modifications (295, 296).

Further WB analysis of nuclear/cytoplasmic fractions revealed a significant reduction of nuclear FLYWCH1 protein and upregulation of cytoplasmic FLYWCH1 protein in the HCT116 treated cells (Figure 3-25 C, D). A clear shift in the molecular weight of FLYWCH1 was perceived in the cytoplasmic fraction (Figure 3-25 C, arrowhead). Data suggest that WNT-activation may also lead to changes in the FLYWCH1 protein posttranslational modification (PTM), such as Phosphorylation, or changes through other PTMs. Further investigations are required to explore and examine FLYWCH1-PTMs possibilities.

In conjugation, the results above suggest a direct effect of Wnt modulation on FLYWCH1 expression and nuclear localisation. Yet the exact mechanism(s) of FLYWCH1 regulation and translocation is still not clear. Thus, we next considered an alternative mean of Wnt activation by inhibiting GSK-3β (using a small molecule 6-bromoindirubin-30-oxime (BIO)). GSK-3 inhibitors activate the Wnt pathway and

ultimately prevent β-catenin degradation (297). BIO was reported by several studies for its high specificity to inhibit GSK3 and is known to maintain self-renewal in human, and mouse embryonic stem cells (ESCs)(298).

3.2.5.2 GSK-3β inhibition reduces the level of FLYWCH1 and modulates its stability

Here, we studied the changes in FLYWCH1 protein expression following GSK-3β inhibition in HEK293T, TIG119 and CRC cell lines. Cells were seeded on coverslips (IF) or 10cm dishes (WB), treated with 5µM BIO or mock treated with medium only for 24h. The concentration of BIO was determined as established in our lab and others (198, 299). GSK-3β inhibition was initially validated, and the effect on FLYWCH1 protein expression and distribution was concurrently examined in HEK293T cells by IF staining (Figure 3-26 A, B) and WB analysis (Figure 3-26 C, D).
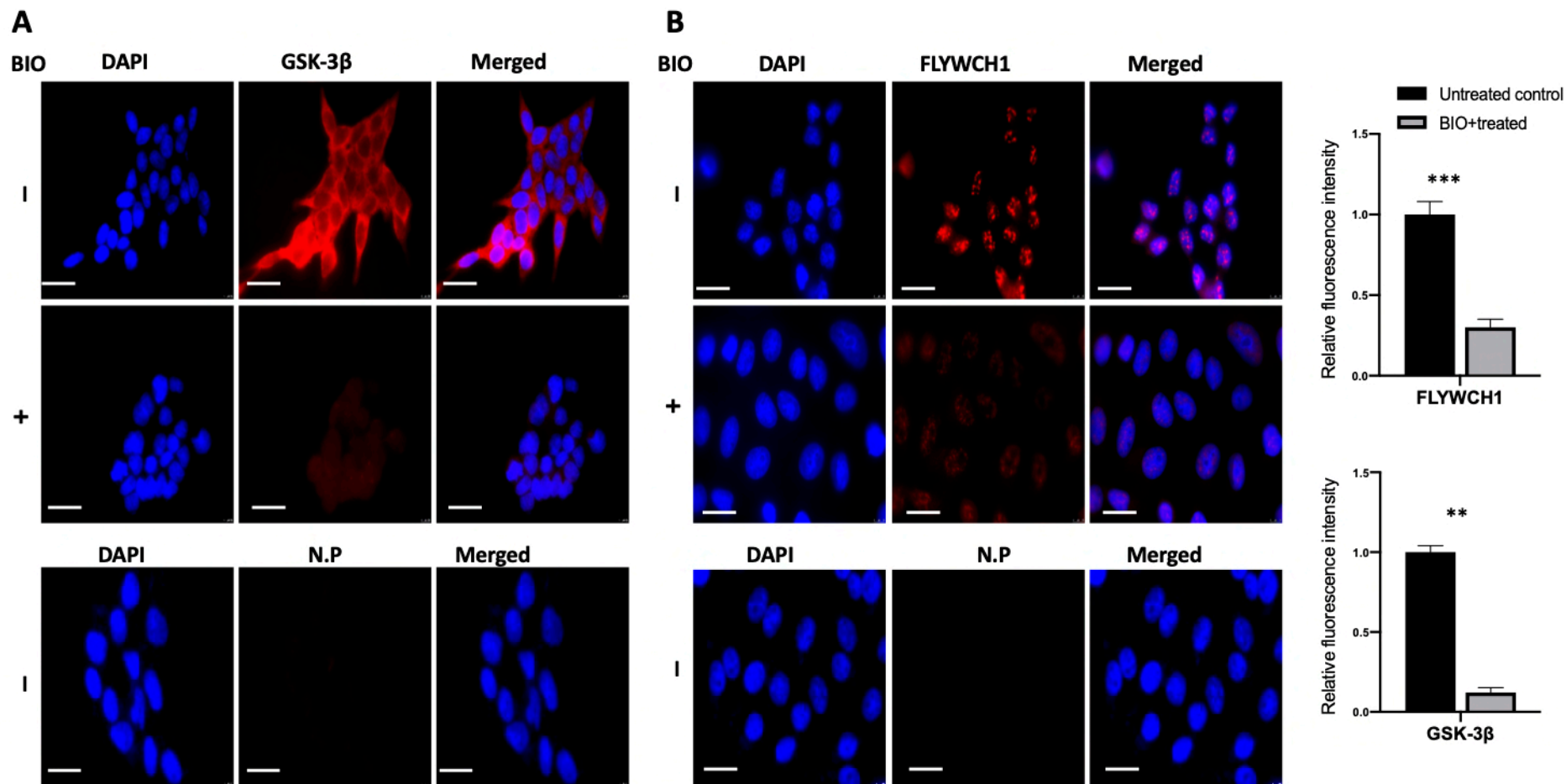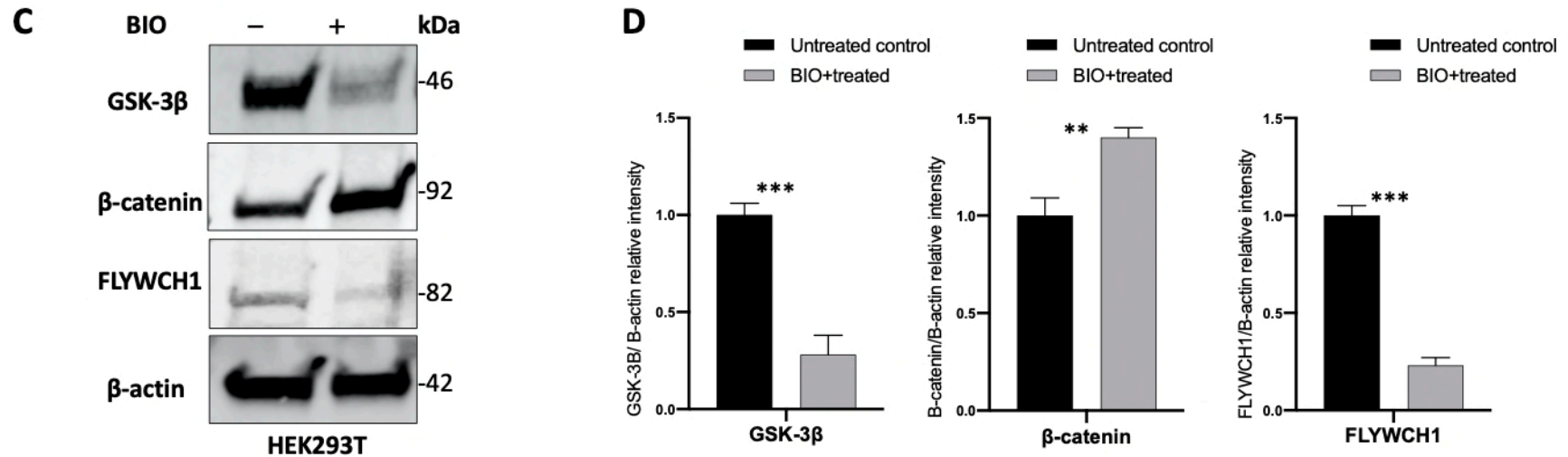
Figure 3-26 Validation of GSK-3β inhibitor in HEK293T cells. A, B) IF staining validates GSK-3β inhibition in HEK293T cells and demonstrates an overall reduction of FLYWCH1 level in the treated cells. Histograms represent the relative fluorescence intensity compared to control and expressed as mean± SD. (N.P, no primary antibody, used as a negative control). Magnification: 100x, Scale bars: 7.5μm. **C)** Validation of GSK-3β inhibition by WB, showing the induction of β-catenin and suggesting a significant reduction of FLYWCH1 protein following BIO treatment (5μM). **D)** Histograms show the relative densitometric quantification of GSK-3β, β-catenin and FLYWCH1 band intensities normalized to β-actin (N=3). P-values were calculated using a Student's *t*-test (**= P ≤ 0.01, ***= P ≤ 0.001).

The effect of GSK-3β inhibitor on FLYWCH1 total protein expression was further studied in CRC and TIG119 cells (Figure 3-27 A). However, because of the strong reduction in the staining intensity in BIO treated cells (Figure 3-26 B), it was not helpful to detect any changes in the cellular distribution by IF staining, and therefore the effect on FLYWCH1 cellular distribution were examined by WB analysis of nuclear/cytoplasmic lysates in HCT116 cells (Figure 3-27 C).
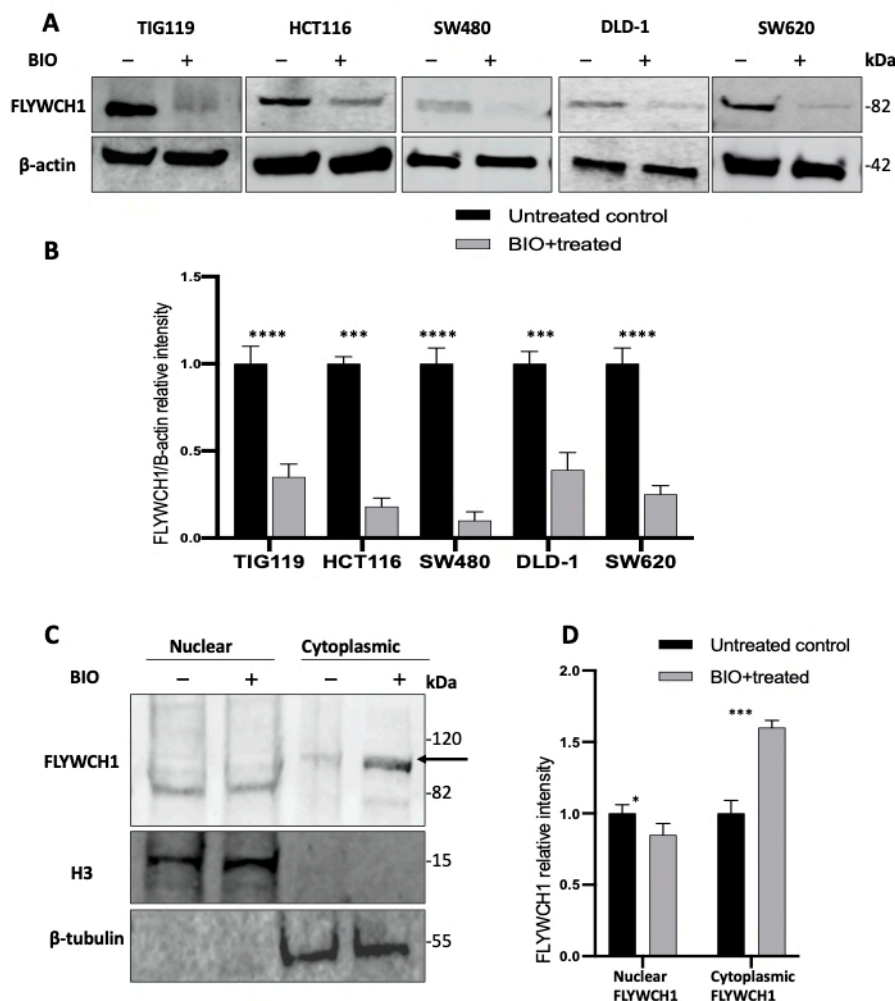
Figure 3-27 GSK-3β inhibition reduces the level of FLYWCH1 in TIG119 and CRC cells. A, B) WB analysis and quantifications showing the significant reduction in FLYWCH1 total protein expression in BIO treated cells. Band intensities were normalized to β-actin and presented as the mean of fold change obtained from three independent experiments. **C)** Immunoblots showing the distribution of FLYWCH1 in the nuclear/cytoplasmic fractions following BIO

treatment in HCT116 cells (N=2). **D)** Graphs show the relative densitometric quantification of nuclear FLYWCH1 band intensity normalized to H3, and the ratio of cytoplasmic proteins normalized to β-tubulin. Data represents the mean fold changes obtained from two independent experiments. P-values were calculated by a Student's *t*-test (ns; not significant, *=P ≤ 0.05, **= P ≤ 0.01, ***= P ≤ 0.001, ****=P ≤ 0.0001).

In line with Wnt3A results, we showed that modulating Wnt signaling by BIO reduces the total protein expression of FLYWCH1 in all tested cell lines (Figure 3-27). Likewise, BIO treatment significantly induced the cytoplasmic FLYWCH1, with less effect on the nuclear protein (Figure 3-27 C, D). Again, an increase in the molecular weight of the cytoplasmic FLYWCH1 were noticed. These repeated observations urged the need to study the stability and potential PTMs of FLYWCH1 under Wnt-modulation.

Given the role of GSK-3β in regulating many other transcription factors (TFs) and transcription activators such as c-Myc (300), Snail (301), Slug (302) including β-catenin (303) by phosphorylation that lead to UB-dependent proteasomal degradation (304), we next explored the possible regulation of FLYWCH1 stability and PTMs by GSK-3β.

3.2.5.3 FLYWCH1 protein stability and turnover.

In order to understand FLYWCH1 protein PTMs activity, FLYWCH1 protein stability was first determined via Cycloheximide (CHX) treatment (an inhibitor of protein biosynthesis and translational elongation (305, 306)). Besides, to address whether inhibition of the proteasome system could counteract the degradation of FLYWCH1 caused by CHX treatment, FLYWCH1 protein stability was determined in the presence or absence of proteasomal inhibitor MG132 (peptide aldehydes that

strongly inhibits multiple peptidase activities of proteasomes and calpain activity (307, 308)). Briefly, HEK293T cells were seeded and synchronized in serum-free medium for 16h, before treatment with 100μg/ml of CHX, and/or MG132 (2μM). Cells treated with just Optimum medium was included as a negative control. At indicated time intervals, lysates were collected for WB analysis (Figure 3-28 A). In parallel, we investigated the effect of GSK-3β inhibition on FLYWCH1 stability and turn-over by blocking the *de novo* protein synthesis with cycloheximide in cells treated with/without BIO (5μM). This was followed by WB analysis of FLYWCH1 protein expression (Figure 3-28 B).
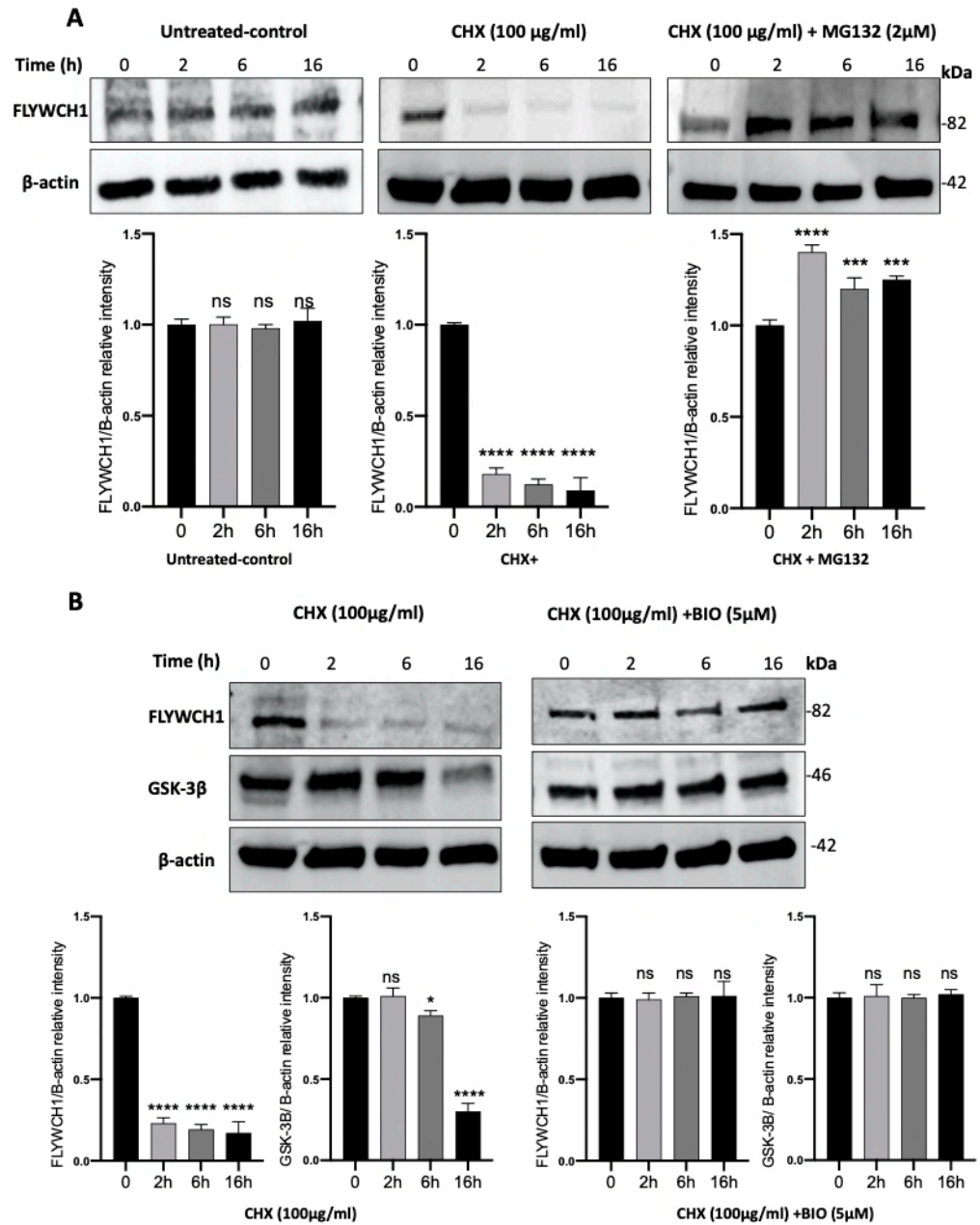
Figure 3-28 FLYWCH1 protein stability and turn-over. A) CHX-chase analysis reveals the half-life of FLYWCH1 protein. HEK293T cells were treated with (Medium only as a negative control, left panel), 100μg/ml CHX (Middle panel), or 100μg/ml CHX+MG132 (2μM) (Right panel). For the proteasome inhibitor MG132, HEK293T cells were seeded and treated with MG132 (2μM), 16h later, cells were washed in Optimum medium and a fresh medium containing cycloheximide (100μg/ml) was then added. At indicated time intervals, lysates were collected and (80μg) protein was loaded on 4-20% SDS-PAGE and blotted with anti-FLYWCH1 and anti-β-actin antibodies. Histograms show FLYWCH1 protein band intensities following normalization with β-actin, obtained from three independent experiments. **B)** BIO treatment extends the half-life of FLYWCH1 protein in cells treated with CHX. HEK293T cells were treated with 5μM of BIO

(right panel) or mock treated with Optimum medium (left panel). 24h later, 100μg/ml cycloheximide (CHX) was added. At the indicated time points, lysates were prepared, and western blotting analysis was performed with the indicated antibodies. Graphs show the densitometric quantification of FLYWCH1 and GSK-3β band intensities normalized to β-actin. Data are represented as the mean fold change obtained from two independent experiments (ns; not significant *=P ≤ 0.05, **= P ≤ 0.01, ***= P ≤ 0.001, ****= P ≤ 0.0001). P-values were calculated using a Student's *t*-test.

Figure 3-28 A demonstrates a rapid degradation of FLYWCH1 within 2h of CHX treatment. Remarkably, inhibiting the proteasome system with MG132 delayed the CHX-mediated degradation of the FLYWCH1 protein by extending the half-life of FLYWCH1 from approximately 2h to 16h (Figure 3-28 A, right panel). Likewise, BIO treatment extended the half-life of FLYWCH1 up to 16h when compared to 2h in the control samples (CHX only, Figure 3-28 B). Therefore, the inactivation of GSK-3β might stop the rapid turnover of FLYWCH1.

Collectively, Wnt3A and BIO controls the stability and cellular distribution of FLYWCH1 in cell lines. Nonetheless, the insufficient knowledge of FLYWCH1 regulation by Wnt or other signaling pathways urges the need to study the potential PTM events that might influence FLYWCH1's stability, function, and localisation within the cells. While PTMs are important determinants of protein stability and cellular localisation, we next explored the possible PTMs of FLYWCH1 protein using online prediction tools.

3.2.5.4 PTMs of FLYWCH1

Due to the lack of previous experimental studies, we first employed PhosphoSitePlus (https://www.phosphosite.org)(309), iPTMnet

(https://research.bioinformatics.udel.edu/iptmnet) (310), and Uniprot (https://www.uniprot.org) (311), to explore the possible PTMs sites of human FLYWCH1 protein. The database showed various PTM sites within the FLYWCH1, these included phosphorylation, ubiquitination and SUMOylation (Figure 3-29). Intriguingly, the phosphorylation sites were predominantly detected at the C-terminal domain (which contains NLS and β-catenin interaction site (198)). This could be an indicative of a possible link between the phosphorylation status of FLYWCH1 protein and its nuclear localisation and/or activity.

A)

B)

Site	PTM type	Source
S7	Phosphorylation	PhosphoSitePlus
S13	Phosphorylation	PhosphoSitePlus
S21	Phosphorylation	HPRD, PhosphoSitePlus and UniProt
K23	Ubiquitination	PhosphoSitePlus
T26	Phosphorylation	PhosphoSitePlus
K142	Ubiquitination	PhosphoSitePlus
K146	Ubiquitination	PhosphoSitePlus
K189	Ubiquitination	PhosphoSitePlus
S192	Phosphorylation	PhosphoSitePlus
S261	Phosphorylation	PhosphoSitePlus, UniProt
S360	Phosphorylation	PhosphoSitePlus
S371	Phosphorylation	PhosphoSitePlus
K393	Sumoylation	PhosphoSitePlus
T498	PhosphoSitePlus	PhosphoSitePlus
S503	Phosphorylation	PhosphoSitePlus, UniProt
S591	Phosphorylation	PhosphoSitePlus, UniProt
S641	Phosphorylation	PhosphoSitePlus
S696	Phosphorylation	PhosphoSitePlus, UniProt
K707	Ubiquitination	PhosphoSitePlus
S715	Phosphorylation	PhosphoSitePlus
S591	Phosphorylation	PhosphoSitePlus

Figure 3-29 Predicted PTM sites of FLYWCH1 and their location within the protein sequence. A) Diagram shows the various PTM modification sites within

the FLYWCH1 protein sequence. Data were generated utilising PhosphoSitePlus (309). **B)** Table shows the position and type of PTM on FLYWCH1 protein.

Afterwards, pilot experiments aimed to investigate the ubiquitination and phosphorylation of FLYWCH1 under modulated Wnt signaling via *in-vitro* Co-IP based assays (Appendix 4). Briefly, we explored the outcomes of Wnt activation by (Wnt3A-CM) and BIO on the ubiquitination and phosphorylation of FLYWCH1 using Co-IP-based approaches. To study the ubiquitination, HEK293T cells were first transfected with HA-UB (HA-tagged ubiquitin was previously used in (231)). 48h post-transfection, cells were either treated with Wnt3A or BIO or mock-treated with medium only. Protein lysates were then extracted and immunoprecipitated with an antibody against endogenous FLYWCH1. Non-immunoprecipitated protein lysates were used as input controls for the protein expression. Samples were immunoblotted using an anti-HA antibody to detect the Ubiquitinated form of FLYWCH1. In parallel, we blotted the anti-Phospho-(Ser/Thr) antibody to detect the phosphorylated protein.

However, due to several technical issues, we failed to get a conclusive/robust statement without repeating the experiment, at least, three times. And therefore, data were excluded from this study. Nonetheless, these preliminary experiments indicated that FLYWCH1 can be ubiquitinated (Appendix 4 A). Also, the Co-IP analysis suggested that FLYWCH1 might be maintained by phosphorylation under untreated conditions. As we detected a band corresponding to the phosphorylated form of FLYWCH1 (Ser/Thr) only in the untreated sample, but lost

in Wnt3A or BIO treated cells (Appendix 4 B, Middle panel). However, these experiments need to be repeated, to ascertain these findings.

In brief, Wnt activation by Wnt3A or BIO suppresses FLYWCH1 expression in normal and CRC cells by mediating FLYWCH1 cytoplasmic translocation. We speculate that activation of Wnt signaling might induce changes in FLYWCH1 PTM status (mainly phosphorylation), which could affect the protein stability and lead to its cytoplasmic translocation. Further studies addressing the mechanism of FLYWCH1 shuttling in relation to WNT activity and its PTM status would be essential to confirm our hypothesis.

To understand and model the impact of Wnt activation on FLYWCH1's tumour suppressive functions, we next examined the effect of GSK-3β inhibition on the growth and proliferation of FLYWCH1-overexpressing PDOs.

3.2.6 The impact of BIO on FLYWCH1-overexpressing PDOs

Both types of PDOs (Cystic/Floral) over-expressing FLYWCH1 (or empty vector), were treated with the 5μM of BIO. Seventy-two hours later, cell proliferation was examined via WST-1 proliferation assay (Figure 3-30). WST-1 is a colorimetric assay that is based on the cleavage of a tetrazolium salt, MTS, by mitochondrial dehydrogenases to form formazan in viable cells (312).
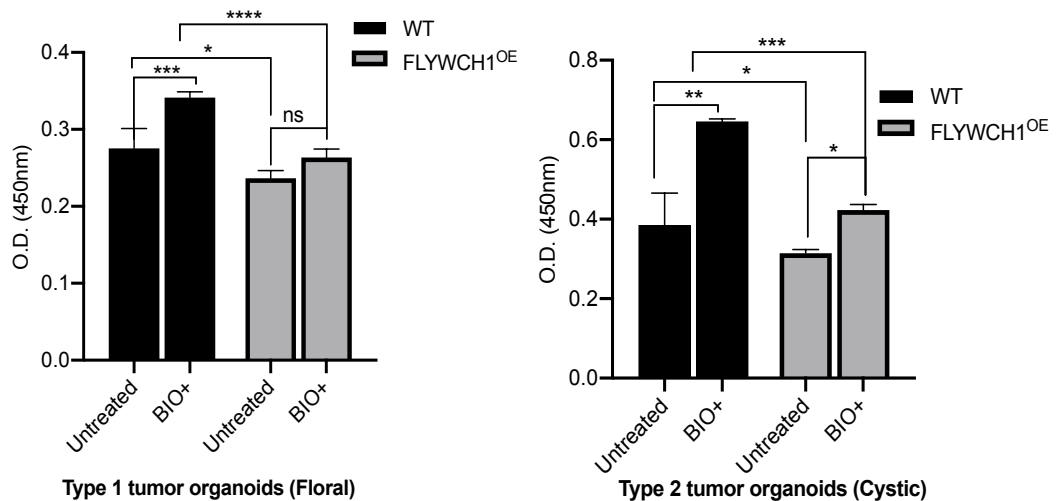
Figure 3-30 BIO treatment induces the proliferation of PDOs, however FLYWCH1-overexpression might antagonise this effect. WST-1 proliferation assay suggesting an increase in the proliferation activity following BIO-treatment. PDOs were transduced with pLVX-lentivirus particles expressing pLVX-Puro-eGFP-FLYWCH1 cDNA (or pLVX-lentivirus expressing empty vector). On day 5, organoids were treated with 5μM of BIO for 72h. The medium was then transferred into a 96 well-plate, and cell viability/proliferation was measured 2h after adding WST-1 reagent. Tumour organoid medium was used as a blank control. (Experimental conditions were determined based on an optimisation experiment piloted on the parental organoids). WST-1 assay was performed in triplicate, and experiment was repeated in two independent occasions. P-values were calculated using the Two-way ANOVA test (*=$P \leq 0.05$, **= $P \leq 0.01$,***= $P \leq 0.001$,****= $P \leq 0.0001$).

As shown in Figure 3-30, BIO treatment stimulated the proliferation of tumour organoids significantly regardless of FLYWCH1[OE], yet the growth stimulation was weaker in FLYWCH1-expressing organoids when compared to control organoids (Figure 3-30, BIO+WT versus BIO+FLYWCH1[OE]). It is likely that FLYWCH1 over-expression antagonises or neutralises the proliferation induction caused by BIO in PDOs.

3.2.6.1 Transcriptional changes associated with BIO treatment in FLYWCH1^{OE}

PDOs

To further explore the underlying transcriptional changes related to BIO treatment

under FLYWCH1-overexpression, gene expression analyses of key Wnt target

genes, intestinal stemness and differentiation markers were carried out in Type 1

(Figure 3-31) and Type 2 (Figure 3-32) tumour organoids.
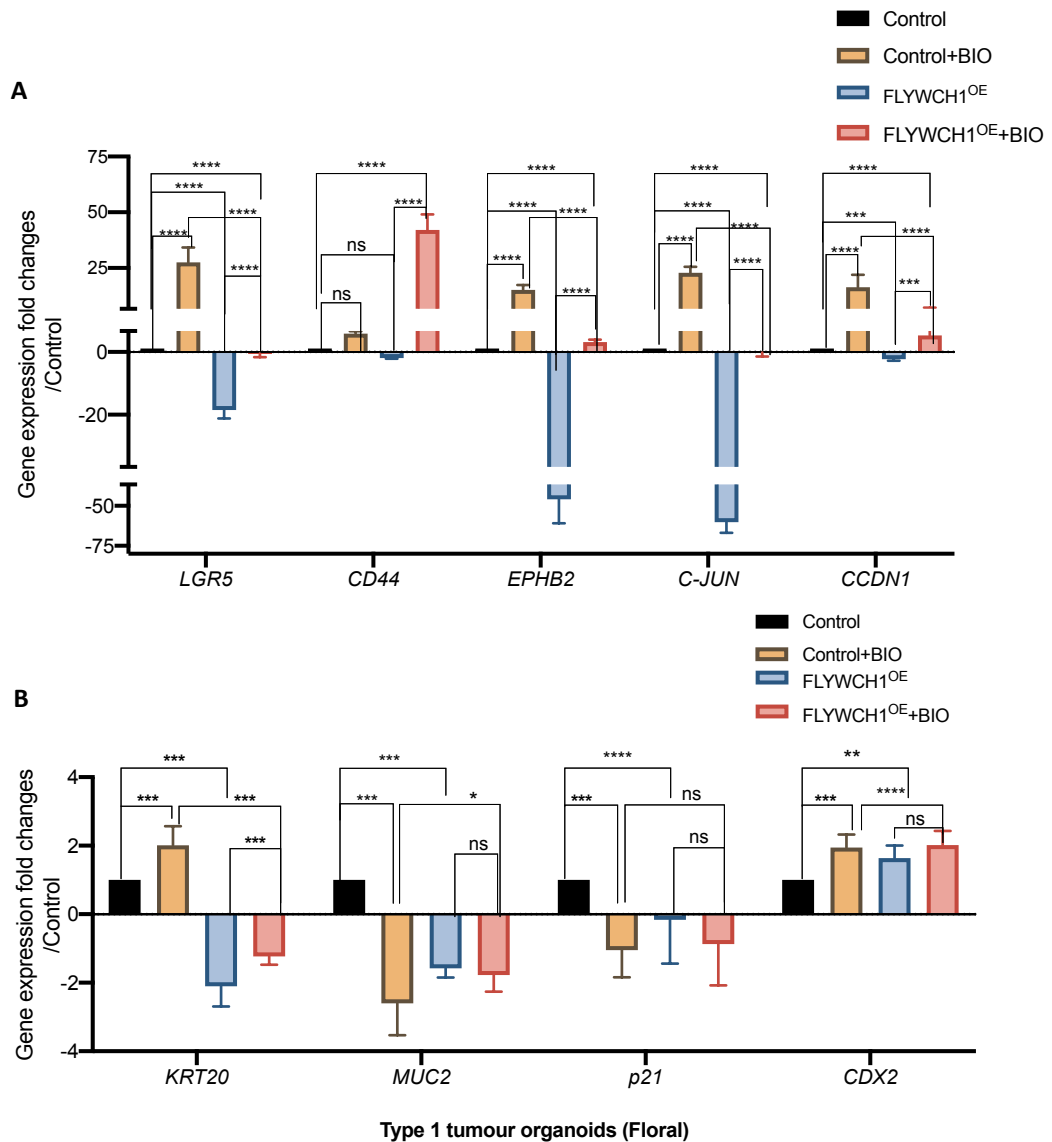
Figure 3-31 Gene expression analysis of A) key Wnt target genes, intestinal stemness, and **B)** differentiation markers in Type 1 tumour organoids (Floral). mRNA expression was obtained by the 2^-(ΔΔCt) method, and all assays were performed in triplicate. Data are mean and SD (N= 3; ns; not significant *=P ≤ 0.05, **= P ≤ 0.01, ***= P ≤ 0.001, ****= P ≤ 0.0001). p-values were estimated using the two-way ANOVA.

In type 1 tumour organoids, BIO treatment increased the stemness markers, and

Wnt-target genes significantly. Whereas, these genes were repressed in

FLYWCH1^OE organoids, in comparison to untreated controls (Figure 3-31 A). Of

note, BIO treatment in FLYWCH1^OE organoids was sufficient to overcome the

negative effect of FLYWCH1-overexpression, in which the expression of Wnt targets and stemness genes, particularly CD44 which were re-increased (Figure 3-31 A, Blue versus Red). However, the effect of BIO on FLYWCH1-overexpressing organoids appeared weaker relatively to BIO-treated controls (Figure 3-31 A, Yellow versus Red).

As demonstrated in Figure 3-31 B, the impact on differentiation markers was dissimilar. BIO treatment reduced MUC2 (Mucin 2, goblet cell marker) and P21 (cyclin-dependent kinase inhibitor) while induced KRT20 (Cytokeratin 20, an epithelial cell marker) and CDX2 (Caudal-type homeobox transcription factor 2) expression. Similarly, FLYWCH1^{OE} significantly reduced all differentiation markers except for CDX2, which was induced in FLYWCH1^{OE} organoids (Figure 3-31 B). In comparison to FLYWCH1^{OE} only, BIO treatment in FLYWCH1-overexpressing organoids did not show significant effects on all differentiation markers except KRT20 (Figure 3-31 B, Blue versus Red).
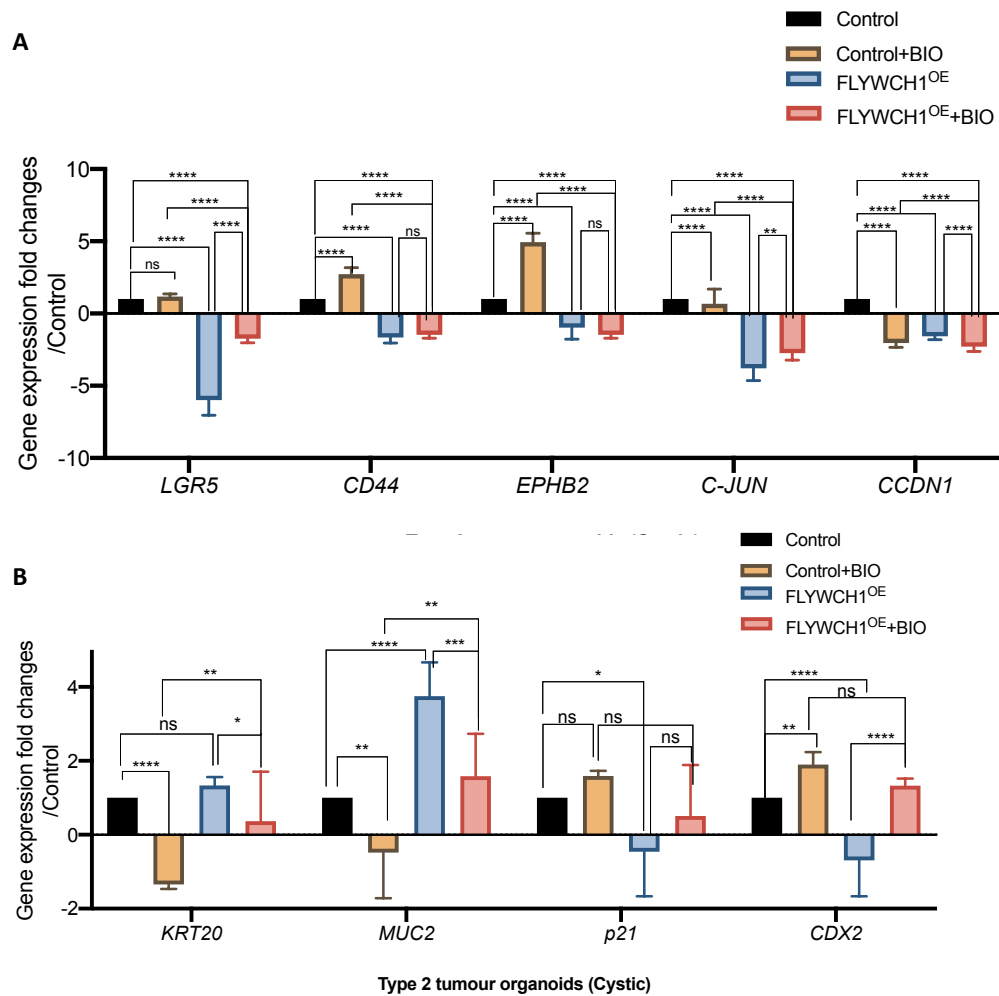
Figure 3-32 Expression analysis of A) key Wnt target genes, intestinal stemness, and **B)** differentiation markers in Type 2 tumour organoids (Cystic). mRNA expression was obtained by the $2^{-(\Delta\Delta Ct)}$ method, and all assays were performed in triplicate. Data are mean and SD (N= 3; ns; not significant *=P $\leq$ 0.05, **= P $\leq$ 0.01, ***= P $\leq$ 0.001, ****= P $\leq$ 0.0001). p-values were estimated using the two-way ANOVA.

Overall, Type 2 organoids (Cystic) showed slightly different outcomes in response to BIO and/or FLYWCH1^{OE} (Figure 3-32 A, B). BIO treatment increased the expression of LGR5, CD44, EPHB2, C-JUN, but CCDN1 (Figure 3-32 A). Yet, similar to Type 1 organoids, FLYWCH1^{OE} reduced the expression of all Wnt targets genes and stemness markers relative to controls (Figure 3-32 A).

Although BIO treatment slightly countered the suppression effects of FLYWCH1 overexpression on the stemness and Wnt target genes (Figure 3-32 A, Red versus Blue), FLYWCH1-overexpressing organoids showed a lower response when compared to BIO+ control organoids (Figure 3-32 A, Red versus Yellow).

On the other hand, the effect of BIO and FLYWCH1^{OE} varied on differentiation markers. For example, the expression of KRT20 and MUC2 were significantly induced by FLYWCH1^{OE}, while CDX2 was reduced (Figure 3-32 B, Blue versus Black). In contrast, BIO+ decreased the expression of KRT20 and MUC2, but induced CDX2 and p21 (Figure 3-32 B, Yellow versus Black). The effect on p21 was not significant. Moreover, the impact of BIO on FLYWCH1-overexpressing organoids was significant on KRT20 and MUC2, but not p21 or CDX2 (Figure 3-32 B).

Overall, we showed that FLYWCH1 over-expression in PDOs significantly alters the stemness and Wnt associated genes expression. Although BIO treatment neutralised the negative effects of FLYWCH1^{OE} on stemness and Wnt target. Yet, the impact of BIO on FLYWCH1^{OE} organoids was significantly lower when compared to control-treated organoids. The impact of FLYWCH1^{OE} on differentiation markers were not conclusive nor consistent across the genes and PDOs. Likewise, the effect of BIO treatment on differentiation markers was dissimilar in each type. The variations observed within the different PDOs, particularly regarding differentiation markers could suggest a potential contribution of other factors such as genetic background/mutations of each type. It is also likely that other signaling pathways are involved in mediating the effect of BIO on cell differentiation, independently of FLYWCH1 expression. Analysing

the genetic profile and mutations of these PDOs would be necessary to explain these variations and the underlying molecular mechanisms.

3.2.7 The clinical significance of FLYWCH1 expression for CRC patients

To obtain a patient-relevant view of FLYWCH1 roles and significance, it is important to evaluate FLYWCH1 expression and cellular localisation in CRC patients. This should also be correlated with the patient's clinicopathological outcomes. To this end, we have employed CRC tissue microarray (TMA) comprising of 1000 samples from a well-characterised patient cohort. Matched normal samples were provided as controls for each patient. The TMA sections were kindly provided by our collaborator (Prof Mohammad Ilyas, University of Nottingham).

Due to the lack of IHC facilities in our lab, sections were probed with a pre-validated FLYWCH1 antibody by Miss Abrar Aljohani (the Histopathology unit, City hospital, University of Nottingham). Before carrying out the IHC staining on the experimental TMA slides, the FLYWCH1 antibody was validated on 15 different TMA slides. IHC staining protocol and Ab concentration were first optimised, the staining specificity was then checked and approved by the pathologist (Dr Mohammed Aleskandarany, Nottingham City Hospital). Subsequently, the stained TMA slides were digitally scanned using VENTANA DP 200 slide scanner (Roche, UK) to high-resolution images, and viewed by Aperio ImageScope (Aperio Technologies, UK) at 20x magnification. The intensity of nuclear and cytoplasmic FLYWCH1 protein expression of epithelial cells was scored by the H-score system,

and calculated as previously described (240) (detailed in chapter 2, Methods Section 2.2.11). After double scoring, the interclass correlation coefficient (ICC) test was applied to assess the concordance rate of the two scores (Appendix 5). Interestingly, FLYWCH1 IHC analysis showed a predominantly detected staining in the nucleus in normal tissues. Whereas in tumour tissues, FLYWCH1 was found mainly in the cytoplasm, and the nuclear staining was almost lost (Figure 3-33, A vs B).
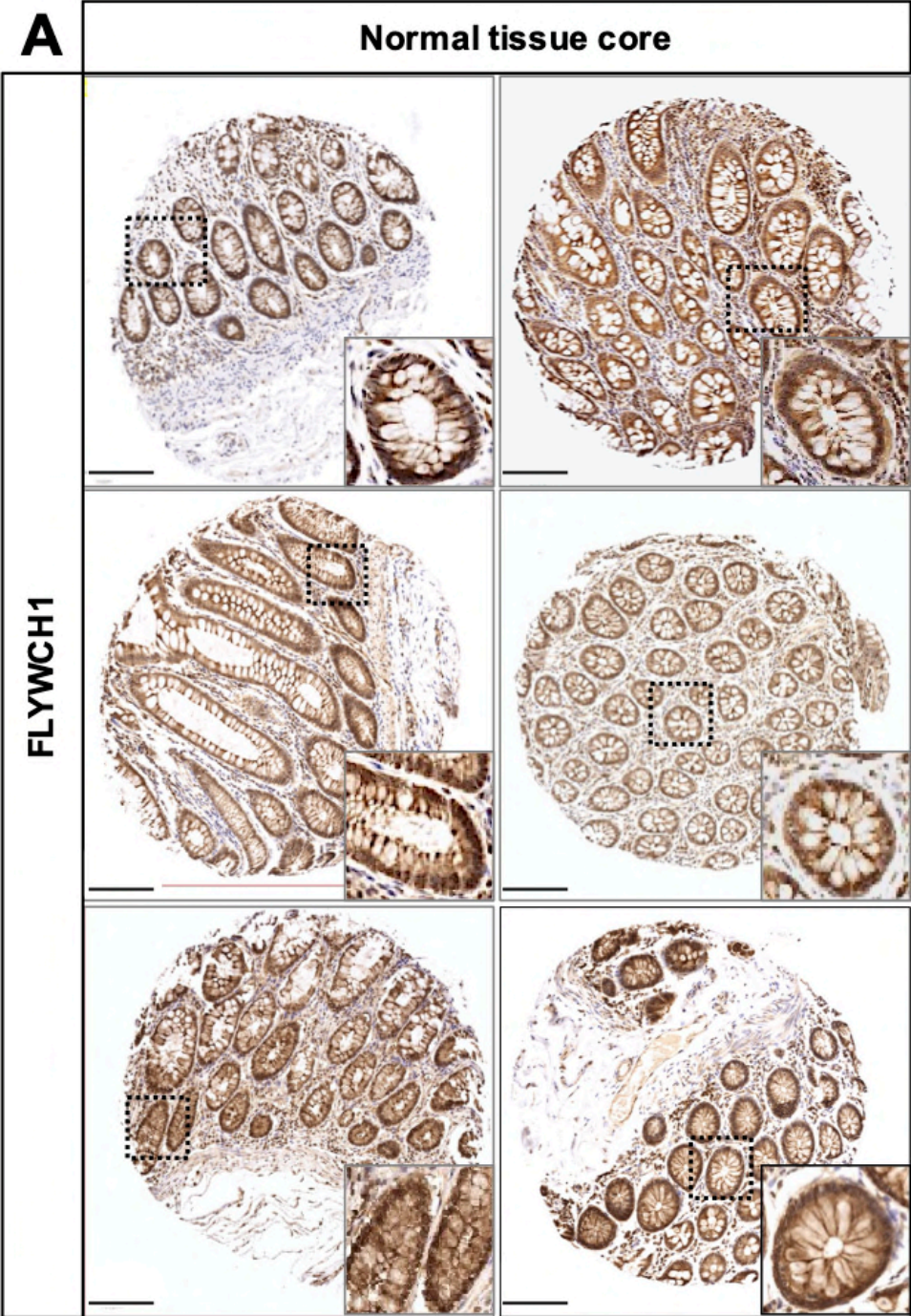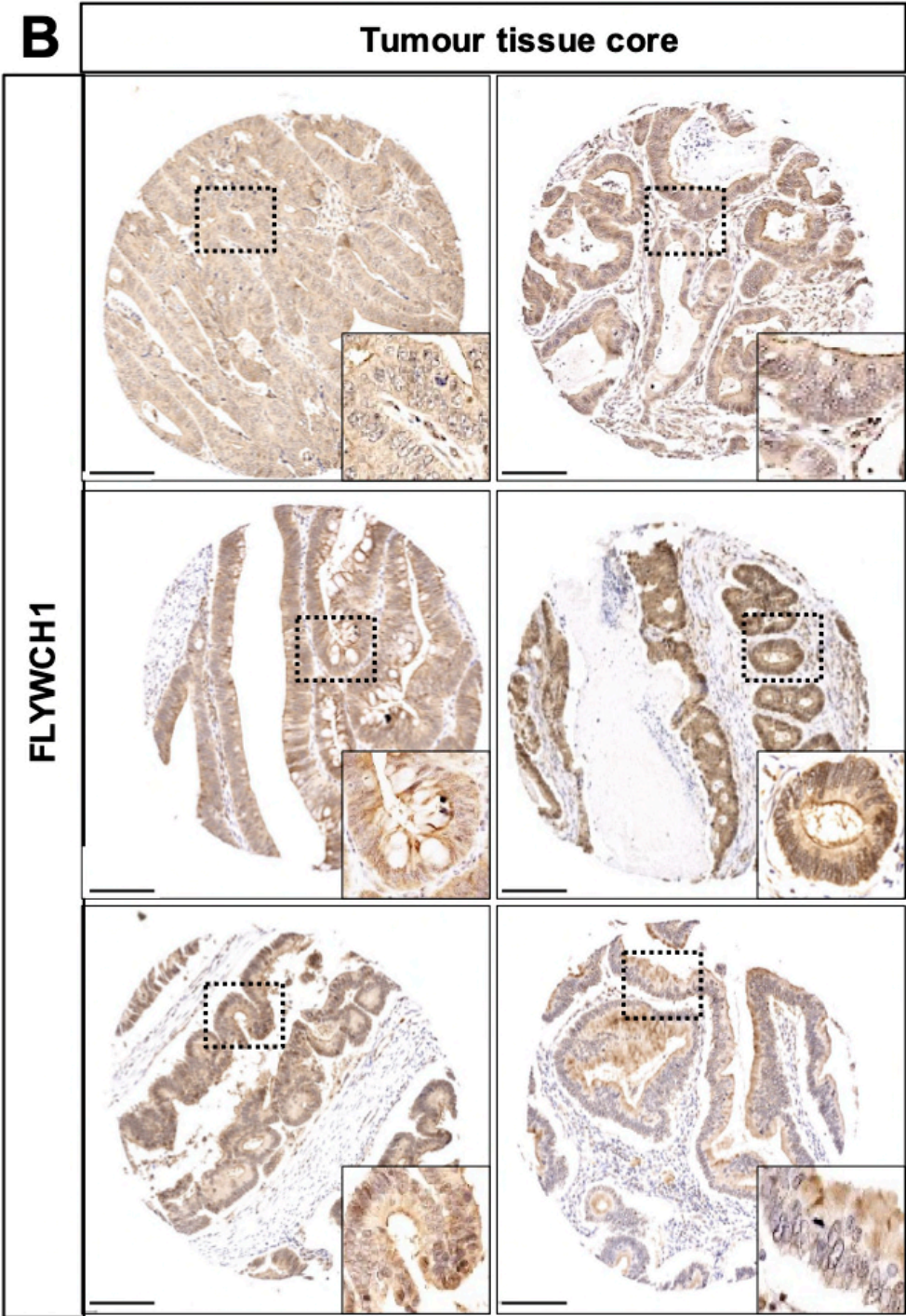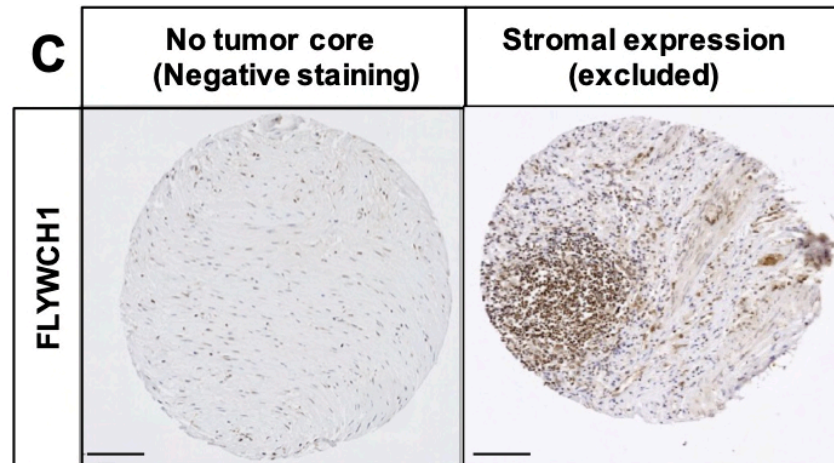
Figure 3-33 Representative examples of IHC staining intensities of FLYWCH1 expression in A) Normal versus **B)** tumour tissues. Intensity of nuclear, and cytoplasmic FLYWCH1 protein expression of epithelial cells was scored by the H-score system. **C)** Representative images of TMA cores that contained less than 15% intact (epithelial) tumour tissue and were therefore excluded from the analysis. Scale bar 200μm.

Our collaborator, Dr William Dalleywater (Pathology Department, University of Nottingham), performed the patients' pathological/outcome by statistical analysis of the scored samples through access to patient's data. According to the initial analysis, it can be suggested that nuclear FLYWCH1 is generally lower in tumour segments than normal tissue. In contrast, cytoplasmic FLYWCH1 expression is higher. Interestingly, as the T-stage increases, cytoplasmic FLYWCH1 expression is significantly lower in intra-tumoural and advancing edge segments of the tumour. This possibly indicates a complete loss of FLYWCH1 expression at the late stages (Figure 3-34 B).
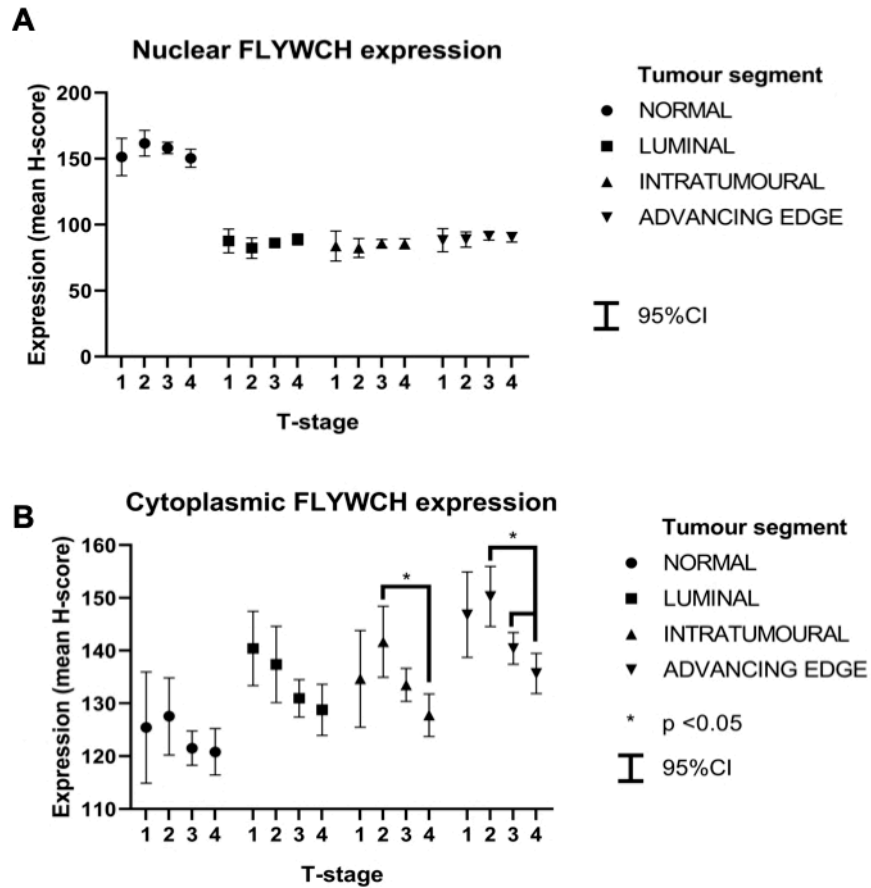
Figure 3-34 Overall expressional analysis of FLYWCH1 in the TMA library used in this study. Graphs showing the mean of **A)** Nuclear, and **B)** Cytoplasmic expression of FLYWCH1 in different tumour segments, and pathological T stages (1, 2, 3, 4 represent T1, T2, T3, and T4 stages), (*=P ≤ 0.05).

Collectively, these data support the notion that FLYWCH1 could be switched off during CRC progression by changing the cellular distribution. Therefore, understanding the regulation of FLYWCH1 is essential to reveal the precise mechanism of FLYWCH1 inactivation. Considering that GSK-3β-mediated regulation of FLYWCH1 could be a key mechanism of this process, we addressed the clinical significance of FLYWCH1/GSK-3β expressions and their correlation in the patients' samples. Here, the same TMA library of CRC-tissues was probed with a pre-validated GSK-3β antibody. The IHC validation and staining was performed under the supervision of Dr Roya Babaei-Jadidi, Division of respiratory medicine, University of Nottingham. The intensity of nuclear, and cytoplasmic GSK-3β protein expression of epithelial cells was scored by the H-score system, as explained above. The interclass correlation coefficient (ICC) test was then performed to assess the concordance rate of the two scores (Appendix 5 D and E).
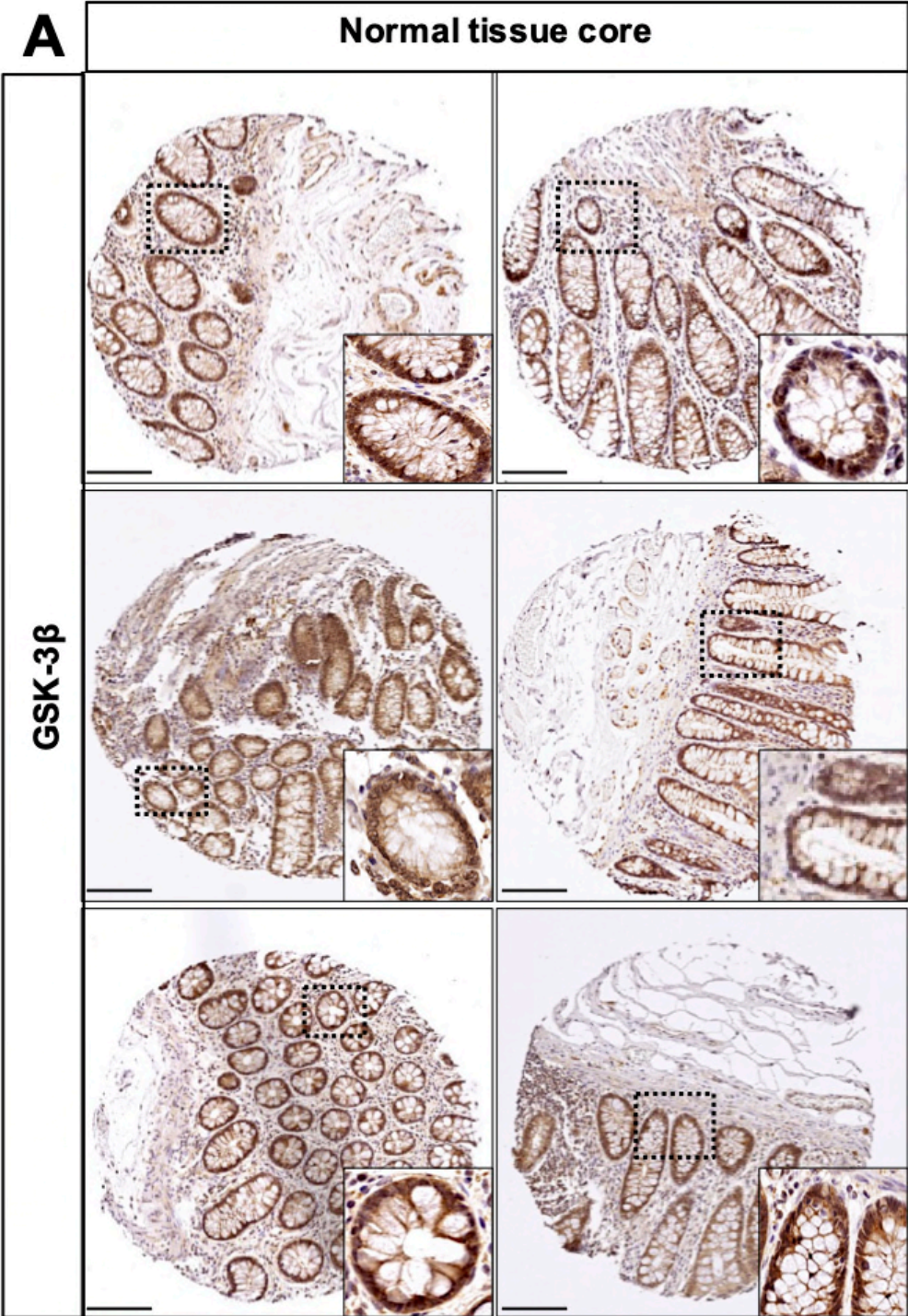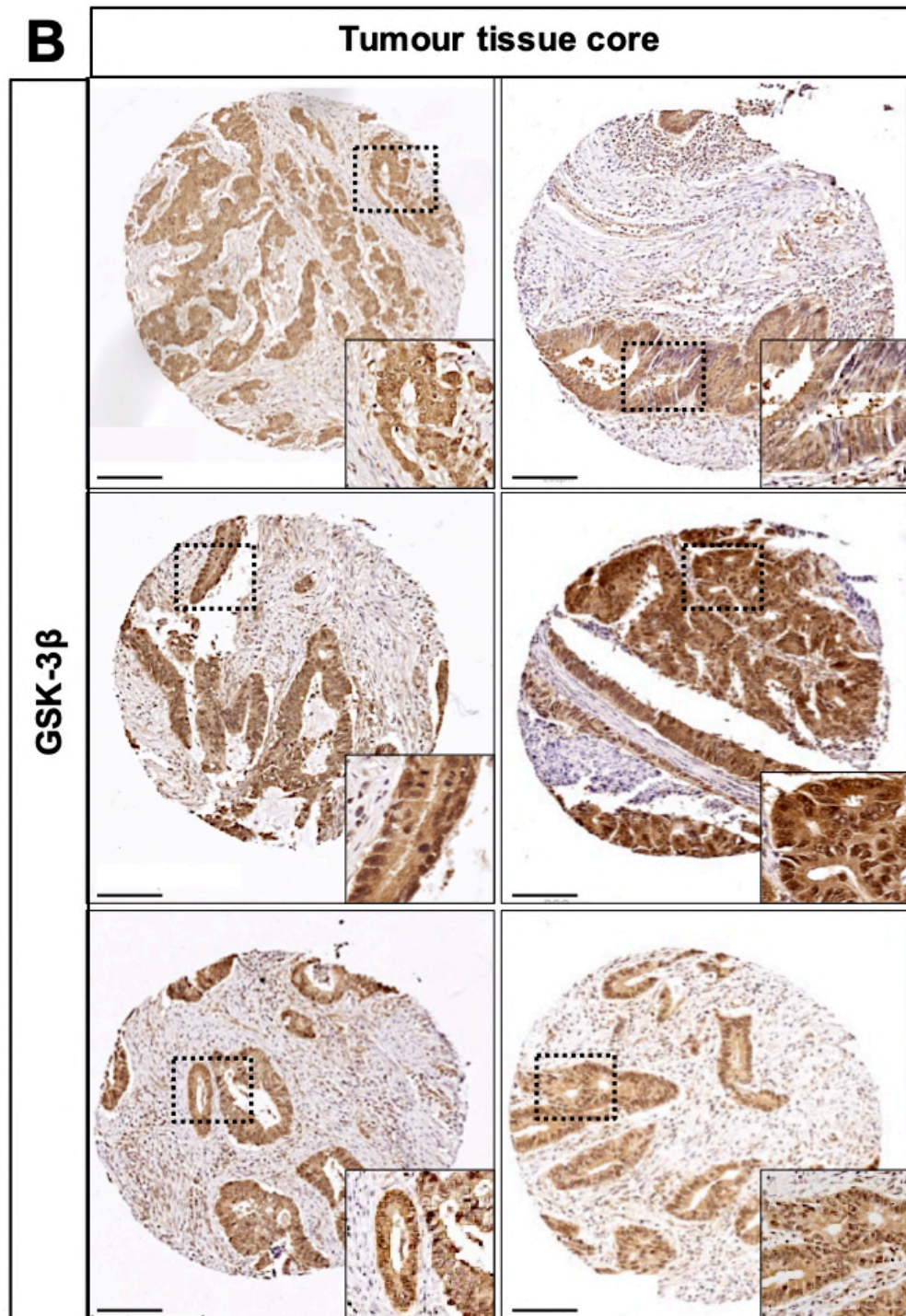
Figure 3-35 Representative examples of IHC staining of GSK-3β in CRC-TMA. IHC analysis displayed uniform intensities of nuclear and cytoplasmic staining in **A)** normal samples, and **B)** tumour samples. Scale bar 200μm.

Generally, similar to FLYWCH1, the GSK-3β was highly expressed in the nucleus in

the normal tissue cores (Figure 3-35 A). However, GSK-3β staining intensity was

variable across the tumour tissues and showed high nuclear and cytoplasmic expression (Figure 3-35 B). According to the statistical analysis performed by Dr William Dalleywater, the nuclear expression of GSK-3β showed an increasing trend with tumour stage, in all tumour segments. While cytoplasmic expression was significantly reduced in higher-stage tumours at the advancing edge (Figure 3-36).
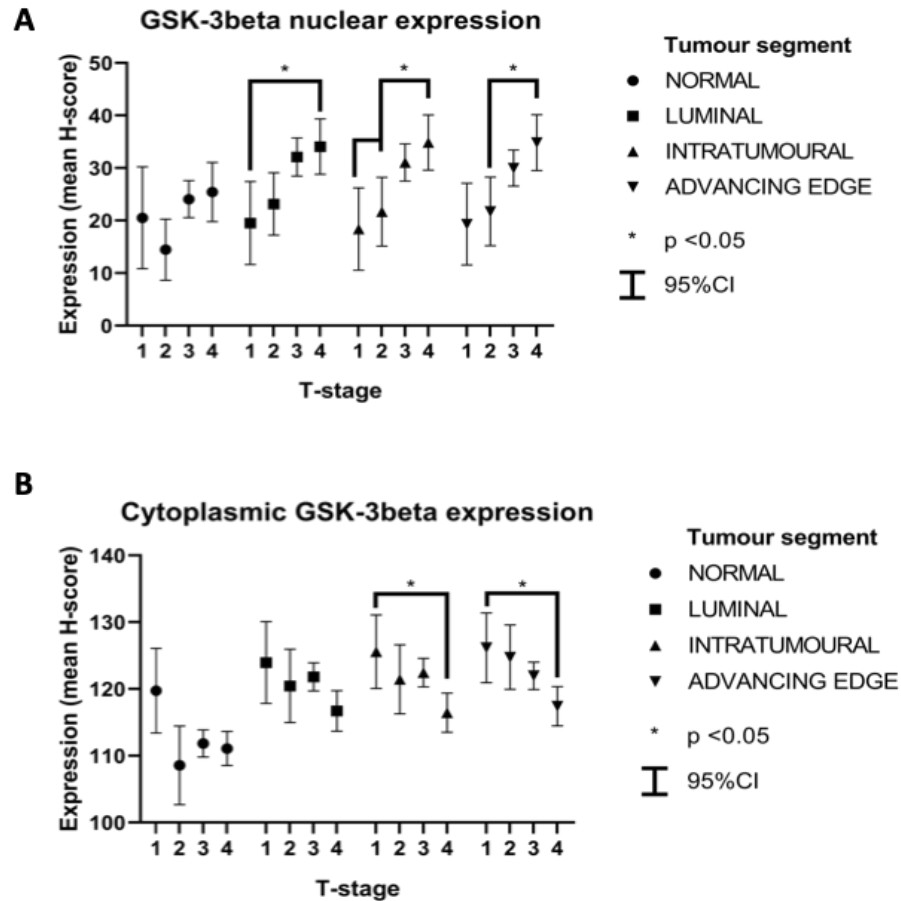
Figure 3-36 Nuclear, and cytoplasmic mean expression of GSK-3β in different tumour segments, and pathological T stages. (1, 2, 3, 4 represent T1, T2, T3, T4 stages), *=P ≤ 0.05.

Interestingly, in higher T-stage tumours, the cytoplasmic expression of FLYWCH1, and GSK-3β was reduced compared to lower T-stage tumours. Additionally, a correlation between tumour, and normal expression of both FLYWCH1, and GSK-3β was observed. Therefore, tumour expression was standardised to normal tissue. This accounted for differences in biological activity at baseline (Figure 3-37). Moreover, the association of cytoplasmic/nuclear expression of both FLYWCH1 and GSK-3β was evaluated in relation to various clinicopathological parameters (Figure 3-38).
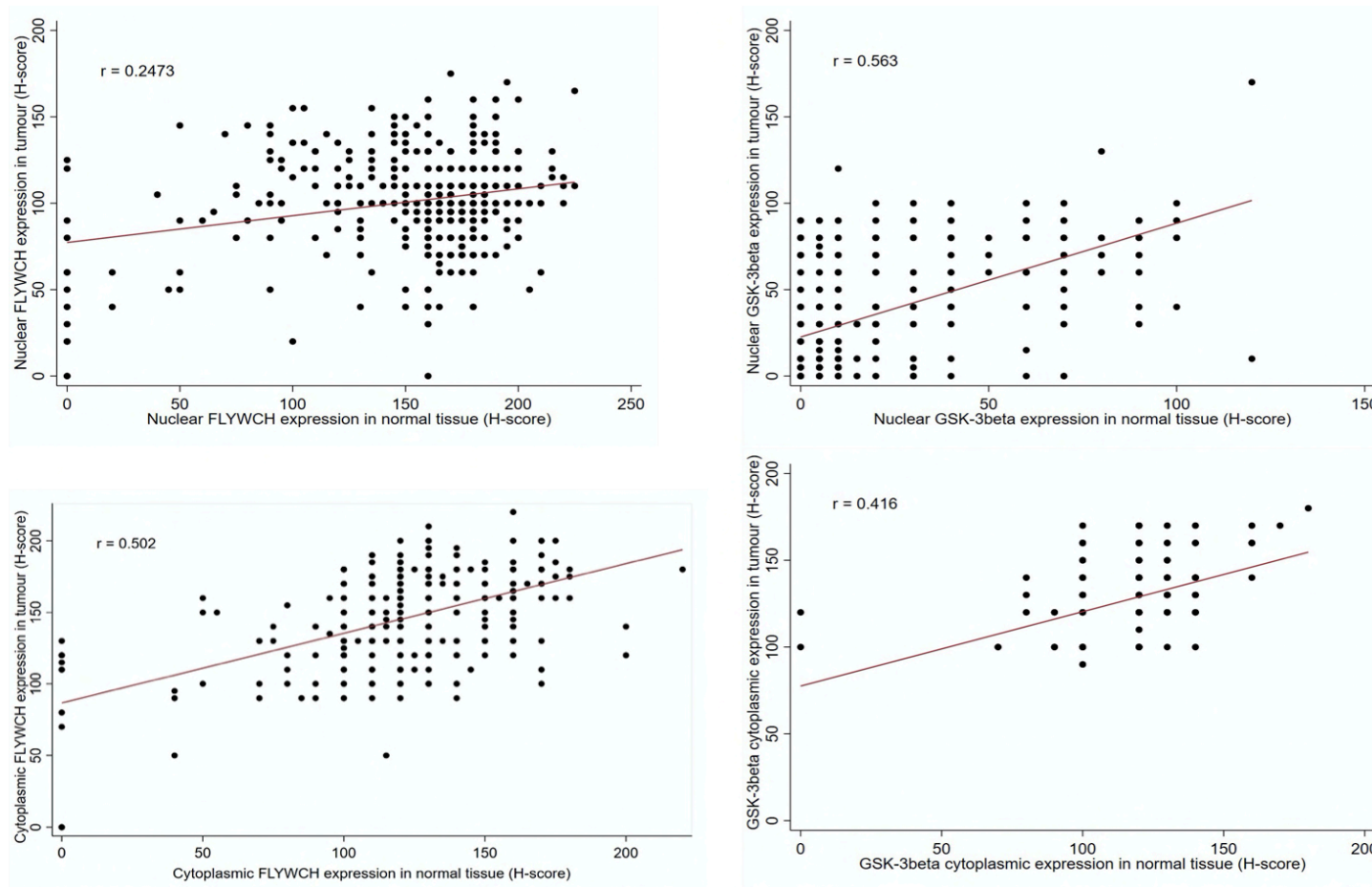
Figure 3-37 The correlation of FLYWCH1/GSK-3β expression in CRC-TMA. Nuclear, and cytoplasmic expression of FLYWCH1, and GSK-3β is correlated between maximum expression across all tumour segments, and adjacent normal tissue.
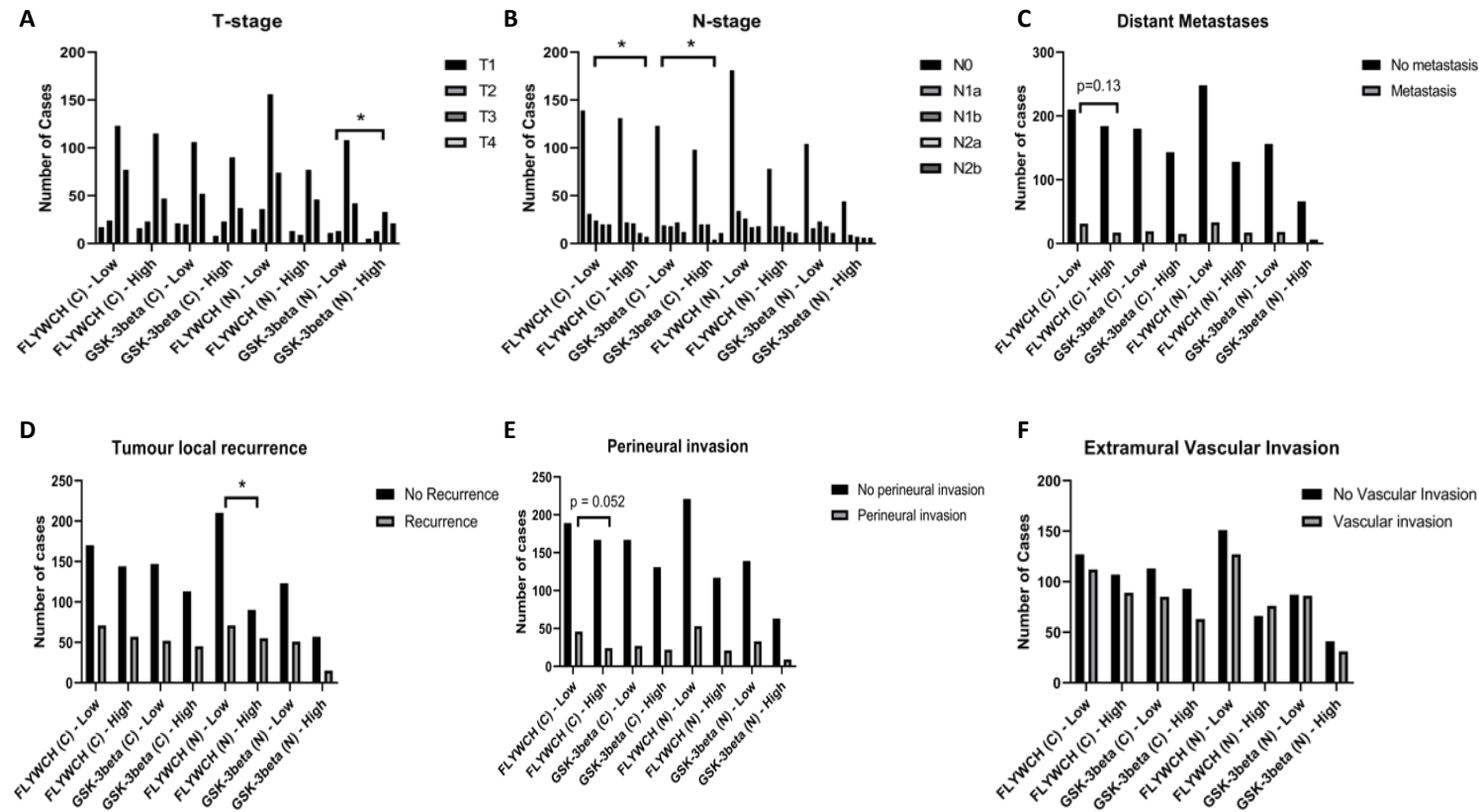
Figure 3-38 The association of FLYWCH1, and GSK-3β expression with various clinicopathological parameters. A) T-stage, **B)** N-stage, **C)** Distant Metastases, **D)** Tumour local recurrence, **E)** Perineural invasion and **F)** Extramural Vascular invasion. FLYWCH1(C)= FLYWCH1 cytoplasmic expression group, FLYWCH1(N)= FLYWCH1 nuclear expression group, GSK-3β(C)= GSK-3β cytoplasmic expression group, and GSK-3β (N)= GSK-3β nuclear expression group, (*=P ≤ 0.05).

As shown in Figure 3-38 B, low cytoplasmic FLYWCH1 expression was significantly associated with an increased rate of higher stage (N1+) lymph node metastases, reflecting a higher number of lymph nodes, involved. Likewise, high cytoplasmic GSK-3β expression was also associated with higher stage lymph node involvement (Figure 3-38 B). Comparatively, tumours with low cytoplasmic FLYWCH1 also showed a trend towards higher rates of distant metastases (Figure 3-38 C). Nonetheless, there was no significant association between differential FLYWCH1/GSK-3β expression, and vascular invasion (Figure 3-38 F). In follow-up data, the association between FLYWCH1/GSK-3β expression at the time of diagnosis, and subsequent recurrence of the tumour was evaluated. High nuclear FLYWCH1 expression was associated with a significantly greater rate of local recurrence when compared to low expression (Figure 3-38 D). This suggested that nuclear FLYWCH1 could be a useful predictive marker of tumour recurrence. Furthermore, low cytoplasmic FLYWCH1 expression was associated with a strong trend towards increased rates of perineural invasion (Figure 3-38 E).

Our clinical data revealed that loss of nuclear and low FLYWCH1 expression is correlated with CRC progression and poor pathological parameters. However, focusing on the effect that nuclear expression of FLYWCH1 might have on overall survival (OS) via Kaplan-Meier analysis showed no statistical significance between patient groups of low versus high nuclear expression of FLYWCH1 (Figure 3-39 A, $P = 0.77$). Likewise, no statistical significance had been discovered between patient groups of low versus high GSK-3β nuclear expression with the overall survival (Figure 3-39 C, $P = 0.159$). Nonetheless, the cytoplasmic expression of both FLYWCH1 and GSK-3β was significantly associated with the overall survival. (Figure

3-39 B, D). Kaplan Meier curves showed a superior overall survival of CRCs with

high cytoplasmic FLYWCH1 expression compared to low cytoplasmic FLYWCH1

expression (Figure 3-39 B). In contrast, low cytoplasmic expressors of GSK-3β had

significantly better survival than those with high cytoplasmic GSK-3β (Figure 3-38

D).
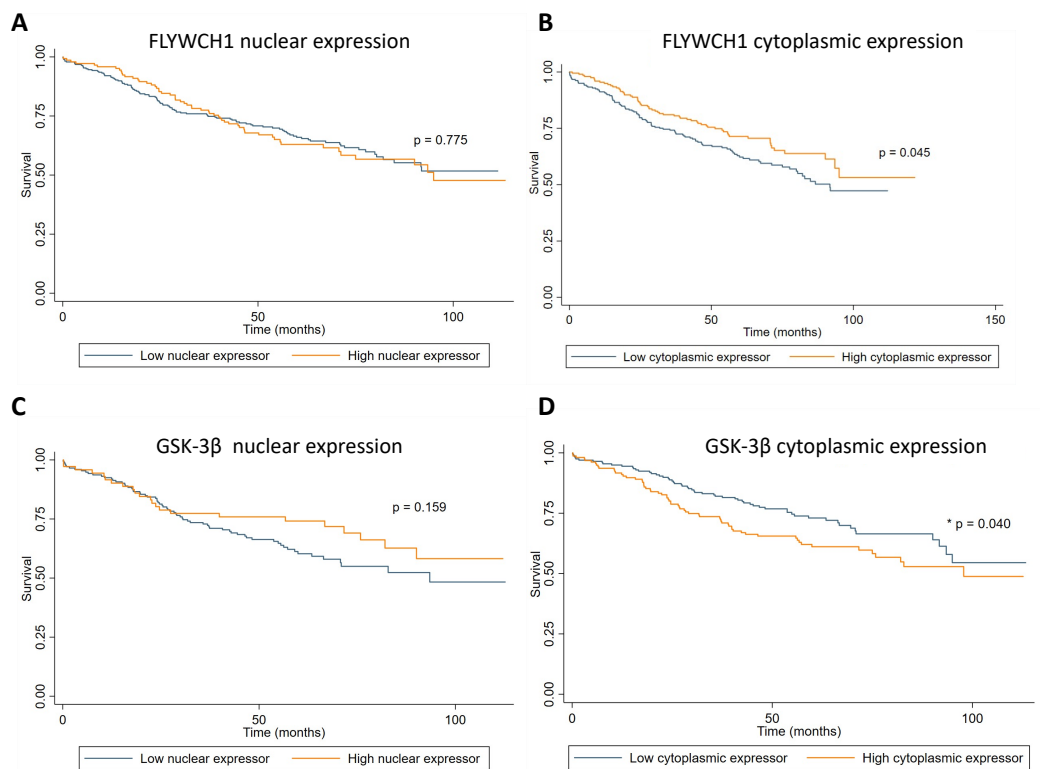
Figure 3-39 Kaplan-Meier modelling of overall survival related to low and high tumour expression of FLYWCH and GSK-3β in the nucleus and cytoplasm. A) FLYWCH1 nuclear expression, **B)** FLYWCH1 cytoplasmic expression. (High vs. low cytoplasmic expression). Mean survival time–Low expressors: 74.9, High expressors: 88.3. HR: 0.72 (95% CI: 0.53 – 0.99), n=241/201. **C)** GSK-3β nuclear expression, and **D)** GSK-3β cytoplasmic expression. (High vs. low cytoplasmic expression), Mean survival time – Low expressors: 85.1, High expressors: 75.7. HR: 1.45 (95% CI: 1.01 – 2.06), n=199/158. (*=P ≤ 0.05).

Interestingly, when we combined FLYWCH1/GSK-3β expressions into a composite group, patients with low cytoplasmic FLYWCH1 and high cytoplasmic GSK-3β had the shortest OS, while low cytoplasmic GSK-3β and high cytoplasmic FLYWCH1 had a better prognostic value (Figure 3-40).
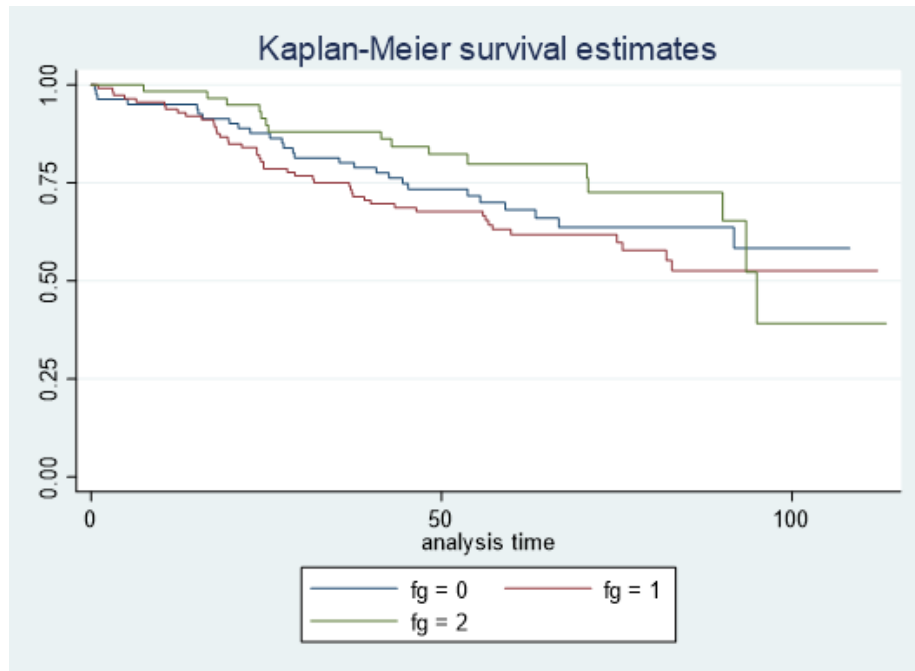
Figure 3-40 Kaplan–Meier survival curves depicting outcomes of overall survival (OS) according to the cytoplasmic expression of FLYWCH1/GSK-3β. In this model, FG = 1 is high cytoplasmic GSK-3β /low cytoplasmic FLYWCH1. FG = 0 is either low cytoplasmic GSK-3β and low cytoplasmic FLYWCH1 or high cytoplasmic GSK-3β and high cytoplasmic FLYWCH1. FG = 2 is low cytoplasmic GSK, high cytoplasmic FLYWCH1. (*=P ≤ 0.05).

To sum up, our data showed a significant correlation between low cytoplasmic FLYWCH1 expression with CRC staging and patients' overall survival. We further revealed an inverse correlation between cytoplasmic expression of FLYWCH1 and GSK-3β. The combination of low cytoplasmic FLYWCH1 and high cytoplasmic GSK-3β conferred a worse prognosis and shorter OS, on the clustering analysis.

Findings together point toward a potential clinical impact of FLYWCH1 expression in CRC, highlighting the significance of FLYWCH1 localisation in CRC staging and tumour progression.

3.3 Discussion

We previously indicated a significant tumour suppressive function of FLYWCH1 in CRC cells by regulating the transcriptional activity of β-catenin/TCF4 (198). However, all observations were focused on the late-stage, or metastatic CRC. This is the first study to explore the biological implications, functions, and regulation of FLYWCH1 in normal intestinal cells versus cancer cells.

On the strength of previous findings in our lab (Chapter 1, Figure 1-12), we predicted that FLYWCH1-crypt expression might be crucial for intestinal crypt growth. Henceforth, using 3D intestinal organoid model, as a representative tool for mimicking the *in-vivo* intestinal structure (313, 314), we modelled the effect of FLYWCH1-depletion on intestinal cells proliferation and growth. So far, organoid systems have a proven ability as robust and promising research tools within many research areas. They can be used as significant experimental or diagnostic tools, and new attractive therapeutic tools (315). Moreover, owing to their strict dependence on Wnt signaling, employing intestinal organoids in this study offered an opportunity to examine FLYWCH1 roles in regulating Wnt-driven activities in normal physiology and cancer.

Our data showed that loss of FLYWCH1 drives a hyperproliferative phenotype of normal intestinal organoids and significantly accelerates their growth. The

expression of the proliferation marker Ki-67 paralleled the growth characteristics in FLYWCH1 depleted organoids, where it was strongly expressed in the basal area of the crypt but low in the control organoids. Cell hyper-proliferation is known to be the first cytological and histological evidence of abnormal epithelial growth, which might give rise to aberrant crypts and may eventually develop into adenomas and invasive adenocarcinoma, over time (316).

Several genetic changes occur in the epithelial cells long before any visible changes in the mucosal structure. Gradually, these changes alter the regular cellular activity leading to abnormal growth and/or differentiation (317). In this sense, we showed that FLYWCH1-depletion drives significant transcriptional changes in the normal organoids to induce their proliferation. Our preliminary data may suggest that loss of FLYWCH1 could drive the proliferation by inducing the transcription of Lgr5+/Olmf4+ (actively cycling cell markers) and reducing the transcription of quiescence Tert+/Lrig1+ cell markers. Several experiments are required at the organoid culture to fully address this phenomenon.

It is plausible that the loss of FLYWCH1 encourages the transition of the relatively quiescent position 4 ISCs or (+4 ISCs, Tert+) into actively proliferating cells via regulating β-catenin mediated activation of Tert+ cells (318). Suh HN et al. reported that Tert+ cells could serve as a reservoir for Lgr5+cells during regeneration. More importantly, the report showed that Wnt/β-catenin signaling is essential for the transition, and mitotic activation of Tert+ cells (318). Yet, the exact mechanism was not fully elucidated. Hence, the potential role of FLYWCH1 in the β-catenin-induced quiescence exit of Tert+ cells is worth future investigations. Our findings generally underline the impact of FLYWCH1 crypt-

expression for regulating intestinal cell growth and proliferation, in part via its suppression activity on Wnt/β-catenin signaling.

Furthermore, the role of FLYWCH1 in controlling Wnt-mediated tumorigenesis was examined in this study using patient-derived CRC organoids (PDOs). Intriguingly, the growth-suppressive phenotype reported in the FLYWCH1-overexpressing PDOs was associated with significant changes in gene signatures involved in important Wnt-driven biological activities including migration, cancer stemness, and EMT. Therefore, our findings indicated that FLYWCH1 mediates changes in the size and growth of tumour organoids, relatively via transcriptional regulation of selected Wnt targets.

Despite all PDOs having common characteristics of CRC tumours, each patient will display a unique proteomic signature that can be detected in tumour organoids (319). Therefore, it was beneficial to explore the phenotypical and transcriptional changes under altered FLYWCH1 expression in two different types of PDOs. Interestingly, irrespective of genetic background variation, and characteristics of these organoids, enforced FLYWCH1-expression significantly affected their growth rates. However, this can be achieved via distinct mechanisms, in a genetic-background dependent manner. Screening the mutational status of the PDOs used in this study would allow for a more specific interpretation of the mechanism by which FLYWCH1 acts. Additionally, screening the outcomes of FLYWCH1 overexpression on a library of different characterised PDOs would enrich our understanding of the tumour suppressive functions of FLYWCH1 under various tumour microenvironments.

Moving forward, our data suggested a likely relevance of altered FLYWCH1 expression with cancer stem-like properties. It is widely accepted that a small sub-population of poorly differentiated cancer stem-like cells (CSCs), are responsible for drug resistance and relapse (274). CSCs possess the ability to self-renew, differentiate, and proliferate like normal stem cells (320). We showed that loss of FLYWCH1 enriches CSCs properties, by enhancing the colonosphere forming efficiency in SW620 cells. Moreover, our PCR array and gene expressional analysis showed significant changes in the gene signatures associated with EMT, and cancer stemness. Therefore, we suggest that FLYWCH1 can be inversely correlated with Wnt signaling activity in CRC, counteracting the cancer stem cell phenotype when ectopically expressed.

While FLYWCH1 controls β-catenin transcriptional activity, the connection between FLYWCH1 and the Wnt/β-catenin signaling can be more complicated than initially thought. Prior to this study, it was unclear how FLYWCH1 is endogenously regulated in normal intestinal cells and tumour cells. We here proposed FLYWCH1 as a new downstream target of the Wnt/β-catenin signaling pathway that is regulated through nuclear/cytoplasmic shuttling. Findings here provide a significant contribution to our knowledge regarding FLYWCH1 regulation by Wnt/β-catenin signaling in normal versus cancer cells.

When Wnt signaling was activated by Wnt3A-CM both transcriptional and translational activity of FLYWCH1 were suppressed. This was coinciding with cytoplasmic translocation of FLYWCH1 and reduction in the nuclear expression. It is well-known that the function of several TFs involved in Wnt/β-catenin (e.g. Chibby, Axin2, GSK-3β etc.) is determined by their cellular distribution (321-323).

Henceforth, FLYWCH1 functions may also be affected by changes in the cellular distribution.

Furthermore, despite having defined mechanisms for nuclear imports and exports, the stability, functions, and activity of a protein in each cellular compartment are mainly determined by PTM modifications (324, 325). It should be emphasized that both post-transcriptional and post-translational modifications contribute substantially to regulate the fate of the protein under different stimuli. While alternative splicing and RNA-mediated silencing control the amount of specific transcripts (326, 327), after translation, a protein can be modified by a plethora of molecules that in turn modulate its activity, subcellular localisation and half-life (328). These modifications may occur at different levels during the transcriptional/translational process, whilst also acting on the same transcript/protein target. Predominantly, the PTM status of a protein controls its N/C shuttling and subsequent activation or degradation (328). Although FLYWCH1 has a defined NLS, the fundamental aspects of FLYWCH1 shuttling and how Wnt activation influences FLYWCH1 localisation remains undefined. Likewise, mediators involved in FLYWCH1 shuttling require further exploration.

In this study, we explored the potential PTMs and studied the half-life and stability of FLYWCH1. These are all crucial aspects for addressing the modes of regulation and accelerating future identification of mechanisms by which FLYWCH1 can be controlled in cancer cells. Initial screening of PTMs on the FLYWCH1 protein sequence revealed various phosphorylation, ubiquitination and SUMOylation sites within its sequence. Protein phosphorylation is a well-established mechanism for

stress signal transmission (328, 329). Ubiquitin and SUMO conjugations are also major post-translational regulatory processes in all eukaryotes (330-332). For example, SUMOylation of a target protein can influence protein stability, subcellular localisation, protein-protein interactions and/or transcriptional activity (330, 333). Like the case of PLK1 protein, where SUMOylation causes its nuclear import and significantly increases the protein stability (334). Another example is the Transducin β-like proteins (TBL1-TBLR1), a transcriptional coactivator, that is SUMOylated in a Wnt signaling-dependent manner. The SUMOylation of TBL1 and TBLR1 releases TBL1-TBLR1 from the NCoR/SMRT corepressor complexes and consequently leads to Wnt signaling activation (335). Overall, the combination of different modifications shapes the final amount of the targeted protein and its corresponding process/function.

To explore this, we first studied the stability and turn-over rate of FLYWCH1 protein and subsequently examined the outcome of BIO on FLYWCH1 protein stability. Our results revealed that FLYWCH1 is a short-lived protein with a maximum half-life of 2h (Figure 3-28 A). Remarkably, the half-life of FLYWCH1 protein in cells treated with BIO was approximately 2 times longer than that of untreated FLYWCH1 (Figure 2-28 B). While GSK-3β is a well-established kinase that regulates the localisation and functions of several TFs such as Snail (301, 302), Slug (302), FoxM1 (336)and c-Myc (337), our data indicates a potential regulation of FLYWCH1 stability, possibly via GSK-3β mediated PTMs.

Further preliminary *in-vitro* phosphorylation assay suggested that FLYWCH1 could be maintained in the nucleus by phosphorylation (at Ser/Thr). Wnt activation/GSK-

3β inhibition hindered the phosphorylation of FLYWCH1 (Appendix 4). Overall, the current findings imply that the localisation of FLYWCH1 is highly dynamic under Wnt modulation. We propose that Wnt-mediated regulation and translocation of FLYWCH1 is primarily achieved by GSK-3β dependent mechanism(s). However, further research is necessary to explore whether FLYWCH1 is a direct substrate of GSK-3β. Specifically, studies that identify and manipulate GSK-3β phosphorylation motifs in FLYWCH1 would further elucidate this mechanism. Future research addressing 'how FLYWCH1 is maintained in the nucleus, and whether the GSK-3β-interaction/mediated-phosphorylation is sufficient to maintain the active nuclear form of FLYWCH1?' would substantially enhance our understanding of this protein. Moreover, the identification of strategies that enhance the nuclear import and stability of FLYWCH1 would provide a novel approach for controlling Wnt-mediated tumorigenesis.

Moreover, we questioned the impact of GSK-3β inhibition on the growth and proliferation of FLYWCH1-expressing PDOs. Reports have shown that inhibiting GSK-3β in human cortical organoids increased the organoid size and caused massive derangement of cortical tissue architecture (338). Alternate research (339) has also reported that GSK3 inhibitor increased the colony formation efficiency of intestinal stem cells through Wnt signaling (339).

We showed that BIO treatment significantly induces the proliferation of CRC-PDOs, as proven by WST-1 assay. Whilst FLYWCH1^{OE} reduces the proliferation of PDOs. BIO treatment in FLYWCH1-overexpressing organoids slightly neutralises FLYWCH1's anti-proliferation effect. Yet, this response was weaker when compared to BIO-treated control organoids. Likewise, the expression of Wnt

targets and stemness genes was lower in BIO-treated FLYWCH1[OE] organoids relative to BIO untreated control organoids.

Nonetheless, the outcomes on the differentiation markers were contradictory within the different PDOs. The variations might suggest that FLYWCH1/GSK-3β might provoke specific responses in a genetic background dependent manner. Though, it is yet to be determined whether this mechanism works independently or concurrently with other mechanisms to induce specific biological outcomes.

To sum up, FLYWCH1-overexpression suppressed the growth, Wnt-mediated stemness, and metastatic activities in CRC-PDOs. Inhibiting GSK-3β counteracted FLYWCH1's suppression activity. Still, the proliferation of BIO+FLYWCH1-overexpressing organoids was less than BIO-treated control organoids. Accordingly, it can be predicted that GSK-3β plays a role in mediating FLYWCH1 functions in CRC-PDOs. Further research would enable the discovery of a mechanism to decipher and manipulate FLYWCH1's cellular mechanism(s).

Another new finding of this chapter was addressing the clinical significance and relevance of FLYWCH1 expression for CRC patients. FLYWCH1 protein expression was examined by scoring and analysing TMA that contained tissue biopsies from 1000 different cases/stages of CRC cancers. Notably, the nuclear expression of FLYWCH1 was significantly repressed in tumour samples compared to normal ones. Whereas cytoplasmic FLYWCH1 increased in tumour tissues.

Moreover, the statistical analysis indicated a disparate expression of FLYWCH1 within different CRC segments/stages. Whereby cytoplasmic FLYWCH1 expression was significantly lower at the late stages in intratumoural and the advancing edge

segments of the tumour. This indicates a potential loss of expression in the late stages of CRC.

We further studied the expression of nuclear versus cytoplasmic GSK-3β and addressed its correlation with FLYWCH1 expression. GSK-3β expression in tumours was localised in both cytoplasmic and nuclear compartments. We identified a statistically significant association between the high nuclear/and the low cytoplasmic GSK-3β expression with the advanced stages. GSK-3β overexpression has been linked to adverse tumour features in many cancers (340-342). Our findings are consistent with the reported association between high expression of GSK-3β with the shorter survival and worse prognosis of colon carcinomas (343).

Other observations entailed, low cytoplasmic FLYWCH1, as well as low nuclear/high cytoplasmic GSK-3β, is associated with markers of poor prognosis (T-stage, N-stage, local recurrence) in colorectal adenocarcinoma. The survival curve showed that patients with high cytoplasmic FLYWCH1 had significantly better OS than those with low FLYWCH1 expression. We also showed that the combination of the low cytoplasmic FLYWCH1 and high cytoplasmic GSK-3β expression status had the worse survival. While the group with high cytoplasmic FLYWCH1/low cytoplasmic GSK-3β had a better prognostic value.

The nuclear expression of FLYWCH1 was very low in tumour tissues, and the association between higher versus lower nuclear expression of FLYWCH1 with the OS was not significant. This could be because only a few tumour samples expressed FLYWCH1 in the nucleus. FLYWCH1 expression was mainly cytoplasmic in tumour tissues. However, it had to be noted that FLYWCH1 cytoplasmic expression was undergoing a gradual reduction at the higher CRC stages.

Overall, low expression of FLYWCH1 was associated with a more advanced tumour stage and worse overall survival in CRC. To the best of our knowledge, this is the first study to identify the expression of FLYWCH1 as a potential marker for overall survival and establish an association of FLYWCH1/GSK-3β expression in CRC. Future studies will seek to address FLYWCH1 localisation as an indicator of patient survival and therapy outcomes.

In conclusion, our findings together indicate that FLYWCH1 can be switched off during CRC progression via delocalisation of FLYWCH1 protein into the cytoplasmic compartment. This could be trigged by PTMs such as phosphorylation and ubiquitination. However, FLYWCH1 inactivation is not typically limited to Wnt-mediated cytoplasmic shuttling but could be a consequence of various mutations in the FLYWCH1 gene.

Holistically, experiments indicated that upon Wnt stimulation, FLYWCH1 is downregulated and translocated into the cytoplasm in different cell lines. This proposes a likely model of FLYWCH1 inactivation during tumorigenesis. Clinical data presented here uncover a potential value of FLYWCH1 as a biomarker for CRC patients, which urges the need for future studies addressing FLYWCH1 as an indicator of patient survival and therapy outcomes. While it has not been examined in other tumours, it would be interesting to test whether differential cellular localisation of FLYWCH1 in various cancer cells may determine the response to the increased Wnt signaling.

CHAPTER 4

FLYWCH1 is a new player in DNA damage response pathways

4.1 Summary

Human cells are continuously under various endogenous and exogenous stresses, which may ultimately result in DNA damage. The maintenance of genome stability is of paramount importance for cell viability. Thus, cells have evolved multiple pathways, including the DNA damage response (DDR) pathway, to preserve genomic integrity and function (344, 345). The molecular mechanisms governing these processes are detailed and complex, with an immense interplay between the various signaling pathways. Nevertheless, the cellular response to DNA damage and the efficiency of the repair machinery are the main determinant of patient outcomes following treatments, especially as the majority of anti-tumour therapies exploit DNA damage to target the rapidly dividing cancer cells. Therefore, understanding and identifying novel players that govern the DNA repair process is crucial to improving anti-tumour therapies' effectiveness and developing novel targeted strategies.

Although FLYWCH1 belongs to Cys2-His2 (C2H2)-type Zinc Finger Protein family, knowledge regarding FLYWCH1 requires greater exploration. Several C2H2 domain-containing proteins have emerged as critical players in repairing DNA double-strand break (DSB) (346-348). Enigmatically, a noticeable similarity is perceived between DNA-damage foci and nuclear foci formed by FLYWCH1. Henceforth, a preliminary idea exploring the genes that share similar function to FLYWCH1 based on their interactions was created by employing proteomic prediction tools named STRING (https://string-db.org) (349) and GeneMANIA (http://genemania.org) (Figure 4-1) (350). These computational approaches

integrate all known and predicted associations between proteins, including both physical interactions as well as functional associations. This is based on data using patterns of gene co- annotation in the Gene Ontology biological function hierarchy (351). Our screening revealed substantial similarities and meaningful potential interactions of FLYWCH1 with proteins involved in DNA damage and repair, such as breast cancer type 1 susceptibility protein (BRCA1) and MDC1 (Figure 4-1 A, B). The potential interaction of FLYWCH1 with MDC1 protein is based on experimental evidence of protein-protein interaction reported in (352).

Known Interactions

- ○━○ *from curated databases*
- ○━○ *experimentally determined*

Predicted Interactions

- ○━○ *gene neighborhood*
- ○━○ *gene fusions*
- ○━○ *gene co-occurrence*

Others

- ○━○ *textmining*
- ○━○ *co-expression*
- ○━○ *protein homology*

Your Input:

● FLYWCH1   *FLYWCH-type zinc finger 1 (715 aa)*

Predicted Functional Partners:

		Neighborhood	Gene Fusion	Cooccurence	Coexpression	Experiments	Databases	Textmining	[Homology]	Score
● ANKRD9	*Ankyrin repeat domain-containing protein 9; Ankyrin repeat domain containing (317 aa)*							•		0.756
● MARCH3	*E3 ubiquitin-protein ligase MARCH3; E3 ubiquitin-protein ligase which may be involved in endosomal trafficking. E3 ubi...*							•		0.735
● AHRR	*Aryl hydrocarbon receptor repressor; Mediates dioxin toxicity and is involved in regulation of cell growth and differentia...*							•		0.719
● MYO1G	*Unconventional myosin-Ig; Unconventional myosin required during immune response for detection of rare antigen-pres...*							•		0.719
● MDC1	*Mediator of DNA damage checkpoint protein 1; Required for checkpoint mediated cell cycle arrest in response to DNA ...*					•				0.693
● ACSM3	*Acyl-coenzyme A synthetase ACSM3, mitochondrial; Has medium-chain fatty acid-CoA ligase activity with broad substr...*							•		0.677
● KIAA1586	*E3 SUMO-protein ligase KIAA1586; E3 SUMO-protein ligase; facilitates UBE2I/UBC9-mediated SUMO2 modification of t...*							•		0.652
● OR1C1	*Olfactory receptor 1C1; Odorant receptor; Olfactory receptors, family 1 (314 aa)*							•		0.583
● FAM89B	*Leucine repeat adapter protein 25; Negatively regulates TGF-beta-induced signaling; in cooperation with SKI prevents t...*							•		0.574
● ODF3L2	*Outer dense fiber of sperm tails 3 like 2 (289 aa)*							•		0.560

Figure 4-1 Predicted Protein interaction network generated by A) GeneMANIA software (351), showing association data including potential protein and genetic interactions, pathways, co-expression, co-localisation and protein domain similarity **B)** STRING software (353), the interactions include direct

(physical) and indirect (functional) associations; they stem from computational prediction, and from interactions aggregated from other (primary) databases.

Indeed, the localisation of proteins to DNA damage sites is believed to be a hallmark of participation in the DNA damage and repair processes (354). At the site of DNA double-strand breaks (DNA-DSB), several proteins such as γH2AX, ATM, 53BP1, RAD51, and the MRE11/RAD50/NBS1 complex accumulate and/or modify to form microscopically visible subnuclear foci (355-357).

The following study is novel in assessing the expression, role, and regulation of FLYWCH1 in the context of DNA-damage response signaling pathways. Interestingly, we here uncover a significant similarity between DNA-damage formed foci and FLYWCH1 nuclear foci. We showed a direct effect of FLYWCH1 expression on the H2AX phosphorylation independent of ATM protein. Additionally, for the first time, we envisaged the regulation of endogenous FLYWCH1 under the various DNA-damage stimuli. With a further clinical investigation in the future, such knowledge may not only lead to a better understanding of the complicated DDR signalling mechanisms but may also offer a new target for anticancer therapies.

4.2 Results

4.2.1 FLYWCH1 is localised in nuclear speckles and co-localised with γH2AX

In Chapter 3, we demonstrated the FLYWCH1 protein in both nuclear and cytoplasmic compartments of the colon tissues and various cell lines. The nucleus

contains various punctuate structures associated with transcription factories, such as PML bodies, Cajal bodies, and nucleolus (358, 359). Additional nuclear domains were also described comprising cleavage bodies, nuclear stress bodies, histone locus bodies, and DNA damage foci (358, 359). Various sub-cellular localisations may contribute to regulating nuclear pathways and differing biological activity (360, 361). Thus, understanding the sub-cellular distribution of FLYWCH1 may be crucial for understanding its biological functions. Previously, in our laboratory, Dr Emenike K. Onyido (2016) analysed the relationship between the nuclear pattern of FLYWCH1 and the mechanisms involved in the formation of foci, such as splicing activity. Following the observation of several nuclear speckles markers, findings indicated FLYWCH1 is co-localised with splicing factor SC-35 using an anti-FLYWCH1 antibody that was the only commercially available from Santa Cruz. However, all knockdown and overexpressing FLYWCH1 studies showed that the anti-FLYWCH1 antibody (from Santa Cruz) is non-specific. Furthermore, Dr Onyido showed that FLYWCH1 was not involved in the splicing activity (Santa Cruz discontinued this antibody). To this end, fortunately, with the recent development of anti-FLYWCH1 antibody, we were able to evaluate the specificity in overexpressing GFP-FLYWCH1, MYC-FLYWCH1 and *FLYWCH1*-knockdown experiments of the current commercial antibody from Sigma (Prestige) as outlined in chapter 3 (Section 3.2.2).

Next, we carried out the co-localisation studies of FLYWCH1 with known mechanisms that are involved in the formation of nuclear foci (such as DNA damage foci, chromatin foci, RNA foci and splicing activity). However, as the majority of antibodies used in this study were raised in the same host (Rabbit) with

our new anti-FLYWCH1 antibody, we had to transiently transfect the cells with GFP-tagged FLYWCH1 (GFP-FLYWCH1) for immunofluorescence colocalisation studies with the γH2AX, 53BP1, Drosha, HP1BP3 and HP1α antibodies.

The γH2AX encodes the phosphorylated form of H2AX (Ser139), a biomarker for DNA double-strand breaks (DSB) (356). 53BP1 encodes tumour suppressor p53 binding protein 1, an important DNA damage response factor (355). Drosha is a double-stranded RNA-specific ribonuclease (RNase) III, and a subunit of the microprocessor protein complex, contributing to DDR activation by generating small non-coding RNAs (362). HP1BP3, or heterochromatin protein 1 binding protein 3, is a novel chromatin-binding protein (363). HP1α (heterochromatin protein 1 isoform α) is the main factor responsible for heterochromatin maintenance and gene silencing and is necessary for binding the main DNA damage-related protein 53BP1 at DNA repair foci (364).

The initial co-localisation study with γH2AX, 53BP1, and Drosha in TIG119 cells, indicated a co-localisation of GFP-FLYWCH1 with γH2AX, but not Drosha or 53BPl (Figure 4-2). These were therefore excluded from the ensuing experiments. Unexpectedly, apart from the co-localisation with γH2AX, an upregulation of γH2AX was detected in GFP-FLYWCH1-expressed cells compared to control cells (Figure 4-2 B, arrowhead).
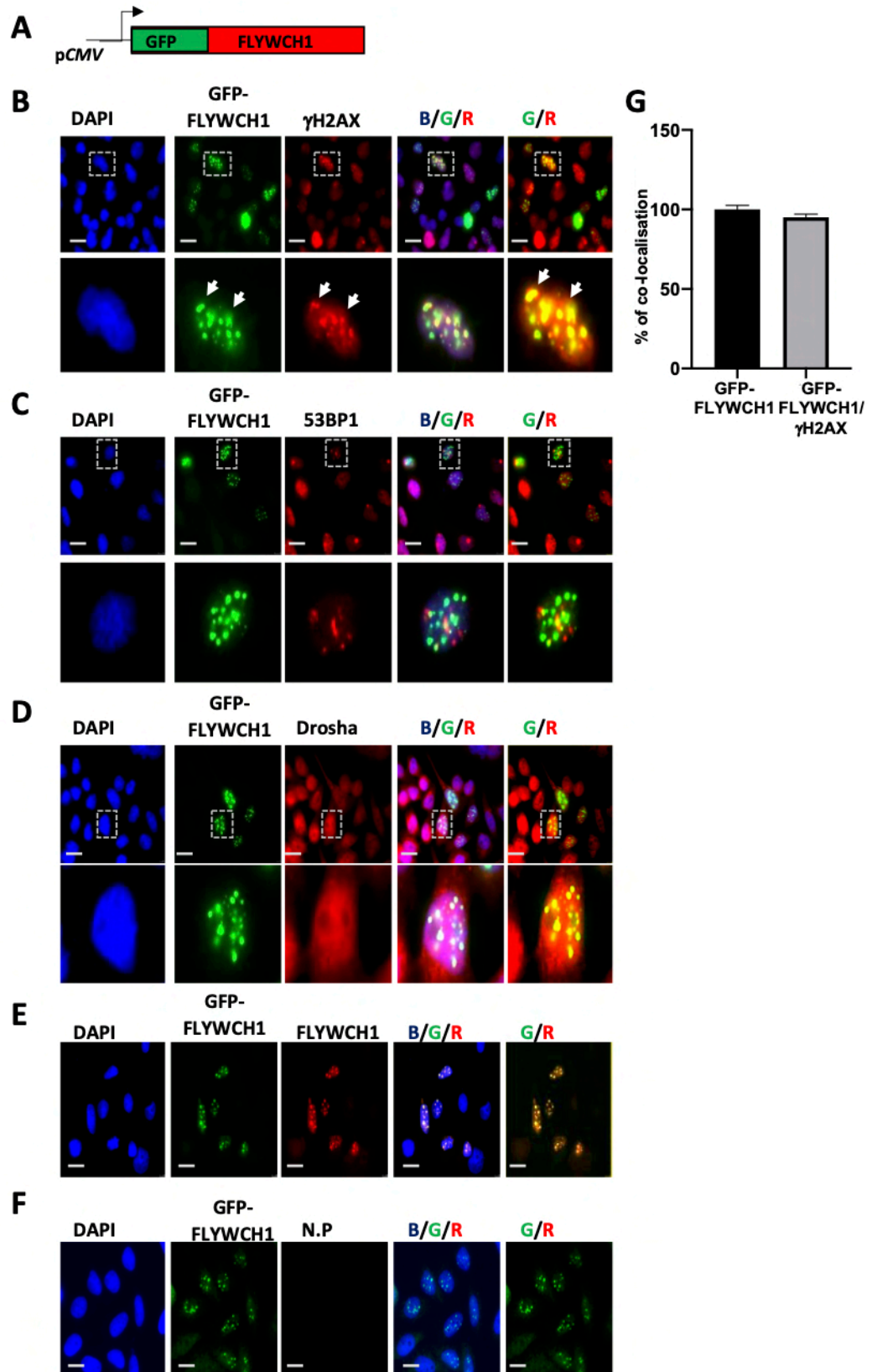
Figure 4-2 Immunostaining shows co-localisation of GFP-FLYWCH1 with γH2AX in TIG119 cells. Cells were transfected with A) GFP-tagged FLYWCH1, fixed and stained with **B)** γH2AX, **C)** 53BP1, **D)** Drosha and **E)** Anti-FLYWCH1 antibody (used as a positive control, confirming GFP-tagged FLYWCH1 exogenous expression). **F)** Negative control (N.P, no primary antibody).

Arrowheads in B show representative co-localised FLYWCH1 and γH2AX foci. Dotted boxes indicate enlarged cell/s. Magnification, 100x. Scale bars, 7.5μm. **G)** Quantification analysis showing the percentage of GFP-FLYWCH1 foci that co-localise with γH2AX. The number of foci formed by GFP-FLYWCH1was counted in 80 cells (from two independent experiments) and the percentage of co-localised foci was calculated and averaged. Data represent the mean of co-localisation %, and error bars indicate the standard deviation.

Next, to study the co-localisation in CRC cells, HCT116 cells were transiently transfected with GFP-tagged FLYWCH1 and were then co-stained with HP1a, HPB1P3, and γH2AX (Figure 4-3). Our results below indicated that GFP-FLYWCH1 does not co-localise with HP1BP3 or HP1a. However, similar to the TIG119 cells, γH2AX was induced in GFP-FLYWCH1-expressing cells, in HCT116 cells (Figure 4-3 B, arrowhead).
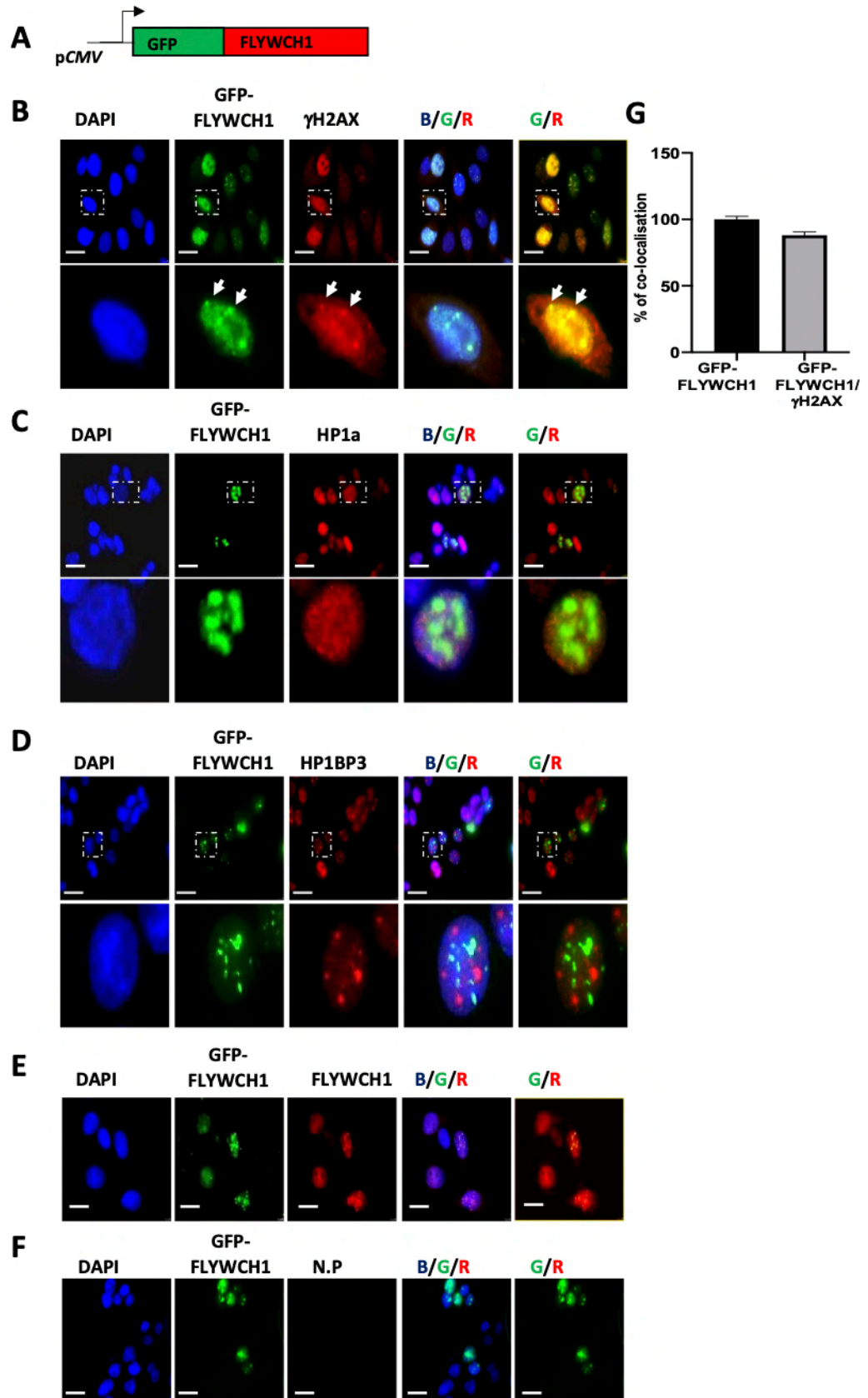
Figure 4-3 Immunostaining shows the co-localisation of GFP-FLYWCH1 with γH2AX in HCT116. A) Schematic representation of GFP-tagged FLYWCH1 (GFP-FLYWCH1) construct. HCT116 cells were transfected with GFP-

FLYWCH1, fixed, and stained with **B)** γH2AX, **C)** HP1a, **D)** HP1BP3, **E)** anti-FLYWCH1 antibody staining confirms GFP-tagged FLYWCH1 exogenous expression (positive control), **F)** is a Negative control (N.P, no primary antibody). Arrowheads in B show representative co-localised FLYWCH1 and γH2AX foci. Dotted boxes indicate enlarged cell/s. Magnification, 100x. Scale bars, 7.5μm. **G)** Histogram shows the percentage of FLYWCH1 foci that co-localise with γH2AX. Data are represented as the mean of co-localisation % obtained from two independent experiments; error bars indicate the standard deviation.

While the minor histone H2A variant is a biomarker for DNA double-strand breaks (DSB), the phosphorylation of H2AX at ser-139 is one of the most well-established chromatin modifications linked to DNA damage and repair (365). The phosphorylation of H2AX (Ser139) occurs in response to DSB formation and plays a role in the assembly of DNA repair proteins at the sites of damage and activation of checkpoints protein (356). The co-localisation, and the induction of γH2AX in FLYWCH1-expressing cells (Figures 4-2 and 4-3) led to the speculation that FLYWCH1 protein may play a role in the DNA-damage response pathway. Therefore, we aimed to investigate how FLYWCH1 mediates its effect on H2AX, and whether FLYWCH1 requires DNA damage and DBS break (a.k.a DNA-damage dependent). Initially, we examined the effects of DNA damaging agents (i.e UV and Cisplatin) on the endogenous expression level and pattern of FLYWCH1, in human fibroblast and CRC cell lines.

4.2.2 The effects of UV-radiation on FLYWCH1 expression in normal versus CRC cells

Ultra-violet light is a classical DNA-damage agent that induces H2AX phosphorylation (366). Here, its influence on endogenous FLYWCH1 expression

was examined in different cell lines. Initially, cells were cultured either on coverslips (for IF staining), or on 10cm dishes, for protein extraction. Confluent cells were then exposed to 50mJ/cm^2 UV light using UV-crosslinker (STRATAGENE UV Stratalinker 1800, UK). 3h later, cells were fixed and stained for IF assay or lysed for WB analysis. For control conditions, untreated cells were cultured at the same time and followed similar conditions without exposure to UV. The activation of the ATM/ATR signalling pathway in response to UV-induced DNA damage was initially validated by monitoring the foci formed by H2AX and ATM before and after UV-light treatment (Figure 4-4).
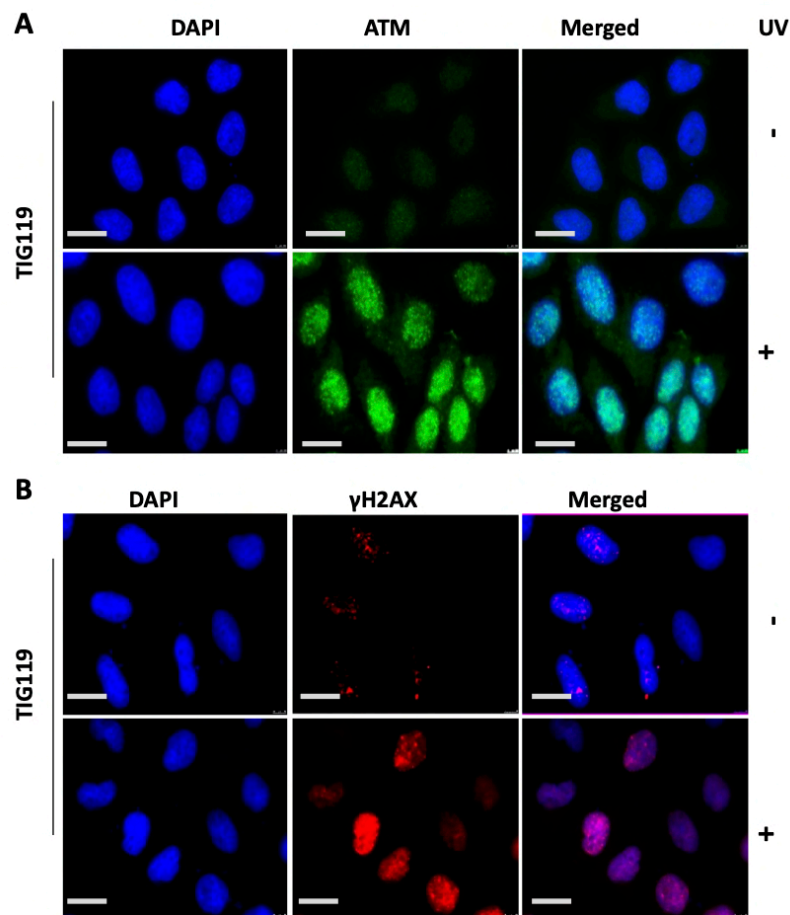
Figure 4-4 Validation of UV-light treatment in TIG119 cell line. Cells were exposed to 50mJ/cm^2 UV light and immunostained with A) ATM and **B)** γH2AX, as a positive control for UV-induced DNA damage response. Images demonstrate the induction of ATM and γH2AX following UV treatment. Nuclei

were detected with DAPI-blue fluorescent stain. Magnification, 100x. Scale bars: 7.5μm.

Afterwards, FLYWCH1 expression was studied in these cells by IF and WB analysis. As shown below, IF staining of endogenous FLYWCH1 in TIG119, and CRC cells, revealed an increase, but no changes in the expression pattern, after UV-exposure (Figure 4-5 A, B). Further investigation by WB analysis indicated a significant induction in FLYWCH1 protein expression in the UV+treated TIG119 and CRC cells (Figure 4-5 C, D). This was also supported by a significant upregulation of FLYWCH1 transcription, as demonstrated by qRT-PCR analysis (Figure 4-5 E). These results together verified the induction of both FLYWCH1 mRNA and protein level in response to UV-mediated DNA damage.
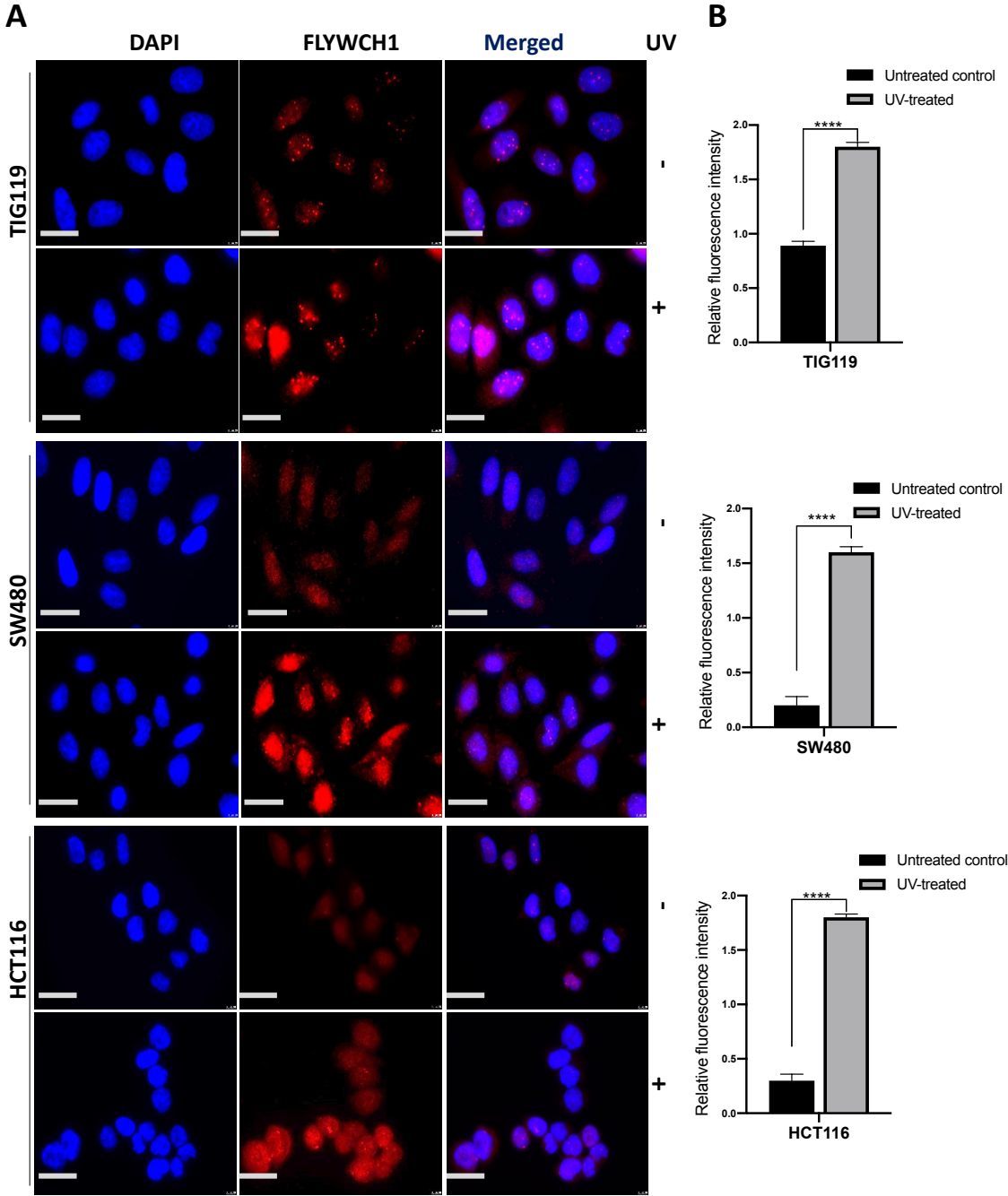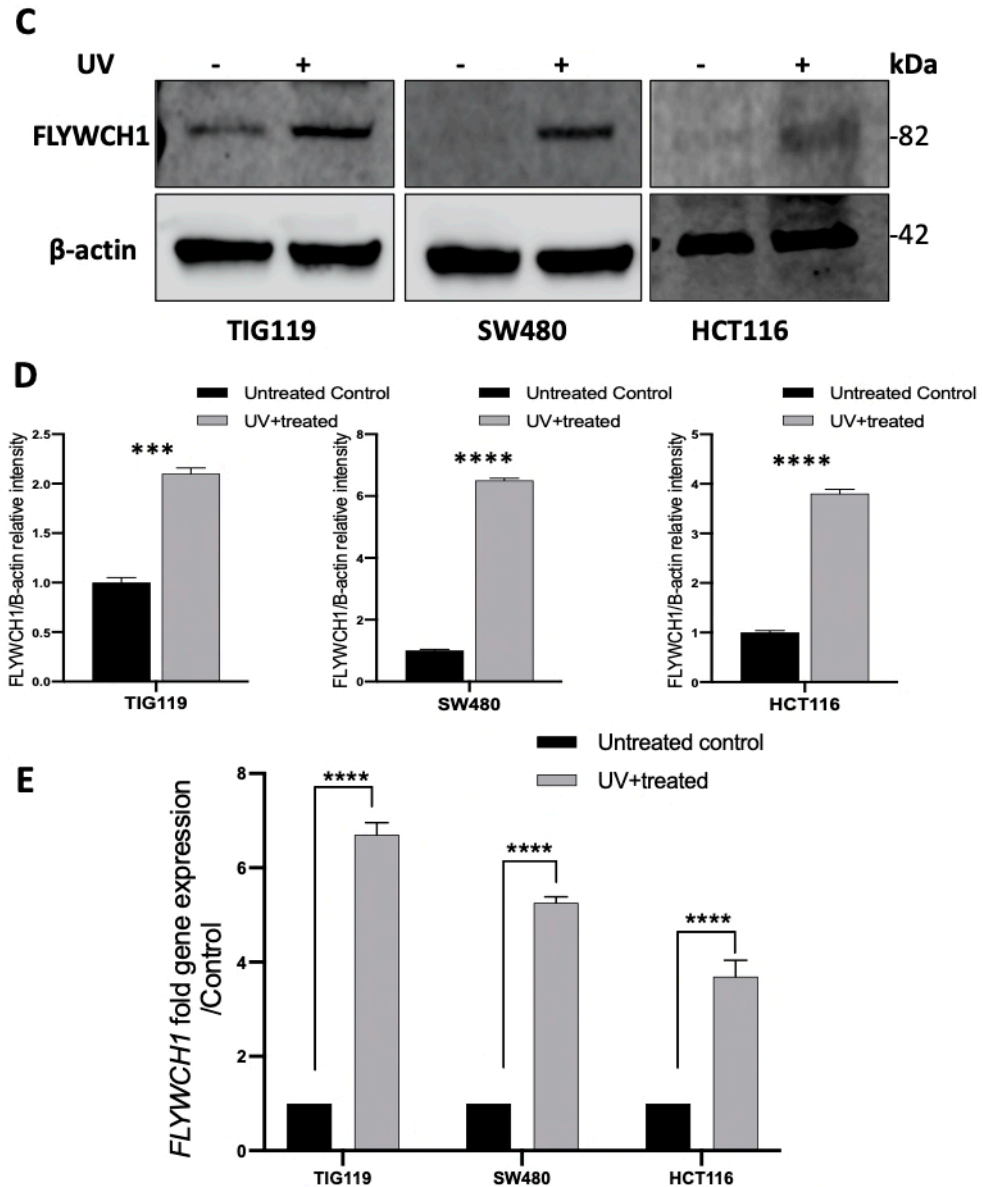
Figure 4-5 UV-treatment induces the endogenous FLYWCH1 expression in TIG119 and CRC cell lines. A, B) IF staining and quantification showing the effect of UV on the expression level and pattern of FLYWCH1, Magnification, 100x, Scale bars: 7.5μm. The relative fluorescence intensity (fold) was measured using ImageJ software. **C)** WB analysis confirming the upregulation of FLYWCH1 protein in UV treated cells. Cells were synchronized by starvation in serum-free medium before treatment with UV (50mJ/cm^2), 100μg of total cell total lysates was loaded in 4-20% gradient pre-cast gel. N=4. **D)** Graphs show the relative densitometric quantification of FLYWCH1 band intensities normalized to β-actin and presented as the mean fold changes obtained from three independent experiments. **E)** qRT-PCR analysis of *FLYWCH1* mRNA in TIG119 and CRC cells following UV-treatment. mRNA expression was obtained by using the 2^-(ΔΔCt) method. Experiments were carried out in triplicates and repeated on three

independent occasions, data are mean and SD (**= $P \leq 0.01$, ***= $P \leq 0.001$, ****= <0.0001). P-values were estimated by Student's *t*-test

In parallel, the impact of enforced-FLYWCH1 expression on some key DDR-proteins was examined and compared to UV-mediated outcomes. For this, TIG119 Myc-control and MYC-tagged-FLYWCH1-IRES-GFP (MYC-FLYWCH1[OE]) overexpressing cells were treated (or untreated) with UV-light. Cells were then analysed by IF staining and WB for the expression of several DDR proteins and endogenous FLYWCH1 protein (Figure 4-6).
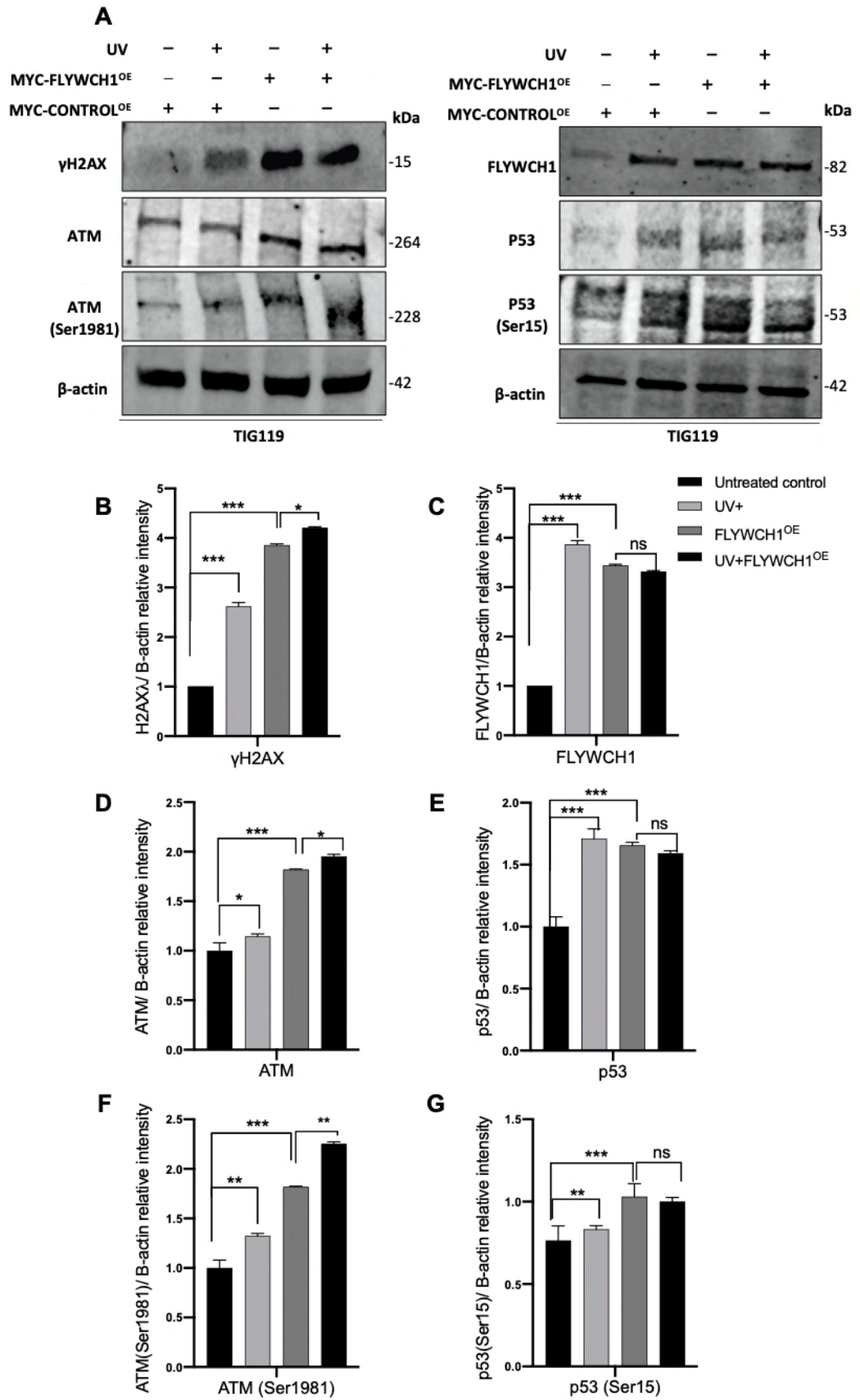
Figure 4-6 The association of FLYWCH1 expression in UV-mediated DNA damage. A) WB analysis demonstrates the recruitment of DDR proteins in response to UV exposure under normal versus enforced FLYWCH1 expression. Protein lysates (120μg) extracted from UV-treated, and untreated fibroblasts were immunoblotted with the indicated antibodies. Histograms represent quantification of **B)** γH2AX (ser139), **C)** FLYWCH1, **D)** ATM, **E)** p53, **F)** ATM (ser1981) and **G)** p53(ser15), band intensities normalized to β-actin. Data are represented as the mean of fold change obtained from three independent experiments; error bars indicate the standard deviation. (ns; not significant, *, $p < 0.05$; **, $p < 0.01$, ***= $P \leq 0.001$, ****= <0.0001).

The activation of ATM/ATR signalling pathway, in response to UV-induced DNA damage, was confirmed by the induction of H2AX and ATM protein level, before and after UV-treatment (Figure 4-6, left panel). In line with co-localisation data, FLYWCH1^{OE}–induced γH2AX protein was higher than that caused by UV treatment. Likewise, FLYWCH1^{OE} cells showed an elevated level of ATM, p53, p53(Ser15) proteins, regardless of UV-treatment condition. This suggests a positive correlation between FLYWCH1 expression and γH2AX induction (ATM/ATR activation).

Collectively, our data implied an impact of FLYWCH1 expression on H2AX phosphorylation, and foci formation. Since the ATM/ATR pathway is the main signalling pathway implicated in UV-mediated DNA damage (366), it can be predicted that the recruitment and activation of ATM/ATR kinases could be the essential mediator to execute FLYWCH1's effect on γH2AX. Therefore, using CRISPR-Cas9 technology, we generated a stable ATM knockout model in TIG119 cells. This was particularly useful in revealing FLYWCH1's relationship with ATM expression and ATM-dependent DNA-damage repair functions.

4.2.2.1 FLYWCH1-mediated induction of phosphorylated H2AX level is independent of ATM protein

Through our work, an ATM-knockout (ATM^KO) model of TIG119 cells and HCT116 cell lines was generated (219). To achieve this, an ATM-gRNA-CRISPR plasmid construct was used (Figure 4-7). The construct was previously generated in our laboratory by Dr Makhliyo Normatova. Specifically, ATM gRNA was cloned into pSpCas9 (BB)-2A-Puro (pX459) (Addgene plasmid ID 48139) backbone vector. The provided plasmid construct was amplified, and revalidated by DNA-sequencing, using U6-Forward primer as shown in Figure 4-7 B.

Sequencing Output:

AGGCCCTTTCCCGTTTTATGATTTAAAGAAATAGCAAGTTAAAATAAGGCTAGTCCGTTATCAACTTGAAAAAGTGGCAC
CGAGTCGGTGCTTTTTTGTTTTAGAGCTAGAAATAGCAAGTTAAAATAAGGCTAGTCCGTTTTTAGCGCGTGCGCCAATT
CTGCAGACAAATGGCTCTAGAGGTACCCGTTACATAACTTACGGTAAATGGCCCGCCTGGCTGACCGCCCAACGACCCCC
GCCCATTGACGTCAATAGTAACGCCAATAGGGACTTTCCATTGACGTCAATGGGTGGAGTATTTACGGTAAACTGCCCAC
TTGGCAGTACATCAAGTGTATCATATCCAAGTACGCCCCCTATTGACGTCAATGACGGTAAATGGCCCGCCTGGCATTG
TGCCCAGTACATGACCTTATGGGACTTTCCTACTTGGCAGTACATCTACGTATTAGTCATCGCTATTACCATGGTCGAGG
TGAGCCCCACGTTCTGCTTCACTCTCCCCATCTCCCCCCCCTCCCCACCCCCAATTTTGTATTTATTTATTTTTTAATTA
TTTTGTGCAGCGATGGGGGCGGGGGGGGGGGGGGGGG

Figure 4-7 Validation of the ATM-CRISPR construct used in this study. A) Diagram of the plasmid construct map. The construct contains resistance genes for Ampicillin and Puromycin, and the U6 promoter drives expression of the guide RNA (sequence in red box). **B)** The sequencing readout of the amplified plasmid downstream of the U6 promoter. The green and red text show the desired gRNA sequence. This was verified through automated DNA sequencing (Sequencing Facilities, Queen's Medical Centre, Nottingham University).

Initially, TIG119 cells were transfected with ATM-CRISPR construct. After 10 days of puromycin selection, the cells were diluted into one cell/well, and distributed among a 96 well-plate to encourage the growth of colonies derived from a single cell. For validation purposes, these colonies were further examined for ATM expression via WB and IF staining (Figure 4-8 A, C), and the expression of FLYWCH1 was thence investigated (Figure 4-8 B, C).
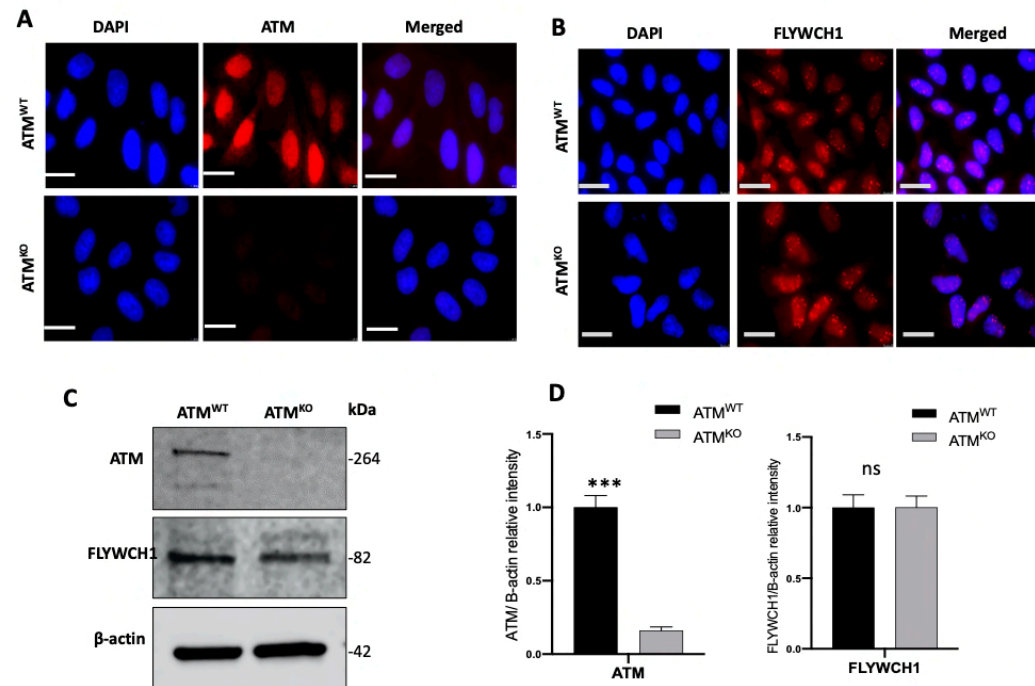
Figure 4-8 The depletion of ATM in TIG119 cells has no effects on the endogenous FLYWCH1 level and pattern. A, B) Immunofluorescence staining of the ATM protein and FLYWCH1 in TIG119, validating the depletion of ATM in the KO cells, and showing no underlying changes of FLYWCH1 level, magnification 100x. Scale bars: 7.5μm. **C)** Western blot analysis, and **D)** quantification of ATM^{WT} versus ATM^{KO} TIG119 cells. β-actin was used as a control. Experiments were repeated in three independent times. (ns; not significant, ***= P ≤ 0.001).

As demonstrated in Figure 4-8 C, WB analysis revealed no detectable levels of ATM protein in the ATM^{KO} lysates compared to the untransfected cells (ATM^{WT}), indicating the successful knockout. This was backed up by IF staining of ATM protein (Figure 4-8 A), where the ATM^{KO} cells showed a reduction in ATM staining compared to the control cells. Furthermore, the endogenous expression of FLYWCH1 was studied in the ATM^{KO} cells by IF and WB assays. Initial screening showed no notable differences in the protein level and/or the pattern of FLYWCH1 in ATM-depleted TIG119 cells (Figure 4-8).

Furthermore, several attempts by James Coulton (M.Sc. student) were undertaken to generate ATM^{KO} in HCT116 cell lines, using a similar strategy and construct. However, it was immediately apparent that the ATM knockout had a significant impact on growth, morphology, and cell proliferation in CRC cells (Appendix 6). Substantial difficulty was experienced in culturing enough cells, and due to time restrictions, it was not possible to carry out the intended experiments in HCT116 cells knockout for ATM. So, TIG119-ATM^{KO} cells were the only ATM^{KO} model used for further experiments. To further assess the need for ATM protein in FLYWCH1-mediated induction of γH2AX, FLYWCH1 was overexpressed in both control (ATM^{WT}) and ATM^{KO} cells (Figure 4-9). The effects on γH2AX foci formation and its co-localisation with FLYWCH1 were thence examined.
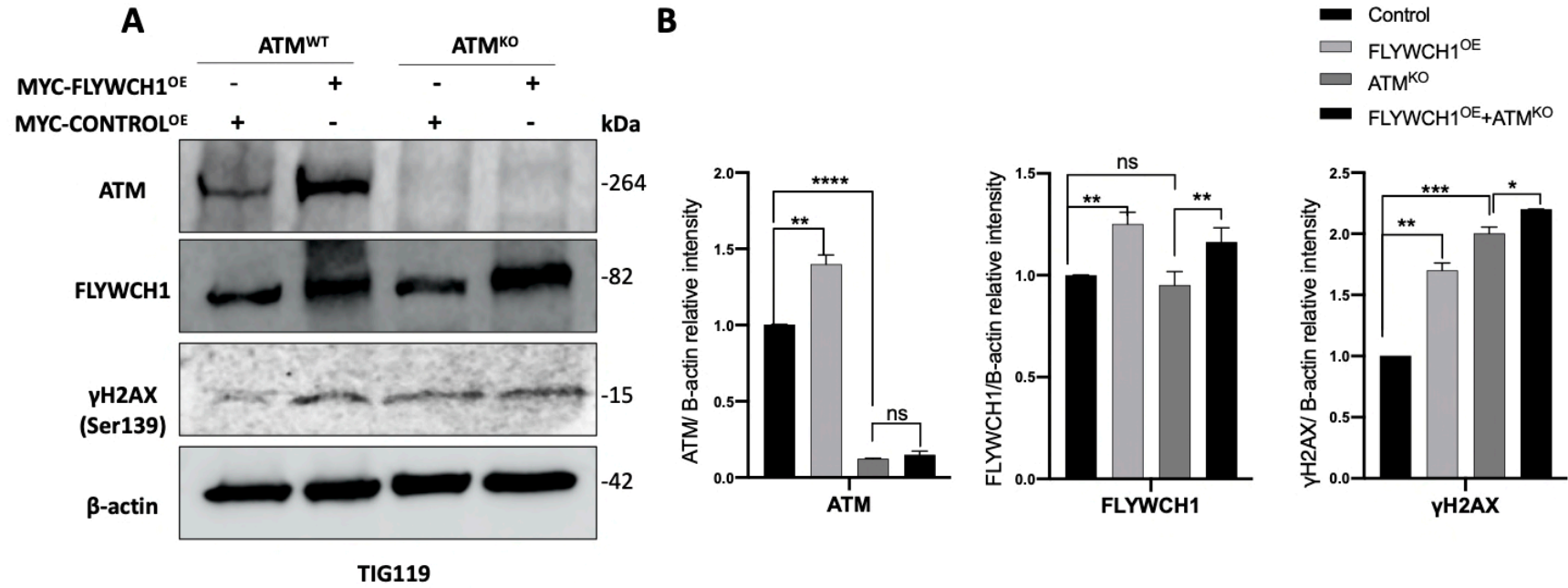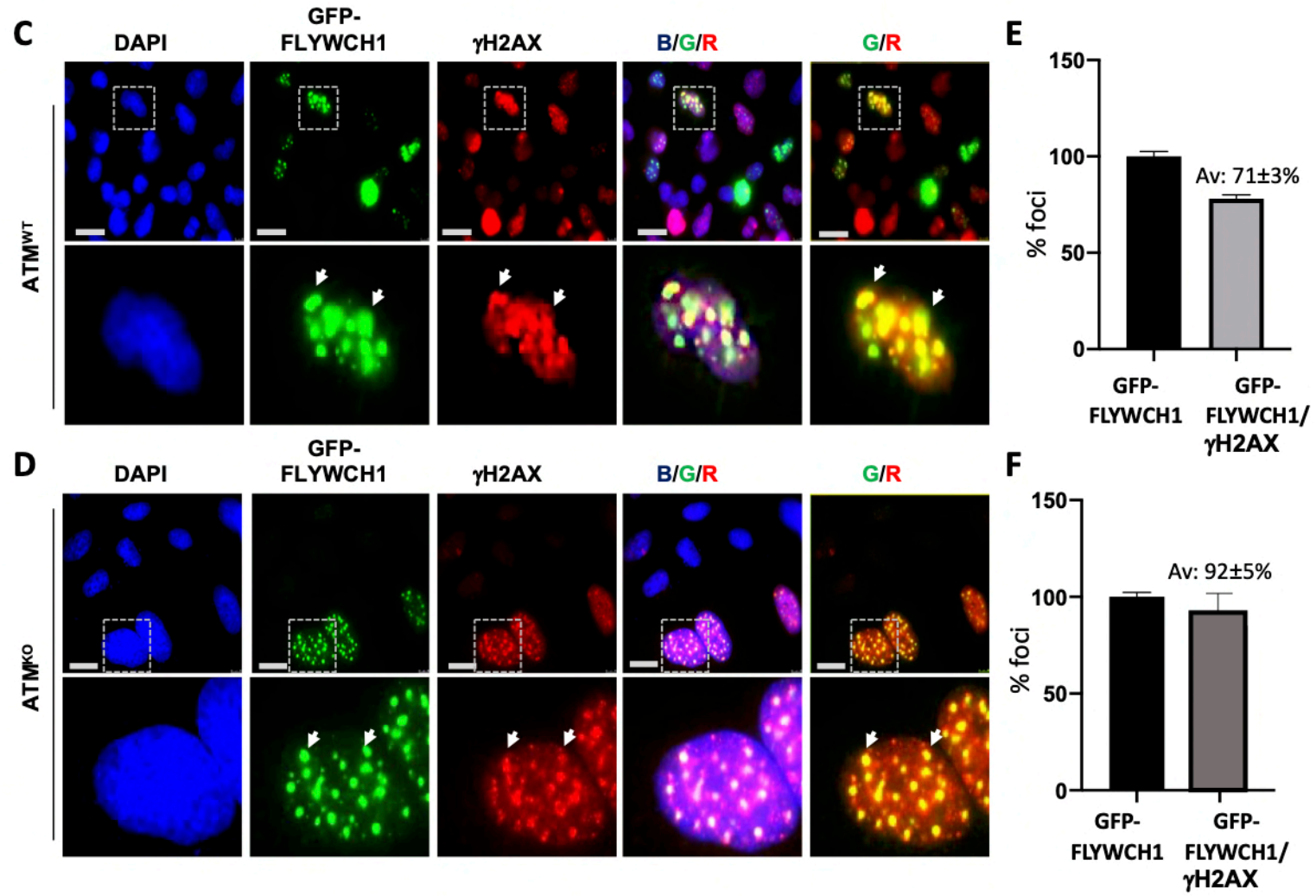
Figure 4-9 FLYWCH1-mediated induction of phosphorylated H2AX level is independent to ATM protein. A) WB analysis showing that ectopic expression of FLYWCH1 induces γH2AX in both cells regardless of ATM depletion. 120ug of protein was loaded in 4-20% gradient precast gel, experiments were repeated in two independent occasions. **B)** Quantification analysis of ATM, γH2AX and FLYWCH1 relative protein expression following normalization with β-actin, Data are represented as the mean fold change obtained from two independent experiments (ns; not significant, *, $p < 0.05$; **, $p < 0.01$, ***= $P \leq 0.001$, ****= <0.0001). P-values were estimated by Student's *t*-test. **C, D)** IF staining confirming the induction and co-localisation of FLYWCH1 (GREEN) with γH2AX foci (RED) in the absence of ATM protein, dotted boxes are magnified cells. Arrowheads in C & D show representative co-localised GFP-FLYWCH1 and γH2AX foci. Magnification: 100x, Scale bars: 7.5μm. **E, F)** Histograms show the mean of the percentage of FLYWCH1 foci that co-localise with γH2AX obtained from two independent experiments; error bars indicate the standard deviation.

As demonstrated in Figure 4-9 A, in the control cells, enforced-FLYWCH1 expression induced both ATM and γH2AX proteins. However, more importantly, overexpressing FLYWCH1 in ATM^KO cells was sufficient to induce the foci formed by γH2AX irrespective of ATM expression (Figure 4-9). Accordingly, these results imply that FLYWCH1-mediated phosphorylation of H2AX could be independent of ATM activation. Therefore, the ATM regulated activity of FLYWCH1 can be excluded in TIG119 cells. Nevertheless, more information is required regarding the potential effects of ATM alterations, and other possible kinases, such as ATR and DNA-PKcS on FLYWCH1 expression in CRC cells.

4.2.3 Cisplatin treatment reduced FLYWCH1 protein level in SW480, DLD-1, and SW620 but not in HCT116

Considering the effects of UV-treatment on endogenous FLYWCH1 protein, the response to different DNA-damaging mediators was investigated by applying a Chemotherapeutic treatment (Cisplatin) strategy as another well-established type of DNA damaging agent. Cisplatin is an antitumor drug widely used to treat several types of cancer, targeting the genomic DNA, causing adducts that block transcription and synthesis of DNA, and leading to cell death if not appropriately repaired (367, 368). Most of the major DNA repair systems are involved in removing cisplatin-induced DNA damage. Examples include: nucleotide excision repair (NER), mismatch repair (MMR), homologous recombination (HR) and non-homologous end-joining (NHEJ) (369). Yet, despite the several players that are implicated in response to cisplatin treatment, and drug sensitivity in general (e.g.

DNA binding and repair, and thiol binding, and drug uptake (368)), a functional p53 is known to be essential in the cellular response to cisplatin (370). Therefore, employing cisplatin would be useful to address the potential linkage between FLYWCH1 and p53-mediated cellular response. To study the effect of cisplatin on the FLYWCH1 protein expression, CRC cells were exposed to 16μM of cisplatin for 24h and 48h. The concentration of cisplatin was determined based on the literatures (253, 371), and a piolet optimisation experiment carried in our lab. It was indicated that a concentration between 10-20μM is sufficient to induce the foci formation by H2AX and activate DNA damage pathway, without causing a significant cell death. Thence, cisplatin-mediated DNA damage was validated by the activation of γH2AX, as well as the induction of p53.

As shown in Figure 4- 10 below, cisplatin treatment triggered a rapid formation of γH2AX foci within 24h of treatment. This validates the treatment condition used in this experiment. Subsequently, the level of FLYWCH1 was examined in CRC cell lines (Figure 4-10 B, E).
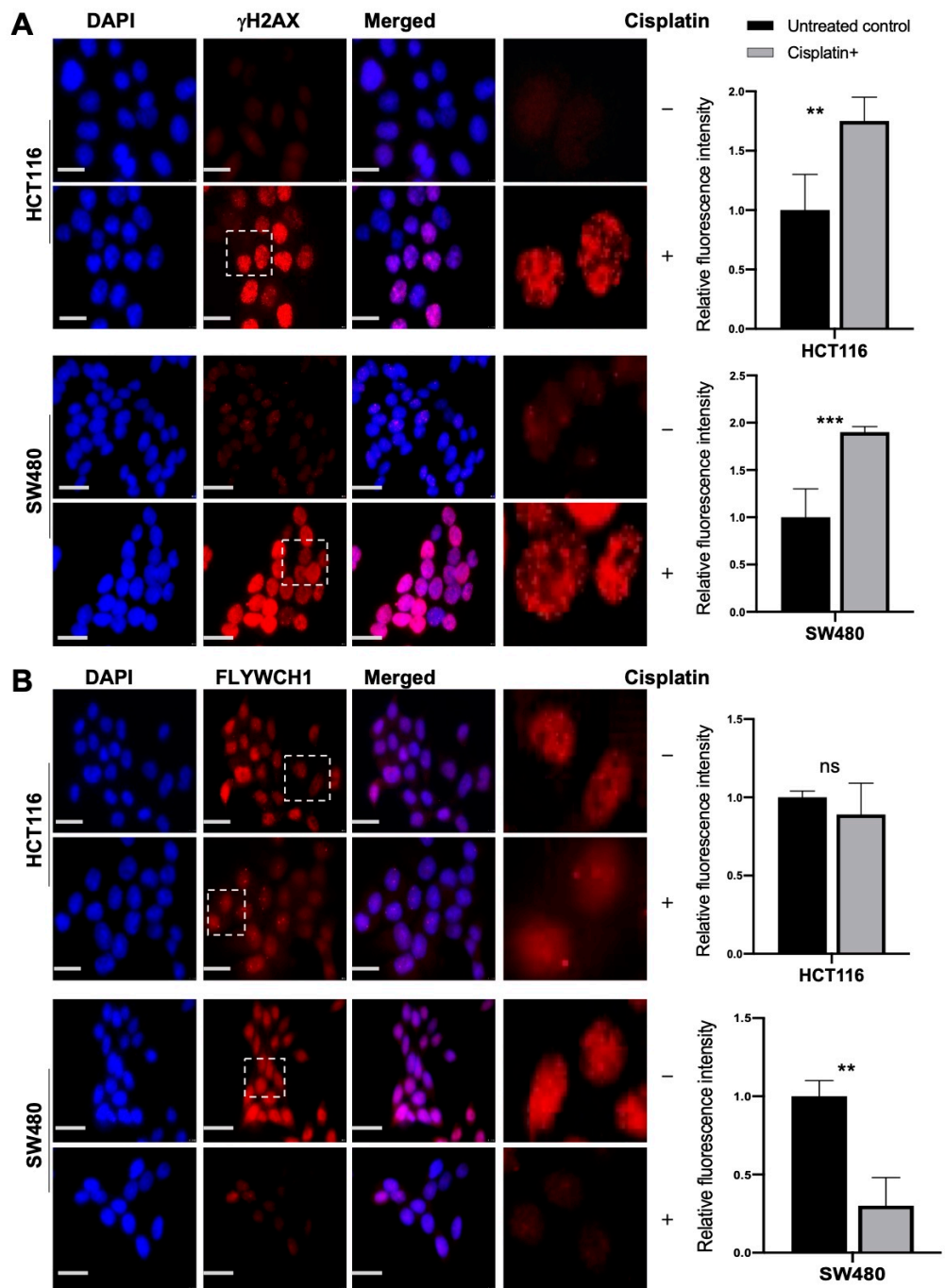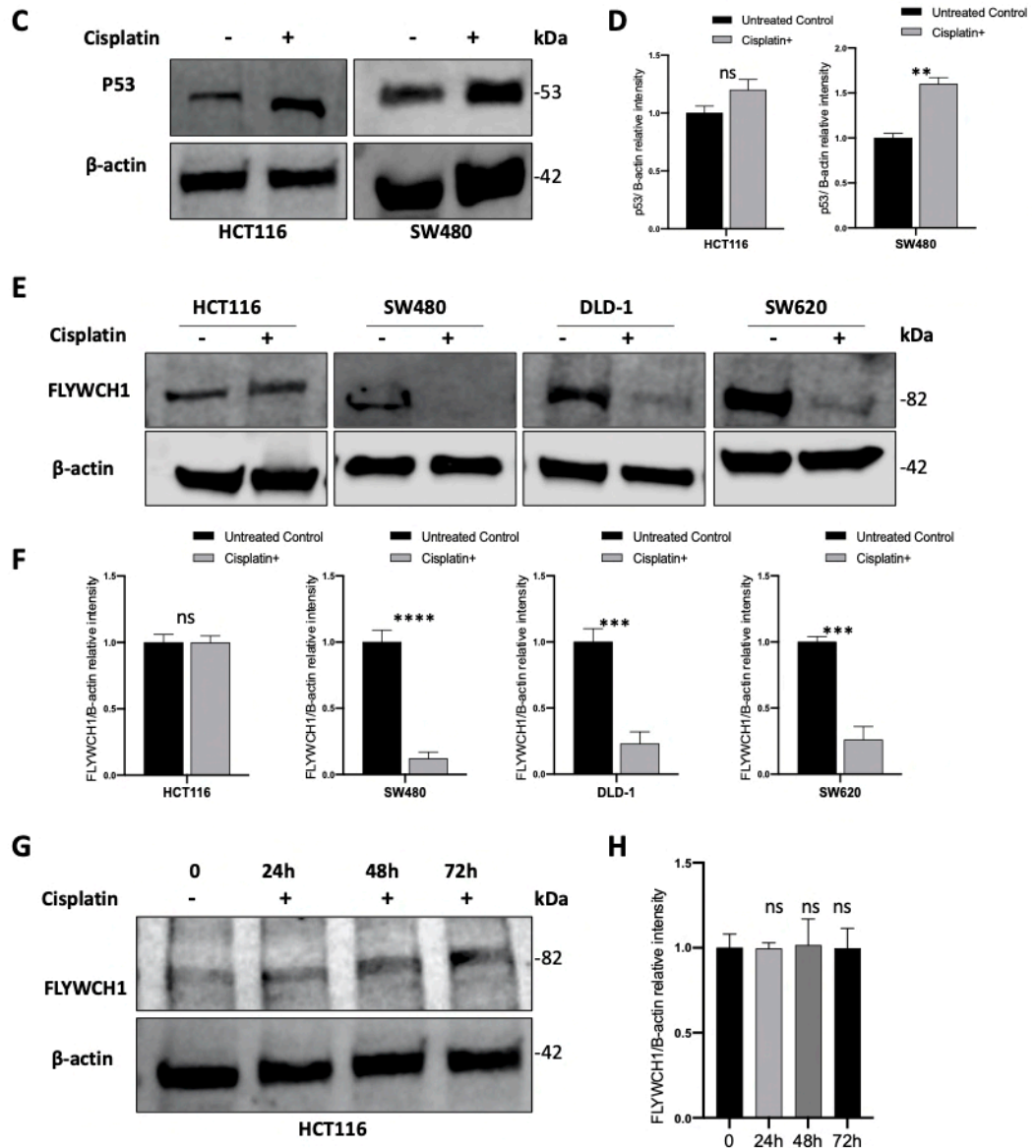
Figure 4-10 Cisplatin treatment reduces FLYWCH1 protein level considerably in CRC cell lines but HCT116. A) IF staining and quantification showing the induction and quick foci formation by γH2AX after 24h of cisplatin treatment, **B)** IF staining and quantification showing the effect of cisplatin on FLYWCH1 protein level in CRC cells. The relative fluorescence intensity (fold) was measured using ImageJ software. Magnification: 100x, Scale bars: 7.5μm. **C, D)** WB analysis and quantification of p53 level in HCT116 and SW480 cells following cisplatin treatment (N=2). **E, F)** WB analysis and quantification showing the effect of cisplatin on FLYWCH1 protein expression (N=3). **G, H)** WB analysis and quantification confirm the steady expression of FLYWCH1 in HCT116 cells treated with 16μM of cisplatin at different time point. All cells were synchronised by starvation in a serum-free medium before treatment and were maintained under similar conditions, and passage number. 120μg of protein lysate was loaded per well, and protein loading levels are monitored by probing for β-actin. For WB quantification, band intensities were normalized to β-actin. Data are represented as

the mean fold change obtained from two or three independent experiments; error bars indicate the standard deviation. P-values were estimated by Student's *t*-test (ns; not significant, *, p < 0.05; **, p < 0.01,***= P ≤ 0.001, ****= <0.0001).

Unlike the UV+ effects, we here showed that cisplatin significantly reduces FLYWCH1 protein level in all p53-mutated CRC cell lines, except for HCT116 (p53^{WT}) (Figure 4-10 D-F). FLYWCH1 expression in HCT116 cells was examined separately at various time points. This repeatedly demonstrated a stable expression of FLYWCH1, when compared to other CRC cell lines (P53^{mut}) (Figure 4-10, G-H). These observations might imply a p53-dependent notion of FLYWCH1 response to cisplatin-induced DNA damage.

Although it was indicated that the HCT116 cell line purchased from the American Type Culture Collection (Manassas, VA, USA) is cisplatin-sensitive (372). Yet, Shen H et al. has reported that the HCT116 cell line contains a mixture of clones that vary broadly in their sensitivity to cisplatin (373). In their study, HCT116 cells were plated at single-cell density and several clones were isolated. It was then shown that some clones of HCT116 cell lines are cisplatin-resistant, while other cisplatin-sensitive (373). Accordingly, the steady expression of FLYWCH1 in HCT116 could also be due to the possible mixed status of cisplatin-resistant in these cells.

While cisplatin treatment was validated in HCT1116 cells by the induction of γH2AX and p53 (Figure 4-10 A, C), to understand their sensitivity to cisplatin, it would be important to examine the apoptosis (e.g., by cell cycle analysis or Annexin-V staining) following 24-72h of cisplatin treatment. Likewise, studying this under enforced FLYWCH1 expression would be beneficial to examine the potential link between FLYWCH1 expression and cisplatin sensitivity.

Moreover, as indicated in Figure 4-6 above, enforced FLYWCH1 expression was able to induce both the total and active forms of p53 (Ser15) in TIG119, regardless of the UV-treatment condition. Therefore, to address the association between FLYWCH1 expression and p53 in CRC cells, the impact of enforced FLYWCH1 expression on p53 was examined by WB (Figure 4-11).
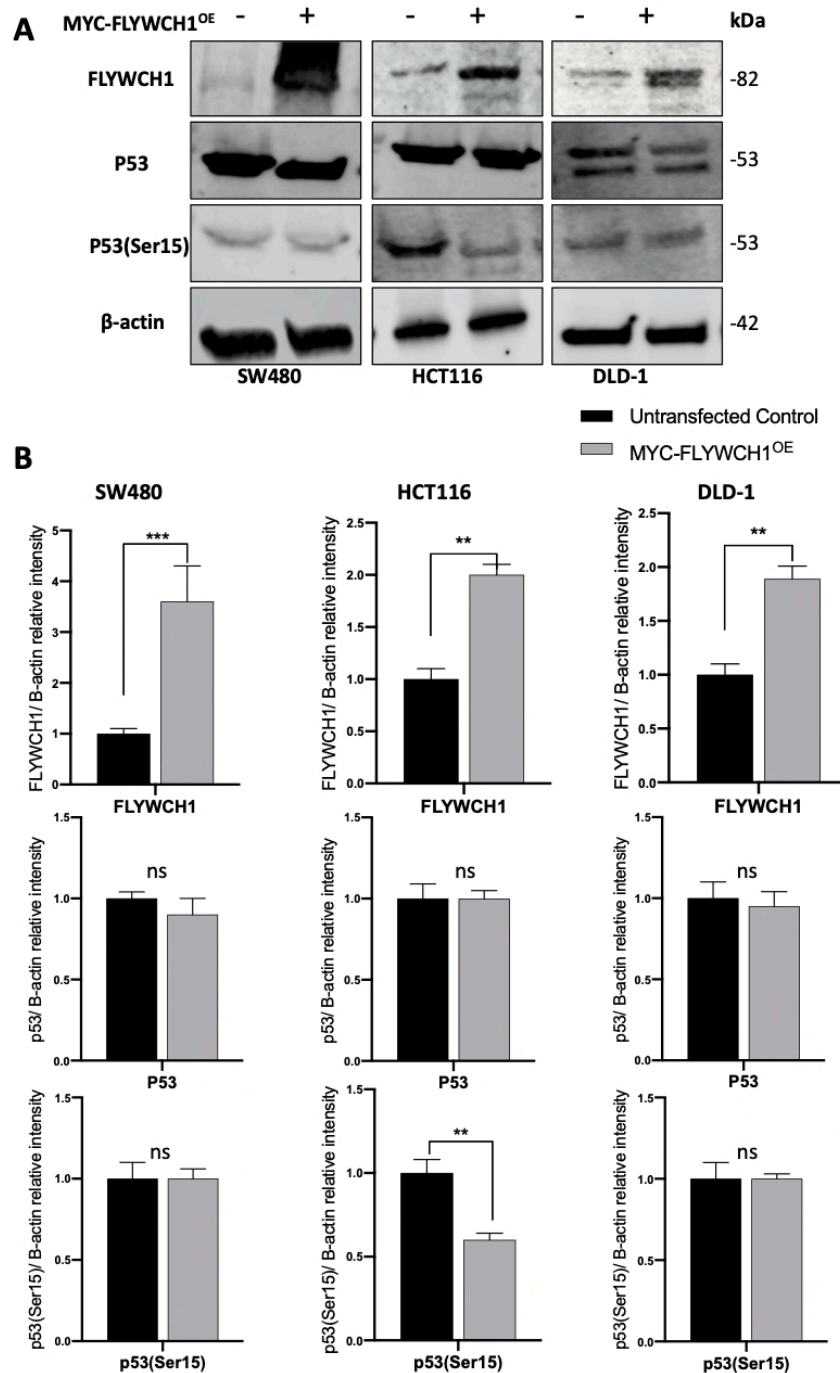
Figure 4-11 Expression and activity of p53 under ectopic expression of FLYWCH1 in CRC cell lines. A) HCT116, SW480 and DLD-1 cells were transiently transfected with Myc-tagged FLYWCH1 to over-express the full length of FLYWCH1, protein lysates were immunoblotted with anti-FLYWCH1(to validate the over-expression), anti-p53 and p53(Ser15) antibodies. **B)** Histograms show the relative band intensities of FLYWCH1, p53 and p53(Ser15) normalized to β-actin and presented as the mean fold change obtained from two independent experiments. Error bars indicate the standard deviation. (ns; not significant, *, $p < 0.05$; **, $p < 0.01$,***= $P \leq 0.001$).

Figure 4-11 revealed that ectopic expression of FLYWCH1 has no significant impact on the level/activity of p53 in SW480 or DLD-1 (p53^{mut}, molecular details in Chapter 2, Methods Table 2-1). Though, the active form of p53 (Ser15) in HCT116 (p53^{WT}) was reduced. These findings together would indicate a potential contribution of p53 in the mechanism by which FLYWCH1 is regulated in response to cisplatin-mediated DNA-damage. However, to elucidate the association between the two proteins, further analysis would be essential. For example, addressing the impact of p53 inhibition or depletion on FLYWCH1 would be necessary to examine the direct effect of P53.

Despite the substantial role of p53 in cisplatin-induced DNA damage response, there is increasing evidence suggesting the contribution of several signalling pathways such as Akt, PKC, and MAPKs (e.g., ERK, JNK, and p38 MAPK) in cisplatin sensitivity, and cisplatin-induced apoptosis in p53-negative cells. (369). Thus, future experiments using a combination of specific inhibitors of these signalling pathways (e.g., Akt (MK2206), MEK (UO126) or Chk1 and Chk2 inhibitors) with cisplatin treatment and studying their effect on FLYWCH1 expression would be beneficial for understanding the upstream players involved in regulating FLYWCH1 in DDR.

Nonetheless, for this chapter, and to ascertain a sparse yet informative perspective on the transcriptional signalling outputs activated under altered FLYWCH1 expression and cisplatin treatment. qPCR analysis of selected markers (p53, P21, RNF8, RAD51C and RUNX2) was carried out in TIG119 cells (Figure 4-12).
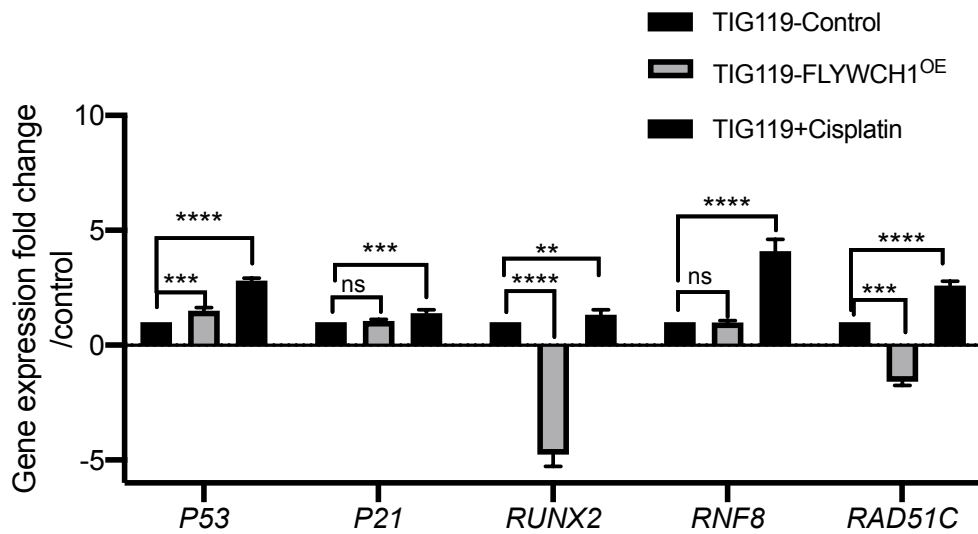
Figure 4-12 qRT-PCR analysis of different DNA-damage targets under enforced FLYWCH1 expression and cisplatin treatment in TIG119 cells. mRNA expression was obtained by using the $2^{\wedge}-(\Delta\Delta Ct)$ method. Each set of experiment was carried out in triplicate and repeated on two independent occasions. Data are mean ± SD. P-values were calculated using Two-way ANOVA test (ns; not significant *=$P \leq 0.05$, **= $P \leq 0.01$, ***= $P \leq 0.001$).

In line with our hypothesis, genes affected by FLYWCH1 alteration were mainly p53-dependent targets and, as expected, cisplatin treatment displayed an opposing effect to FLYWCH1[OE], which aligned with the observed downregulation of FLYWCH1 in cisplatin-treated cells (Figure 4-10).

In cisplatin-treated cells, a significant induction of p53, RUNX2, RNF8 and P21 was demonstrated. These findings validate the activation of DNA damage signaling following cisplatin treatment. Remarkably, over-expression of FLYWCH1 in TIG119 cells increased the transcriptional activity of p53 and P21 (a direct target for p53 and associated with the cell cycle arrest response(374)). While RNF8 (an ATM-dependent target (375, 376)) was not affected by FLYWCH1-expression, supporting the notion of FLYWCH1's ATM-independent function. In addition,

RUNX2 was significantly reduced by FLYWCH1[OE]. RUNX2 mediates p53 associated DNA damage response by repressing p53-dependent apoptotic cell death following DNA damage (377, 378). Likewise, RAD51C was reduced by FLYWCH1-expression which is crucial for the early and late stages of HR and required for ATM-mediated phosphorylation of CHK2 (379).

Our preliminary findings propose that FLYWCH1 might be involved in mediating p53 output signals. Results also imply a contribution of p53-mediated signalling on FLYWCH1's functions and regulation. Though, further investigations are still required, these initial observations suggest a potential new role of FLYWCH1 in DNA-damage response signaling pathways.

4.3 Discussion

This chapter explores a new potential role of FLYWCH1 protein in the DNA-damage response signaling pathways. The tumour-suppressive function of FLYWCH1 is undoubtedly not limited to suppressing nuclear β-catenin transcriptional activity, also the upstream regulation of FLYWCH1 is not restricted to the Wnt signalling. The localisation and function of FLYWCH1, particularly in cancer, could be modulated through multiple signalling pathways. This chapter aimed to uncover the role of nuclear FLYWCH1 that may shed new insights into its function, and biological significance.

Several co-localisation studies were conducted, and the results revealed a co-localisation of FLYWCH1 with γH2AX (Figure 4-2 and 4-3). FLYWCH1's nuclear speckles could be highly similar to those proteins recruited under DNA damage

(e.g. γH2AX). When a cell encounters stress (e.g. elevated reactive oxygen species (ROS) levels, nutrient starvation, or DNA damage), several nuclear proteins and markers are activated in order to partake in re-establishing cellular homeostasis (380). It was, therefore, important to question the possible association of FLYWCH1 foci in the mechanisms involved in DNA-damage response and examine whether it can be recruited under DNA damage, by considering the impact of DNA damaging agents on FLYWCH1 expression, and cellular distribution.

As aforementioned, the phosphorylation of H2AX, a minor histone H2A variant at ser-139, is one of the most well-established chromatin modifications linked to DNA-damage response (365). Interestingly, we indicated that FLYWCH1 over-expression triggers the foci formed by γH2AX, regardless of DNA damage. Our analysis showed that enforced FLYWCH1 expression causes a significant induction of γH2AX protein compared to UV-treatment only. UV and FLYWCH1 overexpression combination demonstrated the highest level of H2AX compared to UV-treatment only or FLYWCH1[OE] (Figure 4-6). Likewise, enforced FLYWCH1 expression upregulated the expression of ATM and p53 proteins. On the other hand, UV treatment increased the endogenous FLYWCH1 protein, and this was correlated with induction of DDR proteins (e.g. ATM, γH2AX), suggesting that FLYWCH1 could also be recruited under DNA damage.

Cisplatin and UV mediate DNA damage via recruiting different players. Unlike Cisplatin, ATM/ATR activation is the primary DNA damaging pathway accountable for the response to the UV-induced DNA lesions (366, 381, 382). Additionally, It is well-established that phosphorylation of H2AX in response to DSBs is mediated by PIKK family proteins involved in both ATM/ATR and DNA-PKcs (365). Thus, we

hypothesised a potential contribution of FLYWCH1 in the recruitment and activation of ATM/ATR and subsequent phosphorylation of H2AX. Accordingly, the necessity of ATM in FLYWCH1's functions was first examined using the ATM^{KO} model (Figure 4-8). Experimental evidence showed no direct effect of ATM depletion on the endogenous FLYWCH1 expression or its action on H2AX. FLYWCH1 was still able to induce γH2AX level, and this was independent of ATM expression. Hence, it is plausible that FLYWCH1 mediates the phosphorylation of γH2AX in an ATM independent manner, and perhaps without DNA damage.

While the phosphorylation of H2AX, at ser-139, is a well-known biomarker for DNA double-strand breaks (DSB) (365), γH2AX induction does not always indicate the presence of DSBs. For instance, H2AX phosphorylation can be induced by serum starvation, which does not cause DNA damage (383). H2AX can also be phosphorylated in a cell cycle-dependent manner. Particularly, the DNA-PKcs/CHK2 pathway mediates the mitotic phosphorylation of H2AX in the absence of DNA damage, and without the recruitment of DNA damage response proteins (384).

Accordingly, the foci formed by γH2AX under altered FLYWCH1-expression could be related to cell-cycle, or other unknown reasons. However, little is known about the regulation of γH2AX in association with cell cycle progression or DNA-damage independent factors. Thus, the contribution of FLYWCH1 expression in γH2AX foci formation out of DNA-damage context is still unclear. Further experiments on the effects of FLYWCH1 on γH2AX at different stages of the cell cycle might provide more significant evidence on how FLYWCH1 functions. However, this is beyond the scope of the current project.

In keeping with the role of the ATM/ATR signalling pathway in UV-mediated DNA damage, our preliminary findings might suggest a contribution of ATM protein expression in the mechanism by which UV/Cisplatin initiates their action on FLYWCH1. Nevertheless, the involvement of ATR protein cannot be excluded. Another intriguing observation in this chapter was the contrasting effects of different DNA damaging agents on the endogenous FLYWCH1 in normal and CRC cells. Unlike UV treatment, cells treated with cisplatin showed a significant reduction in FLYWCH1 expression. Moreover, cisplatin treatment suppressed the FLYWCH1 protein level in all CRC cells (P53^{mut}), except for HCT116 (p53^{WT}) (Figure 4-10). Several pathways are involved for sensing cisplatin-induced DNA damage, including Akt, PKC, and MAPKs (e.g., ERK, JNK, and p38 MAPK). However, the tumour suppressor protein p53 plays the most critical role in DNA-damage response to cisplatin and is known to be the main mediator (367, 385). When cells receive DNA damage, p53 is quickly activated, induces cell cycle arrest, and/or apoptotic cell death by trans-activating its target genes. These genes are implicated in the promotion of cell cycle arrest and/or apoptotic cell death such as p21^{WAF1}, BAX, and PUMA (385). Clarke, P et al. has shown that the induction of apoptosis followed by genotoxic damage caused by cisplatin needs a functional p53 (370). An additional but important player that influences the response to cisplatin treatment is the activation of c-ABL, which in turn requires: the ATM protein, DNA-PK, and a functional DNA mismatch repair response (368). With all the above considerations, the potential role of p53 in regulating FLYWCH1's response to cisplatin cannot be neglected.

Nonetheless, the effects of ectopic-FLYWCH1 expression on the level and activity of p53 were examined in CRC cell lines. Our preliminary data suggest no impact of over-expressing the full length of FLYWCH1 on the total level of p53, in all 3 CRC cell lines (p53$^{wt/mut}$). However, this was able to reduce the phosphorylated form of p53 (Ser15) in the HCT116 cells only, which harboured WT-p53. The aforementioned indicates that FLYWCH1 might need an intact p53 to facilitate its influence. However, this was a preliminary experiment and must be repeated on at least 3-independent experiments for any conclusive statement to be made. (Due to lack of p53-antibody, experiments were postponed for future investigations). Furthermore, transcriptional analyses of several genes targeted by either p53/ATM and/or cell-cycle signalling mechanisms were considered under enforced FLYWCH1 expression. Here, an apparent effect of FLYWCH1-expression was perceived on p53 and p53-putative targets (p21, RUNX2), but not ATM-targets (RNF8) (Figure 4-12). Therefore, our results suggest a direct link between FLYWCH1 and p53-dependent DNA damage response. Once more, addressing the impact of p53 gain/loss of function on FLYWCH1 expression would provide greater insight into their association.

In conclusion, the data provided evidence supporting a novel role of FLYWCH1 in the DNA-damage response signalling pathways. Our results suggest a mechanism by which different DNA-damage stimuli act to regulate FLYWCH1 endogenously in normal and CRC cell lines. Future research studying the upstream mediators in regulating the FLYWCH1 response to DNA damage; and examining FLYWCH1 recruitment at the damage sites will provide a better understanding of FLYWCH1's role in DNA damage/repair processes. While FLYWCH1's role in DNA damage and

repair is still unknown, our findings here suggest that enforced FLYWCH1 expression would trigger the induction and recruitment of DDRP, which does not involve ATM protein. In contrast, the response of endogenous FLYWCH1 to DNA damage might require a functional ATM protein. Such knowledge will expand our understanding of the various functions mediated by FLYWCH1, adding a novel C2H2 ZF-containing player to the DNA damage and repair processes.

Moreover, studying the contribution of FLYWCH1 in the formation of non-DNA damage foci by H2AX would also provide more information regarding the multi-functions of FLYWCH1. To sum up, we can speculate that FLYWCH1 interacts with core components of the DNA repair machinery, yet our knowledge remains limited. Thus, future work could help to disclose the exact contribution and other relevant roles of FLYWCH1 in this context.

CHAPTER 5

General Discussion

5.1 Overview

Colorectal cancer is the prime example of step-wise carcinogenesis and predominantly occurs due to the accumulation of mutations in the tumour suppressor genes and oncogenes (26). Deregulation of nuclear Wnt/β-catenin signaling is the primary oncogenic driver in CRC (222). Hence, this pathway was largely targeted in cancer therapy and scientists began to elucidate and explore mechanisms underpinning the earliest stages of Wnt/β-catenin-driven tumorigenesis (386). Uncovering novel regulators of β-catenin and resolving molecular mechanisms for modulating Wnt-mediated tumorigenesis could improve future detection and treatment approaches used in CRC. Several regulators (both co-repressors and activators) of β-catenin have been discovered, which has significantly improved our understanding of this pathway (171, 174, 387, 388).

Human FLYWCH1 is a novel nuclear β-catenin interacting protein that expresses differentially between normal and various stages of colorectal cancers. We have recently demonstrated that restoring FLYWCH1 expression in several cancer cell lines suppresses their growth and migration by regulating β-catenin transcriptional activity (198). However, the role and mechanism of action of FLYWCH1 in Intestinal homeostasis and tumorigenesis was not explored.

Therefore, the focus of this study was to explore and understand the biological significance and regulation of FLYWCH1 during intestinal homeostasis and CRC development. This was accomplished by applying multidisciplinary approaches, combining cellular and molecular genetic editing with various *in-vitro* cell/tissue

engineering techniques. Overall, this study revealed the following fundamental discoveries:

1. The loss of FLYWCH1 accelerates the proliferation of intestinal cells in organoids by increasing the number of proliferating cells (Ki-67+) and the transcription of intestinal stem cell markers Lgr5+/Olmf4+.

2. Over-expressing FLYWCH1 in the CRC patient-derived tumour organoids (PDOs) strongly reduces organoid size and growth via alteration of selected Wnt target genes.

3. FLYWCH1-depletion enriches CSCs properties and colonospheres formation ability of SW620 cell lines. This is potentially by regulating gene signatures associated with EMT and cancer stemness.

4. FLYWCH1 is a new downstream target of the Wnt signaling pathway that is regulated through nuclear/cytoplasmic translocation. This process is in part mediated by the GSK-3β-dependent mechanism.

5. FLYWCH1 plays a novel role in DNA damage and repair pathways via induction of H2AX phosphorylation, independently of ATM expression. While under DNA damage, endogenous FLYWCH1 can be recruited and regulated in a mechanism that requires functional ATM, and P53 proteins.

6. Clinical data revealed potential prognostic value and clinical significance of FLYWCH1 expression/localisation for CRC patients.
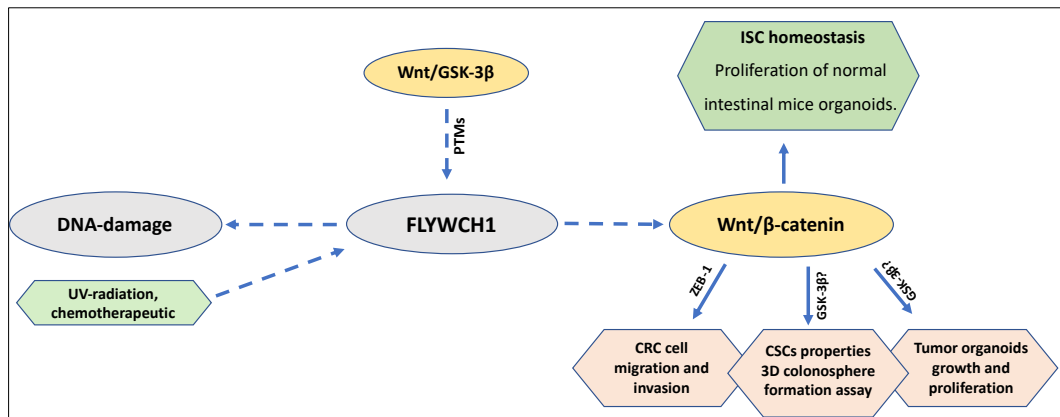
Figure 5-1 An overview of research findings in this study.

5.2 FLYWCH1 is a downstream target of Wnt/β-catenin signaling

The canonical Wnt/β-catenin signaling pathway operates through an extensive network of molecules to fine-tune the signaling ratio and regulate tissue- and stage-specific transcriptional responses during development (168). In many instances, Wnt signaling forms a negative/positive feedback loop to regulate the activity of β-catenin repressor/activators (114, 389). While FLYWCH1 controls β-catenin transcriptional activity (198), the connection between FLYWCH1 and the Wnt pathway may be more complex than initially considered. It is likely that aberrant Wnt signaling, during CRC development forms a negative feedback loop to stop the suppression of FLYWCH1 on β-catenin. However, no information was available on how FLYWCH1 is endogenously regulated in normal intestinal homeostasis and tumorigenesis. Hence, a novelty of this study was uncovering the regulation of endogenous FLYWCH1 via the Wnt/β-catenin signaling pathway. In cultured cells, we found that FLYWCH1 is not only a negative regulator of β-catenin activity but also a potential target of the Wnt pathway, in a process mediated through nuclear/cytoplasmic shuttling of FLYWCH1.

Chapter 5: General Discussion

Investigation of protein localisation at the subcellular level is highly essential to better understand protein activity, cellular signaling cascades, and interaction networks (361). For instance, reports showed that the activity of many TFs involved in Wnt/β-catenin (e.g. Chibby, Axin2, and GSK-3β) is mainly determined by their cellular distribution (185). FLYWCH1 has a putative NLS and is generally considered a nuclear protein. Yet, we showed when Wnt signaling was activated by Wnt3A-CM, FLYWCH1 expression was suppressed, and was shifted into the cytoplasm.

Interestingly, further evidence presented in this study suggests that cellular distribution, and stability of FLYWCH1 is mainly governed by GSK-3β-dependent mechanism. We speculated that phosphorylation/ubiquitination of FLYWCH1 are key events to regulate FLYWCH1 nuclear stability. It is likely that the phosphorylation of FLYWCH1 may well position its NLS for interaction with the nuclear import transporters, and therefore facilitate its nuclear import (390). However, further explorations of upstream regulators of FLYWCH1 and the relation between its phosphorylation status and nuclear localisation would offer a better understanding of how FLYWCH1 can be targeted in cancers.

This study provides a novel perspective by introducing FLYWCH1 as a downstream target of Wnt/β-catenin signaling, in cultured cells. In conclusion, whilst the relative distribution of FLYWCH1 between the nucleus, and cytoplasm varies between normal, and within different cancer cell lines, its localisation could be dynamic in all cases. This could involve continual shuttling between the nucleus and cytoplasm in response to different stimuli. Accordingly, nuclear-cytoplasmic shuttling of FLYWCH1 may be considered a general phenomenon that could have

biological implications in a broad range of cell types. Understanding the impact of FLYWCH1 translocation, and nuclear/cytoplasmic expression in CRC would offer a novel clinical indication for CRC patients.
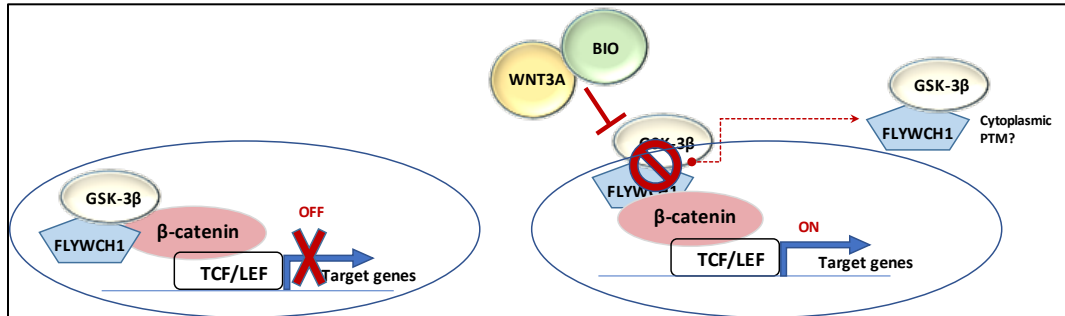
Figure 5-2 Schematic presentation showing the potential regulation of FLYWCH1 by Wnt signaling.

5.3 FLYWCH1 linked with Wnt/β-catenin-mediated control of cell proliferation in organoids.

The intestinal crypt is the main powerhouse for intestinal regeneration and encompasses stem and progenitor cells. Crypt bottom cells (such as Lgr5+, or the actively cycling stem cells) drive the replenishment of all epithelial cells lining the crypt-villus axis. These are also considered as regulated Wnt targets required for intestinal homeostasis (74, 386). Recently, several crypt-expressed Wnt repressors have been identified, for example, AXIN2 (292), SH3BP4 (391), Sox9 (388), and RNF4 (247). These proteins are localised in the stem cell area and can suppress Wnt activity at the cytoplasmic destruction complex, nuclear level, and receptor levels, respectively. Initial data from our lab indicated that *Flywch1* mRNA is highly expressed in the crypt bottom cells and lost in the differentiated cells in the

intestine. Hereafter, we uncovered that FLYWCH1 plays a role in intestinal cell proliferation and Wnt-mediated tumorigenesis in organoids.

Organoid culture is considered a powerful tool that accurately reproduces the *in-vivo* structure of the intestinal/colon epithelium (315). Research using organoid systems permits deciphering the molecular mechanisms involved in regulating stem cell compartments and tumorigenesis (392). Irrespective of their tissue origin, all adult stem cell-derived organoids highly depend on the canonical Wnt signaling pathway for their propagation and maintenance of stemness activity. Therefore, the organoid culture model is effectively used to study Wnt/β-catenin signaling and its regulation during tissue homeostasis and cancers.

In this study, we denoted phenotypical and transcriptional changes in FLYWCH1-depleted intestinal organoids. Firstly, the hyper-proliferative phenotype observed in FLYWCH1-depleted intestinal organoids was supported by the increasing number of Ki-67+ cells compared to control (Figure 3-3, 3-5). This indicates the direct impact of FLYWCH1 loss on intestinal cells proliferation and activity. Further transcriptional data suggest that loss of FLYWCH1 may drive the proliferation via increasing the transcriptional products of actively cycling stem cell markers (Lgr5 and Olmf4) while reducing the quiescence cell markers (Tert and Lrig1). Together, this study revealed the impact of FLYWCH1 crypt-expression on intestinal proliferation and stem cell activity. However, further investigations are essential to understand whether FLYWCH1 inactivation impacts intestinal cells differentiation.

On the other hand, experimental evidence using Patients derived tumour organoids (PDOs), indicated that over-expressing FLYWCH1 could substantially

reduce the size and proliferation of organoids. This could be mediated via upregulating selected Wnt suppressive components such as WNT11 and downregulating transcriptional co-activators such as FOXN1 (Figure 3-15).

Moreover, using colonosphere formation assay, we established that loss of FLYWCH1 in SW620 cells triggers their ability to form colonospheres, and enhances CSCs properties by enriching stemness and EMT gene signatures. The latter supports the notion of FLYWCH1 anti-metastatic functions, reported in CRC cells (198).

Our study also highlighted the significance of GSK-3β-mediated regulation of FLYWCH1 in controlling FLYWCH's anti-proliferation effects in the PDOs (Figure 3-30). Overall, it is likely that the tumour suppressive action of FLYWCH1 is restricted to its nuclear localisation, which could be dis-localised at different CRC stages due to aberrant Wnt activity. Utilising PDOs is now widely accepted as an efficient tool in understanding Wnt pathway-dependent cancer growth and predicting tumour sensitivity to Wnt-targeted therapies (245, 264). Future studies should employ a library of various CRC-PDOs, which may offer a new strategy to decipher and manipulate FLYWCH1's cellular mechanism in individual patients and its involvement in Wnt-driven tumorigenesis.

5.4 The clinical impact of FLYWCH1 expression for CRC patients

Colorectal cancer is a disease with heterogeneous molecular subtypes, leading to a diverse patient prognosis and treatment outcomes. Several mutations in the tumour suppressors or oncogenes have been implicated in CRC development, including APC, KRAS, SMAD4, and TP53 (393). Currently, mutations in these genes

are routinely tested in clinics and used for CRC classification and staging (22). Undoubtedly, screening for molecular biomarkers offers a prognostic value for patients survival, drug response, relapse, and recurrence (394). Additionally, screening for these biomarkers provides patients with personalised profiles, and this facilitates the choice regarding the best treatment options. Also, such genetic information is increasingly used to identify individuals whom are at 'high risk' of developing CRC or other cancers (2). Yet, despite the current advances in biomarker research, there is an unmet clinical need to identify biomarkers for early-stage CRC patients.

Our findings on FLYWCH1 in CRC cell lines and organoids point towards a potential clinical impact of FLYWCH1 expression for CRC patients. Therefore, it was essential to address its clinical significance for patient's pathological outcomes with respect of nuclear/cytoplasmic shuttling. In this study, a TMA library of 1000 cases, including different stages of CRC samples was examined for FLYWCH1 expression by IHC analysis (in collaborations with Prof M. Ilyas, University of Nottingham). Interestingly, the overall nuclear expression of FLYWCH1 was significantly downregulated in tumour tissues when compared to normal ones. Whereas the cytoplasmic FLYWCH1 appeared to be higher in tumour samples. Yet, the expression of FLYWCH1 varied within different CRC stages and segments. Our data also denotes a significant reduction in the cytoplasmic expression, as the T-stage increases. This indicates a possible complete loss of FLYWCH1 expression at the late stages of CRC.

We also showed that FLYWCH1 expression, and localisation could be correlated with different clinicopathological outcomes, including vascular invasion, and local

recurrence. Importantly, the low cytoplasmic expression of FLYWCH1 was also associated with shorter overall survival. Based on the current analysis, it is feasible that FLYWCH1 nuclear/cytoplasmic translocation might occur early in CRC and might contribute to the initiating capacity of CRC cells. However, these require further exploration.

Indeed, the identification of prognostic and predictive molecular biomarkers is attracting many researchers and drug companies. This highlights the importance of discovering new potential biomarkers that might significantly influence the surveillance, and treatment of CRC patients. We are hopeful that with the rapid advancement of molecular testing, as well as greater understanding of CRC genetics, and molecular events, further research on FLYWCH1 could offer a novel biomarker, which may be added to concurrent mutational landscape. Therefore, additional studies implementing more advanced approaches such as, multi-omics and *in vivo* GEM animal CRC models will provide new insights into molecular signatures of FLYWCH1 in different patient stratifications and help to validate FLYWCH1 as a new biomarker for CRC patients.

5.5 FLYWCH1, a new player in the DNA-damage response pathways

Several studies suggest that proteins with the classical Cys_2His_2 zinc finger motif, can exhibit various functional tendencies (395). These proteins may act as transcription factors that function by recognition of specific DNA, and/or RNA sequences (194, 199). We strove to uncover new functions of FLYWCH1 out of the scope of Wnt/β-catenin signaling. This would assist in understanding the roles of FLYWCH1 in intestinal development, and cancers. Preliminary proteomics analysis

revealed high similarities, and potential interactions of FLYWCH1 with proteins involved in DNA damage response (DDR) signaling pathway. Examples include, breast cancer type 1 susceptibility protein (BRAC1) and Mediator of DNA damage checkpoint protein 1 (MDC-1). Moreover, the significant similarities between DNA-damage foci and nuclear foci formed by FLYWCH1 have encouraged us to explore the expression and regulation of FLYWCH1 in the context of DNA-damage response signaling. We here showed in chapter 4 that FLYWCH1 co-localises with γH2AX in the nucleus of both normal and CRC cell lines. More interestingly, our experimental evidence suggests that FLYWCH1^{OE} can induce the phosphorylation of H2AX (Ser139) regardless of ATM expression. The histone variant H2AX is the first, and most prominent protein to form foci at the site of DSB. Upon detecting DSB, H2AX is quickly phosphorylated at C-terminal Ser-139 residue, by the DNA damage-activated kinases ATM, ATR, and DNA-PK to form γH2AX (396). However, the foci formed by γH2AX under altered FLYWCH1-expression could also be corresponded to other factors such as cell-cycle, or serum starvation (383, 384). Thus, further studies are needed to investigate this phenomenon.

We also showed that FLYWCH1 transcription, and protein expression is regulated contrarily by the various types of DNA-damaging agents. Ultraviolet light caused a clear induction in the level of FLYWCH1 in both normal and CRC cells. Contrastingly, Cisplatin (chemotherapeutic agent) significantly downregulated the level of endogenous FLYWCH1.

Given the fact that UV-light recruits a DDR mechanism that is different from Cisplatin, FLYWCH1 can be regulated via various upstream mediators depending on the type of damage. According to our initial data, ATM/ATR, and p53 signaling

pathways appear critical upstream players in regulating the endogenous FLYWCH1 expression in response to DNA-damaging agents.

Collectively, this study supports a novel role of FLYWCH1 in DNA-damage response signaling pathways. Our findings suggest, for the first time, a potential contribution of FLYWCH1 in the induction and recruitment of DDRP including H2AX, ATM, and P53. However, FLYWCH1's role in the DNA-damage response pathways requires substantial investigations. Future research studying the upstream kinases involved in regulating the FLYWCH1 response to DNA damage, examining FLYWCH1 foci recruitment at the damage site in responses to more agents and stimuli, as well as exploring P53 dependency using genetically modified CRC cells or organoids, would provide a better understanding of FLYWCH1's role in DNA damage and repair processes.
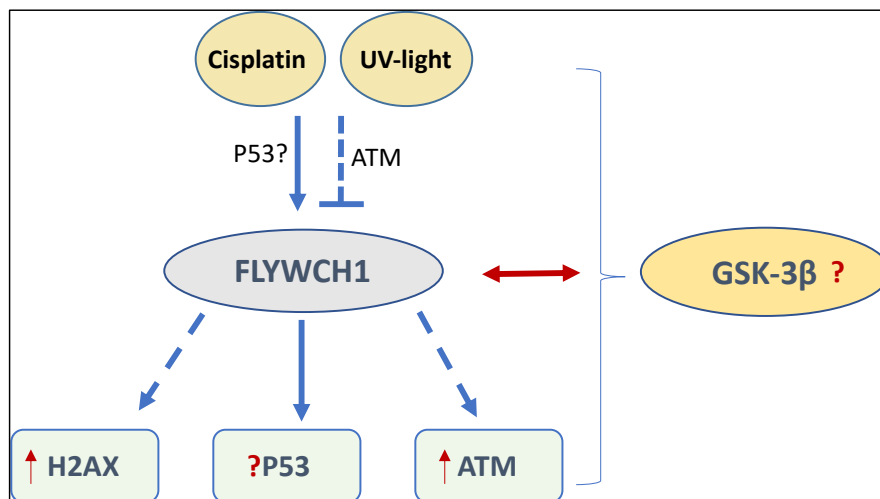
Figure 5-3 Potential association of FLYWCH1 protein in DNA-damage response signaling pathways.

5.6 Experimental limitations

Despite the comprehensive approaches used, the efforts made for effective evaluation, and production of high quality/reliable data, several limitations/challenges were encountered throughout this project. For example:

1. The lack of a robust antibody that could detect endogenous FLYWCH1 protein by WB analysis caused considerable delays in the progress of generating/validating FLYWCH1^{KO} cells and has therefore limited their use throughout the project.

2. Although evidence of using Wnt3A-CM, and BIO (GSK-3β inhibitor) clearly demonstrated FLYWCH1 regulation by Wnt/GSK-3β. Applying and comparing the effects of several other Wnt antagonists (e.g. DKK1), and/or inhibitors of other pathways (e.g. TGF-β) on FLYWCH1 in both CRC cell lines and 3D-organoids, may provide further insight into the mechanism by which FLYWCH1 is regulated endogenously in normal versus cancer cells.

3. Due to time constraints, it was not possible to examine additional differentiation markers such as E-cadherin, cytokeratin 20 (CK20), and mucin 2 (MUC2), as well as apoptotic markers (or epithelial turnover markers) such as Bax, and cleaved Caspase-3, in normal mouse organoids with altered FLYWCH1 expression. Therefore, this study was limited to few stemness, and proliferation markers.

4. The effect of FLYWCH1 deletion on *in vitro* stemness activity using colonosphere forming efficiency was limited to SW620 cell line only; it would be interesting to expand this further in other CRC cell lines.

5. The molecular profile of PDOs used in this study was not available, and therefore it was difficult to assess the molecular details/mechanisms of action, and the correlations of FLYWCH1 with specific molecular subtypes.

6. The transcriptional analysis associated with FLYWCH1[OE] in PDOs was limited to PCR array of Wnt signaling target genes, a comprehensive genomic analysis by single cell profiling or RNA-seq would provide valuable information regarding FLYWCH1 roles, out the scope of Wnt signaling.

7. PTM of FLYWCH1 by Wnt/GSK-3β signaling needs better clarification, more repeats and further analysis to understand the impact of phosphorylation/ubiquitination on the cytoplasmic translocation of FLYWCH1.

8. Due to the shortage/lack of p53 antibody, experiments assessing the association between FLYWCH1, and p53 was not completed.

9. Due to time/funds restrictions, sequencing the genomic DNA of all generated KO cell lines and organoids was not accomplished within the period of this project.

5.7 Conclusions and future directions

The findings from this thesis highlight the significant roles of FLYWCH1 in regulating Wnt-driven activities in normal and CRC cell lines, and intestinal organoids. In cultured cells, FLYWCH1 protein is localised in the nucleus and crosstalk with nuclear GSK-3β and β-catenin, to regulate β-catenin transcriptional activity. We found that FLYWCH1 expression is repressed via the hyperactivation

of Wnt signaling through changes in the subcellular distribution and stability. Therefore, it can be predicted that during CRC development, the hyperactivation of Wnt signaling drives changes in the stability of FLYWCH1, releasing it into the cytoplasm. Eventually, these changes might hinder the FLYWCH1 suppression activity on β-catenin.

In the patient's tumour tissues, FLYWCH1 expression was mainly cytoplasmic and lost in the nucleus, particularly, at the high stage tumours. Our CRC TMA analyses suggested that low cytoplasmic FLYWCH1 expression is correlated with worse survival and poor prognosis. Therefore, FLYWCH1 can potentially be used as prognostic markers in CRC patients.

Moreover, several inactivation mutations or deletion of Wnt repressors have previously been reported in CRCs (e.g. AXIN2, and RNF43) (397-399). Despite the limited studies on FLYWCH1, missense mutations and deletions of FLYWCH1 were also reported in various cancers including CRCs, in accord with the TCGA dataset (see chapter 1, figure 1-8).

While FLYWCH1 regulates specific Wnt-mediated biological responses in CRC, it is conceivable that FLYWCH1 inactivation might be linked with Wnt signaling status and staging of CRC. Further understanding of mechanisms/mutations that drive FLYWCH1 inactivation would help to discover a new therapeutic strategy for targeting Wnt signaling in cancer. Also, identification, and characterisation of specific drugs that induce nuclear localisation of FLYWCH1, and lead to inhibition of the oncogenic WNT/β-catenin pathway, might improve survival in colorectal cancers.

However, more extensive follow-up investigations are needed to enhance the clinical applicability of our research, and to greater impact the therapeutic field. Thus, we propose a series of research ideas that could be implemented in the future:

1. *In-vivo* animal studies such as knockout mice, and/or xenograft could be useful in appreciating the significance of FLYWCH1 in the *in-vivo* development of intestinal epithelium, and tumorigenesis. Additionally, it will enable tracing the stem cells, and their lineage compartments in the murine intestine.

2. A comprehensive genomic analysis to identify the direct target genes regulated by FLYWCH1, using both ChIP-sequencing, and RNA-sequencing or RIP-sequencing analyses, will further clarify alternate functions of this protein.

3. Further investigations of the post-transcriptional, and/or post-translational modification mechanism(s) governing FLYWCH1 expression, and/or activity would facilitate approaches to regulate FLYWCH1.

4. Identifying E3 UB-ligases that could target FLYWCH1 for degradation would improve our understanding of how FLYWCH1 is generally downregulated in CRC.

5. Screening the mutation status of FLYWCH1 in different CRC cell lines, and/or organoids would resolve the discrepancy observed in FLYWCH1 expression and actions.

6. Further investigations of the different FLYWCH1 isoforms, and splicing activity mediated under Wnt modulation, and DNA damaging agents.

7. Further IHC, and/or gene expression analysis of FLYWCH1 impacts on differentiation, apoptosis, and cell-cycle markers in organoids, would improve our understanding of FLYWCH1 association in various cellular activities.

8. Understanding the possible crosstalk of FLYWCH1/GSK-3β with DDRPs, might offer a new axis for regulating DNA-damage response signaling and could enhance the effectiveness of anti-tumour drugs.

9. Studying the different cellular localisation of FLYWCH1 in various cancer cells may help to determine the response to aberrant Wnt activation in different cancers.

References

1.   Bray F, Ferlay J, Soerjomataram I, Siegel RL, Torre LA, Jemal A. Global cancer statistics 2018: GLOBOCAN estimates of incidence and mortality worldwide for 36 cancers in 185 countries. CA Cancer J Clin. 2018;68(6):394-424.
2.   Rawla P, Sunkara T, Barsouk A. Epidemiology of colorectal cancer: incidence, mortality, survival, and risk factors. Przeglad gastroenterologiczny. 2019;14(2):89-103.
3.   Ferlay J, Colombet M, Soerjomataram I, Mathers C, Parkin DM, Piñeros M, et al. Estimating the global cancer incidence and mortality in 2018: GLOBOCAN sources and methods. Int J Cancer. 2019;144(8):1941-53.
4.   Jass JR, Walsh MD, Barker M, Simms LA, Young J, Leggett BA. Distinction between familial and sporadic forms of colorectal cancer showing DNA microsatellite instability. Eur J Cancer. 2002;38(7):858-66.
5.   Fleming M, Ravula S, Tatishchev SF, Wang HL. Colorectal carcinoma: Pathologic aspects. J Gastrointest Oncol. 2012;3(3):153-73.
6.   Nguyen HT, Duong HQ. The molecular characteristics of colorectal cancer: Implications for diagnosis and therapy. Oncol Lett. 2018;16(1):9-18.
7.   Dekker E, Tanis PJ, Vleugels JLA, Kasi PM, Wallace MB. Colorectal cancer. The Lancet. 2019;394(10207):1467-80.
8.   Burt R. Inheritance of Colorectal Cancer. Drug Discov Today Dis Mech. 2007;4(4):293-300.
9.   Kuipers EJ, Grady WM, Lieberman D, Seufferlein T, Sung JJ, Boelens PG, et al. Colorectal cancer. Nat Rev Dis Primers. 2015;1:15065.
10.   Dominguez G. Deciphering the epigenetic network in colorectal cancer. J Pathol. 2013;229(1):1-3.
11.   Juarez-Vazquez CI, Rosales-Reynoso MA. [Colorectal cancer (CCR): genetic and molecular alterations]. Gac Med Mex. 2014;150(2):154-64.
12.   Valle L. Genetic predisposition to colorectal cancer: where we stand and future perspectives. World J Gastroenterol. 2014;20(29):9828-49.
13.   Fearon ER, Vogelstein B. A genetic model for colorectal tumorigenesis. Cell. 1990;61(5):759-67.
14.   Sameer A. Colorectal Cancer: Molecular Mutations and Polymorphisms. Frontiers in Oncology. 2013;3(114).
15.   Smith G, Carey FA, Beattie J, Wilkie MJ, Lightfoot TJ, Coxhead J, et al. Mutations in APC, Kirsten-ras, and p53--alternative genetic pathways to colorectal cancer. Proc Natl Acad Sci U S A. 2002;99(14):9433-8.
16.   Crabtree MD, Tomlinson IP, Talbot IC, Phillips RK. Variability in the severity of colonic disease in familial adenomatous polyposis results from differences in tumour initiation rather than progression and depends relatively little on patient age. Gut. 2001;49(4):540-3.
17.   Armaghany T, Wilson JD, Chu Q, Mills G. Genetic alterations in colorectal cancer. Gastrointestinal cancer research : GCR. 2012;5(1):19-27.
18.   Testa U, Pelosi E, Castelli G. Colorectal cancer: genetic abnormalities, tumor progression, tumor heterogeneity, clonal evolution and tumor-initiating cells. Med Sci (Basel). 2018;6(2):31.

References

19.   Bienz M, Clevers H. Linking colorectal cancer to Wnt signaling. Cell. 2000;103(2):311-20.
20.   van de Wetering M, Sancho E, Verweij C, de Lau W, Oving I, Hurlstone A, et al. The beta-catenin/TCF-4 complex imposes a crypt progenitor phenotype on colorectal cancer cells. Cell. 2002;111(2):241-50.
21.   Friedl W, Caspari R, Sengteller M, Uhlhaas S, Lamberti C, Jungck M, et al. Can APC mutation analysis contribute to therapeutic decisions in familial adenomatous polyposis? Experience from 680 FAP families. Gut. 2001;48(4):515-21.
22.   Schell MJ, Yang M, Teer JK, Lo FY, Madan A, Coppola D, et al. A multigene mutation classification of 468 colorectal cancers reveals a prognostic role for APC. Nat Commun. 2016;7:11743.
23.   Jaiswal AS, Narayan S. A novel function of adenomatous polyposis coli (APC) in regulating DNA repair. Cancer Lett. 2008;271(2):272-80.
24.   Fearon ER. Molecular genetics of colorectal cancer. Annu Rev Pathol. 2011;6:479-507.
25.   Hermsen M, Postma C, Baak J, Weiss M, Rapallo A, Sciutto A, et al. Colorectal adenoma to carcinoma progression follows multiple pathways of chromosomal instability. Gastroenterology. 2002;123(4):1109-19.
26.   Huang D, Sun W, Zhou Y, Li P, Chen F, Chen H, et al. Mutations of key driver genes in colorectal cancer progression and metastasis. Cancer Metastasis Rev. 2018;37(1):173-87.
27.   Coppede F. Epigenetic biomarkers of colorectal cancer: Focus on DNA methylation. Cancer Lett. 2014;342(2):238-47.
28.   Pancione M, Remo A, Colantuoni V. Genetic and epigenetic events generate multiple pathways in colorectal cancer progression. Patholog Res Int. 2012;2012:509348.
29.   Mundade R, Imperiale TF, Prabhu L, Loehrer PJ, Lu T. Genetic pathways, prevention, and treatment of sporadic colorectal cancer. Oncoscience. 2014;1(6):400-6.
30.   Pino MS, Chung DC. The chromosomal instability pathway in colon cancer. Gastroenterology. 2010;138(6):2059-72.
31.   Campbell FC, Loughrey MB, McClements J, Deevi RK, Javadi A, Rainey L. Mechanistic Insights into Colorectal Cancer Phenomics from Fundamental and Organotypic Model Studies. Am J Pathol. 2018;188(9):1936-48.
32.   Puppa G, Sonzogni A, Colombari R, Pelosi G. TNM staging system of colorectal carcinoma: a critical appraisal of challenging issues. Arch Pathol Lab Med. 2010;134(6):837-52.
33.   Wang S, Guan X, Ma M, Zhuang M, Ma T, Liu Z, et al. Reconsidering the prognostic significance of tumour deposit count in the TNM staging system for colorectal cancer. Scientific Reports. 2020;10(1):89.
34.   Guinney J, Dienstmann R, Wang X, de Reyniès A, Schlicker A, Soneson C, et al. The consensus molecular subtypes of colorectal cancer. Nature Medicine. 2015;21(11):1350-6.
35.   Stintzing S, Wirapati P, Lenz HJ, Neureiter D, Fischer von Weikersthal L, Decker T, et al. Consensus molecular subgroups (CMS) of colorectal cancer (CRC)

and first-line efficacy of FOLFIRI plus cetuximab or bevacizumab in the FIRE3 (AIO KRK-0306) trial. Ann Oncol. 2019;30(11):1796-803.

36.   Sveen A, Bruun J, Eide PW, Eilertsen IA, Ramirez L, Murumägi A, et al. Colorectal Cancer Consensus Molecular Subtypes Translated to Preclinical Models Uncover Potentially Targetable Cancer Cell Dependencies. Clin Cancer Res. 2018;24(4):794-806.

37.   Guinney J, Dienstmann R, Wang X, de Reyniès A, Schlicker A, Soneson C, et al. The consensus molecular subtypes of colorectal cancer. Nat Med. 2015;21(11):1350-6.

38.   Thanki K, Nicholls ME, Gajjar A, Senagore AJ, Qiu S, Szabo C, et al. Consensus Molecular Subtypes of Colorectal Cancer and their Clinical Implications. Int Biol Biomed J. 2017;3(3):105-11.

39.   Singh MP, Rai S, Pandey A, Singh NK, Srivastava S. Molecular subtypes of colorectal cancer: An emerging therapeutic opportunity for personalized medicine. Genes & Diseases. 2019.

40.   Shih I-M, Wang T-L, Traverso G, Romans K, Hamilton SR, Ben-Sasson S, et al. Top-down morphogenesis of colorectal tumors. Proceedings of the National Academy of Sciences. 2001;98(5):2640-5.

41.   Yatabe Y, Tavaré S, Shibata D. Investigating stem cells in human colon by using methylation patterns. Proceedings of the National Academy of Sciences. 2001;98(19):10839-44.

42.   Cole JW, McKalen A. STUDIES ON THE MORPHOGENESIS OF ADENOMATOUS POLYPS IN THE HUMAN COLON. Cancer. 1963;16:998-1002.

43.   Preston SL, Wong WM, Chan AO, Poulsom R, Jeffery R, Goodlad RA, et al. Bottom-up histogenesis of colorectal adenomas: origin in the monocryptal adenoma and initial expansion by crypt fission. Cancer Res. 2003;63(13):3819-25.

44.   Barker N, Ridgway RA, van Es JH, van de Wetering M, Begthel H, van den Born M, et al. Crypt stem cells as the cells-of-origin of intestinal cancer. Nature. 2009;457(7229):608-11.

45.   Sangiorgi E, Capecchi MR. Bmi1 is expressed in vivo in intestinal stem cells. Nat Genet. 2008;40(7):915-20.

46.   Will OCC, Deheragoda M, Phillips RKS, Clark SK, Tomlinson IPM. The role of cell proliferation and crypt fission in adenoma aggressiveness: a comparison of ileoanal pouch and rectal adenomas in familial adenomatous polyposis. Colorectal disease : the official journal of the Association of Coloproctology of Great Britain and Ireland. 2011;13(4):387-92.

47.   Wright NA, Poulsom R. Top down or bottom up? Competing management structures in the morphogenesis of colorectal neoplasms. Gut. 2002;51(3):306-8.

48.   Huels DJ, Sansom OJ. Stem vs non-stem cell origin of colorectal cancer. British journal of cancer. 2015;113(1):1-5.

49.   Pardal R, Clarke MF, Morrison SJ. Applying the principles of stem-cell biology to cancer. Nat Rev Cancer. 2003;3(12):895-902.

50.   Jordan CT. Cancer stem cell biology: from leukemia to solid tumors. Curr Opin Cell Biol. 2004;16(6):708-12.

51.   van der Heijden M, Vermeulen L. Stem cells in homeostasis and cancer of the gut. Molecular Cancer. 2019;18(1):66.

References

52.   Westphalen CB, Asfaha S, Hayakawa Y, Takemoto Y, Lukin DJ, Nuber AH, et al. Long-lived intestinal tuft cells serve as colon cancer-initiating cells. J Clin Invest. 2014;124(3):1283-95.

53.   Su LK, Kinzler KW, Vogelstein B, Preisinger AC, Moser AR, Luongo C, et al. Multiple intestinal neoplasia caused by a mutation in the murine homolog of the APC gene. Science. 1992;256(5057):668-70.

54.   Taketo MM, Edelmann W. Mouse models of colon cancer. Gastroenterology. 2009;136(3):780-98.

55.   Itzkowitz SH, Yio X. Inflammation and cancer IV. Colorectal cancer in inflammatory bowel disease: the role of inflammation. Am J Physiol Gastrointest Liver Physiol. 2004;287(1):G7-17.

56.   Clevers H. At the Crossroads of Inflammation and Cancer. Cell. 2004;118(6):671-4.

57.   Hodder MC, Flanagan DJ, Sansom OJ. Intestinal Stem Cell Dynamics: A Story of Mice and Humans. Cell Stem Cell. 2018;22(6):785-7.

58.   Clevers H. The intestinal crypt, a prototype stem cell compartment. Cell. 2013;154(2):274-84.

59.   Umar S. Intestinal stem cells. Curr Gastroenterol Rep. 2010;12(5):340-8.

60.   de Santa Barbara P, van den Brink GR, Roberts DJ. Development and differentiation of the intestinal epithelium. Cell Mol Life Sci. 2003;60(7):1322-32.

61.   Tetteh PW, Basak O, Farin HF, Wiebrands K, Kretzschmar K, Begthel H, et al. Replacement of Lost Lgr5-Positive Stem Cells through Plasticity of Their Enterocyte-Lineage Daughters. Cell Stem Cell. 2016;18(2):203-13.

62.   Li L, Clevers H. Coexistence of quiescent and active adult stem cells in mammals. Science. 2010;327(5965):542-5.

63.   Barker N. Adult intestinal stem cells: critical drivers of epithelial homeostasis and regeneration. Nat Rev Mol Cell Biol. 2014;15(1):19-33.

64.   Philpott A, Winton DJ. Lineage selection and plasticity in the intestinal crypt. Curr Opin Cell Biol. 2014;31:39-45.

65.   Ayyaz A, Kumar S, Sangiorgi B, Ghoshal B, Gosio J, Ouladan S, et al. Single-cell transcriptomes of the regenerating intestine reveal a revival stem cell. Nature. 2019;569(7754):121-5.

66.   Yan KS, Chia LA, Li X, Ootani A, Su J, Lee JY, et al. The intestinal stem cell markers Bmi1 and Lgr5 identify two functionally distinct populations. Proceedings of the National Academy of Sciences. 2012;109(2):466-71.

67.   Takeda N, Jain R, LeBoeuf MR, Wang Q, Lu MM, Epstein JA. Interconversion Between Intestinal Stem Cell Populations in Distinct Niches. Science. 2011;334(6061):1420-4.

68.   Murata K, Jadhav U, Madha S, van Es J, Dean J, Cavazza A, et al. Ascl2-Dependent Cell Dedifferentiation Drives Regeneration of Ablated Intestinal Stem Cells. Cell Stem Cell. 2020;26(3):377-90.e6.

69.   Tan SH, Phuah P, Tan LT, Yada S, Goh J, Tomaz LB, et al. A constant pool of Lgr5(+) intestinal stem cells is required for intestinal homeostasis. Cell Rep. 2021;34(4):108633.

70.   Tian H, Biehs B, Warming S, Leong KG, Rangell L, Klein OD, et al. A reserve stem cell population in small intestine renders Lgr5-positive cells dispensable. Nature. 2011;478(7368):255-9.

References

71.   de Sousa EMF, de Sauvage FJ. Cellular Plasticity in Intestinal Homeostasis and Disease. Cell Stem Cell. 2019;24(1):54-64.

72.   Rees WD, Tandun R, Yau E, Zachos NC, Steiner TS. Regenerative Intestinal Stem Cells Induced by Acute and Chronic Injury: The Saving Grace of the Epithelium? Frontiers in Cell and Developmental Biology. 2020;8(1333).

73.   Sato T, van Es JH, Snippert HJ, Stange DE, Vries RG, van den Born M, et al. Paneth cells constitute the niche for Lgr5 stem cells in intestinal crypts. Nature. 2011;469(7330):415-8.

74.   Barker N, van Es JH, Kuipers J, Kujala P, van den Born M, Cozijnsen M, et al. Identification of stem cells in small intestine and colon by marker gene Lgr5. Nature. 2007;449(7165):1003-7.

75.   Vermeulen L, Snippert HJ. Stem cell dynamics in homeostasis and cancer of the intestine. Nat Rev Cancer. 2014;14(7):468-80.

76.   Buczacki SJA, Zecchini HI, Nicholson AM, Russell R, Vermeulen L, Kemp R, et al. Intestinal label-retaining cells are secretory precursors expressing Lgr5. Nature. 2013;495(7439):65-9.

77.   Lopez-Garcia C, Klein AM, Simons BD, Winton DJ. Intestinal stem cell replacement follows a pattern of neutral drift. Science. 2010;330(6005):822-5.

78.   Frede J, Adams DJ, Jones PH. Mutation, clonal fitness and field change in epithelial carcinogenesis. J Pathol. 2014;234(3):296-301.

79.   Martincorena I, Campbell PJ. Somatic mutation in cancer and normal cells. Science. 2015;349(6255):1483-9.

80.   Vermeulen L, Morrissey E, van der Heijden M, Nicholson AM, Sottoriva A, Buczacki S, et al. Defining stem cell dynamics in models of intestinal tumor initiation. Science. 2013;342(6161):995-8.

81.   Sailaja BS, He XC, Li L. The regulatory niche of intestinal stem cells. J Physiol. 2016;594(17):4827-36.

82.   Jones DL, Wagers AJ. No place like home: anatomy and function of the stem cell niche. Nat Rev Mol Cell Biol. 2008;9(1):11-21.

83.   Vanuytsel T, Senger S, Fasano A, Shea-Donohue T. Major signaling pathways in intestinal stem cells. Biochim Biophys Acta. 2013;1830(2):2410-26.

84.   Tian H, Biehs B, Chiu C, Siebel CW, Wu Y, Costa M, et al. Opposing activities of Notch and Wnt signaling regulate intestinal stem cells and gut homeostasis. Cell Rep. 2015;11(1):33-42.

85.   Tian A, Benchabane H, Wang Z, Ahmed Y. Regulation of Stem Cell Proliferation and Cell Fate Specification by Wingless/Wnt Signaling Gradients Enriched at Adult Intestinal Compartment Boundaries. PLoS Genet. 2016;12(2):e1005822.

86.   Van Camp JK, Beckers S, Zegers D, Van Hul W. Wnt signaling and the control of human stem cell fate. Stem Cell Rev Rep. 2014;10(2):207-29.

87.   van Es JH, Jay P, Gregorieff A, van Gijn ME, Jonkheer S, Hatzis P, et al. Wnt signalling induces maturation of Paneth cells in intestinal crypts. Nat Cell Biol. 2005;7(4):381-6.

88.   Demitrack ES, Samuelson LC. Notch regulation of gastrointestinal stem cells. J Physiol. 2016;594(17):4791-803.

References

89.   Qi Z, Li Y, Zhao B, Xu C, Liu Y, Li H, et al. BMP restricts stemness of intestinal Lgr5(+) stem cells by directly suppressing their signature genes. Nat Commun. 2017;8:13824.
90.   Akyala AI, Peppelenbosch MP. Gastric cancer and Hedgehog signaling pathway: emerging new paradigms. Genes & cancer. 2018;9(1-2):1-10.
91.   Lien WH, Fuchs E. Wnt some lose some: transcriptional governance of stem cells by Wnt/beta-catenin signaling. Genes Dev. 2014;28(14):1517-32.
92.   Basu S, Haase G, Ben-Ze'ev A. Wnt signaling in cancer stem cells and colon cancer metastasis. F1000Res. 2016;5.
93.   Yeung TM, Chia LA, Kosinski CM, Kuo CJ. Regulation of self-renewal and differentiation by the intestinal stem cell niche. Cell Mol Life Sci. 2011;68(15):2513-23.
94.   Bertrand FE, Angus CW, Partis WJ, Sigounas G. Developmental pathways in colon cancer: crosstalk between WNT, BMP, Hedgehog and Notch. Cell Cycle. 2012;11(23):4344-51.
95.   Batlle E, Clevers H. Cancer stem cells revisited. Nature Medicine. 2017;23(10):1124-34.
96.   Ayob AZ, Ramasamy TS. Cancer stem cells as key drivers of tumour progression. J Biomed Sci. 2018;25(1):20.
97.   Hervieu C, Christou N, Battu S, Mathonnet M. The Role of Cancer Stem Cells in Colorectal Cancer: From the Basics to Novel Clinical Trials. Cancers (Basel). 2021;13(5):1092.
98.   Vermeulen L, Sprick MR, Kemper K, Stassi G, Medema JP. Cancer stem cells--old concepts, new insights. Cell Death Differ. 2008;15(6):947-58.
99.   Visvader JE, Lindeman GJ. Cancer stem cells: current status and evolving complexities. Cell Stem Cell. 2012;10(6):717-28.
100.   Sun Z, Wang L, Dong L, Wang X. Emerging role of exosome signalling in maintaining cancer stem cell dynamic equilibrium. Journal of Cellular and Molecular Medicine. 2018;22(8):3719-28.
101.   Olmez I, Shen W, McDonald H, Ozpolat B. Dedifferentiation of patient-derived glioblastoma multiforme cell lines results in a cancer stem cell-like state with mitogen-independent growth. Journal of Cellular and Molecular Medicine. 2015;19(6):1262-72.
102.   Oshima N, Yamada Y, Nagayama S, Kawada K, Hasegawa S, Okabe H, et al. Induction of cancer stem cell properties in colon cancer cells by defined factors. PLoS One. 2014;9(7):e101735.
103.   Ingangi V, Minopoli M, Ragone C, Motti ML, Carriero MV. Role of Microenvironment on the Fate of Disseminating Cancer Stem Cells. Frontiers in Oncology. 2019;9(82).
104.   Ciardiello C, Leone A, Budillon A. The Crosstalk between Cancer Stem Cells and Microenvironment Is Critical for Solid Tumor Progression: The Significant Contribution of Extracellular Vesicles. Stem Cells International. 2018;2018:6392198.
105.   Ye J, Wu D, Wu P, Chen Z, Huang J. The cancer stem cell niche: cross talk between cancer stem cells and their microenvironment. Tumor Biology. 2014;35(5):3945-51.

References

106.   Muncie JM, Weaver VM. Chapter One - The Physical and Biochemical Properties of the Extracellular Matrix Regulate Cell Fate. In: Litscher ES, Wassarman PM, editors. Current Topics in Developmental Biology. 130: Academic Press; 2018. p. 1-37.

107.   Zhao Y, Dong Q, Li J, Zhang K, Qin J, Zhao J, et al. Targeting cancer stem cells and their niche: perspectives for future therapeutic targets and strategies. Semin Cancer Biol. 2018;53:139-55.

108.   Zeuner A, Todaro M, Stassi G, De Maria R. Colorectal cancer stem cells: from the crypt to the clinic. Cell Stem Cell. 2014;15(6):692-705.

109.   Moon BS, Jeong WJ, Park J, Kim TI, Min do S, Choi KY. Role of oncogenic K-Ras in cancer stem cell activation by aberrant Wnt/β-catenin signaling. J Natl Cancer Inst. 2014;106(2):djt373.

110.   Basu S, Haase G, Ben-Ze'ev A. Wnt signaling in cancer stem cells and colon cancer metastasis. F1000Res. 2016;5:F1000 Faculty Rev-699.

111.   Nusse R, Varmus HE. Many tumors induced by the mouse mammary tumor virus contain a provirus integrated in the same region of the host genome. Cell. 1982;31(1):99-109.

112.   Nusse R. Wnt signaling in disease and in development. Cell Res. 2005;15(1):28-32.

113.   Nusse R, Brown A, Papkoff J, Scambler P, Shackleford G, McMahon A, et al. A new nomenclature for int-1 and related genes: the Wnt gene family. Cell. 1991;64(2):231.

114.   MacDonald BT, Tamai K, He X. Wnt/beta-catenin signaling: components, mechanisms, and diseases. Dev Cell. 2009;17(1):9-26.

115.   Grumolato L, Liu G, Mong P, Mudbhary R, Biswas R, Arroyave R, et al. Canonical and noncanonical Wnts use a common mechanism to activate completely unrelated coreceptors. Genes Dev. 2010;24(22):2517-30.

116.   Mohammed MK, Shao C, Wang J, Wei Q, Wang X, Collier Z, et al. Wnt/beta-catenin signaling plays an ever-expanding role in stem cell self-renewal, tumorigenesis and cancer chemoresistance. Genes Dis. 2016;3(1):11-40.

117.   Nusse R, Clevers H. Wnt/beta-Catenin Signaling, Disease, and Emerging Therapeutic Modalities. Cell. 2017;169(6):985-99.

118.   Angers S, Moon RT. Proximal events in Wnt signal transduction. Nat Rev Mol Cell Biol. 2009;10(7):468-77.

119.   Lustig B, Jerchow B, Sachs M, Weiler S, Pietsch T, Karsten U, et al. Negative feedback loop of Wnt signaling through upregulation of conductin/axin2 in colorectal and liver tumors. Mol Cell Biol. 2002;22(4):1184-93.

120.   Bernkopf DB, Brückner M, Hadjihannas MV, Behrens J. An aggregon in conductin/axin2 regulates Wnt/β-catenin signaling and holds potential for cancer therapy. Nature Communications. 2019;10(1):4251.

121.   Koo B-K, Spit M, Jordens I, Low TY, Stange DE, van de Wetering M, et al. Tumour suppressor RNF43 is a stem-cell E3 ligase that induces endocytosis of Wnt receptors. Nature. 2012;488(7413):665-9.

References

122. Hao H-X, Xie Y, Zhang Y, Charlat O, Oster E, Avello M, et al. ZNRF3 promotes Wnt receptor turnover in an R-spondin-sensitive manner. Nature. 2012;485(7397):195-200.

123. Spit M, Fenderico N, Jordens I, Radaszkiewicz T, Lindeboom RG, Bugter JM, et al. RNF43 truncations trap CK1 to drive niche-independent self-renewal in cancer. EMBO J. 2020;39(18):e103932.

124. de Lau W, Peng WC, Gros P, Clevers H. The R-spondin/Lgr5/Rnf43 module: regulator of Wnt signal strength. Genes Dev. 2014;28(4):305-16.

125. Lebensohn AM, Rohatgi R. R-spondins can potentiate WNT signaling without LGRs. Elife. 2018;7.

126. Zebisch M, Jones EY. ZNRF3/RNF43--A direct linkage of extracellular recognition and E3 ligase activity to modulate cell surface signalling. Prog Biophys Mol Biol. 2015;118(3):112-8.

127. Bugter JM, Fenderico N, Maurice MM. Mutations and mechanisms of WNT pathway tumour suppressors in cancer. Nature Reviews Cancer. 2021;21(1):5-21.

128. Chen PH, Chen X, Lin Z, Fang D, He X. The structural basis of R-spondin recognition by LGR5 and RNF43. Genes Dev. 2013;27(12):1345-50.

129. Ackers I, Malgor R. Interrelationship of canonical and non-canonical Wnt signalling pathways in chronic metabolic diseases. Diabetes & vascular disease research. 2018;15(1):3-13.

130. Gómez-Orte E, Sáenz-Narciso B, Moreno S, Cabello J. Multiple functions of the noncanonical Wnt pathway. Trends in Genetics. 2013;29(9):545-53.

131. Komiya Y, Habas R. Wnt signal transduction pathways. Organogenesis. 2008;4(2):68-75.

132. Corda G, Sala A. Non-canonical WNT/PCP signalling in cancer: Fzd6 takes centre stage. Oncogenesis. 2017;6(7):e364-e.

133. Wang Y. Wnt/Planar cell polarity signaling: A new paradigm for cancer therapy. Molecular Cancer Therapeutics. 2009;8(8):2103-9.

134. Wang HY, Malbon CC. Wnt signaling, Ca2+, and cyclic GMP: visualizing Frizzled functions. Science. 2003;300(5625):1529-30.

135. Cerpa W, Latorre-Esteves E, Barria A. RoR2 functions as a noncanonical Wnt receptor that regulates NMDAR-mediated synaptic transmission. Proceedings of the National Academy of Sciences. 2015;112(15):4797-802.

136. Gallegos TF, Kouznetsova V, Kudlicka K, Sweeney DE, Bush KT, Willert K, et al. A protein kinase A and Wnt-dependent network regulating an intermediate stage in epithelial tubulogenesis during kidney development. Developmental Biology. 2012;364(1):11-21.

137. Semenov MV, Habas R, Macdonald BT, He X. SnapShot: Noncanonical Wnt Signaling Pathways. Cell. 2007;131(7):1378.

138. Flanagan DJ, Vincan E, Phesse TJ. Wnt Signaling in Cancer: Not a Binary ON:OFF Switch. Cancer Res. 2019;79(23):5901-6.

139. Hergovich A, Hemmings BA. TAZ-Mediated Crosstalk between Wnt and Hippo Signaling. Developmental Cell. 2010;18(4):508-9.

140. Gao B. Wnt regulation of planar cell polarity (PCP). Curr Top Dev Biol. 2012;101:263-95.

References

141.   Parri M, Chiarugi P. Rac and Rho GTPases in cancer cell motility control. Cell Communication and Signaling. 2010;8(1):23.

142.   Kohn AD, Moon RT. Wnt and calcium signaling: β-Catenin-independent pathways. Cell Calcium. 2005;38(3):439-46.

143.   De A. Wnt/Ca2+ signaling pathway: a brief overview. Acta Biochim Biophys Sin (Shanghai). 2011;43(10):745-56.

144.   Martin-Orozco E, Sanchez-Fernandez A, Ortiz-Parra I, Ayala-San Nicolas M. WNT Signaling in Tumors: The Way to Evade Drugs and Immunity. Frontiers in immunology. 2019;10:2854-.

145.   Tian A, Benchabane H, Ahmed Y. Wingless/Wnt Signaling in Intestinal Development, Homeostasis, Regeneration and Tumorigenesis: A Drosophila Perspective. J Dev Biol. 2018;6(2).

146.   Crosnier C, Stamataki D, Lewis J. Organizing cell renewal in the intestine: stem cells, signals and combinatorial control. Nat Rev Genet. 2006;7(5):349-59.

147.   Dunn SJ, Osborne JM, Appleton PL, Nathke I. Combined changes in Wnt signaling response and contact inhibition induce altered proliferation in radiation-treated intestinal crypts. Mol Biol Cell. 2016;27(11):1863-74.

148.   Riemer P, Sreekumar A, Reinke S, Rad R, Schafer R, Sers C, et al. Transgenic expression of oncogenic BRAF induces loss of stem cells in the mouse intestine, which is antagonized by beta-catenin activity. Oncogene. 2015;34(24):3164-75.

149.   Yang K, Wang X, Zhang H, Wang Z, Nan G, Li Y, et al. The evolving roles of canonical WNT signaling in stem cells and tumorigenesis: implications in targeted cancer therapies. Lab Invest. 2016;96(2):116-36.

150.   Gregorieff A, Grosschedl R, Clevers H. Hindgut defects and transformation of the gastro-intestinal tract in Tcf4(-/-)/Tcf1(-/-) embryos. The EMBO journal. 2004;23(8):1825-33.

151.   van Es JH, Haegebarth A, Kujala P, Itzkovitz S, Koo BK, Boj SF, et al. A critical role for the Wnt effector Tcf4 in adult intestinal homeostatic self-renewal. Mol Cell Biol. 2012;32(10):1918-27.

152.   Korinek V, Barker N, Moerer P, van Donselaar E, Huls G, Peters PJ, et al. Depletion of epithelial stem-cell compartments in the small intestine of mice lacking Tcf-4. Nat Genet. 1998;19(4):379-83.

153.   Hrckulak D, Janeckova L, Lanikova L, Kriz V, Horazna M, Babosova O, et al. Wnt Effector TCF4 Is Dispensable for Wnt Signaling in Human Cancer Cells. Genes (Basel). 2018;9(9):439.

154.   Shao W, Wang D, Chiang Y-T, Ip W, Zhu L, Xu F, et al. The Wnt signaling pathway effector TCF7L2 controls gut and brain proglucagon gene expression and glucose homeostasis. Diabetes. 2013;62(3):789-800.

155.   Wenzel J, Rose K, Haghighi EB, Lamprecht C, Rauen G, Freihen V, et al. Loss of the nuclear Wnt pathway effector TCF7L2 promotes migration and invasion of human colorectal cancer cells. Oncogene. 2020;39(19):3893-909.

156.   Koch S, Nava P, Addis C, Kim W, Denning TL, Li L, et al. The Wnt antagonist Dkk1 regulates intestinal epithelial homeostasis and wound repair. Gastroenterology. 2011;141(1):259-68, 68.e1-8.

157.   Kuhnert F, Davis CR, Wang H-T, Chu P, Lee M, Yuan J, et al. Essential requirement for Wnt signaling in proliferation of adult small intestine and colon

revealed by adenoviral expression of Dickkopf-1. Proceedings of the National Academy of Sciences. 2004;101(1):266-71.

158.   Fevr T, Robine S, Louvard D, Huelsken J. Wnt/beta-catenin is essential for intestinal homeostasis and maintenance of intestinal stem cells. Mol Cell Biol. 2007;27(21):7551-9.

159.   Kinzler KW, Nilbert MC, Su LK, Vogelstein B, Bryan TM, Levy DB, et al. Identification of FAP locus genes from chromosome 5q21. Science. 1991;253(5020):661-5.

160.   Nishisho I, Nakamura Y, Miyoshi Y, Miki Y, Ando H, Horii A, et al. Mutations of chromosome 5q21 genes in FAP and colorectal cancer patients. Science. 1991;253(5020):665-9.

161.   Nieuwenhuis MH, Vasen HF. Correlations between mutation site in APC and phenotype of familial adenomatous polyposis (FAP): a review of the literature. Crit Rev Oncol Hematol. 2007;61(2):153-61.

162.   Ficari F, Cama A, Valanzano R, Curia MC, Palmirotta R, Aceto G, et al. APC gene mutations and colorectal adenomatosis in familial adenomatous polyposis. Br J Cancer. 2000;82(2):348-53.

163.   Castellsague E, Gonzalez S, Guino E, Stevens KN, Borras E, Raymond VM, et al. Allele-specific expression of APC in adenomatous polyposis families. Gastroenterology. 2010;139(2):439-47, 47.e1.

164.   Christie M, Jorissen RN, Mouradov D, Sakthianandeswaren A, Li S, Day F, et al. Different APC genotypes in proximal and distal sporadic colorectal cancers suggest distinct WNT/beta-catenin signalling thresholds for tumourigenesis. Oncogene. 2013;32(39):4675-82.

165.   Buchert M, Athineos D, Abud HE, Burke ZD, Faux MC, Samuel MS, et al. Genetic dissection of differential signaling threshold requirements for the Wnt/beta-catenin pathway in vivo. PLoS Genet. 2010;6(1):e1000816.

166.   Dienstmann R, Vermeulen L, Guinney J, Kopetz S, Tejpar S, Tabernero J. Consensus molecular subtypes and the evolution of precision medicine in colorectal cancer. Nat Rev Cancer. 2017;17(2):79-92.

167.   Willert K, Jones KA. Wnt signaling: is the party in the nucleus? Genes Dev. 2006;20(11):1394-404.

168.   Cadigan KM, Waterman ML. TCF/LEFs and Wnt signaling in the nucleus. Cold Spring Harb Perspect Biol. 2012;4(11).

169.   Hrckulak D, Kolar M, Strnad H, Korinek V. TCF/LEF Transcription Factors: An Update from the Internet Resources. Cancers (Basel). 2016;8(7).

170.   Pronobis MI, Peifer M. Wnt signaling: the many interfaces of beta-catenin. Curr Biol. 2012;22(4):R137-9.

171.   van Tienen LM, Mieszczanek J, Fiedler M, Rutherford TJ, Bienz M. Constitutive scaffolding of multiple Wnt enhanceosome components by Legless/BCL9. Elife. 2017;6.

172.   Ling X-H, Chen Z-Y, Luo H-W, Liu Z-Z, Liang Y-K, Chen G-X, et al. BCL9, a coactivator for Wnt/β-catenin transcription, is targeted by miR-30c and is associated with prostate cancer progression. Oncology letters. 2016;11(3):2001-8.

173.   Mani M, Carrasco DE, Zhang Y, Takada K, Gatt ME, Dutta-Simmons J, et al. BCL9 Promotes Tumor Progression by Conferring Enhanced Proliferative,

References

Metastatic, and Angiogenic Properties to Cancer Cells. Cancer Research. 2009;69(19):7577-86.

174.   Mieszczanek J, de la Roche M, Bienz M. A role of Pygopus as an anti-repressor in facilitating Wnt-dependent transcription. Proceedings of the National Academy of Sciences. 2008;105(49):19324.

175.   Gay DM, Ridgway RA, Müller M, Hodder MC, Hedley A, Clark W, et al. Loss of BCL9/9l suppresses Wnt driven tumourigenesis in models that recapitulate human cancer. Nature communications. 2019;10(1):723-.

176.   de la Roche M, Ibrahim AE, Mieszczanek J, Bienz M. LEF1 and B9L shield β-catenin from inactivation by Axin, desensitizing colorectal cancer cells to tankyrase inhibitors. Cancer Res. 2014;74(5):1495-505.

177.   Takada K, Zhu D, Bird GH, Sukhdeo K, Zhao JJ, Mani M, et al. Targeted disruption of the BCL9/β-catenin complex inhibits oncogenic Wnt signaling. Sci Transl Med. 2012;4(148):148ra17.

178.   Barker N, Hurlstone A, Musisi H, Miles A, Bienz M, Clevers H. The chromatin remodelling factor Brg-1 interacts with beta-catenin to promote target gene activation. The EMBO journal. 2001;20(17):4935-43.

179.   Takemaru KI, Moon RT. The transcriptional coactivator CBP interacts with beta-catenin to activate gene expression. J Cell Biol. 2000;149(2):249-54.

180.   Mosimann C, Hausmann G, Basler K. Parafibromin/Hyrax activates Wnt/Wg target gene transcription by direct association with beta-catenin/Armadillo. Cell. 2006;125(2):327-41.

181.   Sinner D, Kordich JJ, Spence JR, Opoka R, Rankin S, Lin SC, et al. Sox17 and Sox4 differentially regulate beta-catenin/T-cell factor activity and proliferation of colon carcinoma cells. Mol Cell Biol. 2007;27(22):7802-15.

182.   Vadlamudi U, Espinoza HM, Ganga M, Martin DM, Liu X, Engelhardt JF, et al. PITX2, beta-catenin and LEF-1 interact to synergistically regulate the LEF-1 promoter. J Cell Sci. 2005;118(Pt 6):1129-37.

183.   Perissi V, Jepsen K, Glass CK, Rosenfeld MG. Deconstructing repression: evolving models of co-repressor action. Nat Rev Genet. 2010;11(2):109-23.

184.   Daniels DL, Weis WI. Beta-catenin directly displaces Groucho/TLE repressors from Tcf/Lef in Wnt-mediated transcription activation. Nat Struct Mol Biol. 2005;12(4):364-71.

185.   Takemaru K-I, Fischer V, Li F-Q. Fine-tuning of nuclear-catenin by Chibby and 14-3-3. Cell cycle (Georgetown, Tex). 2009;8(2):210-3.

186.   Daniels DL, Weis WI. ICAT inhibits beta-catenin binding to Tcf/Lef-family transcription factors and the general coactivator p300 using independent structural modules. Mol Cell. 2002;10(3):573-84.

187.   Ito K, Lim AC, Salto-Tellez M, Motoda L, Osato M, Chuang LS, et al. RUNX3 attenuates beta-catenin/T cell factors in intestinal tumorigenesis. Cancer Cell. 2008;14(3):226-37.

188.   Ju X, Ishikawa TO, Naka K, Ito K, Ito Y, Oshima M. Context-dependent activation of Wnt signaling by tumor suppressor RUNX3 in gastric cancer cells. Cancer Sci. 2014;105(4):418-24.

189.   Hudson GM, Watson PJ, Fairall L, Jamieson AG, Schwabe JW. Insights into the Recruitment of Class IIa Histone Deacetylases (HDACs) to the SMRT/NCoR Transcriptional Repression Complex. J Biol Chem. 2015;290(29):18237-44.

References

190.   Evans PM, Chen X, Zhang W, Liu C. KLF4 interacts with beta-catenin/TCF4 and blocks p300/CBP recruitment by beta-catenin. Mol Cell Biol. 2010;30(2):372-81.

191.   Ramalingam S, Daughtridge GW, Johnston MJ, Gracz AD, Magness ST. Distinct levels of Sox9 expression mark colon epithelial stem cells that form colonoids in culture. Am J Physiol Gastrointest Liver Physiol. 2012;302(1):G10-20.

192.   Sellak H, Wu S, Lincoln TM. KLF4 and SOX9 transcription factors antagonize beta-catenin and inhibit TCF-activity in cancer cells. Biochim Biophys Acta. 2012;1823(10):1666-75.

193.   Olson LE, Tollkuhn J, Scafoglio C, Krones A, Zhang J, Ohgi KA, et al. Homeodomain-mediated beta-catenin-dependent switching events dictate cell-lineage determination. Cell. 2006;125(3):593-605.

194.   Razin SV, Borunova VV, Maksimenko OG, Kantidze OL. Cys2His2 zinc finger protein family: classification, functions, and major members. Biochemistry (Mosc). 2012;77(3):217-26.

195.   Jen J, Wang Y-C. Zinc finger proteins in cancer progression. Journal of biomedical science. 2016;23(1):53-.

196.   Mosimann C, Hausmann G, Basler K. Beta-catenin hits chromatin: regulation of Wnt target gene activation. Nat Rev Mol Cell Biol. 2009;10(4):276-86.

197.   Nateri AS, Riera-Sans L, Costa CD, Behrens A. The Ubiquitin Ligase SCF[Fbw7] Antagonizes Apoptotic JNK Signaling. Science. 2004;303(5662):1374-8.

198.   Muhammad BA, Almozyan S, Babaei-Jadidi R, Onyido EK, Saadeddin A, Kashfi SH, et al. FLYWCH1, a Novel Suppressor of Nuclear beta-Catenin, Regulates Migration and Morphology in Colorectal Cancer. Mol Cancer Res. 2018;16(12):1977-90.

199.   Cassandri M, Smirnov A, Novelli F, Pitolli C, Agostini M, Malewicz M, et al. Zinc-finger proteins in health and disease. Cell death discovery. 2017;3:17071-.

200.   Najafabadi HS, Mnaimneh S, Schmitges FW, Garton M, Lam KN, Yang A, et al. C2H2 zinc finger proteins greatly expand the human regulatory lexicon. Nature Biotechnology. 2015;33(5):555-62.

201.   Fedotova AA, Bonchuk AN, Mogila VA, Georgiev PG. C2H2 Zinc Finger Proteins: The Largest but Poorly Explored Family of Higher Eukaryotic Transcription Factors. Acta Naturae. 2017;9(2):47-58.

202.   Zhang W, Xu C, Bian C, Tempel W, Crombet L, MacKenzie F, et al. Crystal structure of the Cys2His2-type zinc finger domain of human DPF2. Biochem Biophys Res Commun. 2011;413(1):58-61.

203.   Nandan MO, Ghaleb AM, Bialkowska AB, Yang VW. Krüppel-like factor 5 is essential for proliferation and survival of mouse intestinal epithelial stem cells. Stem Cell Res. 2015;14(1):10-9.

204.   Zhang Y, Xu L, Li A, Han X. The roles of ZEB1 in tumorigenic progression and epigenetic modifications. Biomedicine & Pharmacotherapy. 2019;110:400-8.

205.   Hahn S, Hermeking H. ZNF281/ZBP-99: a new player in epithelial-mesenchymal transition, stemness, and cancer. J Mol Med (Berl). 2014;92(6):571-81.

References

206.   Essien BE, Sundaresan S, Ocadiz-Ruiz R, Chavis A, Tsao AC, Tessier AJ, et al. Transcription Factor ZBP-89 Drives a Feedforward Loop of β-Catenin Expression in Colorectal Cancer. Cancer Res. 2016;76(23):6877-87.
207.   Dai MS, Sun XX, Qin J, Smolik SM, Lu H. Identification and characterization of a novel Drosophila melanogaster glutathione S-transferase-containing FLYWCH zinc finger protein. Gene. 2004;342(1):49-56.
208.   Ow MC, Martinez NJ, Olsen PH, Silverman HS, Barrasa MI, Conradt B, et al. The FLYWCH transcription factors FLH-1, FLH-2, and FLH-3 repress embryonic expression of microRNA genes in C. elegans. Genes Dev. 2008;22(18):2520-34.
209.   Beaster-Jones L, Okkema PG. DNA binding and in vivo function of C.elegans PEB-1 require a conserved FLYWCH motif. J Mol Biol. 2004;339(4):695-706.
210.   Castello A, Fischer B, Eichelbaum K, Horos R, Beckmann BM, Strein C, et al. Insights into RNA biology from an atlas of mammalian mRNA-binding proteins. Cell. 2012;149(6):1393-406.
211.   Hodel MR, Corbett AH, Hodel AE. Dissection of a nuclear localization signal. J Biol Chem. 2001;276(2):1317-25.
212.   Uhlén M, Fagerberg L, Hallström BM, Lindskog C, Oksvold P, Mardinoglu A, et al. Proteomics. Tissue-based map of the human proteome. Science. 2015;347(6220):1260419.
213.   Cerami E, Gao J, Dogrusoz U, Gross BE, Sumer SO, Aksoy BA, et al. The cBio Cancer Genomics Portal: An Open Platform for Exploring Multidimensional Cancer Genomics Data. Cancer Discovery. 2012;2(5):401-4.
214.   Gao J, Aksoy BA, Dogrusoz U, Dresdner G, Gross B, Sumer SO, et al. Integrative analysis of complex cancer genomics and clinical profiles using the cBioPortal. Sci Signal. 2013;6(269):pl1.
215.   Almars A, Chondrou PS, Onyido EK, Almozyan S, Seedhouse C, Babaei-Jadidi R, et al. Increased FLYWCH1 Expression is Negatively Correlated with Wnt/β-catenin Target Gene Expression in Acute Myeloid Leukemia Cells. Int J Mol Sci. 2019;20(11):2739.
216.   Foroughi Asl H, Talukdar HA, Kindt AS, Jain RK, Ermel R, Ruusalepp A, et al. Expression quantitative trait Loci acting across multiple tissues are enriched in inherited risk for coronary artery disease. Circ Cardiovasc Genet. 2015;8(2):305-15.
217.   Haskell GT, Jensen BC, Skrzynia C, Pulikkotil T, Tilley CR, Lu Y, et al. Genetic Complexity of Mitral Valve Prolapse Revealed by Clinical and Genetic Evaluation of a Large Family. The Journal of heart valve disease. 2017;26(5):569-80.
218.   Santos-Barriopedro I, van Mierlo G, Vermeulen M. Off-the-shelf proximity biotinylation for interaction proteomics. Nature Communications. 2021;12(1):5015.
219.   Almozyan S, Coulton J, Babaei-Jadidi R, Nateri AS. FLYWCH1, a Multi-Functional Zinc Finger Protein Contributes to the DNA Repair Pathway. Cells. 2021;10(4):889.
220.   Kim MJ, Huang Y, Park JI. Targeting Wnt Signaling for Gastrointestinal Cancer Therapy: Present and Evolving Views. Cancers (Basel). 2020;12(12).

References

221.   Jung Y-S, Jun S, Kim MJ, Lee SH, Suh HN, Lien EM, et al. TMEM9 promotes intestinal tumorigenesis through vacuolar-ATPase-activated Wnt/β-catenin signalling. Nature Cell Biology. 2018;20(12):1421-33.

222.   Jung Y-S, Park J-I. Wnt signaling in cancer: therapeutic targeting of Wnt signaling beyond β-catenin and the destruction complex. Experimental & Molecular Medicine. 2020;52(2):183-91.

223.   Berg KCG, Eide PW, Eilertsen IA, Johannessen B, Bruun J, Danielsen SA, et al. Multi-omics of 34 colorectal cancer cell lines - a resource for biomedical studies. Molecular Cancer. 2017;16(1):116.

224.   Sawayama H, Miyamoto Y, Ogawa K, Yoshida N, Baba H. Investigation of colorectal cancer in accordance with consensus molecular subtype classification. Annals of Gastroenterological Surgery. 2020;4(5):528-39.

225.   Li Z, Wang J, Zhou T, Ye X. Establishment of a colorectal cancer nude mouse visualization model of HIF-1α overexpression. Oncol Lett. 2016;11(4):2725-32.

226.   Ran FA, Hsu PD, Wright J, Agarwala V, Scott DA, Zhang F. Genome engineering using the CRISPR-Cas9 system. Nature Protocols. 2013;8(11):2281-308.

227.   Lino CA, Harper JC, Carney JP, Timlin JA. Delivering CRISPR: a review of the challenges and approaches. Drug delivery. 2018;25(1):1234-57.

228.   Johnston S, Gallaher Z, Czaja K. Exogenous reference gene normalization for real-time reverse transcription-polymerase chain reaction analysis under dynamic endogenous transcription. Neural regeneration research. 2012;7(14):1064-72.

229.   Shaheen S, Ahmed M, Lorenzi F, Nateri AS. Spheroid-Formation (Colonosphere) Assay for in Vitro Assessment and Expansion of Stem Cells in Colon Cancer. Stem Cell Rev Rep. 2016;12(4):492-9.

230.   Ibrahim SA, Yip GW, Stock C, Pan JW, Neubauer C, Poeter M, et al. Targeting of syndecan-1 by microRNA miR-10b promotes breast cancer cell motility and invasiveness via a Rho-GTPase- and E-cadherin-dependent mechanism. Int J Cancer. 2012;131(6):E884-96.

231.   Babaei-Jadidi R, Li N, Saadeddin A, Spencer-Dene B, Jandke A, Muhammad B, et al. FBXW7 influences murine intestinal homeostasis and cancer, targeting Notch, Jun, and DEK for degradation. J Exp Med. 2011;208(2):295-312.

232.   Langan TJ, Chou RC. Synchronization of mammalian cell cultures by serum deprivation. Methods Mol Biol. 2011;761:75-83.

233.   Melak M, Plessner M, Grosse R. Actin visualization at a glance. J Cell Sci. 2017;130(3):525-30.

234.   de Lau W, Barker N, Low TY, Koo B-K, Li VSW, Teunissen H, et al. Lgr5 homologues associate with Wnt receptors and mediate R-spondin signalling. Nature. 2011;476(7360):293-7.

235.   Kashfi SMH, Almozyan S, Jinks N, Koo B-K, Nateri AS. Morphological alterations of cultured human colorectal matched tumour and healthy organoids. Oncotarget. 2018;9(12):10572-84.

References

236.   Sato T, Vries RG, Snippert HJ, van de Wetering M, Barker N, Stange DE, et al. Single Lgr5 stem cells build crypt-villus structures in vitro without a mesenchymal niche. Nature. 2009;459(7244):262-5.

237.   Andersson-Rolf A, Fink J, Mustata RC, Koo B-K. A video protocol of retroviral infection in primary intestinal organoid culture. Journal of visualized experiments : JoVE. 2014(90):e51765-e.

238.   Fujii E, Yamazaki M, Kawai S, Ohtani Y, Watanabe T, Kato A, et al. A simple method for histopathological evaluation of organoids. Journal of toxicologic pathology. 2018;31(1):81-5.

239.   Danbolt NC, Zhou Y, Furness DN, Holmseth S. Strategies for immunohistochemical protein localization using antibodies: What did we learn from neurotransmitter transporters in glial cells and neurons. Glia. 2016;64(12):2045-64.

240.   McCarty KS, Jr., Miller LS, Cox EB, Konrath J, McCarty KS, Sr. Estrogen receptor analyses. Correlation of biochemical and immunohistochemical methods using monoclonal antireceptor antibodies. Arch Pathol Lab Med. 1985;109(8):716-21.

241.   Barker N, van de Wetering M, Clevers H. The intestinal stem cell. Genes & Development. 2008;22(14):1856-64.

242.   Barker N, van Es JH, Kuipers J, Kujala P, van den Born M, Cozijnsen M, et al. Identification of stem cells in small intestine and colon by marker gene Lgr5. Nature. 2007;449(7165):1003-7.

243.   Spit M, Koo BK, Maurice MM. Tales from the crypt: intestinal niche signals in tissue renewal, plasticity and cancer. Open Biol. 2018;8(9).

244.   Harnack C, Berger H, Antanaviciute A, Vidal R, Sauer S, Simmons A, et al. R-spondin 3 promotes stem cell recovery and epithelial regeneration in the colon. Nat Commun. 2019;10(1):4368.

245.   Merenda A, Fenderico N, Maurice MM. Wnt Signaling in 3D: Recent Advances in the Applications of Intestinal Organoids. Trends Cell Biol. 2020;30(1):60-73.

246.   Qian L, Mahaffey JP, Alcorn HL, Anderson KV. Tissue-specific roles of Axin2 in the inhibition and activation of Wnt signaling in the mouse embryo. Proceedings of the National Academy of Sciences. 2011;108(21):8692-7.

247.   Koo BK, Spit M, Jordens I, Low TY, Stange DE, van de Wetering M, et al. Tumour suppressor RNF43 is a stem-cell E3 ligase that induces endocytosis of Wnt receptors. Nature. 2012;488(7413):665-9.

248.   Shimomura Y, Agalliu D, Vonica A, Luria V, Wajid M, Baumer A, et al. APCDD1 is a novel Wnt inhibitor mutated in hereditary hypotrichosis simplex. Nature. 2010;464(7291):1043-7.

249.   Zhan T, Rindtorff N, Boutros M. Wnt signaling in cancer. Oncogene. 2017;36(11):1461-73.

250.   Sato T, Clevers H. Growing Self-Organizing Mini-Guts from a Single Intestinal Stem Cell: Mechanism and Applications. Science. 2013;340(6137):1190-4.

251.   Sato T, Stange DE, Ferrante M, Vries RGJ, van Es JH, van den Brink S, et al. Long-term Expansion of Epithelial Organoids From Human Colon, Adenoma,

References

Adenocarcinoma, and Barrett's Epithelium. Gastroenterology. 2011;141(5):1762-72.

252.   Serra D, Mayr U, Boni A, Lukonin I, Rempfler M, Challet Meylan L, et al. Self-organization and symmetry breaking in intestinal organoid development. Nature. 2019;569(7754):66-72.

253.   Li N, Babaei-Jadidi R, Lorenzi F, Spencer-Dene B, Clarke P, Domingo E, et al. An FBXW7-ZEB2 axis links EMT and tumour microenvironment to promote colorectal cancer stem cells and chemoresistance. Oncogenesis. 2019;8(3):13.

254.   Lorenzi F, Babaei-Jadidi R, Sheard J, Spencer-Dene B, Nateri AS. Fbxw7-associated drug resistance is reversed by induction of terminal differentiation in murine intestinal organoid culture. Mol Ther Methods Clin Dev. 2016;3:16024-.

255.   Kashfi H, Jinks N, Nateri AS. Generating and Utilizing Murine Cas9-Expressing Intestinal Organoids for Large-Scale Knockout Genetic Screening. Methods Mol Biol. 2020;2171:257-69.

256.   Au - Andersson-Rolf A, Au - Fink J, Au - Mustata RC, Au - Koo B-K. A Video Protocol of Retroviral Infection in Primary Intestinal Organoid Culture. JoVE. 2014(90):e51765.

257.   Ringel T, Frey N, Ringnalda F, Janjuha S, Cherkaoui S, Butz S, et al. Genome-Scale CRISPR Screening in Human Intestinal Organoids Identifies Drivers of TGF-β Resistance. Cell Stem Cell. 2020;26(3):431-40.e8.

258.   Ahmed M, Jinks N, Babaei-Jadidi R, Kashfi H, Castellanos-Uribe M, May ST, et al. Repurposing Antibacterial AM404 as a Potential Anticancer Drug for Targeting Colorectal Cancer Stem-Like Cells. Cancers (Basel). 2019;12(1):106.

259.   Cai T, Qi Y, Jergens A, Wannemuehler M, Barrett TA, Wang Q. Effects of six common dietary nutrients on murine intestinal organoid growth. PLoS One. 2018;13(2):e0191517.

260.   Nam MO, Hahn S, Jee JH, Hwang TS, Yoon H, Lee DH, et al. Effects of a small molecule R-spondin-1 substitute RS-246204 on a mouse intestinal organoid culture. Oncotarget. 2018;9(5):6356-68.

261.   Pastuła A, Middelhoff M, Brandtner A, Tobiasch M, Höhl B, Nuber AH, et al. Three-Dimensional Gastrointestinal Organoid Culture in Combination with Nerves or Fibroblasts: A Method to Characterize the Gastrointestinal Stem Cell Niche. Stem Cells Int. 2016;2016:3710836.

262.   Munoz J, Stange DE, Schepers AG, van de Wetering M, Koo BK, Itzkovitz S, et al. The Lgr5 intestinal stem cell signature: robust expression of proposed quiescent '+4' cell markers. The EMBO journal. 2012;31(14):3079-91.

263.   Young M, Reed KR. Organoids as a Model for Colorectal Cancer. Curr Colorectal Cancer Rep. 2016;12(5):281-7.

264.   Vlachogiannis G, Hedayat S, Vatsiou A, Jamin Y, Fernández-Mateos J, Khan K, et al. Patient-derived organoids model treatment response of metastatic gastrointestinal cancers. Science. 2018;359(6378):920-6.

265.   Prasetyanti PR, Medema JP. Intra-tumor heterogeneity from a cancer stem cell perspective. Mol Cancer. 2017;16(1):41.

266.   Punt CJ, Koopman M, Vermeulen L. From tumour heterogeneity to advances in precision treatment of colorectal cancer. Nat Rev Clin Oncol. 2017;14(4):235-46.

References

267. Wang T, Song P, Zhong T, Wang X, Xiang X, Liu Q, et al. The inflammatory cytokine IL-6 induces FRA1 deacetylation promoting colorectal cancer stem-like properties. Oncogene. 2019;38(25):4932-47.
268. Wu J, Long Z, Cai H, Du C, Liu X, Yu S, et al. High expression of WISP1 in colon cancer is associated with apoptosis, invasion and poor prognosis. Oncotarget. 2016;7(31):49834-47.
269. Laissue P. The forkhead-box family of transcription factors: key molecular players in colorectal cancer pathogenesis. Molecular cancer. 2019;18(1):5-.
270. Murillo-Garzón V, Gorroño-Etxebarria I, Åkerfelt M, Puustinen MC, Sistonen L, Nees M, et al. Frizzled-8 integrates Wnt-11 and transforming growth factor-β signaling in prostate cancer. Nature Communications. 2018;9(1):1747.
271. Yu J, Wu WKK, Li X, He J, Li X-X, Ng SSM, et al. Novel recurrently mutated genes and a prognostic mutation signature in colorectal cancer. Gut. 2015;64(4):636-45.
272. Maye P, Zheng J, Li L, Wu D. Multiple mechanisms for Wnt11-mediated repression of the canonical Wnt signaling pathway. J Biol Chem. 2004;279(23):24659-65.
273. Ali I, Medegan B, Braun DP. Wnt9A Induction Linked to Suppression of Human Colorectal Cancer Cell Proliferation. International journal of molecular sciences. 2016;17(4):495-.
274. Papaccio F, Paino F, Regad T, Papaccio G, Desiderio V, Tirino V. Concise Review: Cancer Cells, Cancer Stem Cells, and Mesenchymal Stem Cells: Influence in Cancer Development. STEM CELLS Translational Medicine. 2017;6(12):2115-25.
275. Gonzalez-Villarreal CA, Quiroz-Reyes AG, Islas JF, Garza-Treviño EN. Colorectal Cancer Stem Cells in the Progression to Liver Metastasis. Frontiers in Oncology. 2020;10(1511).
276. Das PK, Islam F, Lam AK. The Roles of Cancer Stem Cells and Therapy Resistance in Colorectal Carcinoma. Cells. 2020;9(6):1392.
277. Yang L, Shi P, Zhao G, Xu J, Peng W, Zhang J, et al. Targeting cancer stem cell pathways for cancer therapy. Signal Transduction and Targeted Therapy. 2020;5(1):8.
278. Jiao ZY, Cao HT, Li YM. Possible Role of Cancer Stem Cells in Colorectal Cancer Metastasizing to the Liver. Curr Stem Cell Res Ther. 2016;11(5):440-3.
279. Olejniczak A, Szaryńska M, Kmieć Z. In vitro characterization of spheres derived from colorectal cancer cell lines. Int J Oncol. 2018;52(2):599-612.
280. Xu Y, Zhang L, Wang Q, Zheng M. Comparison of Different Colorectal Cancer With Liver Metastases Models Using Six Colorectal Cancer Cell Lines. Pathology & Oncology Research. 2020;26(4):2177-83.
281. Zhao H, Yan C, Hu Y, Mu L, Huang K, Li Q, et al. Sphere-forming assay vs. organoid culture: Determining long-term stemness and the chemoresistant capacity of primary colorectal cancer cells. Int J Oncol. 2019;54(3):893-904.
282. Xu H, Niu M, Yuan X, Wu K, Liu A. CD44 as a tumor biomarker and therapeutic target. Experimental Hematology & Oncology. 2020;9(1):36.
283. Huang T, Wang L, Liu D, Li P, Xiong H, Zhuang L, et al. FGF7/FGFR2 signal promotes invasion and migration in human gastric cancer through upregulation of thrombospondin-1. International journal of oncology. 2017;50(5):1501-12.

References

284.   Yao Y, Zhou D, Shi D, Zhang H, Zhan S, Shao X, et al. GLI1 overexpression promotes gastric cancer cell proliferation and migration and induces drug resistance by combining with the AKT-mTOR pathway. Biomed Pharmacother. 2019;111:993-1004.

285.   Wang J, Liang W-J, Min G-T, Wang H-P, Chen W, Yao N. LTBP2 promotes the migration and invasion of gastric cancer cells and predicts poor outcome of patients with gastric cancer. International journal of oncology. 2018;52(6):1886-98.

286.   Wang Z, Li R, He Y, Huang S. Effects of secreted frizzled-related protein 1 on proliferation, migration, invasion, and apoptosis of colorectal cancer cells. Cancer cell international. 2018;18:48-.

287.   Ren D-n, Chen J, Li Z, Yan H, Yin Y, Wo D, et al. LRP5/6 directly bind to Frizzled and prevent Frizzled-regulated tumour metastasis. Nature Communications. 2015;6(1):6906.

288.   Yu J, Liu D, Sun X, Yang K, Yao J, Cheng C, et al. CDX2 inhibits the proliferation and tumor formation of colon cancer cells by suppressing Wnt/β-catenin signaling via transactivation of GSK-3β and Axin2 expression. Cell Death & Disease. 2019;10(1):26.

289.   Fender AW, Nutter JM, Fitzgerald TL, Bertrand FE, Sigounas G. Notch-1 promotes stemness and epithelial to mesenchymal transition in colorectal cancer. J Cell Biochem. 2015;116(11):2517-27.

290.   Ueno K, Hazama S, Mitomori S, Nishioka M, Suehiro Y, Hirata H, et al. Down-regulation of frizzled-7 expression decreases survival, invasion and metastatic capabilities of colon cancer cells. British Journal of Cancer. 2009;101(8):1374-81.

291.   Blache P, van de Wetering M, Duluc I, Domon C, Berta P, Freund J-Nl, et al. SOX9 is an intestine crypt transcription factor, is regulated by the Wnt pathway, and represses the CDX2 and MUC2 genes. Journal of Cell Biology. 2004;166(1):37-47.

292.   Jho E-h, Zhang T, Domon C, Joo C-K, Freund J-N, Costantini F. Wnt/β-Catenin/Tcf Signaling Induces the Transcription of Axin2, a Negative Regulator of the Signaling Pathway. Molecular and Cellular Biology. 2002;22(4):1172-83.

293.   MacDonald BT, Tamai K, He X. Wnt/β-Catenin Signaling: Components, Mechanisms, and Diseases. Developmental Cell. 2009;17(1):9-26.

294.   Anderson P, Kedersha N. RNA granules. Journal of Cell Biology. 2006;172(6):803-8.

295.   Slawson C, Housley MP, Hart GW. O-GlcNAc cycling: how a single sugar post-translational modification is changing the way we think about signaling networks. J Cell Biochem. 2006;97(1):71-83.

296.   Ohn T, Kedersha N, Hickman T, Tisdale S, Anderson P. A functional RNAi screen links O-GlcNAc modification of ribosomal proteins to stress granule and processing body assembly. Nature cell biology. 2008;10(10):1224-31.

297.   Meijer L, Skaltsounis AL, Magiatis P, Polychronopoulos P, Knockaert M, Leost M, et al. GSK-3-selective inhibitors derived from Tyrian purple indirubins. Chem Biol. 2003;10(12):1255-66.

298.   Sato N, Meijer L, Skaltsounis L, Greengard P, Brivanlou AH. Maintenance of pluripotency in human and mouse embryonic stem cells through activation of

References

Wnt signaling by a pharmacological GSK-3-specific inhibitor. Nature Medicine. 2004;10(1):55-63.

299.   Thorne CA, Wichaidit C, Coster AD, Posner BA, Wu LF, Altschuler SJ. GSK-3 modulates cellular responses to a broad spectrum of kinase inhibitors. Nat Chem Biol. 2015;11(1):58-63.

300.   Gregory MA, Qi Y, Hann SR. Phosphorylation by glycogen synthase kinase-3 controls c-myc proteolysis and subnuclear localization. J Biol Chem. 2003;278(51):51606-12.

301.   Zhou BP, Deng J, Xia W, Xu J, Li YM, Gunduz M, et al. Dual regulation of Snail by GSK-3beta-mediated phosphorylation in control of epithelial-mesenchymal transition. Nat Cell Biol. 2004;6(10):931-40.

302.   Kao SH, Wang WL, Chen CY, Chang YL, Wu YY, Wang YT, et al. GSK3beta controls epithelial-mesenchymal transition and tumor metastasis by CHIP-mediated degradation of Slug. Oncogene. 2014;33(24):3172-82.

303.   Wu D, Pan W. GSK3: a multifaceted kinase in Wnt signaling. Trends in biochemical sciences. 2010;35(3):161-8.

304.   Beurel E, Grieco SF, Jope RS. Glycogen synthase kinase-3 (GSK3): regulation, actions, and diseases. Pharmacol Ther. 2015;148:114-31.

305.   Schneider-Poetsch T, Ju J, Eyler DE, Dang Y, Bhat S, Merrick WC, et al. Inhibition of eukaryotic translation elongation by cycloheximide and lactimidomycin. Nature chemical biology. 2010;6(3):209-17.

306.   Kao S-H, Wang W-L, Chen C-Y, Chang Y-L, Wu Y-Y, Wang Y-T, et al. Analysis of Protein Stability by the Cycloheximide Chase Assay. Bio-protocol. 2015;5(1):e1374.

307.   Kisselev AF, Goldberg AL. Proteasome inhibitors: from research tools to drug candidates. Chemistry & Biology. 2001;8(8):739-58.

308.   Yasuda S, Tsuchiya H, Kaiho A, Guo Q, Ikeuchi K, Endo A, et al. Stress- and ubiquitylation-dependent phase separation of the proteasome. Nature. 2020;578(7794):296-300.

309.   Hornbeck PV, Zhang B, Murray B, Kornhauser JM, Latham V, Skrzypek E. PhosphoSitePlus, 2014: mutations, PTMs and recalibrations. Nucleic Acids Res. 2015;43(Database issue):D512-20.

310.   Huang H, Arighi CN, Ross KE, Ren J, Li G, Chen SC, et al. iPTMnet: an integrated resource for protein post-translational modification network discovery. Nucleic Acids Res. 2018;46(D1):D542-d50.

311.   Consortium TU. UniProt: the universal protein knowledgebase in 2021. Nucleic Acids Research. 2020;49(D1):D480-D9.

312.   Tukler Henriksson J, Coursey TG, Corry DB, De Paiva CS, Pflugfelder SC. IL-13 Stimulates Proliferation and Expression of Mucin and Immunomodulatory Genes in Cultured Conjunctival Goblet Cells. Invest Ophthalmol Vis Sci. 2015;56(8):4186-97.

313.   Min S, Kim S, Cho S-W. Gastrointestinal tract modeling using organoids engineered with cellular and microbiota niches. Experimental & Molecular Medicine. 2020;52(2):227-37.

314.   Costa J, Ahluwalia A. Advances and Current Challenges in Intestinal in vitro Model Engineering: A Digest. Frontiers in Bioengineering and Biotechnology. 2019;7(144).

References

315.   Angus HCK, Butt AG, Schultz M, Kemp RA. Intestinal Organoids as a Tool for Inflammatory Bowel Disease Research. Frontiers in Medicine. 2020;6(334).
316.   Takayama T, Ohi M, Hayashi T, Miyanishi K, Nobuoka A, Nakajima T, et al. Analysis of K-ras, APC, and beta-catenin in aberrant crypt foci in sporadic adenoma, cancer, and familial adenomatous polyposis. Gastroenterology. 2001;121(3):599-611.
317.   Yuasa Y. Control of gut differentiation and intestinal-type gastric carcinogenesis. Nat Rev Cancer. 2003;3(8):592-600.
318.   Suh HN, Kim MJ, Jung Y-S, Lien EM, Jun S, Park J-I. Quiescence Exit of Tert(+) Stem Cells by Wnt/β-Catenin Is Indispensable for Intestinal Regeneration. Cell reports. 2017;21(9):2571-84.
319.   Cristobal A, van den Toorn HWP, van de Wetering M, Clevers H, Heck AJR, Mohammed S. Personalized Proteome Profiles of Healthy and Tumor Human Colon Organoids Reveal Both Individual Diversity and Basic Features of Colorectal Cancer. Cell Rep. 2017;18(1):263-74.
320.   Ray K. Two sides to cancer stem cells in colorectal cancer. Nature Reviews Gastroenterology & Hepatology. 2017;14(6):325-.
321.   Li FQ, Mofunanya A, Fischer V, Hall J, Takemaru K. Nuclear-cytoplasmic shuttling of Chibby controls beta-catenin signaling. Mol Biol Cell. 2010;21(2):311-22.
322.   Cong F, Varmus H. Nuclear-cytoplasmic shuttling of Axin regulates subcellular localization of β-catenin. Proceedings of the National Academy of Sciences of the United States of America. 2004;101(9):2882-7.
323.   Bechard M, Dalton S. Subcellular localization of glycogen synthase kinase 3beta controls embryonic stem cell self-renewal. Mol Cell Biol. 2009;29(8):2092-104.
324.   Eisenberg-Lerner A, Ciechanover A, Merbl Y. Post-translational modification profiling - A novel tool for mapping the protein modification landscape in cancer. Exp Biol Med (Maywood). 2016;241(14):1475-82.
325.   He M, Zhou Z, Shah AA, Hong Y, Chen Q, Wan Y. New insights into posttranslational modifications of Hippo pathway in carcinogenesis and therapeutics. Cell Div. 2016;11:4.
326.   Wang Y, Liu J, Huang BO, Xu Y-M, Li J, Huang L-F, et al. Mechanism of alternative splicing and its regulation. Biomedical reports. 2015;3(2):152-8.
327.   Park Y-J, Lee J-H, Kim JY, Park C-M. Alternative RNA Splicing Expands the Developmental Plasticity of Flowering Transition. Frontiers in Plant Science. 2019;10(606).
328.   Venne AS, Kollipara L, Zahedi RP. The next level of complexity: crosstalk of posttranslational modifications. Proteomics. 2014;14(4-5):513-24.
329.   Ardito F, Giuliani M, Perrone D, Troiano G, Lo Muzio L. The crucial role of protein phosphorylation in cell signaling and its use as targeted therapy (Review). International journal of molecular medicine. 2017;40(2):271-80.
330.   Han Z-J, Feng Y-H, Gu B-H, Li Y-M, Chen H. The post-translational modification, SUMOylation, and cancer (Review). International journal of oncology. 2018;52(4):1081-94.
331.   Wei W, Lin H-K. The key role of ubiquitination and sumoylation in signaling and cancer: a research topic. Frontiers in oncology. 2012;2:187-.

References

332.   Su S, Zhang Y, Liu P. Roles of Ubiquitination and SUMOylation in DNA Damage Response. Current issues in molecular biology. 2020;35:59-84.

333.   Wilkinson KA, Henley JM. Mechanisms, regulation and consequences of protein SUMOylation. Biochem J. 2010;428(2):133-45.

334.   Wen D, Wu J, Wang L, Fu Z. SUMOylation Promotes Nuclear Import and Stabilization of Polo-like Kinase 1 to Support Its Mitotic Function. Cell reports. 2017;21(8):2147-59.

335.   Choi H-K, Choi K-C, Yoo J-Y, Song M, Ko Suk J, Kim Chul H, et al. Reversible SUMOylation of TBL1-TBLR1 Regulates β-Catenin-Mediated Wnt Signaling. Molecular Cell. 2011;43(2):203-16.

336.   Hsu CL, Chung FH, Chen CH, Hsu TT, Liu SM, Chung DS, et al. Genotypes of cancer stem cells characterized by epithelial-to-mesenchymal transition and proliferation related functions. Sci Rep. 2016;6:32523.

337.   Doble BW, Woodgett JR. GSK-3: tricks of the trade for a multi-tasking kinase. J Cell Sci. 2003;116(Pt 7):1175-86.

338.   López-Tobón A, Villa CE, Cheroni C, Trattaro S, Caporale N, Conforti P, et al. Human Cortical Organoids Expose a Differential Function of GSK3 on Cortical Neurogenesis. Stem Cell Reports. 2019;13(5):847-61.

339.   Wang F, Scoville D, He XC, Mahe MM, Box A, Perry JM, et al. Isolation and characterization of intestinal stem cells based on surface marker combinations and colony-formation assay. Gastroenterology. 2013;145(2):383-95.e1-21.

340.   Zeng J, Liu D, Qiu Z, Huang Y, Chen B, Wang L, et al. GSK3β overexpression indicates poor prognosis and its inhibition reduces cell proliferation and survival of non-small cell lung cancer cells. PLoS One. 2014;9(3):e91231-e.

341.   Ugolkov AV, Matsangou M, Taxter TJ, O'Halloran TV, Cryns VL, Giles FJ, et al. Aberrant expression of glycogen synthase kinase-3β in human breast and head and neck cancer. Oncol Lett. 2018;16(5):6437-44.

342.   Alves M, Borges DdP, Kimberly A, Martins Neto F, Oliveira AC, Sousa JCd, et al. Glycogen Synthase Kinase-3 Beta Expression Correlates With Worse Overall Survival in Non-Small Cell Lung Cancer—A Clinicopathological Series. Frontiers in Oncology. 2021;11(343).

343.   Salim T, Sjölander A, Sand-Dejmek J. Nuclear expression of Glycogen synthase kinase-3β and lack of membranous β-catenin is correlated with poor survival in colon cancer. International Journal of Cancer. 2013;133(4):807-15.

344.   Fleck O, Nielsen O. DNA repair. Journal of Cell Science. 2004;117(4):515-7.

345.   Hakem R. DNA-damage repair; the good, the bad, and the ugly. The EMBO journal. 2008;27(4):589-605.

346.   Helfricht A, Thijssen PE, Rother MB, Shah RG, Du L, Takada S, et al. Loss of ZBTB24 impairs nonhomologous end-joining and class-switch recombination in patients with ICF syndrome. Journal of Experimental Medicine. 2020;217(11).

347.   Nicolai S, Mahen R, Raschellà G, Marini A, Pieraccioli M, Malewicz M, et al. ZNF281 is recruited on DNA breaks to facilitate DNA repair by non-homologous end joining. Oncogene. 2020;39(4):754-66.

348.   Chen G, Chen J, Qiao Y, Shi Y, Liu W, Zeng Q, et al. ZNF830 mediates cancer chemoresistance through promoting homologous-recombination repair. Nucleic acids research. 2018;46(3):1266-79.

References

349.   Szklarczyk D, Franceschini A, Wyder S, Forslund K, Heller D, Huerta-Cepas J, et al. STRING v10: protein-protein interaction networks, integrated over the tree of life. Nucleic Acids Res. 2015;43(Database issue):D447-52.

350.   Warde-Farley D, Donaldson SL, Comes O, Zuberi K, Badrawi R, Chao P, et al. The GeneMANIA prediction server: biological network integration for gene prioritization and predicting gene function. Nucleic Acids Res. 2010;38(Web Server issue):W214-20.

351.   Franz M, Rodriguez H, Lopes C, Zuberi K, Montojo J, Bader GD, et al. GeneMANIA update 2018. Nucleic acids research. 2018;46(W1):W60-W4.

352.   Gupta R, Somyajit K, Narita T, Maskey E, Stanlie A, Kremer M, et al. DNA Repair Network Analysis Reveals Shieldin as a Key Regulator of NHEJ and PARP Inhibitor Sensitivity. Cell. 2018;173(4):972-88.e23.

353.   Szklarczyk D, Gable AL, Lyon D, Junge A, Wyder S, Huerta-Cepas J, et al. STRING v11: protein-protein association networks with increased coverage, supporting functional discovery in genome-wide experimental datasets. Nucleic Acids Res. 2019;47(D1):D607-d13.

354.   Izhar L, Adamson B, Ciccia A, Lewis J, Pontano-Vaites L, Leng Y, et al. A Systematic Analysis of Factors Localized to Damaged Chromatin Reveals PARP-Dependent Recruitment of Transcription Factors. Cell Rep. 2015;11(9):1486-500.

355.   Mirman Z, de Lange T. 53BP1: a DSB escort. Genes Dev. 2020;34(1-2):7-23.

356.   Podhorecka M, Skladanowski A, Bozko P. H2AX Phosphorylation: Its Role in DNA Damage Response and Cancer Therapy. J Nucleic Acids. 2010;2010.

357.   Polo SE, Jackson SP. Dynamics of DNA damage response proteins at DNA breaks: a focus on protein modifications. Genes & development. 2011;25(5):409-33.

358.   Galganski L, Urbanek MO, Krzyzosiak WJ. Nuclear speckles: molecular organization, biological function and role in disease. Nucleic Acids Research. 2017;45(18):10350-68.

359.   Sleeman JE, Trinkle-Mulcahy L. Nuclear bodies: new insights into assembly/dynamics and disease relevance. Curr Opin Cell Biol. 2014;28:76-83.

360.   Birbach A, Bailey ST, Ghosh S, Schmid JA. Cytosolic, nuclear and nucleolar localization signals determine subcellular distribution and activity of the NF-κB inducing kinase NIK. Journal of Cell Science. 2004;117(16):3615-24.

361.   Hung M-C, Link W. Protein localization in disease and therapy. Journal of Cell Science. 2011;124(20):3381-92.

362.   Lu W-T, Hawley BR, Skalka GL, Baldock RA, Smith EM, Bader AS, et al. Drosha drives the formation of DNA:RNA hybrids around DNA break sites to facilitate DNA repair. Nature Communications. 2018;9(1):532.

363.   Liu H, Liang C, Kollipara RK, Matsui M, Ke X, Jeong B-C, et al. HP1BP3, a Chromatin Retention Factor for Co-transcriptional MicroRNA Processing. Molecular cell. 2016;63(3):420-32.

364.   Bartova E, Malyskova B, Komurkova D, Legartova S, Suchankova J, Krejci J, et al. Function of heterochromatin protein 1 during DNA repair. Protoplasma. 2017;254(3):1233-40.

365.   Mah LJ, El-Osta A, Karagiannis TC. γH2AX: a sensitive molecular marker of DNA damage and repair. Leukemia. 2010;24(4):679-86.

References

366.   Rastogi RP, Richa, Kumar A, Tyagi MB, Sinha RP. Molecular mechanisms of ultraviolet radiation-induced DNA damage and repair. J Nucleic Acids. 2010;2010:592980.

367.   Rocha CRR, Silva MM, Quinet A, Cabral-Neto JB, Menck CFM. DNA repair pathways and cisplatin resistance: an intimate relationship. Clinics (Sao Paulo, Brazil). 2018;73(suppl 1):e478s-es.

368.   Heijink AM, Everts M, Honeywell ME, Richards R, Kok YP, de Vries EGE, et al. Modeling of Cisplatin-Induced Signaling Dynamics in Triple-Negative Breast Cancer Cells Reveals Mediators of Sensitivity. Cell Rep. 2019;28(9):2345-57.e5.

369.   Basu A, Krishnamurthy S. Cellular responses to Cisplatin-induced DNA damage. J Nucleic Acids. 2010;2010.

370.   Clarke PA, Pestell KE, Di Stefano F, Workman P, Walton MI. Characterisation of molecular events following cisplatin treatment of two curable ovarian cancer models: contrasting role for p53 induction and apoptosis in vivo. Br J Cancer. 2004;91(8):1614-23.

371.   Englinger B, Mair M, Miklos W, Pirker C, Mohr T, van Schoonhoven S, et al. Loss of CUL4A expression is underlying cisplatin hypersensitivity in colorectal carcinoma cells with acquired trabectedin resistance. Br J Cancer. 2017;116(4):489-500.

372.   Luo P, Wu S, Ji K, Yuan X, Li H, Chen J, et al. LncRNA MIR4435-2HG mediates cisplatin resistance in HCT116 cells by regulating Nrf2 and HO-1. PLoS One. 2020;15(11):e0223035.

373.   Shen H, Perez RE, Davaadelger B, Maki CG. Two 4N Cell-Cycle Arrests Contribute to Cisplatin-Resistance. PLoS One. 2013;8(4):e59848.

374.   Fischer M. Census and evaluation of p53 target genes. Oncogene. 2017;36(28):3943-56.

375.   Mailand N, Bekker-Jensen S, Faustrup H, Melander F, Bartek J, Lukas C, et al. RNF8 Ubiquitylates Histones at DNA Double-Strand Breaks and Promotes Assembly of Repair Proteins. Cell. 2007;131(5):887-900.

376.   Bartocci C, Denchi EL. Put a RING on it: regulation and inhibition of RNF8 and RNF168 RING finger E3 ligases at DNA damage sites. Frontiers in genetics. 2013;4:128-.

377.   Ozaki T, Wu D, Sugimoto H, Nagase H, Nakagawara A. Runt-related transcription factor 2 (RUNX2) inhibits p53-dependent apoptosis through the collaboration with HDAC6 in response to DNA damage. Cell death & disease. 2013;4(4):e610-e.

378.   Ozaki T, Nakagawara A, Nagase H. RUNX Family Participates in the Regulation of p53-Dependent DNA Damage Response. Int J Genomics. 2013;2013:271347.

379.   Badie S, Liao C, Thanasoula M, Barber P, Hill MA, Tarsounas M. RAD51C facilitates checkpoint signaling by promoting CHK2 phosphorylation. The Journal of cell biology. 2009;185(4):587-600.

380.   Chatterjee N, Walker GC. Mechanisms of DNA damage, repair, and mutagenesis. Environ Mol Mutagen. 2017;58(5):235-63.

381.   Shiloh Y. ATM and ATR: networking cellular responses to DNA damage. Curr Opin Genet Dev. 2001;11(1):71-7.

References

382. Yajima H, Lee KJ, Zhang S, Kobayashi J, Chen BP. DNA double-strand break formation upon UV-induced replication stress activates ATM and DNA-PKcs kinases. J Mol Biol. 2009;385(3):800-10.
383. Lu C, Shi Y, Wang Z, Song Z, Zhu M, Cai Q, et al. Serum starvation induces H2AX phosphorylation to regulate apoptosis via p38 MAPK pathway. FEBS Lett. 2008;582(18):2703-8.
384. Tu WZ, Li B, Huang B, Wang Y, Liu XD, Guan H, et al. gammaH2AX foci formation in the absence of DNA damage: mitotic H2AX phosphorylation is mediated by the DNA-PKcs/CHK2 pathway. FEBS Lett. 2013;587(21):3437-43.
385. Williams AB, Schumacher B. p53 in the DNA-Damage-Repair Process. Cold Spring Harbor perspectives in medicine. 2016;6(5):a026070.
386. Cheng X, Xu X, Chen D, Zhao F, Wang W. Therapeutic potential of targeting the Wnt/β-catenin signaling pathway in colorectal cancer. Biomedicine & Pharmacotherapy. 2019;110:473-81.
387. Mosimann C, Hausmann G, Basler K. β-Catenin hits chromatin: regulation of Wnt target gene activation. Nature Reviews Molecular Cell Biology. 2009;10(4):276-86.
388. Huang C-Z, Xu J-H, Zhong W, Xia Z-S, Wang S-Y, Cheng D, et al. Sox9 transcriptionally regulates Wnt signaling in intestinal epithelial stem cells in hypomethylated crypts in the diabetic state. Stem Cell Research & Therapy. 2017;8(1):60.
389. Georgopoulos NT, Kirkwood LA, Southgate J. A novel bidirectional positive-feedback loop between Wnt–β-catenin and EGFR–ERK plays a role in context-specific modulation of epithelial tissue regeneration. Journal of Cell Science. 2014;127(13):2967-82.
390. Nardozzi JD, Lott K, Cingolani G. Phosphorylation meets nuclear import: a review. Cell communication and signaling : CCS. 2010;8:32-.
391. Antas P, Novellasdemunt L, Kucharska A, Massie I, Carvalho J, Oukrif D, et al. SH3BP4 Regulates Intestinal Stem Cells and Tumorigenesis by Modulating beta-Catenin Nuclear Localization. Cell Rep. 2019;26(9):2266-73.e4.
392. Dieterich W, Neurath MF, Zopf Y. Intestinal ex vivo organoid culture reveals altered programmed crypt stem cells in patients with celiac disease. Scientific Reports. 2020;10(1):3535.
393. Grady WM, Pritchard CC. Molecular alterations and biomarkers in colorectal cancer. Toxicologic pathology. 2014;42(1):124-39.
394. Alves Martins BA, de Bulhões GF, Cavalcanti IN, Martins MM, de Oliveira PG, Martins AMA. Biomarkers in Colorectal Cancer: The Role of Translational Proteomics Research. Frontiers in Oncology. 2019;9(1284).
395. Schmitges FW, Radovani E, Najafabadi HS, Barazandeh M, Campitelli LF, Yin Y, et al. Multiparameter functional diversity of human C2H2 zinc finger proteins. Genome Res. 2016;26(12):1742-52.
396. Stiff T, O'Driscoll M, Rief N, Iwabuchi K, Löbrich M, Jeggo PA. ATM and DNA-PK function redundantly to phosphorylate H2AX after exposure to ionizing radiation. Cancer Res. 2004;64(7):2390-6.
397. Li Y, Li J, Wang R, Zhang L, Fu G, Wang X, et al. Frequent RNF43 mutation contributes to moderate activation of Wnt signaling in colorectal signet-ring cell carcinoma. Protein & cell. 2020;11(4):292-8.

References

398.   Yaeger R, Chatila WK, Lipsyc MD, Hechtman JF, Cercek A, Sanchez-Vega F, et al. Clinical Sequencing Defines the Genomic Landscape of Metastatic Colorectal Cancer. Cancer cell. 2018;33(1):125-36.e3.

399.   Giannakis M, Hodis E, Jasmine Mu X, Yamauchi M, Rosenbluh J, Cibulskis K, et al. RNF43 is frequently mutated in colorectal and endometrial cancers. Nature genetics. 2014;46(12):1264-6.

400.   Koo TK, Li MY. A Guideline of Selecting and Reporting Intraclass Correlation Coefficients for Reliability Research. J Chiropr Med. 2016;15(2):155-63.

Appendices

Appendix 1
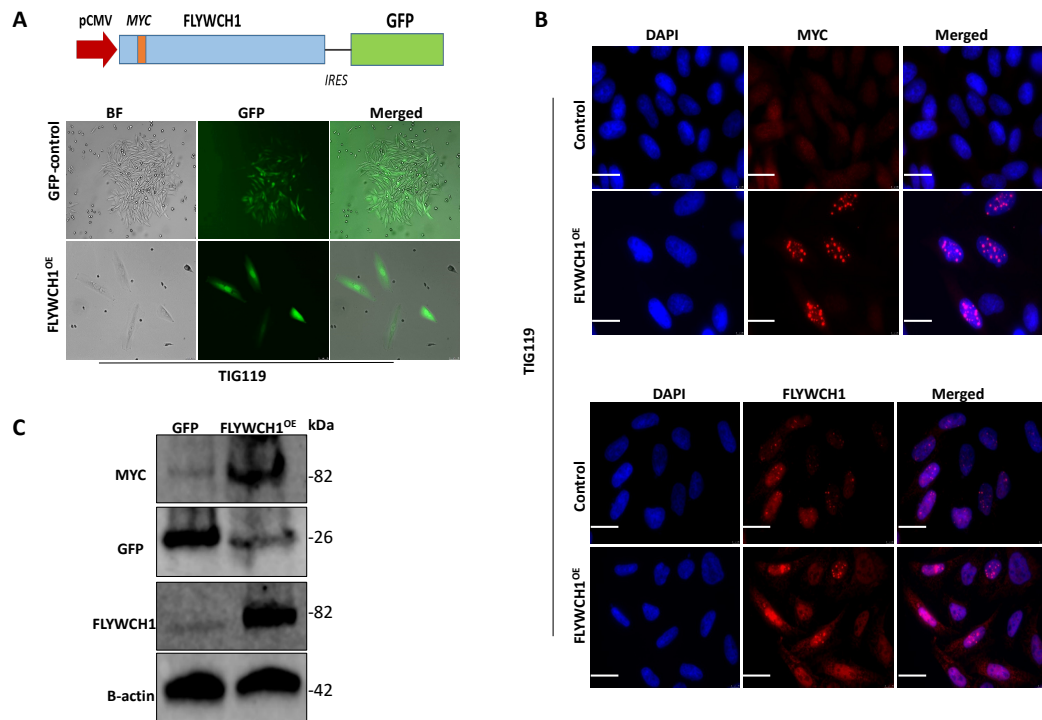
Appendix 1: Generation and validation of TIG119 Stable cell lines over-expressing the full length of FLYWCH1. A) Schematic presentation of plasmid construct used to generate the cell line and microscopic images showing the GFP expression after selection with Neomycin (G418). **B)** Immunofluorescence staining shows the expressing of Myc-tagged FLYWCH1 and endogenous FLYWCH1 in both control cells (transfected with empty vector) and FLYWCH1-expressing cells. **C)** WB analysis validates the stable expression of Myc-tagged FLYWCH1 in TIG119 cells. Cells were blotted with the indicated Abs. anti-β-actin was used a loading control. Lysate derived from GFP trasnfected cells were used as controls.

Appendix 2
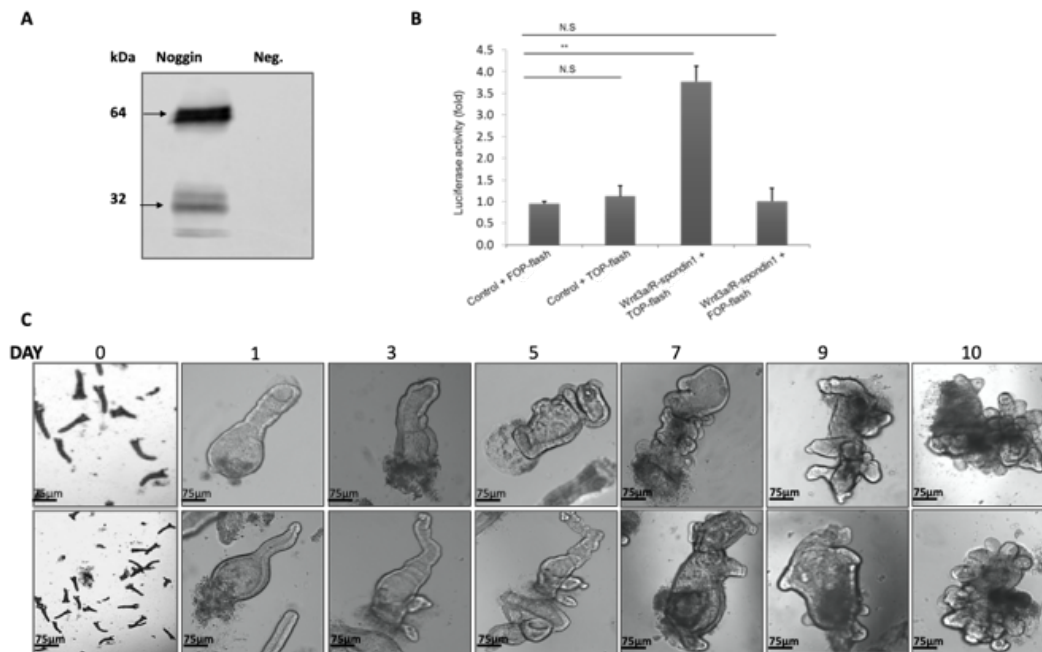
Appendix 2: Validation of essential culture components produced in house and used in our organoid growth medium. A) Western Blot analysis of Noggin protein secreted by transfected HEKT293. Cells were transfected with 15µg of Noggin plasmid, and the noggin conditioned medium was filtered and run in 10% SDS-gel. **B)** Luciferase analysis of Wnt-3a and R-spondin in HEK293T cells confirms the activity of Wnt-3a+R-spondin1 function used in our organoid culture. Figure shows a significant increase of the activity in the combination of Wnt3a+R-spondin **P < 0.01. C)** Representative Images for Human colonic crypts embedded in Matrigel and cultured for 10 days. Images were taken daily to monitor the growth and expansion of crypts before freezing. Magnification 10x, Scale bars; 75µm.

Appendix 3
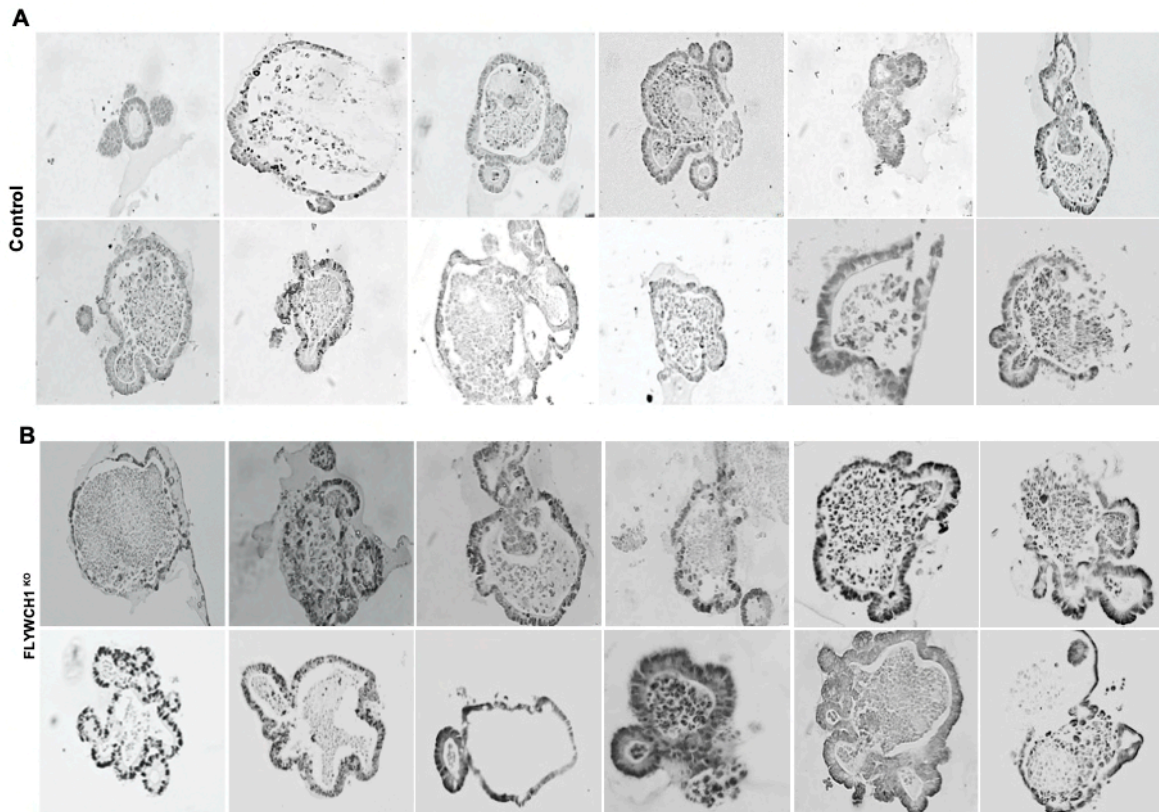
Appendix 3: Images used for the quantificational analysis of Ki-67 in A) Control & **B)** FLYWCH1^KO**.** The expression of Ki-67 was quantified from 10 organoids and the percentage of positive cells was calculated.

Appendix 4

A

B
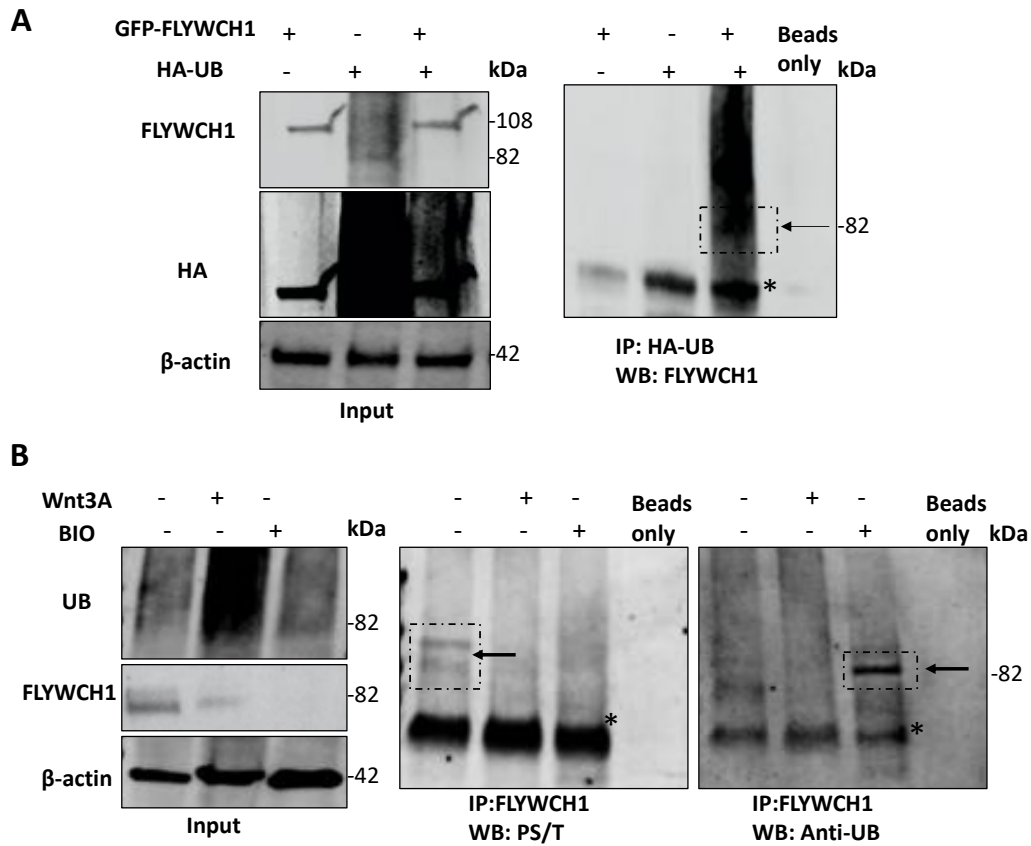
Appendix 4: PTM of FLYWCH1 by Wnt/GSK-3β signaling. A) Ubiquitination assay shows that FLYWCH1 can be modified by UB protein. HEK293T cells were transiently transfected with GFP-FLYWCH1 and/or HA-UB. 48h post transfection, lysates were prepared, and cells were immunoprecipitated with HA-tagged antibody and then blotted against FLYWCH1 antibody. The experiment was repeated in two independent occasions. **B)** Co-IP-based in-vitro phosphorylation and UB assay showing the impact of Wnt activation using (Wnt3A-CM, BIO) on FLYWCH1 phosphorylation and ubiquitination. HEK293T cells were treated with (Wnt3A /BIO) or mock treated with just Optimum for 24h. Lysates were then immunoprecipitated for endogenous FLYWCH1 and blotted against either anti-Phospho-(Ser/Thr) or anti-UB. Beads only was used as a negative control for IP and β-actin was used as loading control for input samples. N=2. *Indicates non-specific bands (correspond to IgG heavy chain).

Appendix 5

A

Intraclass Correlation Coefficient

	Intraclass Correlation[b]	95% Confidence Interval		F Test with True Value .	
		Lower Bound	Upper Bound	Value	df1
Single Measures	.761[a]	.354	.886	11.737	282
Average Measures	.864[c]	.522	.940	11.737	282

Intraclass Correlation Coefficient

	F Test with True Value 0	
	df2	Sig
Single Measures	282	.000
Average Measures	282	.000

Two-way mixed effects model where people effects are random and measures effects are fixed.

  a. The estimator is the same, whether the interaction effect is present or not.

  b. Type A intraclass correlation coefficients using an absolute agreement definition.

  c. This estimate is computed assuming the interaction effect is absent, because it is not estimable otherwise.

B

Intraclass Correlation Coefficient

	Intraclass Correlation[b]	95% Confidence Interval		F Test with True Value .	
		Lower Bound	Upper Bound	Value	df1
Single Measures	.717[a]	.207	.871	10.519	368
Average Measures	.835[c]	.342	.931	10.519	368

Intraclass Correlation Coefficient

	F Test with True Value 0	
	df2	Sig
Single Measures	368	.000
Average Measures	368	.000

Two-way mixed effects model where people effects are random and measures effects are fixed.

  a. The estimator is the same, whether the interaction effect is present or not.

  b. Type A intraclass correlation coefficients using an absolute agreement definition.

  c. This estimate is computed assuming the interaction effect is absent, because it is not estimable otherwise.

C

Intraclass Correlation Coefficient

	Intraclass Correlation[b]	95% Confidence Interval		F Test with True Value .	
		Lower Bound	Upper Bound	Value	df1
Single Measures	.965[a]	.930	.980	68.882	101
Average Measures	.982[c]	.964	.990	68.882	101

Intraclass Correlation Coefficient

	F Test with True Value 0	
	df2	Sig
Single Measures	101	.000
Average Measures	101	.000

Two-way mixed effects model where people effects are random and measures effects are fixed.

a. The estimator is the same, whether the interaction effect is present or not.

b. Type A intraclass correlation coefficients using an absolute agreement definition.

c. This estimate is computed assuming the interaction effect is absent, because it is not estimable otherwise.

D

Intraclass Correlation Coefficient

	Intraclass Correlation[b]	95% Confidence Interval		F Test with True Value .	
		Lower Bound	Upper Bound	Value	df1
Single Measures	.884[a]	.810	.927	18.582	104
Average Measures	.939[c]	.895	.962	18.582	104

Intraclass Correlation Coefficient

	F Test with True Value 0	
	df2	Sig
Single Measures	104	.000
Average Measures	104	.000

Two-way mixed effects model where people effects are random and measures effects are fixed.

a. The estimator is the same, whether the interaction effect is present or not.

b. Type A intraclass correlation coefficients using an absolute agreement definition.

c. This estimate is computed assuming the interaction effect is absent, because it is not estimable otherwise.

Appendix 5: Intraclass Correlation Coefficient (ICC) of TMA analysis for: **A)** Nuclear and **B)** Cytoplasmic FLYWCH1, **D)** Nuclear & **E)** Cytoplasmic GSK-3β. ICC test was used to assess the concordance rate of the two scoring. Values between 0.75 and 0.9 indicate good reliability, and values greater than 0.90 indicate excellent reliability (400). ICC results indicate an excellent correlation and agreement between the two scoring.

Appendix 6

A

B

Appendix 6: Growth pattern and validation HCT116 ATM^KO cells.
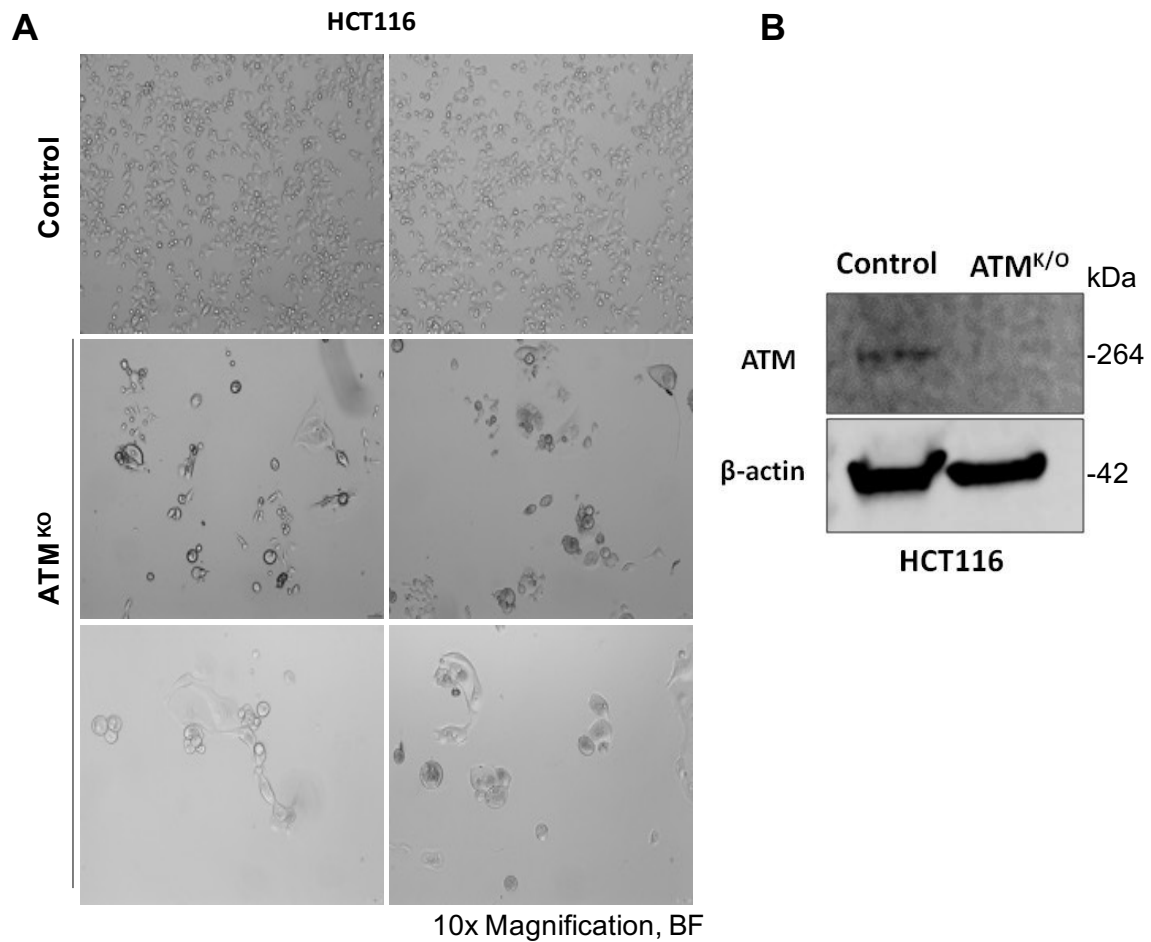
Appendix 6: Growth pattern and validation HCT116 ATM^KO cells. A) Representative images showing the growth pattern and morphology of the control HCT116 (top two images) versus the ATM^KO cells (Bottom two images). Images taken by bright field light microscope. Scale bar 75μm. **B)** Validation of the knockout in HCT116 cells by Western blot technique. WB confirms the depletion of ATM in the knockout. 100μg of protein was loaded, blotted with ATM antibody and β-actin was used as a loading control, N=1.